Dissertation zur Erlangung des Doktorgrades
der Fakultät für Chemie und Pharmazie
der Ludwig-Maximilians-Universität München

The role of glucocorticoids in the hepatic
adaptive response to caloric restriction

Konstantinos Makris

aus

Cholargos (Athens), Greece

2022

Acknowledgements

Index of Contents

Contents

Abstract

Glucocorticoids (GCs) are adrenal hormones that control vital functions such as metabolism, cell differentiation, behavior and immune responses. Glucocorticoids bind to the glucocorticoid receptor (GR), which belongs to the nuclear hormone receptor family. Upon ligand binding, GR migrates into the nucleus, binds to promoters or enhancers and induces or represses the expression of target genes. Transcriptional regulation of GR involves recruitment of and interplay with co-regulatory partners such as Mediator (MED1), histone modifiers, chromatin remodelers and other transcription factors such as E47 and STAT5. Glucocorticoids are secreted in a diurnal rhythm at the beginning of the feeding phase and in response to stress and caloric restriction. Patients who either have Cushing's syndrome or are receiving exogenous GC therapy also display higher circulating steroid levels. Caloric restriction has been shown to protect against ageing and metabolic disease by triggering numerous positive molecular signaling pathways. In the presence of increased GC secretion, such as in Cushing's syndrome, the classical treatment regimen typically leads to severe side effects such as hyperglycemia and obesity. The aim of this work was therefore to perform a functional characterization of GC responses during caloric restriction

During the highest GC values, an interaction of GR with FOXO1, the main component in caloric restriction, could be detected in the liver by ChIP MS (immunoprecipitation coupled with mass spectrometry). At the same time, liver-specific GR interacted with the SIN3A/HDAC complex, a FOXO1 corepressor complex whose function is to deacetylate proteins and histones. Comparing *ad-libitum* fed to caloric restricted mice, an enrichment of hepatic FOXO1 and PPARα motifs at maximal glucocorticoid action was demonstrated by chromatin immunoprecipitation sequencing (Chip-seq) of GR. Application of ChIP-seq for FOXO1 under caloric restriction revealed overlap with GR in many cis regulatory elements of carbohydrate and lipid homeostatic genes. In ChIP-seq for the catalytic subunit SIN3A, there was common binding of GR/FOXO1 at cis-regulatory elements of circadian and insulin-related genes. Transcriptome analysis confirmed a transition from PPARα to FOXO1 signaling at the peak of hormone release in caloric restricted mice compared to *ad-libitum* fed mice. In parallel, caloric restriction upregulated beneficial molecular signaling pathways such as autophagy, carbohydrate catabolism, circadian clock genes and antioxidant mechanisms. However, deletion of GR in the liver, during caloric restriction resulted in a switch of transcription from FOXO1 to PPARα signaling and

a loss of beneficial mechanisms such as autophagy, circadian rhythms, glycogen degradation and lipid homeostasis. Furthermore, in the absence of hepatic GR postprandially, transcriptomic analysis revealed a defective transition from fatty acid to carbohydrate metabolism. Metabolic phenotyping of liver-specific GR knockout mice with caloric restriction recapitulated resistance to glycogen consumption, a shift in cholesterol secretion and a postprandial increase in energy expenditure.

Taken together, our results show that GR/FOXO1 act synergistically in the expression of metabolic genes. The absence of GR in the liver may switch the FOXO1-driven program to PPARα responses. In summary, we found that GR controls the major molecular pathways of caloric restriction and contributes significantly to this dietary adaptation.

Zusammenfassung

Glukokortikoide (GCs) sind Nebennierenhormone, die lebenswichtige Funktionen wie Stoffwechsel, Zelldifferenzierung, Verhalten und Immunreaktionen steuern. Glukokortikoide binden an den Glukokortikoidrezeptor (GR), der zur Familie der nuklearen Hormonrezeptoren gehört. Nach der Ligandenbindung wandert der GR in den Zellkern, bindet an Promotoren oder Enhancer und induziert oder unterdrückt die Expression von Zielgenen. Die Transkriptionsregulation von GR beinhaltet die Rekrutierung von und das Zusammenspiel mit koregulatorischen Partnern wie Mediator (MED1), Histonmodifikatoren, Chromatin-Remodelern und anderen Transkriptionsfaktoren, wie E47 und STAT5. Glucocorticoide werden im Tagesrhythmus zu Beginn der Fütterungsphase und als Reaktion auf Stress und Kalorienrestriktion ausgeschüttet. Auch Patienten, die entweder am Cushing-Syndrom leiden, oder eine exogene GC-Therapie erhalten weisen höhere zirkulierende Steroidspiegel auf. Es hat sich gezeigt, dass Kalorienrestriktion vor Alterung und Stoffwechselkrankheiten schützt, indem es zahlreiche positive molekulare Signalwege auslöst. Sogar in Gegenwart erhöhter GC-Sekretion, wie beim Cushing-Syndrom, wo das klassische Behandlungsschema typischerweise zu schweren Nebenwirkungen wie Hyperglykämie und Fettleibigkeit führt. Das Ziel dieser Arbeit war daher eine funktionelle Charakterisierung der GC-Reaktionen während einer kalorischen Restriktion durchzuführen.

Während der höchsten GC-Werte konnte eine Interaktion von GR mit FOXO1, dem Hauptkomponenten bei kalorischer Restriktion, in der Leber mittels Chip-MS (Immunopräzipitation gekoppelt mit Massenspektrometrie) nachgewiesen werden. Gleichzeitig interagierte der leberspezifische GR mit dem SIN3A/HDAC-Komplex, einem FOXO1-Korepressorkomplex, dessen Funktion in der Deacetylierung von Proteinen und Histonen liegt. Im Vergleich von *ad-libitum* gefütterten zu mit kalorischer Restriktion gefütterten Mäusen konnte eine Anreicherung von hepatischen FOXO1 und PPARα-Motiven bei maximaler Glukokortikoidwirkung mittels Chromatin Immunpräzipitations Sequenzierung (Chip-seq) von GR gezeigt werden. Die Anwendung von ChIP-seq für FOXO1 bei kalorischer Restriktion ergab eine Überschneidung mit GR in vielen cis-regulatorischen Elementen von Kohlenhydrat- und lipid-homöostatischen Genen. Bei ChIP-seq für die katalytische Untereinheit SIN3A gab es eine gemeinsame Bindung des GR/FOXO1 an cis-regulatorischen Elementen von zirkadian- und insulinbezogenen Genen. Die Transkriptomanalyse bestätigte bei kalorienrestriktiven Mäusen im Vergleich

zu ad-libitum-gefütterten Mäusen einen Übergang von PPARα zu FOXO1-Signalen auf dem Höhepunkt der Hormonausschüttung. Parallel dazu wurden durch die Kalorienrestriktion vorteilhafte molekulare Signalwege wie Autophagie, Kohlenhydratabbau, zirkadiane Uhrgene und antioxidative Mechanismen hochreguliert. Die Deletion von GR in der Leber, während der Kalorienrestriktion führte jedoch zu einer Umstellung der Transkription von FOXO1 auf PPARα-Signale und zu einem Verlust förderlicher Mechanismen wie Autophagie, zirkadiane Rhythmen, Glykogenabbau und Lipidhomöostase. Darüber hinaus zeigte die transkriptomische Analyse in Abwesenheit von hepatischem GR postprandial einen defekten Übergang vom Fettsäurezum Kohlenhydratstoffwechsel. Die metabolische Phänotypisierung von Leber-spezifischen GRKnockout-Mäusen mit Kalorienrestriktion rekapituliert eine Resistenz gegen den Glykogenverbrauch, eine Verschiebung der Cholesterinsekretion und einen postprandialen Anstieg des Energieverbrauchs.

Zusammengenommen zeigen unsere Ergebnisse, dass GR/FOXO1 bei der Expression von Stoffwechselgenen synergistisch wirken. Das Fehlen von GR in der Leber kann das FOXO1-gesteuerte Programm auf PPARα-Reaktionen umstellen. Zusammenfassend haben wir festgestellt, dass GR die wichtigsten molekularen Wege der Kalorienrestriktion steuert und wesentlich zu dieser Ernährungsanpassung beiträgt

Abbreviations

ACSS1	acetyl-CoA-generating acyl-CoA synthase short-chain family member 1
ACTH	adrenocorticotropic hormone
AF	activation function domain
AD	*ad-libitum*
Alb	albumin
ALT	alanine transaminase
AMPK	AMP-activated kinase
ANCOVA	analysis of covariance
ANOVA	analysis of variance
AR	Androgen receptor
AST	aspartate transaminase
ATM	adipose tissue macrophages
ATP	adenosine tri-phosphate
BA	bile acid
BAT	brown adipose tissue
BCAAs	Brain chain amino acids
bp	base pair
BSA	bovine serum albumin
CCGs	clock-controlled genes
CDCA	chenodeoxycholic acid
cDNA	complementary DNA
ChIP	chromatin immuno-precipitation
ChIP-MS	chromatin immune-precipitation coupled with mass spectrometry
co-IPs	co-Immunoprecipitation
CR	caloric restriction
CRH	corticosteroid-releasing hormone
Ct	threshold cycle
DBD	DNA binding domain
Dex	dexamethasone
dKO	double KO
DNA	deoxyribonucleic acid
DNL	*de novo* lipogenesis

DR	direct repeat
DTT	dithiothreitol
ECL	enzymatic chemoluminescence
EDTA	ethylenediaminetetraacetic acid
EE	energy expanditure
e.g.	exempli gratia
ER	Estrogen receptor
EtOH	ethanol
FFA	free fatty acid
fl	floxed
FOX	Forkhead domain
Fw	forward
GCs	Glucocorticoids
GEO	gene expression omnibus
GO	gene ontology
GR	Glucocorticoid receptor
GRE	Glucocorticoids receptor element
GTT	glucose tolerance test
H&E	hematoxylin and eosin
HCC	hepatocellular carcinoma
HCR	highly conserved domain
HDL	high density lipoprotein
HEPES	4-(2-hydroxyethyl)-1-piperazineethanesulfonic acid
HFD	high fat diet
HPA	Hypothalamus-Pituitary Axis
HRE	hormone response element
HRP	horse radish peroxidase
IgG	immunoglobin G
IP	immunoprecipitation
IR	insulin receptor
IGF-1	Insulin growth factor 1
KATs	lysine acetyl-transferases
KDACs	lysine deacetylases
KCl	potassium chloride

KO	knockout
KOH	potassium hydroxide
L-dKO	liver specific double knockout
LBD	ligand binding domain
LCDA-CoA	long-chain dicarboxylic acyl coenzyme
LDF	lineage determining factor
LDL	low density lipoprotein
LTP	Long term potentiation
MCD	methionine choline deficient diet
$MgCl_2$	magnesium chloride
MR	Mineralocorticoid receptor
mRNA	messenger RNA
mTOR	mechanistic target of rapamycin
NaCl	natrium chloride
NAD^+	nicotine adenine dinucleotide
NAFLD	non-alcoholic fatty liver disease
NaOH	natrium hydroxide
NASH	non-alcoholic steato-hepatitis
NEFA	Non-esterified fatty acids
NP-40	nonyl phenoxypolyethoxylethanol
NR	nuclear receptor
ORF	open reading frame
PAH	Paired amphipathic helix
PAS	Periodic Acid Staining
PBS	phosphate buffered saline
PCR	polymerase chain reaction
pH	potential of hydrogen
qPCR	quantitative PCR
PR	Progesterone receptor
RER	respiratory exchange ratio
RNA	ribonucleic acid
ROS	reactive oxygen species
rpm	rotation per minute
RT-qPCR	real-time qPCR

Rv	reverse
SCN	suprachiasmatic nucleus
SD	standard deviation
SDS	sodium dodecyl sulfate
SEM	standard error of the mean
Seq	sequencing
SIRT	sirtuins
SGK	serum glucocorticoid-induced kinase
TAD	Transactivation domain
TAG	Triglycerides
T2DM	type 2 diabetes mellitus
TBS-T	TRIS buffered saline with Tween 20
TCA	tricarboxylic acid
TF	transcription factor
TRF	time restricted feeding
TRIS	tris(hydroxymethyl)aminomethane
TSS	transcription start site
TTFLs	transcriptional and translational feedback loops
UV	ultraviolet
vLCA-CoA	very long-chain acyl coenzyme
WB	western blot
WT	wild type
ZT	zeitgeber

All gene names are indicated in *italics*. All proteins are written in regular font with capital letters. Compounds and chemical elements are abbreviated according to common chemical nomenclature.

Index of Figures

Index of Tables

1. Introduction

1.1 The effects of caloric restriction and its molecular connection

1.1.1 The physiological output of caloric restriction

Caloric restriction (CR) by definition is the reduced consumption of calories without deprivation of essential nutrients and minerals. The first evidences showing that caloric restriction has an anti-aging role and can extend life span were first presented by McCay et al in the 1930s (McCay et al., 1935). Simultaneously, caloric restriction can improve health span and protect from metabolic diseases, such as obesity, diabetes and cardiovascular diseases (Madeo et al., 2019). The concept of caloric restriction has been applied to many different model species including mice, rats, fishes, monkeys, flies, worms and yeast. In the case of primates such as rhesus monkeys, caloric restriction lowers body temperature and insulin secretion and improves overall their health status and survival (Colman et al., 2014; Mattison et al., 2017; Schneider et al., 2017). Primates, including human and monkeys, show that body composition and age can affect the caloric restriction regimen efficiency (Roth et al., 2006). Human studies have shown that this nutritional status leads to reduced insulin secretion and simultaneously to enhanced insulin sensitivity. Body temperature and resting energy expenditure are diminished because the metabolism tries to adapt to the conditions of the reduced calories. The lower consumption of calories is also connected with less oxidative stress and utilization of fat mass (Bordone & Guarente, 2005; Someya et al., 2010). This physiological condition leads to reduced secreted thyroid hormone and disrupts the reproductive capacity of the subjects. In healthy humans, caloric restriction reduces many cardiometabolic risk factors, such as triglycerides, cholesterol, blood pressure, and the circulating tumor necrosis factor-α (TNFα) (Most et al., 2018; Most & Redman, 2020; Ravussin et al., 2015).

In rodents, the application of different caloric restriction regimens impacts differently on each tissue. In short term caloric restriction, a favorable utilization of the fat depots and the reproductive accessory system are observed, while metabolic organs such as liver, pancreas, and heart are protected by losing their mass (Mitchell et al., 2015). Even upon extreme lack of food the body tries to protect the essential metabolic organs and consumes all the potential energy sources creating a hierarchy in energy utilization

1

(Mitchell et al., 2015). Moreover, the caloric restriction regimen reprograms the transcriptional landscape boosting innate immunity, protects from age-associated cognitive decline and entrains the diurnal rhythms (Acosta-Rodríguez et al., 2017; Collins et al., 2019; Kishi et al., 2015; Ma et al., 2020).

1.1.2 Caloric restriction: link with the molecular pathways and autophagy

Caloric restriction (CR) is tightly connected with specific molecular pathways related with insulin-like growth factor 1 (IGF-1), sirtuins (SIRTs), target of rapamycin (mTOR), and adenosine monophosphate (AMP)-activated protein kinase (AMPK) (Duszka et al., 2020). This complex hub of signaling regulates downstream autophagy, a mechanism which is able to process and eliminate dysfunctional proteins, organelles and aggregates from the cytoplasmic pool (Levine & Klionsky, 2004).

In rodents, caloric restriction reduces the overall caloric intake and leads to reduced circulating IGF-1 levels increasing their maximal life span and health span (Fontana, 2007). In opposition, human in caloric and protein restriction have not shown reduced serum IGF-1 and IGF-1/IGF Binding Protein (IGFBP)-3 ratio levels (Fontana et al., 2008). The caloric restriction-mediated reduction of serum IGF-1 in rodents is believed to play a critical role against cancer and aging (**Figure 1**) (Dunn et al., 1997; Fontana, 2007; Sonntag et al., 1999). In parallel, growth hormone (GH)-deficient and GH receptor-deficient mice show low IGF-1 signaling and increased longevity (Bonkowski et al., 2006; Flurkey et al., 2001; Ikeno et al., 2003). Undoubtedly, caloric restriction in rodents reduces the IGF-1 signaling, playing thus a significant role in metabolism, growth and development (Jones & Clemmons, 1995).

Caloric restriction dampens the carbon flow inside the glycolytic pathway and the conversion of ADP to ATP, increasing AMP: ATP and ADP: ATP ratios and activating the AMPK signaling, a nutrient sensing pathway (**Figure 1**) (Duszka et al., 2020;Oakhill et al., 2011; Ruderman et al., 2013; Xiao et al., 2011). AMPK is a heterotrimeric complex composed of the catalytic subunit α (α1 and α2), the regulatory subunit β (β1 and β2), and the non-catalytic subunit γ (γ1, γ2, and γ3) (Hardie & Alessi, 2013; Ruderman et al., 2013). The subunit α transfers phosphate groups from the ATP molecules to target proteins (Hardie & Alessi, 2013; Ruderman et al., 2013). AMPK is activated by phosphorylation at

Thr172 in the α-subunit by upstream kinases, such as LKB1, CaMKK, TAK1, and MLK3 (Luo et al., 2015; Shaw et al., 2004; Woods et al., 2003). Active AMPK inhibits mTOR activity either by activating the TSC1/2 pathway that represses mTOR and by phosphorylating Raptor, a component of the mTOR complex (Alers et al., 2012; Gwinn et al., 2008; Inoki et al., 2003; Meley et al., 2006). AKT inhibits TSC2 leading to the activation of mTOR, which is responsible for the cell growth and is antagonistic to the AMPK signaling (Holczer et al., 2019). The balance between AMPK/mTOR signaling leads to activation or repression of autophagy, as a final molecular output (Holczer et al., 2019). Therefore, CR increases AMPK and lowers mTOR signaling for tuning the cell growth with the existing nutrients (**Figure 1**).
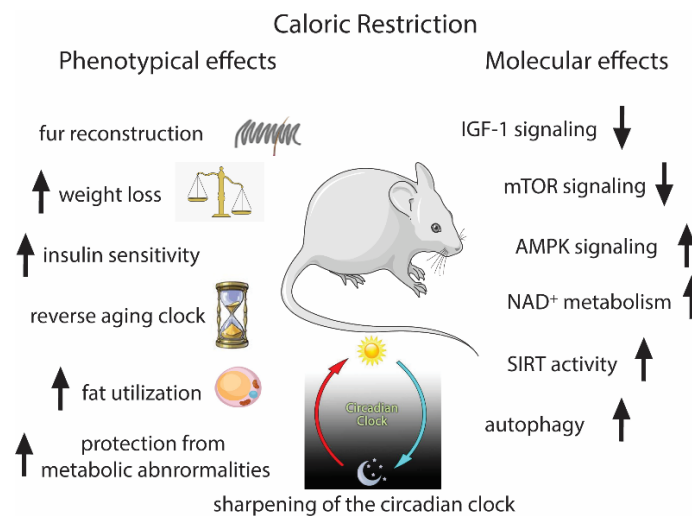
Figure 1: Phenotypical and molecular effects of caloric restriction.

Caloric restriction impacts on both phenotypical and molecular aspects. All these characterized changes have been connected with the molecular aspects of this diet regimen. Individual pictures taken from Servier Medical Art (https://smart.servier.com/).

Caloric restriction not only activates AMPK, but also increases the expression levels of sirtuins (SIRTs), such as SIRT1, SIRT3, and SIRT5 (Cohen et al., 2004; Lombard et al., 2007; Nakagawa et al., 2009). Sirtuins are NAD^+-dependent deacetylases, which remove acetyl groups from histone and non-histone proteins, such as certain transcription factors and cytoplasmic proteins (Trapp, 2006). SIRT1 induces mitochondrial biogenesis, fat homeostasis and stress resistance, by deacetylating related-transcription factors, such as FOXO1, PGC-1α, and PPARα (Brunet et al., 2004; Gerhart-Hines et al., 2007; Motta et al., 2004; Purushotham et al., 2009; Rodgers et al., 2005). SIRT1 is commonly induced in

CR by both mice and humans and is related with ageing (Civitarese et al., 2007; Cohen et al., 2004). Indeed, SIRT1 activity is closely interconnected with AMPK, since AMPK activates the synthesis of the nicotinamide (NAD) synthetic enzyme nicotinamide phosphoribosyltransferase (NAMPT) and in return, SIRT1 deacetylates and activates the AMPK kinase LKB1 (Cantó et al., 2009, 2010; Feige et al., 2008; Fulco et al., 2008; Hou et al., 2008; Lan et al., 2008). Afterwards, SIRT1 switches off the glycolysis pathway by deacetylating glycolytic enzymes and their transcriptional inducer, HIF-1α (Hallows et al., 2012; J.-H. Lim et al., 2010). To conclude, in CR the elevated AMPK and SIRT activity boost the NAD$^+$ cellular metabolism, deactivate specific factors and glycolytic enzymes and activate autophagy (**Figure 1**) (Kume et al., 2010).

Protein acetylation is another modulator of autophagy affecting the molecular output of caloric restriction. One of the most phylogenetically conserved post-translational protein modifications is the Ne acetylation of lysines in proteins, which is catalyzed by lysine acetyltransferases (KATs) and removed by lysine deacetylases (KDACs) (Madeo et al., 2019). It is known that protein acetylation can inhibit the autophagic machinery. A lot of members of the autophagic machinery undergo changes in their acetylation status and core mediators of autophagy such as the transcription factor p53 and the forkhead box P3 (FoxP3) (Contreras et al., 2013; C. Lee et al., 2010; I. H. Lee & Finkel, 2009; Morselli et al., 2011; Sacitharan et al., 2019; Yi et al., 2012).

Intriguingly, protein acetylation and autophagy follow circadian fluctuations (Sato et al., 2017). This oscillation is dampened through aging and is restored by CR (Sato et al., 2017). It is proposed that the rhythmic deacetylation is maintained by CR and associated with the elevated NAD$^+$ levels. These events are coupled with SIRT1 activation and the rhythmic changes in the inhibitory acetylation of acetyl-CoA-generating acyl-CoA synthase short-chain family member 1 (ACSS1) (Sato et al., 2017). Acetylation is lowered in aged mouse liver and CR can reverse this phenomenon, leading to hepatic protein hyperacetylation (Sato et al., 2017). Interestingly, autophagy is responsible for CRY1 degradation, a CLOCK/BMAL1 repressor in liver (Toledo et al., 2018). Since CRY1 suppresses hepatic gluconeogenesis by rhythmic repression of glucocorticoid receptor, by regulating CREB/cAMP signaling, and by decreasing nuclear FOXO1 levels led to the conclusion that autophagy and glucose metabolism are interconnected (Jang et al., 2016; Lamia et al., 2011; E. E. Zhang et al., 2010). Since CRY1 is destined to the lysosomes for degradation by autophagy, then gluconeogenesis is activated, increasing the blood

glucose levels (Toledo et al., 2018) (**Figure 1**). Consequently, autophagy, glucose metabolism and acetylation of cytoplasmic and histone proteins are tightly connected with the circadian fluctuations, which are amplified by CR.

1.1.3   Effects of caloric restriction in the circadian clock

Most living organisms are adapted to daily environmental changes enforced by the 24h rotation of the Earth around its own axis. To anticipate all environmental cues, organisms developed a timekeeping system, called the circadian clock (coming from Latin *circa* and *diem* meaning "about 24 h"), which regulates both behavior and physiology (Atger et al., 2017; Hughes et al., 2009). Despite the fact that every cell contains the circadian clock machinery, the mammalian clock is hierarchically organized, and the main pacemaker, located in the suprachiasmatic nucleus (SCN) of the hypothalamus is entrained by the light/dark cycles and drives the synchronization of the subsidiary peripheral oscillators located in every organ (Panda, 2016; C. B. Green et al., 2008; Potter et al., 2016; Reppert & Weaver, 2001).

The molecular clock in all living organisms is highly conserved throughout evolution and consists in interconnected Transcription Translation Feedback Loops (TTFLs) (Partch et al., 2014). Circadian Locomotor Output Cycles Kaput (CLOCK) or NPAS2 heterodimerize with Brain and Muscle ARNTL Like protein 1 (BMAL1) protein, which belong to the bHLH-PAS (basic helix-loop-helix; Per-Arnt-Sim domain) family. These two transcription factors heterodimerize and initiate transcription by binding to E box-related DNA (5'-CACGT[G/T]) motifs in the promoters of clock-controlled genes (CCGs), such as the repressors Period (Per) 1-3 and Cryptochrome (Cry) 1 and 2. CLOCK without BMAL1 cannot facilitate transcription and vice versa. The expression of their own repressors completes a self-regulated transcriptional-translational loop (Atger et al., 2017; Masri & Sassone-Corsi, 2018).
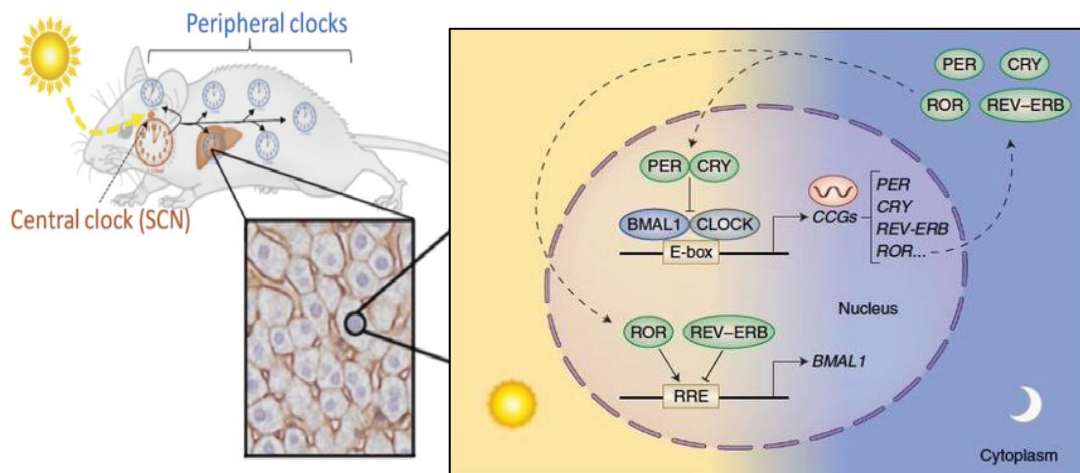
Figure 2: Molecular mechanism of the mammalian circadian clock.

The master clock resides in the suprachiasmatic nucleus of the hypothalamus entrained by the light/dark cycles and drives the peripheral clocks, such as the liver clock. The molecular clock is a transcriptional-translational feedback loop oscillating within the time period of roughly 24 h. Picture modified by (Atger et al., 2017)and (Masri & Sassone-Corsi, 2018).

Peripheral clocks can be reset primarily by the light and secondarily by the food (Oosterman et al., 2015). Caloric restriction is one potent example of modulating the circadian clock. It is known that 30% CR increases the amplitude and affects the expression of many core clock genes (S. A. Patel, Velingkaar, et al., 2016). It is remarkable that CR effects fail to improve the physiological output of BMAL1 deficient mice, including the effect in longevity, pointing the necessity for a functional clock (S. A. Patel, Velingkaar, et al., 2016). Further insight from studying polysome-bound mRNAs around the clock in both AL and CR showed diurnal rhythmicity in protein translation (Jouffe et al., 2013; Makwana et al., 2019) . CR increased the translation of enzymes related with the oxidation of very long-chain acyl coenzyme (vLCA-CoA) and long-chain dicarboxylic acyl coenzyme (LCDA-CoA) in peroxisomes. Increased activation of these enzymes generates long-chain acyl-CoA (LCA-CoA) and short-chain dicarboxylic acyl-CoA, which are hydrolyzed by the enzymes ACOT3 and ACOT4 producing free fatty acids and CoA enzyme in their inactive form. These free fatty acids are destined via the CPT1α enzyme to the mitochondria, where β-oxidation transform them into β-ketones. This β-oxidation reaction is coupled with the ATP production supplementing hepatocytes with energy and producing ketones, with the process of ketogenesis (Makwana et al., 2019a). Previous studies have shown that

chronic caloric restriction leads to the shift towards increased fatty acid oxidation and gluconeogenesis and reduced glycolysis (Dhahbi et al., 1999, 2001; Hagopian et al., 2004, 2013). Fractionation of mitochondrial sub-populations from caloric restricted mice showed higher acyl-CoA dehydrogenase (β-oxidation) and β-hydroxybuterate dehydrogenase (ketogenesis) activities (Hagopian et al., 2013). Therefore, CR boosts the rhythm in protein translation and the activity of enzymes related with β-oxidation and ketogenesis.

1.2   Glucocorticoid signaling in hepatic metabolism

1.2.1   Glucocorticoid receptor, as a nuclear receptor member

Glucocorticoids are steroid hormones, secreted by the adrenal glands either due to the circadian rhythms or environmental stress, such as starvation or exercise (Challet, 2015; Præstholm et al., 2020; Spencer et al., 2018) Their whole mechanism of secretion is based on the hypothalamus-pituitary-adrenal (HPA) axis (Vegiopoulos & Herzig, 2007). These hormones bind to the ubiquitously expressed glucocorticoid receptor (GR) to mediate their effects. GR belongs to the nuclear receptor superfamily (NR) of transcription factors (S. Green et al., 1986; Greene et al., 1986; Hollenberg et al., 1985). That also includes the estrogen receptor (ER), the mineralocorticoid receptor (MR), the androgen receptor (AR), and the progesterone receptor (PR) (Gustafsson, 2016). The founding members of this family were GR and ER with the isolation of their cDNAs in the 1980s (Gustafsson, 2016). Overall, the nuclear receptor family regulates processes, such as reproduction, metabolism, inflammation, development and homeostasis (Evans, 1988; Evans & Mangelsdorf, 2014; Mangelsdorf et al., 1995).

The synthesis and secretion of GCs is diurnal and can be modulated by the circadian clock (Lightman, 2008; Son et al., 2011; Young et al., 2004). At the beginning of the day, light resets the SCN, which is responsible for the stimulation of the hypothalamus producing corticosteroid-releasing hormone (CRH) (Son et al., 2011). In turn, CRH stimulates further the pituitary adrenal gland to secrete adrenocorticotropic hormone (ACTH), which promotes the final secretion of GCs (**Figure 3**) (Son et al., 2011; Vegiopoulos & Herzig, 2007). The SCN is the main modulator of the GC rhythmicity, as it is able to regulate the hypothalamic-hypophysial portions of the HPA axis influencing the CRH levels (Herman et al., 2016).
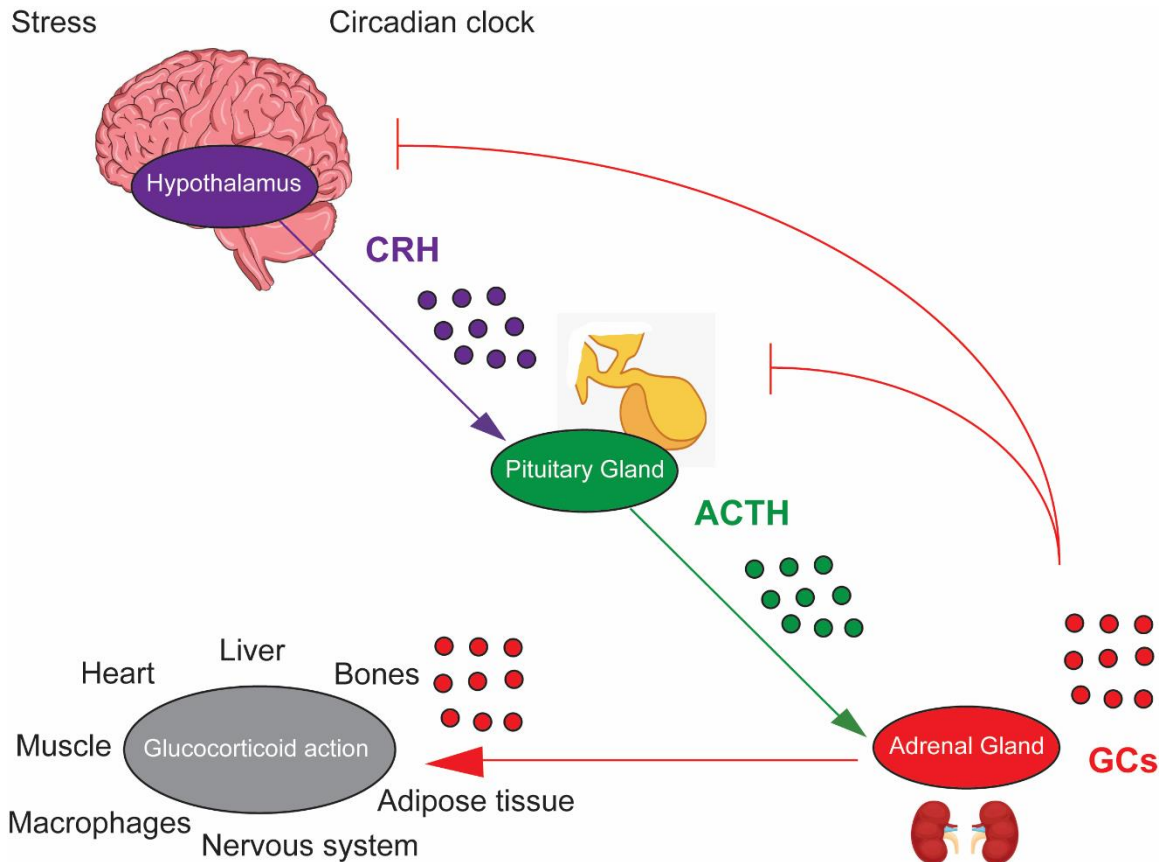
Figure 3: The diurnal secretion of glucocorticoids by the hypothalamus-pituitary-adrenal axis.

Stress or diurnal rhythms trigger the hypothalamus to secrete corticotropin releasing hormone (CRH), which will signal the pituitary gland to secrete adrenocorticotropic hormone (ACTH). Then, ACTH signals the adrenal glands to secrete glucocorticoids (GCs). GCs regulate in a negative feedback loop the secretion of CRH and ACTH. In the same time, GCs activate various processes in metabolic organs, such as gluconeogenesis (liver), fat accumulation (adipose), muscle wasting (muscle). Image adapted from (Oakley & Cidlowski, 2011, 2013). Individual pictures taken from Servier Medical Art (https://smart.servier.com/).

Mechanistically, the binding of glucocorticoids releases GR from the heat shock proteins 70 and 90 (HSP70 and HSP90) in the cytoplasm, and then GR is translocated into the nucleus (Pratt & Toft, 1997). Inside the nucleus, it recognizes as homodimer the canonical binding sites, which are called glucocorticoid response elements (GREs). GREs are two 6bp palindromic sequences with a 3bp spacer, having the consensus 5'-AGAACAnnnTGTTCT-3' (Escoter-Torres et al., 2019; Greulich et al., 2016; H.-W. Lim et al., 2015; Oakley & Cidlowski, 2011; Starick et al., 2015). GR can bind differential motifs,

based on the neighboring transcription factors providing different modes of gene regulation. Beyond the classical GREs, GR can bind to other DNA-bound TFs via protein-protein interactions, which are called "composite elements" (Escoter-Torres et al., 2019; Greulich et al., 2016; H.-W. Lim et al., 2015; Oakley & Cidlowski, 2011; Starick et al., 2015). The composite elements are a combination of GREs and other transcription factor motifs, which are in close proximity (**Figure 4**) (Glass & Saijo, 2010; Langlais et al., 2012).
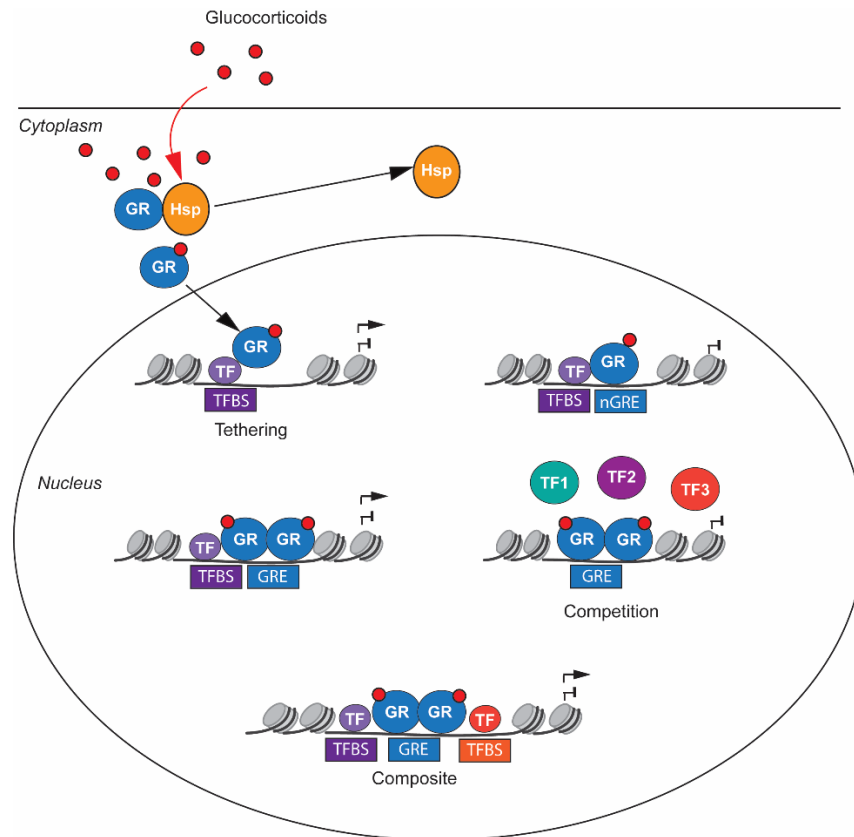
Figure 4: All the proposed models for glucocorticoid receptor as a transcription factor.

Upon ligand (GCs) binding, the glucocorticoid receptor (GR) is released by the heat shock proteins (Hsp) and translocates to the nucleus. Different mechanisms have been proposed GR actions in both inflammation and metabolism, i.e., binding to Glucocorticoid Response Elements (GREs), to negative GREs (nGREs), to composite GREs together with other transcription factors (TF), by tethering to DNA-bound transcription factors, and by competing with other transcription factors for DNA-binding sites and by non-genomic actions (Escoter-Torres et al., 2019). TFBS: Transcription Factor Binding Site.

The human GR (hGR) is encoded by the *NR3C1* gene, is located on chromosome 5q31-32, and contains nine exons and through alternative splicing and alternative initiation of

translation gives multiple isoforms (N. Z. Lu & Cidlowski, 2006). At the protein level, GR has three distinct domains, the N-terminal transactivation domain (NTD), the DNA-binding domain (DBD), and the C-terminal ligand-binding domain (LBD) (**Figure 5**) (Oakley & Cidlowski, 2011, 2013). Inside the DBD, two zinc finger motifs are necessary for the recognition and binding of GREs. Moreover, the second zinc finger has a stretch of amino acids, the D-loop, giving the possibility of GR homodimerization. Between the DBD and LBD, there is a flexible region called "hinge region" (H). In the N terminal, NTD houses a strong transcriptional activation function domain (AF1), necessary for the interaction with the basal transcriptional machinery and multiple co-regulators (Oakley & Cidlowski, 2011, 2013). In the C-terminal, LBD houses a second activation function domain (AF2), which interacts with co-activators and co-repressors (Oakley & Cidlowski, 2011, 2013). Lastly, two nuclear localization signal sequences and the dimerization domain are located at the junction of DBD/hinge region and within the LBD ensuring the efficient transport and dimerization of the protein respectively (Dahlman-Wright et al., 1991; Kumar & Thompson, 2005). Between human and mouse GR proteins, there is roughly 88% homology with conservation of most of the residues and phosphorylation sites (Almlöf et al., 1995). These phosphorylations are mediated by kinases such as glycogen synthase kinase-3 (GSK-3), mitogen-activated protein kinases (MAPK), cyclin-dependent kinases (CDK) and c-Jun N-terminal kinases (JNK) (Almlöf et al., 1995; Itoh et al., 2002; Krstic et al., 1997; Rogatsky et al., 1998).
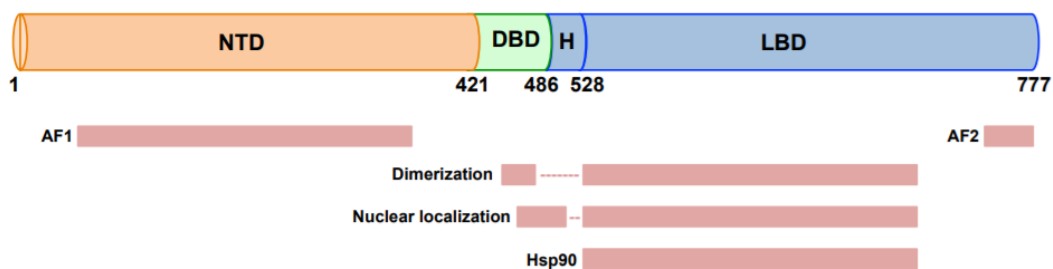
Figure 5: Schematic representation of the structural domains of glucocorticoid receptor.

The glucocorticoid receptor is composed of 4 different structural domains: the N-terminal (NTD), the DNA-binding domain (DBD), the hinge region (H), and the ligand-binding domain (LBD). The red underlined regions are responsible for transcriptional activation (AF1 and AF2), dimerization, nuclear localization, and interaction with the chaperone Hsp90 (heat-shock protein 90). Numbers indicate the amino acids of the human GR. Picture adapted from (Oakley & Cidlowski, 2013).

1.2.2 Hepatic gene regulation by glucocorticoid receptor

In mice, the full body deletion of GR leads to lethality of the pups due to respiratory defects (Cole et al., 1995). Generally, GR regulates basic functions in every metabolic organ, but also shows tissue-specific properties. In the case of hepatic-specific deletion, the mice present various metabolic abnormalities, such as dyslipidemia, bile acid (BA) accumulation and defects in glucose production (Cole et al., 1995; Oakley & Cidlowski, 2013). For energy homeostasis, GR regulates significant genes for the interplay between the lipid uptake/synthesis and gluconeogenesis (Præstholm et al., 2020; Quagliarini et al., 2019). Disruption of glucocorticoid receptor leads to de-repression of lipid uptake and synthesis genes (such as *Cd36* and *Fasn*) and reduction of glucose production due to absence of activated gluconeogenic genes (such as *Pck1* and *G6Pase*) (Lemke et al., 2008; Opherk et al., 2004; Præstholm et al., 2020; Quagliarini et al., 2019). Additionally, hepatic GR is responsible for the activation of the gluconeogenic gene *Gck*, which expresses the rate-limiting enzyme for the glucose uptake and phosphorylation (Præstholm et al., 2021). For this reason, GR liver-specific knockout mice show increased triglyceride and lipid accumulation, being prone to develop hepatic steatosis. In the case of BA homeostasis, GR up-regulates the entero-hepatic BA transporter *Ntcp*, binding to its promoter (Rose et al., 2011). Additional studies showed that hepatic GR increases the expression of bile acid synthesis enzymes (such as *Cyp7a1* and *Cyp27a1*) and modulates bile acid transporters in the crosstalk with FXR (such as *Oatp* and *Btep*) (Jenniskens et al., 2018; Y. Lu et al., 2012; Rosales et al., 2013; Rose et al., 2011). Surprisingly, glucocorticoids in combination with glucagon act as fasting hormones for the induction of the amino acid catabolism by GR/CREB crosstalk both in liver and muscle in order to support hepatic gluconeogenesis (Korenfeld et al., 2021; Kuo et al., 2013). Moreover, the hepatic GR presents a rhythmic binding to chromatin (Quagliarini et al., 2019). It seems that a great number of diurnally oscillating transcripts are regulated by the hepatic GR (Quagliarini et al., 2019). We found in our lab that, upon high-fat diet, glucose and triglyceride homeostasis are boosted by the time-dependent augmented GR binding, increasing its amplitude (Quagliarini et al., 2019). Pharmacological activation of GR by dexamethasone (a synthetic GC) leads to amplified transcriptional responses (Quagliarini et al., 2019). This fact proves the development of hepatic steatosis by the GR over-activation and increased chromatin binding (Quagliarini et al., 2019). So, either reduced

or increased GR activity can have detrimental effects in hepatic homeostasis pointing out its significance.

Genomic data have revealed many aspects of GR function tightly connected to the physiology (Greulich et al., 2016; Præstholm et al., 2020). Based on genomic studies, GR ChIP peaks have in their proximity classical hepatic-specific motifs, such as HNF4α, C/EBP, FOX, PPAR/RXR, HNF6, STAT and E2A motifs (Præstholm et al., 2020, 2021a; Quagliarini et al., 2019). Usually, HNF4α and HNF6 are essential hepatic transcription factors for every developmental liver stage (Clotman et al., 2002; Duncan, 2000). Their absence leads to defects in the liver bud development (Margagliotti et al., 2007; Parviz et al., 2003). Recent genomic data (ChIP-seq and ATAC-seq) revealed that absence of HNF4α remodels the hepatic GR cistrome with gain and loss of GR binding sites (Hunter et al., 2021). Hepatic C/EBPβ plays role in the remodeling of the hepatic GR binding profile, since is associated with chromatin accessibility and 62% co-occupancy with the GR sites (Grøntved et al., 2013). It is also expected the appearance of PPAR/RXR motifs because PPARα interacts with GR for modulation of genes from feeding to fasting (Ratman et al., 2016). Mild fasting leads to antagonistic interaction between GR and PPARα for trans-repression of genes, while prolonged fasting leads to p-AMPK recruitment and their synergistic interaction for the activation of fatty acid oxidation genes (Ratman et al., 2016). Moreover, FOXA factors act as pioneers in order to open the chromatin and keep the nucleosome accessible for other transcription factors (Iwafuchi-Doi et al., 2016; Z. Li et al., 2011). Especially, for FOX motifs, it is known that GR interacts with FOXO1 for the activation of the *Angptl4* and *Pepck* promoters upon dexamethasone treatment (Cournarie et al., 1999; Kuo et al., 2014). In the case of *Pepck* promoter, is known that LXR agonists downregulate by part hepatic gluconeogenesis by suppressing GR (Liu et al., 2006). Additionally, E47 is another GR-copartner, which in association with FOXO1 activate gluconeogenic genes (Hemmer et al., 2019). Upon fasting, increased GR signaling can lead to tighter coordination between GR, FOXO1, and E47 (Hemmer et al., 2019). The ablation of E47 can benefit liver from the chronic GCs' effect pointing another suspicious candidate of GR action (Hemmer et al., 2019). In contrast to fasting, high fat diet gave enrichment of STAT motifs in the GR cistrome (Quagliarini et al., 2019). Unraveling that STAT5 can act as another GR co-partner enhances the role of the latter in circadian rhythmicity and boosts the GR chromatin binding (Quagliarini et al., 2019). In normal conditions, REVERBα promotes the hepatic GR recruitment to the chromatin

during the day affecting the circadian GC sensitivity (Caratti et al., 2018). Conclusively, GR based on the interacting co-partner can impact differently on the genome.

1.2.3 Glucocorticoids and caloric restriction conundrum

Chronic exposure to glucocorticoids in both human and mice can lead in various defects in the body, such as cognitive impairment, hippocampal atrophy, defects in the long-term potentiation (LTP) obesity, osteoporosis, diabetes, and heart abnormalities (Escoter-Torres et al., 2019; R. Patel et al., 2002). CR, due to the reduced calories, leads to the 'caloric stress' boosting the secretion of glucocorticoids in both human (cortisol) and rodents (corticosterone) (Gredilla & Barja, 2005; R. Patel et al., 2002; Sabatino et al., 1991). A long-term increased secretion of glucocorticoids can promote many detrimental effects (Greulich et al., 2016; Vegiopoulos & Herzig, 2007). However, studies in CR have shown a neuronal and metabolic protection from the oversecreted glucocorticoids (Gredilla & Barja, 2005; Patel & Finch, 2002; R. Patel et al., 2002). Not only CR protects from all these abnormalities, but also provides anti-aging role in the physiology extending the lifespan in many model organisms (Cantó & Auwerx, 2009; Gredilla & Barja, 2005; Madeo et al., 2019; Mattison et al., 2017). For these reasons, these opposing effects constitutes a conundrum between the chronic exposure to caloric restriction and the chronic effects of glucocorticoids. Understanding the role of glucocorticoids upon CR can give new insights how to boost metabolism and if it is feasible to manipulate the same pathways in order to have the same positive effects of caloric restriction. It still remains enigmatic though glucocorticoids in one case can lead to detrimental effects while on the other side can potentially protect from metabolic abnormalities (Gredilla & Barja, 2005; R. Patel et al., 2002; Sabatino et al., 1991).

1.3 Insulin signaling and the Forkhead-box protein family

1.3.1 Insulin-related pathways in hepatic homeostasis

In the postprandial state, insulin remotes the transition from glucose production to synthesis and storage of lipids and glycogen in the liver (Titchenell et al., 2016). For promoting *de novo* lipogenesis, insulin represses fatty acid oxidation, favoring the triglyceride esterification and secretion (Leavens & Birnbaum, 2011). This is achieved

through binding to insulin receptor, which is a receptor tyrosine kinase (RTK), and activating the PI3K/PIP2/PIP3/PDK1/AKT (phospho-inositol-3 kinase) cascade signaling (Taniguchi et al., 2006). This activated signaling leads to the phosphorylation of the predominant FOXO1 factor (**Figure 6**). The FOXO1 cytoplasmic sequestration leads to repression of gluconeogenenic genes, such as *G6pc* and *Pck1* (Wu et al., 2018). At the same time, *Gck* is derepressed boosting glycolysis and SREBP1 binding to lipid related genes promotes the uptake and storage of lipids. SREBPs are ubiquitously expressed transcription factors that promote the synthesis of triglycerides, fatty acids, and cholesterol (Horton et al., 2002). Activation of SREBP1 is accomplished by mTORC1 (Porstmann et al., 2008). In parallel, AKT kinase activates GSK3-dependent and independent pathways of glycogen synthesis (Porstmann et al., 2008). It is remarkable that insulin receptor by itself can translocate to the nucleus and in association with the Host Cell Factor 1 (HCF-1) can bind to the promoter regions of the genes (Hancock et al., 2019). Finally, insulin receptor interacts with HCF1 and RNA polymerase II for the up-regulation of lipid homeostatic genes and boosts the protein synthesis of downstream effectors of the whole insulin pathway (Hancock et al., 2019).
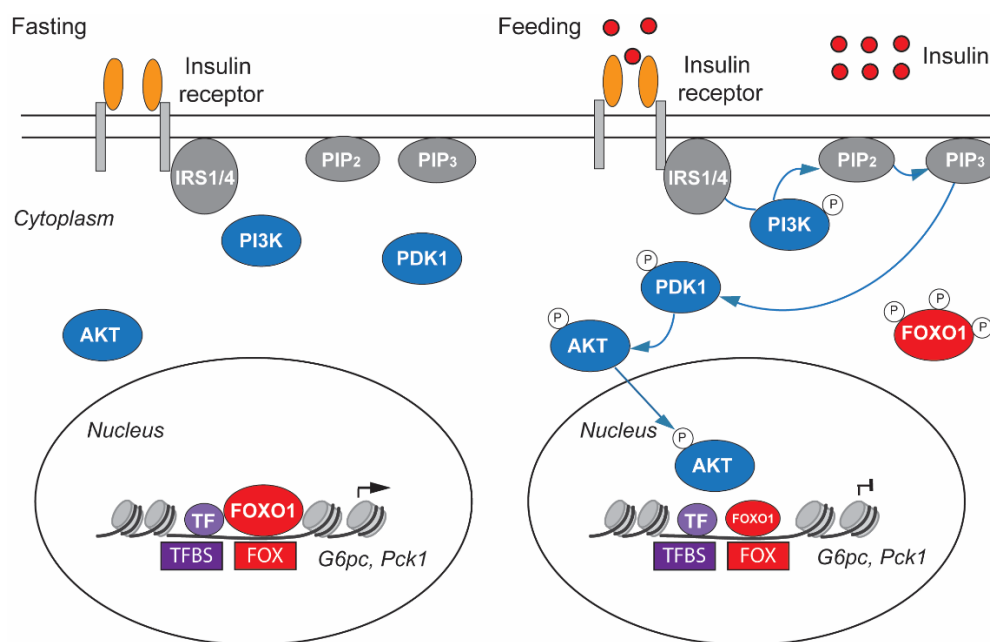
Figure 6: Insulin modulates FOXO1 signaling from fasting to feeding.

Fasting or absence of insulin signaling does not activate PI3K/AKT/PDK1/AKT signaling. In the case of feeding, insulin binds to insulin receptor and activates PI3K/AKT/PDK1/AKT signaling, which phosphorylates FOXO1 and leads to its cytoplasmic sequestration.

1.3.2 The Forkhead-box family: function and physiological outcome

The Forkhead-box family contains a great variety of conserved factors, implicated in many processes, such as cell cycle, senescence, proliferation, metabolism, maintenance and/or cancer progression, and development. This family contains a highly evolutionary conserved forkhead or winged-helix DNA-binding domain (DBD). The founding member of this family was established in the fruitfly *Droshophila melanogaster*, carrying a mutation in the homeotic gene *forkhead* (*fkh*) with ectopic head structures in the embryos (Kaufmann & Knöchel, 1996; Weigel et al., 1989). In various cases, homozygous mutations in Fox genes can lead to embryonic or perinatal lethality. Especially in humans, mutations affecting the regulation of Fox genes are linked with many developmental disorders and diseases, such as cancer, Parkinson's disease, autism spectrum disorder, ocular abnormalities, immune system deregulation, neurological deficiencies, and metabolic abnormalities (Golson & Kaestner, 2016; Zhu, 2016). A great number of members has captivated scientific attention because their role in development and disease is critical for opening new therapeutic avenues.

Focusing on mammals, Forkhead-box factors are categorized into subclasses from A to S. Their classification is based on their sequence similarity inside and outside the Forkhead-box domain. All Forkhead members share this highly conserved FOX-DBD of around 100 amino residues. Structurally, this protein domain consists of three N-terminal α-helices, three β-strands and two loops, shaping butterfly wings or a "winged helix" (Clark et al., 1993). The presence of this domain permits the recognition of the core sequence (5' – (G/A) (T/C) (A/C) AA (C/T) A-3'), which is located on the promoter regions of target genes (Biggs III & Cavenee Karen C., 2001). The wings of the FOX-DBD regulate the DNA binding specificity and affinity (Obsil & Obsilova, 2011).

Despite the similarity in DNA sequence of the Forkhead box domain, Fox factors show differential affinities for the DNA-binding motif. These differences come from the divergent sequences outside of the DNA-binding domain, which define spatial and temporal changes. Structurally among the Fox members, there are various other domains, such as the transactivation domain (TAD), the nuclear localization sequence (NLS) and the nuclear export sequence (NES) (**Figure 7**) (Biggs III & Cavenee Karen C., 2001; Golson & Kaestner, 2016). In opposition to the DBD, all these domains show poor conservation. Until now, different members have shown structural peculiarities pointing out their specific functions. A characteristic example is FoxA members which structurally mimic the linker

histones H1 and H5, giving them access to compacted chromatin. This unique identity allows them nucleosome repositioning and gives the opportunity for other transcription factors to recognize their DNA-binding motifs. Members of the FoxA subfamily are mentioned also with the term "pioneer factors". Their role as pioneer factors is necessary for the DNA binding of many nuclear receptors, such as androgen receptor (AR), glucocorticoid receptor (GR), and estrogen receptor. Among them, it is also found that FoxAs and FoxOs members interact with the SWI/SNF chromatin remodeling complex. Until now, FoxAs, FoxOs, FoxMs, and FoxKs are the most well-studied Fox members for their implication in cancer and metabolism (Golson & Kaestner, 2016; Obsil & Obsilova, 2011).
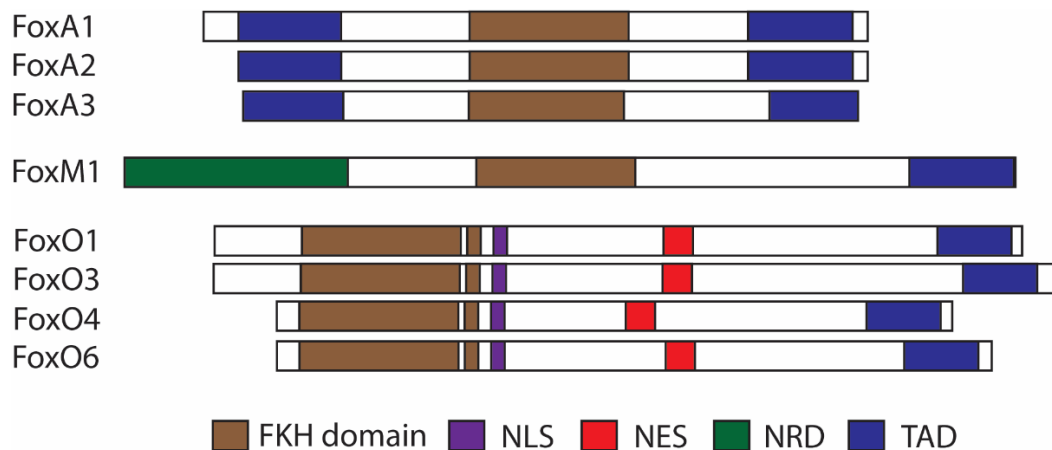
Figure 7: The protein structure of representative Fox members.

The topology of protein domains for the selected mouse Fox members, which are responsible for DNA binding, interaction with other transcription factors and nuclear localization. FKH, forkhead domain; TAD, transactivation domain; NRD, N-terminal repressor domain; NLS, nuclear localization signal; NES, nuclear export signal. Picture adapted from (Golson & Kaestner, 2016).

Among the Forkhead members, FOXOs (FOXO1, FOXO3, and FOXO4) are important transcription factors for the regulation of energy metabolism in liver (Kousteni, 2012). Their role is implicated in processes such as autophagy/mitophagy, gluconeogenesis, lipid homeostasis, stress-resistance, cancer, and cell death (Calnan & Brunet, 2008; Kousteni, 2012; Rui, 2014). They show protective role for the hepatic homeostasis and are responsible for metabolic diseases, such as diabetes, fatty liver disease, metabolic syndrome, and obesity (Golson & Kaestner, 2016). Consequently, describing their structural behavior is an increased interest in order to design novel drugs.

All the FOXO members are modulated by the insulin, insulin-like growth factors and growth factors (Brunet et al., 1999; Guo et al., 1999; Jackson et al., 2000; Lin et al., 1997; Medema et al., 2000; Ogg et al., 1997; Zheng et al., 2002). Upon lack of nutrients, such as caloric restriction or fasting, they are active and subsequently bind to their motif. After feeding or growth factor stimulation, activation of PI3K/AKT or SGK (serum and glucocorticoid-induced) kinase leads to their phosphorylation and inevitably to their cytoplasmic retention (Alessi et al., 1996). Phosphorylation of three conserved phosphorylation sites promotes their binding to the chaperone 14-3-3 and their nuclear exclusion. Afterwards, they are poly-ubiquitinated and destined to the proteasome for degradation. Furthermore, acetylation by CBP/EP300 reduces their transcriptional activity and structurally are more susceptible to phosphorylation (Wondisford et al., 2014). Acetylation and phosphorylation negatively regulate the transcriptional activity and nuclear residency of FOXO factors, reducing the gluconeogenesis induction (Liu et al., 2008). In short-term fasting, acetylation of CRTC2 by EP300 increases its activity for inducing gluconeogenesis and at the same time promoting its degradation (Liu et al., 2008). In the case of prolonged fasting, FOXO1 is de-acetylated by SIRT1 and becomes more active in order to reassure the induction of gluconeogenesis and compensate the CRTC2 downregulation (Liu et al., 2008). Conclusively, FOXOs can potentially regulate different genes based on their post-translational modifications.

FOXO factors are significant mediators of energy metabolism in mouse liver. Hepatic ablation of FOXO1 leads to decreased gluconeogenesis and glycogenolysis in fasted mice, causing hypoglycemia (Matsumoto et al., 2007). Triple hepatic FOXO (FOXO1, -3, and -4) ablation caused more severe hypoglycemia and significantly improved glucose tolerance compared to the single FOXO knockout mice (Haeusler et al., 2010; K. Zhang et al., 2012). In the same time, triple knockout mice showed enhanced insulin sensitivity accompanied by reduced plasma insulin levels (Haeusler et al., 2010; K. Zhang et al., 2012). Beyond glucose levels, hepatic FOXO1/3 and FOXO1/3/4 inactivation in mice caused elevated circulating triglyceride and cholesterol levels (K. Zhang et al., 2012). Total cholesterol content and high-density lipoprotein (HDL)- and VLDL/low-density lipoprotein (LDL)-associated cholesterol were also increased while mice were prone to develop mild hepatic steatosis (K. Zhang et al., 2012). It seems that FOXO1 and FOXO3 have overlapping roles, by up-regulating gluconeogenic genes, such as *Pck1* and *G6pc*, while they can repress lipogenic-related genes, such as *Hmgcr* and *Fasn* (Haeusler et al., 2010; K. Zhang et al., 2012). To summarize, mainly FOXO1 and FOXO3 regulate

transcriptionally the balance between glucose production and lipid homeostasis in the liver (Haeusler et al., 2010; K. Zhang et al., 2012).

1.3.3 FOXO's (FOXO1 & FOXO3) action in the genomic neighborhood

Genome-wide binding profiles for FOXO1 and FOXO3 have defined their target-genes. All the existed non-hepatic FOXO's (mouse/human FOXO1 & FOXO3 data) ChIP-seq showed that these factors bind to genes, related to metabolism/insulin signaling, cellular stress, DNA repair, apoptosis, proteostasis and cell cycle (Webb et al., 2016). There was conservation among the different species within the 200bp of all FOXO ChIP peaks, with Forkhead, ETS, CTCF, bHLH and CTF motifs enriched in mice (Webb et al., 2016). In the case of liver, FOXO1 ChIP-seq in fasted mice at ZT14 (Zeitgeber 14; 8 p.m.) showed roughly 8000 unique peaks, which were located mainly on distal elements (Kalvisa et al., 2018). Gene ontology of the nearest genes in FOXO1 ChIP-seq presented glucose-, fatty acid-, carbohydrate-, steroid- and lipid-related homeostatic genes. HOMER motif analysis showed enriched HNF4α, ERRα, CEBPβ, and GR motifs around the 250bp up- and down-stream of the FOXO1 peaks (Kalvisa et al., 2018; Shin et al., 2012). According to the fasting-feeding cycle, FOXO1 presents co-occupancy with GR in more than 60% of its sites, while significantly small overlap with CREB (Kalvisa et al., 2018). Characteristic example of gluconeogenic genes, such as *Fasn* and *Gck*, were less expressed in the unfed mice over the fed mice (Kalvisa et al., 2018). Similarly, fasting-dependent genes such as *Pck1* and *Angptl4*, were highly expressed in the unfed condition (Kalvisa et al., 2018). Between the unfed and fed conditions at ZT14, Kalvisa et al., clustered the deregulated genes into 5 different groups, based on the expression levels. In parallel, perturbed feeding behavior in obese mice revealed a specific gene behavior because insulin resistance can activate transcription factors, such as PPARα, which may contribute to the altered expression levels of genes, such as *G6pc*, *Angptl4*, and *Insig2* (Kalvisa et al., 2018). Consequently, it seems that pre-prandially FOXO1 binds with GR to distal active enhancers of feeding-related genes, since there are more robust H3K27ac ChIP peaks. Feeding causes the reduced FOXO1/GR chromatin occupancy and repression of these genes which may vary from the response to the insulin signaling in combination with glucocorticoids (Kalvisa et al., 2018). Finally, FOXO1 acetylation by the enhanced binding of ETS1 with CBP reduces FOXO1 chromatin occupancy in gluconeogenic genes after feeding (K. Li et al., 2019).

1.4 The role of SIN3A complex in hepatic homeostasis

1.4.1 Structure and role of SIN3A complex in repression

SIN3 complex is a universal corepressor of transcription from yeast to mammals and it was first introduced from genetic screens in budding yeast as *Sin3* (Silverstein & Ekwall, 2005a; Sternberg et al., 1987). In mammals, they exist in two highly conserved isoforms, SIN3A and SIN3B, although the latter has a shorter amino N terminal region (Halleck et al., 1995a). SIN3A mainly acts as a scaffold protein for the recruitment of histone deacetylases (HDACs) causing transcriptional repression (Laherty et al., 1997). To mediate repression, SIN3A uses protein-mediated interactions since it does not contain a DNA binding domain (Y. Zhang et al., 1997). It is a large acidic protein of 1274 amino acids containing four paired amphipathic α-helices (PAH1-PAH4) (Silverstein & Ekwall, 2005). Each PAH domain contains two helices separated by a 20 amino acid spacer and present high similarity between yeast and mice(Ayer et al., 1995; Halleck et al., 1995). In addition to the PAH domain, SIN3A contains a histone interaction domain (HID) and a sixth highly conserved domain (HCR) (**Figure 8A**). Structural evidence and assays for SIN3A originated from the yeast homologue *Sin3* (Silverstein & Ekwall, 2005).

Mouse SIN3A is part of a multimeric complex, containing other eight components in mammals: HDAC1, HDAC2, RbAp46/RBBP7, RbAp48/RBBP4, SAP30, SAP18, SAP130 and SUDS3 (Hassig et al., 1997; Laherty et al., 1997; Y. Zhang et al., 1997). The SIN3A part adds multiple interactions providing extra functions to the core complex. Some of these interactions are nucleosome-remodeling enzymes, N-acetyltransferases and DNA methyltransferases (Silverstein & Ekwall, 2005). The remaining components have stabilizing role (**Figure 8B**). One of the first indicative work for mSIN3A/HDAC1, was the interaction with the SMRT/NCOR complex, repressing the RXR/RAR and RXR/TR heterodimers (Nagy et al., 1997). Simply tethering of this complex in the vicinity of gene promoters is sufficient for transcriptional repression (H. Wang & Stillman, 1993). Moreover, mSIN3A can interact and block the TFIIB (Transcription factor II B of the RNA polymerase II preinitiation complex) *in vitro* repressing the basal transcriptional machinery (Wong & Privalsky, 1998). Another aspect of SIN3A is the perpetuation of heterochromatic silencing in both centromeres and rDNA. In order to perform compaction, SIN3A interacts with MeCP2, which methylates CpG dinucleotides (Nan et al., 1998). In hepatic circadian biology, mSIN3A interacts with PSF of PER complex for transcriptional inhibition of BMAL-

CLOCK machinery, repressing *Per1* promoter (Duong et al., 2011). Finally, the yeast homologue Sin3 is implicated in deacetylation of H4K16 in response to double strand breaks (DSBs) and tuning the pre-replication complex early in G1 phase underpinning its role in genome stability (Aparicio et al., 2004).
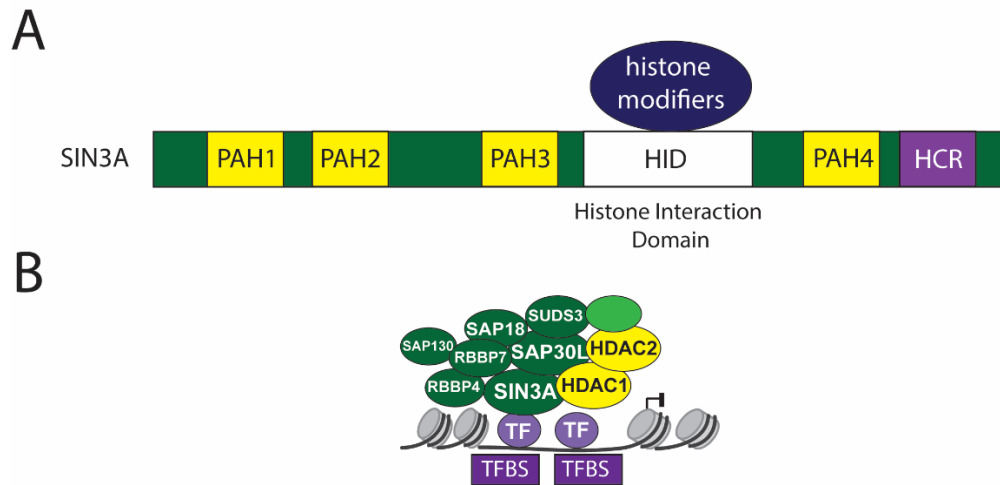
Figure 8: Structure and core interaction partners of SIN3A.

A: Structure of SIN3A catalytic subunit, which contains four PAH (amphipathic helix) domains, the HCR (highly conserved domain) and the HID (Histone Interaction Domain). **B:** The main SIN3A-HDAC complex has the SIN3A, SUDS3, SAP30L, RBBP4, RBBP7, SAP18, HDAC1, HDAC2 subunits. TF: Transcription Factor, TFBS: Transcription Factor Binding Site.

1.4.2 SIN3A as a FOXO1-corepressor complex

The SIN3A complex is crucial for the maintenance of chromatin remodeling and epigenetic regulation in the full SIN3A KO embryos, affecting the lung buds when is missing at the late developmental mouse stages (Yao et al., 2017). Deletion of SIN3A from the liver leads to hypoglycemia, retardation growth, reduced fat mass and increased glucose and pyruvate tolerance (Langlet et al., 2017). The liver-specific SIN3A knock-out mice present cholestasis, with elevated plasma aspartate transaminase (AST), alanine transaminase (ALT), alkaline phosphatase, triglycerides, bile acids and bilirubin, causing hepatomegaly and fibrosis (Langlet et al., 2017). These hepatic abnormalities showed that SIN3A affects the interplay between glucose production and lipid homeostasis. Further investigation showed that SIN3A is a FOXO1 corepressor, blunting the activation of *Gck*, which is the rate-limiting enzyme of glucose production, when FOXO1 binds upon insulin and dexamethasone stimulation (Langlet et al., 2017). More specifically, SIN3A interacts with

the N-terminal domain of FOXO1 (Langlet et al., 2017). Another study showed that SIN3A in association with COREST complex interacts with FOXO1 in the hypothalamus recapitulating its function as a FOXO1 corepressor (Zullo et al., 2019). Pharmacological manipulation of FOXO1 mimicking SIN3A interactions can lead to manipulation of the hepatic glucose production and lipid homeostasis treating various metabolic diseases, such as diabetes and obesity.

2. Scope of the thesis

Past years revealed that caloric restriction has protective role against many metabolic abnormalities and favors many beneficial pathways, which have opposing effect with the chronic exposure to glucocorticoids. Chromatin immunoprecipitation coupled with mass spectrometry (ChIP-MS) for GR in mouse livers identified one of the main modulators of caloric restriction, FOXO1 and its corepressor, SIN3A.

The underlying hypothesis of this PhD thesis was that GR is necessary for the hepatic adaptation to the caloric restriction and that FOXO1 and SIN3A acting as potential copartners to this metabolic adaptation. Three specific aims are detailed as follows:

1. ***Defining the genome-wide binding profile of GR, FOXO1 and SIN3A and their transcriptional targets in caloric restriction***

Caloric restriction regimen protocol was performed in wild type mice around the circadian clock for characterizing the profile of glucocorticoids and insulin levels. ChIP-sequencing was performed to define the genome-wide binding profiles for GR, FOXO1 and SIN3A in caloric restriction at the peak of corticosterone levels. Gene ontology annotations of co-bound regions showed functional pathways related with glucose and lipid homeostasis, commonly affected by the three factors. At the same time, RNA-seq in *ad-libitum* and caloric restricted WT mice, contributed to find the targets which are induced and repressed by this nutritional challenge.

2. ***Loss of hepatic glucocorticoid receptor in caloric restriction deregulates transcriptionally the molecular clock, autophagy and lipid homeostasis***

Based on previous studies, caloric restriction regimen can enhance the function of the molecular clock in the liver. This feeding-fasting imposed behavior can entrain the hepatic circadian rhythms. For this reason, validation of the main circadian factors in expression levels was necessary for checking the functionality of the clock. Moreover, processes enriched in caloric restriction such as autophagy, energy production and lipid species were transcriptionally deregulated in the absence of GR. RNA-seq analysis before and after

feeding in caloric restricted wild type vs GR liver specific knockout mice (GR-LKO) shows the importance of GR in energy cycling and utilization, autophagy and lipid homeostasis.

3. *Hepatic glucocorticoid receptor is necessary for the effects of caloric restriction*

Caloric restriction regimen protocol was performed in GR liver specific knockout (GR-LKO) mice and their WT control littermates. Metabolic phenotyping of the caloric restricted WT and GR-LKO mice and testing of their glycogen liver storage capacity and secreted lipoprotein profile were examined. Additionally, metabolic cages were used for assessing the energy status of the caloric restricted WT versus GR-LKO mice.

3 Material and Methods

3.1 Chemicals, commercial kits, antibodies and primers

Table 1. List of chemicals and reagents.

Chemical/reagent	Provider
Agarose	VWR Chemicals
Bovine serum albumin	Sigma Aldrich
Bradford	Carl Roth GmbH
Charcoal-stripped FBS	Life Technologies GmbH
Chelex	Sigma Aldrich
Complete Mini protease inhibitor	Roche Applied Science
D-(+)-Glucose solution	Sigma Aldrich
Dexamethasone	Sigma Aldrich
Dithiothreitol	Serva Electrophoresis GmbH
DMEM (high glucose) cell culture medium	Sigma Aldrich
DMEM (phenol red-free) cell culture medium	Life Technologies GmbH
dNTP	Thermo Fisher Scientific GmbH
Dynabeads M-280 sheep anti-rabbit IgG-10	Life Technologies GmbH
EDTA	G-Biosciences
Eosin Y	Sigma Aldrich
Ethanol	AppliChem GmbH
Eukitt quick hardening mounting medium	Sigma Aldrich
Fetal bovine serum	Sigma Aldrich
Formaldehyde (w/v)	Thermo Fisher Scientific GmbH
Fugene HD transfection reagent	Promega
Glycerol	Carl Roth GmbH
Glycine	Sigma Aldrich
GoTaq Green DNA Polymerase	Promega
Hematoxylin Gill no.3	Sigma Aldrich
HEPES buffer	Carl Roth GmbH
Igepal (NP-40)	Sigma Aldrich
Igepal (NP-40)	Sigma Aldrich
Isopropyl alcohol	Merck Millipore
Magnesium chloride	Carl Roth GmbH
Methanol	Sigma Aldrich
Milk powder	Carl Roth GmbH
Opti-MEM reduced serum medium	Life Technologies GmbH
Paraformaldehyde	Sigma Aldrich
Penicilin/Streptomycin	Sigma Aldrich
Phosphatase inhibitor	Thermo Fisher Scientific GmbH
Phosphate-buffered saline (PBS)	Thermo Fisher Scientific GmbH

Physiological saline (0.9%)	B-Braun group	
Potassium chloride	Carl Roth GmbH	
Potassium hydroxide	Carl Roth GmbH	
Power SYBR Green Master mix	Thermo Fisher Scientific GmbH	
Protein G-coupled Dynabeads	Life Technologies GmbH	
Proteinase K	Sigma Aldrich	
Rnase A (Dnase-free)	AppliChem GmbH	
Roti-Mount Aqua mounting medium	Carl Roth GmbH	
Schiff's reagent intense	Merck Millipore	
Sepharose A/G beads	Biomol GmbH	
Sodium chloride	Sigma Aldrich	
Sodium dodecyl sulfate (20%)	Sigma Aldrich	
Sodium pyruvate	Sigma Aldrich	
Sucrose	Carl Roth GmbH	
Triton-X	AppliChem GmbH	
Trypsin (0.25%) EDTA	Sigma Aldrich	
Tween-20	AppliChem GmbH	
Xylene	AppliChem GmbH	

Table 2. List of commercial kits and reagents.

Product	Provider	Reference Nº
Ambion DNase Treatment and Removal Kit	Thermo Fischer Scientific	AM2295
BCA reagent	Thermo Fischer Scientific	23228
Bradford reagent	Biorad	500-0205
DNA Maxi Plasmid kit	Qiagen	12965
DNA plasmid plus maxi	Qiagen	12963
Dual-Glo, Luciferase assay	Promega	E2940
High Sensitivity DNA Kit	Agilent Technologies	5067-4626
HindIII restriction enzyme	NEB	R3104
KAPA HyperPrep kit (96rnxs)	Roche	7962363001
KAPA Library Quantification kit (Illumina/ROX)	Roche	7960336001
MinElute PCR purification kit	Qiagen	28006
Mouse Corticosterone ELISA kit	Enzo Life Sciences	ADI-900-097
QIAquick gel extraction kit	Qiagen	28706
QuantiTect reverse transcription kit	Qiagen	205314
Qubit dsDNA HS kit	Thermo Fisher Scientific	Q32854
RNA 6000 Nano reagents	Agilent Technologies	5067-1511
RNeasy micro kit (low input)	Qiagen	74004
RNeasy mini kit	Qiagen	74106
Ulltrasensitive Mouse Insulin ELISA kit	Crystal Chem	90080

XhoI restriction enzyme	NEB		R0146-S

Table 3. List of primary and secondary antibodies.

Antibody*	Source	Method**	Identifier
AKT (R)	Cell Signaling Technology	WB (1:1000)	Cat#4961
AKT (pS473) (R)	Cell Signaling Technology	WB (1:1000)	Cat#4060
ATG16L1 (D6D5) (R)	Cell Signaling Technology	WB (1:1000)	Cat#8089
ATG3 (R)	Cell Signaling Technology	WB (1:1000)	Cat#3415
ATG5 (D5F5U) (R)	Cell Signaling Technology	WB (1:1000)	Cat#12994
ATG7 (D12B11) (R)	Cell Signaling Technology	WB (1:1000)	Cat#8558
BECLIN1 (D40C5) (R)	Cell Signaling Technology	WB (1:1000)	Cat#3495
FOXO1/FOXO3 (pT24/pT32) (R)	Cell Signaling Technology	WB (1:1000)	Cat#9464
FOXO1A (pS256) (R)	Cell Signaling Technology	WB (1:1000)	Cat#9461S
FOXO1A (R)	Abcam	WB (1:1000), ChIP-seq & ChIP-qPCR	Cat#ab39670
FOXO1A (R)	ProteinTech Group	ChIP-seq & ChIP-qPCR	Cat#18592-1-AP
GR (G-5) (M)	Santa Cruz Biotech	WB (1:1000)	Cat#sc-393232
GR (R)	ProteinTech Group	ChIP-seq & ChIP-qPCR	Cat#24050-1-AP
IgG, HRP-conjugated (M)	Bio-Rad	WB (1:10000)	Cat#170-6516
IgG, HRP-conjugated (R)	Cell Signaling Technology	ChIP-qPCR	Cat#7074
LC3A/B (D3U4C) (R)	Cell Signaling Technology	WB (1:1000)	Cat#12741
p62 (R)	Enzo Life Sciences	WB (1:1000)	Cat#BML-PW9860
SIN3A (R)	Abcam	WB (1:1000)	Cat#ab3479
SIN3A (R)	Novus Biologicals	ChIP-seq & ChIP-qPCR	Cat#NB600-1263

*Host species antibody: R = rabbit, M = mouse. ** Chromatin immunoprecipitation (ChIP), Western Blot (WB).

Table 4. List of RT-qPCR primers.

Gene name	Forward (5' ->3')	Reverse (5'->3')
Aldob	ACCTCAATGCTATCAACCGTTT	ATAGGTGTAGGAGGCTGTGAAT
Apoa4	CGTGGACCTGCAAGATCAGA	TCTGCATGCGCTGGATGTAT
Apoc3	GAGCTGAAGAGGTAGAGGGATT	TTGGTCCTCAGGGTTAGAATCT
Bdh2	TCAGTTTGCCTCAGAAATCGAT	GCCACAGACGACATGTTGATAA
Bmal1	GCAGTGCCACTGACTACCAA	TCCTGGACATTGCATTGCAT
Cpt1α	CTCCGCCTGAGCCATGAAG	CACCAGTGATGATGCCATTC
Cry1	ACGTCCCGAGCTGTAGCGGT	CGCGGAGCTTCTCCCTTGCT
Eno1	GCTAGGTCCTCTATCCCTGATT	GCACCCTAGAGATTACACTGGA
Fabp1	AACTTCTCCGGCAAGTACCA	GTCCTCGGGCAGACCTATTG
Fdps	TCTGCAGTCTGCTTTCTTCA	TGTAGATCTTGTTTGCAAGT
Gys2	TCCCTTCTATGAGCCATCTTCA	CCGATGAGTGGGGAGAGAATTA
Hmgcr	TGTTCACCGGCAACAACAAGA	CCGCGTTATCGTCAGGATGA
Per1	GAAAGAAACCTCTGGCTGTTCCT	GCTGACGACGGATCTTTCTTG
Pygl	TACATTCAGGCTGTGCTGGA	AAGGCATCAAACACGGTTCC
Rev-Erbα	GGGCACAAGCAACATTACCA	CACGTCCCCACACACCTTAC
Scarb1	GATCCCTTCGTGCATTTTC	GAAGACAGTGAAGACCCCAG
U36b4	AGATTCGGGATATGCTGTTGGC	TCGGGTCCTAGACCAGTGTTC

Table 5. List of ChIP-qPCR primers.

Locus	Forward (5'->3')	Reverse (5'->3')
Foxl2	GCTGGCAGAATAGCATCCG	TGATGAAGCACTCGTTGAGGC
Trim63	TGGAAACGCTATGGAGAACC	ATGTCGTTGGCACACTTCC
Pdk4	GGGATAGATCCCAGGTCGCT	CTGGCTAGGAATGCGTGACA
Abcg8	GCCAGAGTGTCCTTATCTCG	CTTTCTCCCAGCATTCCTC
Per1-peak#1	TGGAACATCCTGTTCTCAGCG	AAGGAAGGCTGTGGCCAAC
Per1-peak#2	GTAGGTCCCGCAAAGAGAACC	GACAGCGGTCCTGTACAAAAG
Fkbp5	CTCAGCAGCTGGGTAAGTGG	TGCAGGAGCGGTTGATCTG

Table 6. List of cloning primers.

Genomic region	Forward (5' ->3')	Reverse (5'->3')
Apoa4/Apoc3 intergenic enhancer	ATCTTGTGGTATCAGTCGAC	TGGTCCACAGAGACTGTGAA
Apoe intergenic enhancer	AATCTCGAGAGAGGCGGCTG TACACAGGC	AATAAGCTTCAGCAGCACCT GCCTGACAC

3.2   Animal experiments

3.2.1   Transgenic mouse lines

All animal protocols were approved by the relevant animal welfare committee of the state of upper Bavaria (2532-Vet-02-1980 and 1943) - in accordance with Helmholtz Zentrum München –Deutsches Forschungszetrum für Gesundheit und Umwelt (HMGU) guidelines for the care and use of animals. All mice were bred on a C57BL/6J background.

3.2.2   Liver tissue-specific knockout mice

FOXO1 & GR floxed mice (FOXO1$^{flx/flx}$ and GR$^{flx/flx}$) were bred on a C57BL/6J background. GR$^{flx/flx}$ line was generated by Schütz lab (Tronche et al., 1999) while FOXO1$^{flx/flx}$ line was generated by DePinho lab (Paik et al., 2007). FOXO1$^{flx/flx}$ mice were obtained by JAX (Foxo1<tm1Rdp>/J). GR$^{flx/flx}$ and FOXO1$^{flx/flx}$ mice were crossed with hepatocyte-specific Albumin-Cre mice obtained from JAX (B6.Cg-Tg (Alb-cre)21Mgn/J) to generate Albumin-Cre x GR$^{flx/flx}$ and Albumin-Cre x FOXO1$^{flx/flx}$ mice, respectively. Consequently, Albumin-Cre x GR$^{flx/flx}$ and Albumin-Cre x FOXO1$^{flx/flx}$ were produced by the Cre/LoxP recombination system. From now, they will be mentioned as GR-LKO and FOXO1-LKO. Albumin-Cre negative floxed littermates served as control mice.

The *LoxP/Neo* cassette in GR$^{flx/flx}$ mice was inserted between exon 3 and exon 4 in the *Gr* wt allele with the first *loxP* site in the flanking exon 3, while the other *loxP* site was located between the two exons (Tronche et al., 1999). Use of Cre recombinase removes this region ablating the exon 3.

The *LoxP/Neo* cassette in FOXO1$^{flx/flx}$ mice was inserted in the flanking regions of exon 2 of the *Foxo1* wt allele (Paik et al., 2007). Use of Cre recombinase removes this region ablating the exon 2.

3.2.3   Housing and diets

Mice were housed in a controlled pathogen-free (SPF) facility with a 12 h light/dark cycle in groups of 3-4 animals per cage. The cages were constantly ventilated and kept in a

room at 23 °C with steady humidity levels. After weaning, mice were fed with *ad-libitum* chow diet (Altromin GmbH, 1318 diet) until adulthood (12 weeks old).

3.2.4 Genotyping

Genotyping of the GR-LKO and FOXO1-LKO mice was performed on DNA digested ear punches, which were taking during the weaning period. Digestion of the ear punches was performed using 200 µL of 50mM NaOH solution for 30 min at 95 °C and neutralized using 15 µL of 75mM TRIS. In the genotyping PCR, 1 µL of the DNA was used as template. The PCR reaction mix contains 12.5 µL of GoTaq Green DNA polymerase mix (Promega), 40mM $MgCl_2$ (Carl Roth GmbH), 0.2µM of each primer pair und filled up with H_20 to 25µL. Primer pairs were produced by the Eurofin Genomics. The list of primers is listed in the following table (**Table 7**). The PCR reaction is listed in the second following table (**Table 8**). All PCR products were separated on a 2% agarose gel (VWR Chemicals) and detected with a UV detection chamber (Benchtop 2UV Transilluminator and GelDoc-It Imaging System, UVP).

Table 7. Primer list for genotyping.

Primer name	Primer sequence 5'->3'
GR1_Fw	GGCATGCACATTACTGGCCTTCT
GR4_Rv	GTGTAGCAGCCAGCTTACAGGA
GR8_Rv	CCTTCTCATTCCATGTCAGCATGT
FOXO1flx_Fw	ACCACTCTGGACGGCATACT
FOXO1flx_Rv	TGAGTCTGGGGCTAGTTTGA

Table 8. Genotyping PCR reaction.

Step	Temperature (°C)	Duration	Cycles
Initiation	95	5 min	1
Denaturation	95	1 min	
Primer annealing	56	1 min	35
Elongation	72	1 min	
Final elongation	72	10 min	1

For the GR-LKO, primer pairs were used to genotype the two *LoxP* sites,

For the FOXO1-LKO, one primer pair was used to genotype the two *LoxP* sites surrounding the exon 2 of mouse *Foxo1* gene. PCR reaction gives fragments of 247bp and around 300bp for the WT and mutant *Foxo1* allele, respectively.

3.2.5 Glucose tolerance test

For a GTT, mice were fasted overnight for 16 hours with free access only to water. Glucose (45% D-glucose; Sigma Aldrich) was administered by intraperitoneal injection at a dosage of 2g/kg dissolved in sterile 0.9% NaCl (B. Braun) and the injection volume was calculated based on the fasted body mass of each mouse. Blood glucose levels were sampled from the tail vein using a glucometer (AccuCheck Aviva, Roche Diagnostics). Before the intraperitoneal administration, blood glucose was measured as baseline (time = 0) and afterwards at time = 15, 30, 60, 90 and 120 min.

3.2.6 Body fat composition using Echo-MRI

Body composition in lean and fat mass was measured using quantitative magnetic resonance technology (EchoMRI 900, Echo Medical System Houston, USA) before and after caloric restriction. For the measurements, each mouse was placed into a cylindrical tube without anesthesia inside the machine and it was scanning roughly for 1 min.

3.2.7 Caloric restriction regimen

For the caloric restriction regimen, 14 weeks old mice were used and single housed during the whole protocol. Before caloric restriction, the weekly food consumption was measured for each mouse, to determine the amount of food required for each week during the caloric restriction protocol (10-40%). At the end, mice were kept with 40 per cent restricted calories for 3 weeks. As a control, mice were fed *ad-libitum* (AL) without control of their food intake and the last week mice had access to the food only during the night. Overall, the caloric restriction protocol including also the food consumption and single housing lasted 7 weeks.

3.2.8 Indirect calorimetry, food intake and locomotor activity

Mice were trained with special bottles before their entry to the indirect calorimetry system. At the 5th week of caloric restriction regimen, they were placed in the indirect calorimetric cages (Labmaster, TSE systems GmbH, Bad Homburg, Germany). Almost the full first week were acclimatized and the actual measurements were taken from the last week of caloric restriction protocol. Food pellets were inserted before the transition of mice from the light to the dark phase. Body weight of mice was measured through special sensor in the house, while locomotor activity was recorded via a three-dimensional automated infrared beam grid surrounding each cage. Oxygen consumption (VO_2), carbon dioxide production (VCO_2), energy expenditure (EE), and locomotor activity (X+Y) were measured every 15 min during the experiment. The respiratory exchange ratio (RER = VCO_2/VO_2) was calculated for the overall contribution of energy sources, such as lipids and carbohydrates. A RER equals to 1 indicates exclusive glucose consumption while a value of 0.7 corresponds to exclusive lipid oxidation. Energy expenditure was calculated based on Weir's equation, which connects ATP consumption with exchanges of gases (Weir, 1949).

3.2.9 Mouse sacrifice and organ withdrawal

Mice were sacrificed by cervical dislocation and organs were collected every 4 hours for 24 hours. Blood was collected from the heart. Mice were quickly dissected and livers were isolated, snap-frozen in liquid nitrogen and stored at -80 °C. Serum was obtained after centrifugation at 1500 g for 10 min at 4 ºC, and stored after snap-freezing at -80 °C.

3.3   Molecular biology techniques

3.3.1 RNA isolation from tissue

50 mg of frozen tissue was used for RNA extraction. RNA was extracted using the QIAzol lysis reagent (Qiagen) according to the manufacturer's instructions.

3.3.2　cDNA synthesis

1µg of total RNA from liver tissue was reversed transcribed into cDNA (complementary DNA) using the QuantiTect Reverse Trancription Kit (Qiagen) according to the manufacturer's instructions.

3.3.3　Real-time quantitative polymerase chain reaction

Power SYBR Green Master Mix (Life Technologies GmbH) was use for real-time quantitative polymerase chain reaction (RT-qPCR) in a ViiA 7 Real-Time PCR System (Termo Fischer Scientific GmbH). Each sample was run with three technical replicates. The relative gene expression was normalized by the *U36b4* housekeeping gene expression. All RT-qPCR primers were obtained by Eurofins Genomics and are listed in **Table 4**.

3.3.4　Nuclear protein extraction from liver

A piece of 50mg of liver tissue was used for nuclear extraction. The cell lysis was performed in a tissue lyser (Qiagen) for 1.5 minutes at 30 Hz with 5mm stainless beads (Qiagen) in cold cell lysis buffer (Table 9) containing protease inhibitors (Roche Applied Science) and phosphatase inhibitors (Thermo Fisher Scientific).

The cytosolic fraction was separated by centrifugation for 20 minutes at 2700g at 4 °C. The pellet containing the nuclei was washed with PBS and the nuclei were homogenized in a lysis buffer (**Table 9**) and passed through an insulin syringe. After incubation for 1 h at 4°C under rotation, nuclear extracts were centrifuged at 21000g for 45 minutes at 4°C. Nuclear fractions were obtained by collecting supernatants and protein concentrations were measured using the Bradford method (Bio Rad) according to manufacturer's instructions.

Table 9. Cell lysis and nuclear lysis buffer for nuclei isolation.

Cell lysis buffer	Nuclear lysis buffer
10 mM Hepes-KOH pH=7.9	420 mM NaCl
1.5 mM MgCl2	20 mM Hepes-KOH pH=7.9
10 mM KCl	2 mM EDTA
0.5 mM DTT freshly added	0.5 mM DTT freshly added
0.15% NP40 (v/v)	0.1% NP40
	20% glycerol (v/v)

3.3.5 Total protein extraction from liver

30 mg of liver tissue were homogenized in cold RIPA buffer (1M NaCl, 1% NP-40, 0.5% DOC, 0.1% SDS, and 50mM Tris) supplemented with protease inhibitors (Roche Applied Science) and phosphatase inhibitors (Thermo Fisher Scientific). The lysis occurred in a tissue lyser (Qiagen) for 2 minutes at 30Hz. The samples were then centrifuged for 20 minutes at 21000g at 4°C, the supernatants containing the proteins were collected and kept at -80°C.

3.3.6 Western Blot analysis

10 µg of proteins (nuclear extracts) or 20 µg of total proteins were diluted into Laemmli buffer and boiled for 5 minutes at 95 °C. Protein extracts were run in 4-12% Bis-Tris gel (Invitrogen) and transferred on PVDF (Polyvinylidene fluoride) membranes (Merck Millipore). The membranes were blocked in a 10% milk/TBS-T with 0.1% Tween20 for 1h at room temperature. Primary antibodies and secondary antibodies for each protein are reported in **Table 3**.

Membranes were washed three times with TBS-T and incubated for 1h at room temperature with shaking with the secondary antibody secondary antibody. After three consecutive washes with TBS-T, the western blots were revealed using the HRP Western substrate (Merck Millipore) that induced a peroxidase reaction on X-ray films (CEA X-ray).

3.3.7 Cloning of mouse genomic regions in luciferase reporters

The selection of genomic regions to clone was based on ChIP-sequencing data. From GR and FOXO1 ChIP-seq, genomic regions containing at least one GRE or FOX binding motif were selected. Great overlap between the two factors was also desired. After the selection of the peaks, primers (Eurofin Genomics) with 5' overhangs were designed in the *Oligo Explorer* software. In the 5' overhangs, restriction enzyme binding sites were added to allow the cloning of insert into the vector of expression for further experiments. The melting temperature for the PCR production of each fragment was calculated using the NEB Tm calculator. The amplification of the region of interest was performed by PCR using mouse liver genomic DNA and the Q5 High-Fidelity polymerase (NEB) (**Table 10 and 11**).

Table 10. Q5 Polymerase reaction for cloning of mouse genomic regions.

Preparation of the Q5 polymerase master mix	Volume
Template DNA	1 µl
10mM dNTPs	0.5 µl
10 µM Forward primer	1.25 µl
10 µM Reverse primer	1.25 µl
5X Q5 reaction buffer	5 µl
Q5 High-Fidelity DNA polymerase	0.25 µl
Nuclease free water	15.75 µl
V_{final}	25 µl

Table 11. PCR reaction program for cloning.

Step	Temperature (°C)	Duration	Cycles
Initial denaturation	98	30 seconds	1
Denaturation	98	10 seconds	
Primer elongation	Tm	10-30 seconds	30
Elongation	72	20-30 seconds/kb	
Final extension	72	2 minutes	1
Hold	4 to 10		

After PCR reaction, products were run in 0.7% to 2% agarose gel, depending on the expected size of the insert. DNA was extracted using the QIAquick Gel Extraction kit (Qiagen) according to the manufacturer's instructions. Both insert and vector (1 µg) underwent separately a digestion with 2 restriction enzymes (NEB) for 1h at 37 °C. The vector was treated with CIP (Alkaline Phosphatase, Calf Intestinal; NEB) and FastAP de-phosphorylation, preventing thus a potential re-circularization of the vector without insert. After their purification using QIAquick PCR purification kit (Qiagen), the de-phosphorylated vector and fragment were ligated using either the T4 ligase (NEB) with overnight incubation or the quick ligase (NEB) for 2h at room temperature. Finally, the ligation products were transformed into bacteria by heat shock usually in TOP10 cells or in DHS5a cells. Bacterial cells were thawed and mixed with the ligation products for 30 min. Heat shock of bacteria was for 1 min, at 45 ºC. After recovery, bacteria were plated in agarose plates supplemented with ampicillin and incubated at 37 ºC overnight. Afterwards, LB (Luria Bertani) colonies were picked up and screened using mini prep columns (Qiagen). As negative control in the ligation was using for the reaction empty vector without the PCR product. Positive clones were validated by sequencing by Eurofin Genomics (**Table 12**). For cloning of promoter and enhancer regions was used pgl3basic and pgl4.23 vector, respectively. Both vectors carry ampicillin resistance cassette.

Table 12. Sequencing primers used for validation of positive clones.

Primer name	Primer sequence (5'->3')
RVprimer3	CTAGCAAAATAGGCTGTCCC
pGL4.23-Seq	TACCAACAGTACCGGATTGCC

3.4 Luciferase reporter assays

CV1 (a cell line derived from kidney of the African green monkey) were maintained in DMEM supplemented with 10% Fetal Bovine Serum (FBS), and 1% antibiotic cocktail (Pen/Strep) at 37 ºC and 5% CO_2. 2.000 cells per well were seeded in a 96 well-plate (PS, F-bottom, Greiner #655083) in DMEM (DULBECCOS MODIFIED EAGLE #D6429-500; Sigma Aldrich) supplemented with 10% dialyzed Fetal Bovine Serum (Fetal Bovine Serum Heat inactivated #F9665-500; Sigma Aldrich). CV1 cells were transfected with 25ng of the luciferase reporters, 50ng of vectors overexpressing GR/FOXO1 or their empty vectors, and 25ng CMV Renilla reporter for normalization of the luciferase signal (100ng per well)

using Fugene in OptiMEM medium (#31985047; Life Technologies GmbH) (**Table 13**). After overnight incubation, transfected cells were incubated with dexamethasone or vehicle (EtOH) in 50µl PhenolRed free DMEM (#21063029; Life Technologies GmbH) supplemented with 10% dialyzed FBS and pyruvate. The Firefly Dual-Glo Luciferase Assay System (#E2940; Promega) according to the manufacturer's instructions.

Table 13. Preparation of DNAs and transfection system for luciferase assays.

master mix of DNAs	Quantity for one well
luciferase reporter construct	25ng (1 µl)
GR-pDESTV5 or empty vector pDESTV5	50ng (1 µl)
Total amount/volume	75ng (2 µl)
master mix of transfection system	Quantity for one well
CMV-Renilla	25ng (1 µl)
OptiMEM	6.7 µl
Fugene	0.3 µl
Total amount/volume	8 µl

3.5 Tissue assays

3.5.1 Paraffin embedding of liver

Livers were isolated and immediately fixed in 10% formalin solution (Sigma-Aldrich) overnight at 4°C under rotation. After three washes with PBS (pH=7.4), livers were incubated overnight with 70% EtOH at 4°C with rotation. Tissues were dehydrated by incubating in solution containing gradually increased percentages of EtOH for 1h each at room temperature (80%, 90% and 2 times 100%). In order to remove the ethanol, livers were incubated three times for 10minutes in Xylene (AppliChem GmbH). Livers were placed in three consecutive paraffin baths at 65 °C, the last one being an overnight incubation. Livers were embedded in paraffin blocks using a paraffin embedding station (Leica EG1150) and blocks were cut in 6µm sections in a microtome (Leica RM255).

3.5.2 Hematoxylin and Eosin staining

For hematoxylin and eosin (H&E) staining, xylene was used for removal of paraffin from the slides and their re-hydration was accomplished by gradual decreasing concentration

of ethanol (100%, 96%, 70%) and deionized water. Afterwards, slides were incubated in Hematoxylin gill no.3 (GHS332, Sigma Aldrich) and eosin Y (HT110216, Sigma Aldrich) for around 1 min followed by rapid washes with tap water. Stained slides were again dehydrated in increasing concentrations of ethanol and cleared in pure xylene. In the end, for mounting was used the quick-hardening mounting medium (03989, Sigma Aldrich). Pictures of slides in brightfield were captured by a Nikon Eclipse Ci-L microscope.

3.5.3 Periodic-Acid Schiff staining

For periodic acid and Schiff (PAS) staining, xylene was used for removal of paraffin from the slides and their re-hydration was accomplished through gradual decreasing concentration of ethanol (100%, 96%, 70%) and deionized water. Afterwards, slides were incubated in 1% periodic acid in deionized water for 5 min followed by 10 min incubation with the Schiff's reagent and rapid washes with tap water for 3 min. Slides were stained with Mayer's Hematoxylin for 1 min followed by washes again with tap water. Stained slides were again dehydrated in increasing concentrations of ethanol and cleared in pure xylene. In the end was used the quick-hardening mounting medium (03989, Sigma Aldrich). Pictures of slides in brightfield were captured by a Nikon Eclipse Ci-L microscope.

3.5.4 ELISA corticosterone measurement

Plasma corticosterone levels were measured using the Enzo immunoassay kit (Enzo Life science, #ADI-900-097) according to the manufacturer's instructions.

3.5.5 ELISA insulin measurement

Plasma insulin levels were measured using the ultrasensitive mouse insulin Elisa kit (Crystal Chem, #90080) according to the manufacturer's instructions.

3.6 Next generation sequencing techniques

3.6.1 Chromatin-Immunoprecipitation coupled with Sequencing

The ChIP-Seq protocol was followed using the already described method (Mir et al., 2019). 200mg of frozen liver tissues were homogenized in the lysis buffer supplemented with

protease inhibitors (Roche Applied Science) and phosphatase inhibitors (Thermo Fisher Scientific) using a Tissue Lyzer at a frequency 30Hz for 2 min. For the control SIN3A cistrome, mice fed with low fat diet (LFD; Research Diets D12450H, with 10% fat) were used, while all the remaining cistromes were coming from mice fed chow diet (7% simple sugars, 3% fat, 50% polysaccharide, 15% protein (w/w), energy 3.5 kcal/g, n = 20). Afterwards, lysates were passed through a 70 µm cell strainer (Falcon) and then cross-linked in 1% formaldehyde solution (FA) for 15 min at room temperature (for both GR- and FOXO1-ChIP-seq), while a disuccinimidyl glutarate (DSG) solution for 30 min followed by a 15 min incubation in 1% FA solution at room temperature (for SIN3A-ChIP-seq). Cross-linkers were quenched with by 5 min incubation with 0.2M glycine solution in PBS.

Pellets were resuspended in cold Fast-IP (150mM NaCl, 5mM EDTA pH=7.5, 5mM Tris pH=7.5, 1% Triton X-100, 0.5% NP40) buffer and passed through a syringe of 24G twice. The chromatin was sonicated in shearing buffer (1% SDS, 10µM EDTA pH=8, 0.05 Tris pH=8) into a range between 0.1 and 1kb molecular size by using a Bioruptor Plus (Diagenode) with 30sec on/30sec off on low settings. Sonicated chromatin was centrifuged for 10 min at 4 °C at 12.000rpm. A 10% input sheared chromatin was kept at -20°C as internal control. Chromatin immunoprecipitation was performed in dilution buffer (0.01% SDS, 1.1% Triton X-100, 1.2µM EDTA pH=8, 16.7µM Tris pH=8, 0.167M NaCl) and was incubated overnight with 8µg of antibody (**Table 3**) at 4 °C under rotation.

Next day, the antibody-bound chromatin was cleared by centrifugation at 3500 rpm for 20min at 4°C. The 90% of each sample was incubated with Dynabeads M-280 (Invitrogen), which were overnight blocked with 0.5% BSA in PBS. After the 6 hours incubation at 4°C under rotation, the loaded Dynabeads M-280 were washed 6 times with the FAST-IP buffer and once with TE buffer. Elution of samples was achieved by using the elution buffer for 15min at room temperature under 1000 rpm. ChIPed and input DNA were decrosslinked by an overnight incubation with 200mM NaCl at 65°C. Next day, samples were treated with 0.05 µg RNase A (AppliChem GmbH) at 37°C for 30 min and followed by a digestion with a buffer containing 0.05 µg Proteinase K, 10mM EDTA at pH=8 and 40mM Tris at pH=7.5 for 2 hours at 45°C. Both ChIPed and input DNA were isolated by the MiniElute PCR purification kit (Qiagen). ChIP DNA concentration was determined by using the QUBIT dsDNA HS kit (Thermo Fischer Scientific). Lastly, qPCR for negative and positive loci were used for the evaluation of enrichment for each factor (**Supplementary Figure 1**).

Final step is the library preparation using the KAPA Hyperprep Kit (#KK8504, Kapa Biosystems). Illumina compatible adapters were synthesized by IDT (Integrated DNA Technologies) and their final concentration on each reaction was 68nM. The adapter-ligated libraries were size-selected between the 360 and 610bp using a 2% free-dye gel (CDF2010, Sage Science) and a Pippin Gel size selection station (Sage Science). qPCR was performed for the estimation of the library concentration by the KAPA Library Quantification kit (#KK4873, Kapa Biosystems). The quality of each library was assessed by using the Agilent High Sensitivity kit (Agilent) in a 2100 Bioanalyzer (Agilent).

3.6.2   Chromatin-immunoprecipitation coupled with qPCR (ChIP-qPCR)

The preparation of samples, the sonication of the chromatin and the immunoprecipitation followed the protocol of ChIP-seq as in the paragraph 3.6.1. For the IP of each factor, was used 3 μg of antibody and sheared chromatin was kept as input at -20 °C with 3 volumes of pure EtOH overnight. The next day, the IP chromatin was cleared by centrifugation at 12000rpm for 10min at 4°C. The supernatant of IP cleared chromatin was incubated for 2-3hrs at 4°C with Sepharose Protein A/G beads (Rockland Inc.), which were overnight blocked with 0.5% BSA in PBS. Coupled Sepharose Protein A/G beads were washed five times with the FAST IP buffer. For the isolation of the chromatin was using 100 μl of 10% Chelex (Sigma-Aldrich). After vortexing, samples were treated with 0.05 μg RNase A (AppliChem GmbH) at 37°C for 30 min and followed by 0.05 μg Proteinase K digestion for 2 hrs at 55°C under 600rpm. After the incubation, 12000rpm centrifugation and collection of the first 80 μl, and a second step collection of 120 μl, leads to final volume of 200 μl of ChIP chromatin. Both the ChIP DNA and the input were isolated by the MiniElute PCR purification kit (Qiagen).

ChIP-DNA was diluted (1:60) and was used as template for the qPCR by the reaction the Power SYBR Green Master Mix (Life Technologies) in a ViiA 7 Real-Time PCR system (Thermo Fischer Scientific). Each sample was run in total with three different technical replicates on a 384-well plate. Percentage of input was calculated both over IgG and over the negative locus in order to assess the IP of each factor and the enrichment of each locus.

3.6.3 RNA coupled with Sequencing (RNA-Seq)

RNA coupled with sequencing (RNA-Seq) was performed in liver samples. RNA was extracted using the QIAzol lysis reagent (Qiagen) according to the manufacturer's instructions. All samples for RNA-Seq were DNAse-treated with the Ambion DNAse I kit (Thermo Fischer Scientific) according to the manufacturer's instructions. The quality of the total RNA was assessed by using an Agilent 2100 Bioanalyzer with RNA 6000Nano Reagents (Agilent Technologies). Library preparation and rRNA depletion was performed by using the Illumina TruSeq stranded/unstranded mRNA Library Prep Kit v2 chemistry in an automated system (Agilent Bravo liquid handling platform) starting with initial amount of 1µg of total RNA per sample.

3.7 NGS & Lipidomics data analysis

3.7.1 Chromatin-Immunoprecipitation coupled with Sequencing analysis

The ChIP-seq analysis contains multiple steps. The samples were sequenced with 50bp, paired end libraries. Because of the Pair-End (PE) sequencing it was mandatory to read and merged the 2 different reads (read1 and read2) in order to create one merged file with all the reads, from both strands. First step is checking the quality of the sequencing data, using the FASTQC in order to evaluate the quality of the raw data. After the quality check of the raw data, it is necessary to remove the adaptor sequences, using the "Trimmomatic" tool (Bolger et al., 2014). Second step is the alignment to the mouse mm10 reference genome using the BWA-MEM v.0.7.12 (H. Li & Durbin, 2010). Removal of duplicates and multimappers was performed with Samtools and Bamtools v2.4 (Barnett et al., 2011). During the process of removal of duplicates and multimappers, Flagstats was assessing the final number of reads, which will be used for the final stage of the analysis. Picard was used for sorting and indexing of the files. Peaks were called using the MACS2 v2.1.1 with FDR <0.05 and peaks falling into blacklisted peak regions were excluded by the BEDTools v2.25 (Quinlan & Hall, 2010; Y. Zhang et al., 2008). The irreproducibility discovery rate (IDR) gave the reproducible peaks between the replicates after the performance of the BEDTools (Landt et al., 2012; Q. Li et al., 2011). Peaks were annotated with gene names and motif discovery was performed by HOMER v4.8 (Heinz et al., 2010). For the

annotation and visualization of the ChIP-seq data was used ChIPseeker package, which is built-up in R language (Yu et al., 2015).

3.7.2 RNA coupled with Sequencing analysis

The RNA samples were sequenced with 100bp paired end libraries. For the pre-processing, RNA-Seq FASTQ files were mapped against mouse genome mm10 with the STAR v2.4.2a aligner (Dobin et al., 2013). For the mm10 genome annotation was used GENCODE. Format conversions were achieved by using samtools v1.3.1 (H. Li et al., 2008). The feautreCounts program (Liao et al., 2014) was used to count reads located within exonic regions, without having multiple features' overlap and not being chimeric.

For normalization and differential expression analysis, a read count matrix was fed into the DESeq2 v1.23.10 program (Love et al., 2014). Variance stabilization was necessary to be performed for the production of a normalized data matrix. Differential gene expression analysis was performed using a linear model that quantifies the effect of genotype, time, and their interactions, comparing the genotype-time groups with each other. In this case our design formula was: design=~ genotype + time + genotype:time. The number of biological replicates was 4.

For functional enrichment based on the gene ontology was carried out using EnrichR (Kuleshov et al., 2016). Heatmaps and volcano plots were produced using R language (www.R-project.org).

3.7.3 Lipidomic analysis

For Lipidomics analysis, 5 samples per condition were submitted at the Lipidomics platform Unit at the Helmholtz Zentrum München. Samples run into Lipidyzer, which is able to quantify accurately up to 1070 lipid species from 13 different lipid classes using ion mobility mass spectrometry (IM-MS) combined with multiple reaction monitoring (MRM). The lipid quantification is based on internal standards with known concentrations, which have approximately 10 different fatty acids with various amount of carbon atoms and double-bonds per lipid class, which are spiked into the analytical samples prior the extraction procedure.

3.7.4   Statistical analysis

All statistical tests were performed either using GraphPad Prism 6 (GraphPad Software, San Diego, USA) or R language. For difference between two groups, unpaired multiple t-test with threshold $p < 0.05$ has been used in order to evaluate the statistical significance. For cases with more than two groups, two-way ANOVA was used in order to assess differences. All results were given as mean ± SEM.

3.8 Contributions from collaborations

Mouse experiments were performed mainly by Konstantinos Makris with the help from Dr. Kenneth Allen Dyar, Dr. Céline Jouffe and Dr. Fabiana Quagliarini. Hepatocyte experiments were performed by Konstantinos Makris, Teresa Horn and Dr. Revathi Sekar. Samples were sequenced by Inti Alberto De La Rosa Vazquez, Elisabeth Graf, Sandy Lösecke and Thomas Schwarzmayr at the Genomic Facility at Helmholtz Zentrum München. ChIP- and RNA-seq data were processed by Dr. Kinga Balazs. Final processing of ChIP- and RNA-seq analysis and their visualization were performed by Konstantinos Makris. Processing and analysis of samples for lipidomics was performed by Fabien Riols at the Lipidomics platform Unit and analyzed by Dr. Mark Haik at Helmholtz Zentrum München. Serum Analyzer was performed by Daniela Hass and metabolic cages (TSE system) were run with the help of Dr. Adriano Maida at the Helmholtz Zentrum München.

4   Results

4.1   Caloric restriction changes physiological parameters in C57BL6/J mice

4.1.1   Caloric restriction reduces body and liver weight

Evidences from various studies showed that caloric restriction can improve many physiological parameters protecting from underling metabolic diseases. As previously described, caloric restricted mice were single caged and their food consumption was measured during the 1st week, followed by a 10% gradual reduction of their food intake per week up to 40% reduction of calories per week (the maximal reduction applicable for mouse studies). Then, mice were kept under 40% caloric restriction for 3 weeks until the sacrifice. In parallel, *ad-libitum* control fed mice in separate cages were monitored, and the last week of the protocol mice had access to the food only during the night in order to sacrifice them in parallel with the caloric restricted mice. Based on this experimental design, changes in the body and liver mass are expected (**Figure 9A**). Indeed, in wild type mice, we observed a significant reduction in the body mass of caloric restricted mice, while the livers of these mice had reduced mass over the total body mass, validating thus the protocol design for further experiments (**Figure 9B & 9C**). In previous studies, it has been observed that liver is a tissue relevant protective by the effects of the caloric restriction, loosing less mass compared to other organs. For further examination of this cohort, samples were collected every 4 hours around the clock in order to characterize better the physiological output of caloric restriction and understanding its effects in the liver. As first timepoint was ZT0 (Zeitgeber Time 0; 6am), where the lights were on, while as ZT12 (Zeitgeber Time 12; 6pm), where the lights were off. Based on the different timepoints between day and night, liver can absorb lipids and carbohydrates during the active phase of the mice, energy necessary for processes during the whole day-night cycle of 24 hours. In the context of fat and lean mass, the caloric restricted mice loose and gain significantly 4% of fat and 3% of muscle respectively, compared with control mice (**Figure 9D & 9E**). Conclusively, these mice are gaining lean mass, loosing significant percentage of fat mass and having a comparable phenotype with mice having exercise.
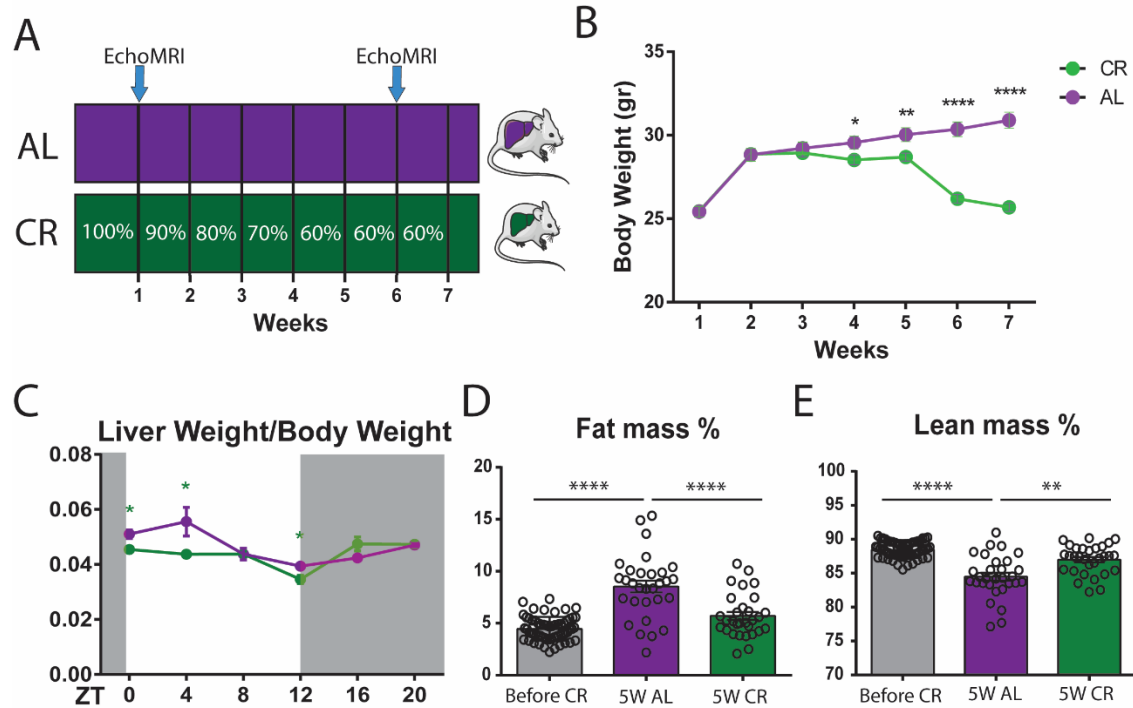
Figure 9: Caloric restriction lessens the body and liver mass.

A: Experimental outline of the caloric restriction regimen showing that caloric restricted mice have 10% gradual restriction of their calories up to 40%, in which they are maintained for 3 consecutive weeks. EchoMRI has been performed after the 1st and 5th week of caloric restriction. **B:** Body mass before and after caloric restriction regimen in wild type mice. **C:** Liver mass from normal-fed and restricted wildtype mice around the circadian clock (ZT0= 6am; ZT12= 6pm). **D:** Percentage of fat mass from normal-fed and caloric restricted mice measured by NMR. **E:** Percentage of lean mass from normal-fed and caloric restricted mice measured by NMR. n= 30 biological replicates per condition, ZT: Zeitgeber Time; W: Weeks; AL: Ad-Libitum; CR: Caloric Restriction. Data are mean ± SEM, n=3 per condition. *$p<0.05$, **$p<0.01$, ***$p<0.001$, ****$p<0.0001$. Student's t-test.

4.1.2 Caloric restriction boosts circulating glucocorticoids and dampens insulin secretion

Caloric restriction leads to the caloric stress, which potentially can affect the total physiological output of the mice. Since in the 40% caloric restriction, it was observed reduced body and liver mass, it was important to understand the impact of caloric stress on the secretion of the glucocorticoids and insulin around the circadian clock. GC secretion in adrenal glands is either rhythmically activated by light or by food deprivation or stress

event. In the case of caloric stress, adrenal glands of the wild type restricted mice secrete about 3 times more corticosterone (the circulating glucocorticoids in mice) in a time-dependent manner, specifically at the peak of the hormones (ZT12), when they are compared to the *ad-libitum* fed mice (**Figure 10A**). Temporal measurements of circulating corticosterone levels exhibit this bigger corticosterone peak in the caloric restricted mice at ZT12, pointing out that caloric stress has presumably an emerging role in the anticipation of the metabolism before food intake. At the same time, caloric restriction reduced the overall levels of insulin, a hormone regulated by food intake. The temporal insulin levels were dampened especially after the food intake (at ZT16) (**Figure 10B**). The fact that caloric restricted mice have lower insulin levels before and after food intake implies that they have become insulin sensitive.
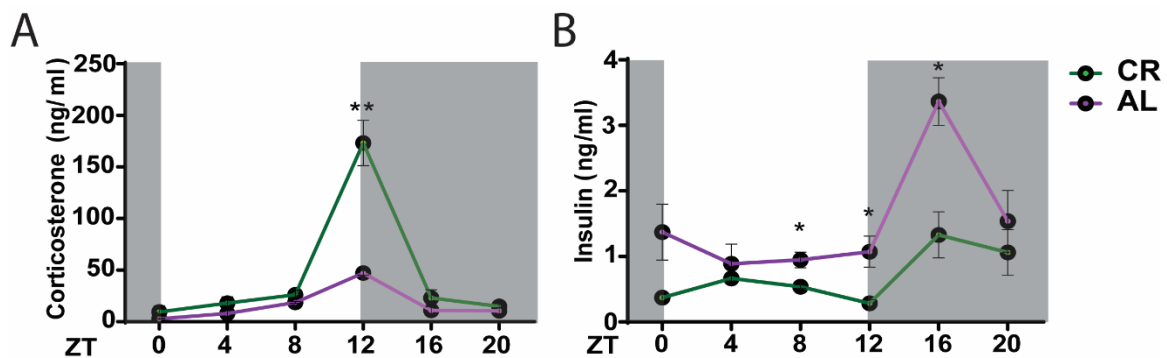
Figure 10: Caloric restriction increases the secretion of glucocorticoids and reduces insulin levels.

A: Measurements of circulating corticosterone levels from the plasma of normal-fed and restricted mice around the clock. **B:** Measurements of circulating insulin from the plasma of normal-fed and restricted mice around the clock. Data are mean ± SEM, n=3 per condition. *$p<0.05$, **$p<0.01$, ***$p<0.001$. Student's t-test. ZT: Zeitgeber Time.

4.2 Increased residency of hepatic FOXO1 factor in restriction

Caloric restriction is connected with many molecular pathways. The initial evidence of increased corticosterone and reduced insulin secretion in restricted mice led to the hypothesis that short term caloric restriction would enhance the glucocorticoid activity. Despite the 3 times more secreted ligand (**Figure 10A**), nuclear protein levels of hepatic glucocorticoid receptor (GR) around the circadian clock exhibit comparable pattern in both caloric restricted and *ad-libitum* mice (**Figure 11A & 11B**). In parallel, restriction of calories reduced the insulin levels affecting the activation of the PI3K/AKT signaling, a major

nutrient sensing signaling. The binding of insulin to its receptor activates the PI3K/AKT signaling affecting many downstream transcription factors. The activation of the AKT kinase phosphorylates transcription factors such as the ones from the FOXO family. In the case of intermittent and prolonged fasting, PI3K/AKT signaling is dampened giving lower pulses of activation in the liver and affecting the FOXO1 factor. In caloric restriction, insulin levels are dampened and there is an increased nuclear residency of FOXO1 in the nuclear hepatic extracts of the restricted mice especially during the night (**Figure 11A & 11B**). Caloric restricted mice show a reverse phase in the phosphorylation status of hepatic FOXO1, compared to the control ad-libitum fed mice. Interestingly, the ration between pFOXO1 and the total FOXO1 protein levels in liver showed a delayed phosphorylation pattern (**Figure 11C & 11D**). This delay in the phosphorylation status follows the nuclear residency of FOXO1. Conclusively, restricted mice gain insulin sensitivity affecting the nuclear residency of FOXO1, without changing the nuclear GR levels.
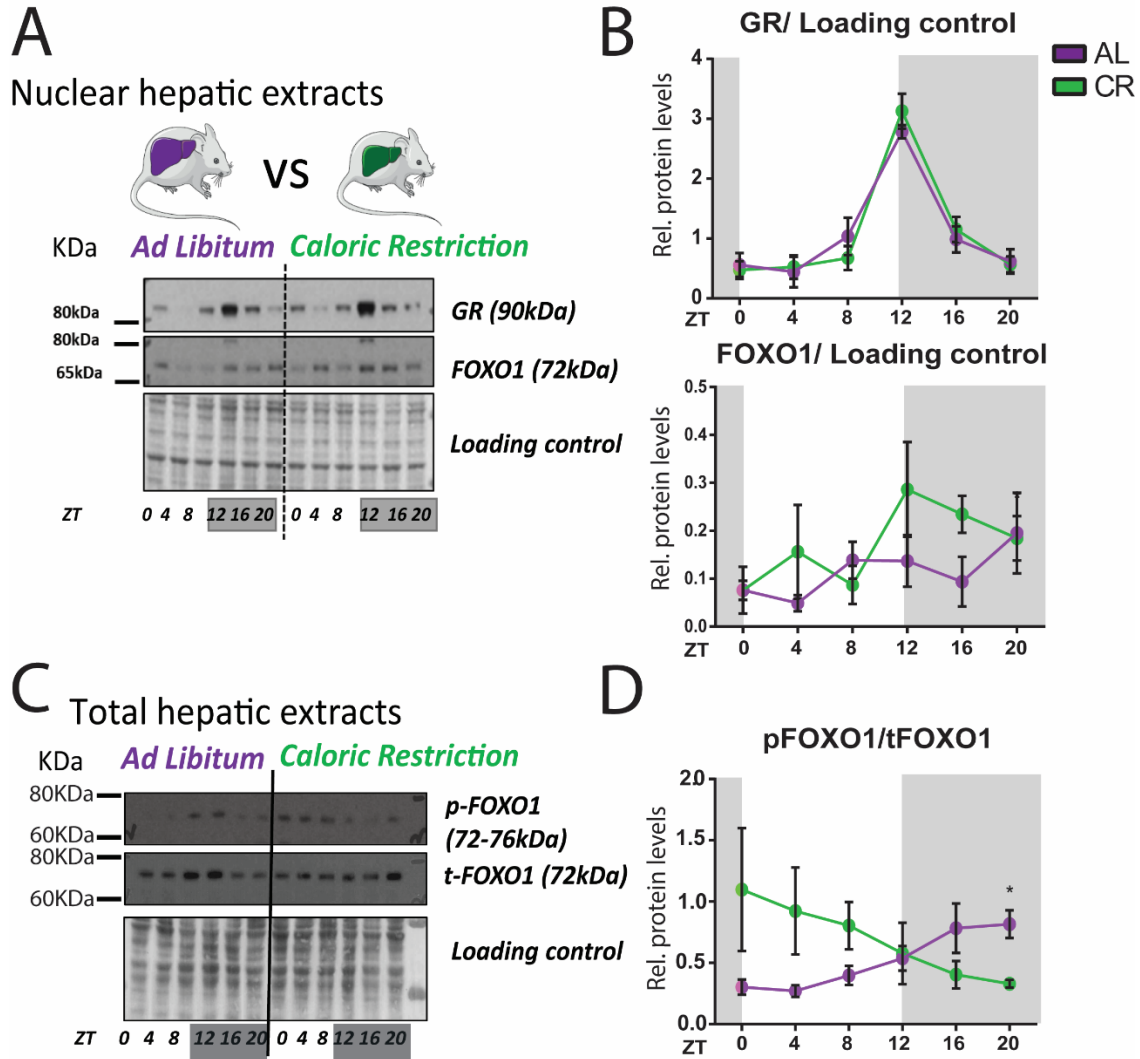
Figure 11: Increased nuclear hepatic GR and FOXO1 levels in caloric restriction.

A: Western blot in nuclear hepatic extracts from control-fed and restricted mice detecting total GR, total FOXO1 and amido black staining was used as a loading control. **B:** Quantification of nuclear hepatic GR and FOXO1 levels normalized over the loading control. **C:** Western blot in total extracts from control-fed and restricted mice detecting phospho-FOXO1 at T24 and T32 (p-FOXO1/FOXO3 at T24/T32), total FOXO1 (t-FOXO1), and amido black staining was used as a loading control. **D:** Quantification of hepatic p-FOXO1 over the t-FOXO1 levels normalized over the loading control. Data are mean ± SEM, n= 3 biological replicates per condition. ZT: Zeitgeber Time.

4.3   Genomic binding of GR and FOXO1 in restriction

4.3.1   Genome-wide binding of hepatic GR in *ad-libitum* and caloric restriction in mice

Caloric restricted mice exhibited enhanced glucocorticoid secretion at the peak of hormones (**Figure 9**). The mechanism of hepatic GR in gene regulation is not fully understood due to many factors affecting GR binding patterns. In caloric restriction, there are several factors influencing gene regulation, which potentially can interact with the GR. Chromatin immunoprecipitation followed by high throughput sequencing (ChIP-Seq) for GR was performed in mouse livers in order to study the diet-specific regulatory elements (promoters and enhancers) that are unique and distinct from the control mice. Moreover, motif analyses of surrounding sequences around differential and *de novo* binding sites will reveal enriched cis-regulatory elements of co-occupying factors (such as nuclear receptors and hepatocyte specific factors) which are likely to crosstalk with GR during the response to caloric restriction. Wild type livers from restricted and normal-fed mice were collected at the peak of hormones (ZT12). ChIP-DNA was prepared for libraries and sequenced reads were aligned to the mouse mm10 reference genome (**Supplemental Table 1**). GR ChIP bound regions (peaks) were called by the MACS2. Overlap between the two biological replicates for each condition gave 6824 and 15258 peaks for GR in normal feeding and caloric restriction, respectively (**Figure 12A**). Among these peaks, IDR (Irreproducibility Discovery Rate) analysis identified 6579 and 14825 reproducible peaks for the two biological replicates (**Figure 12B**).
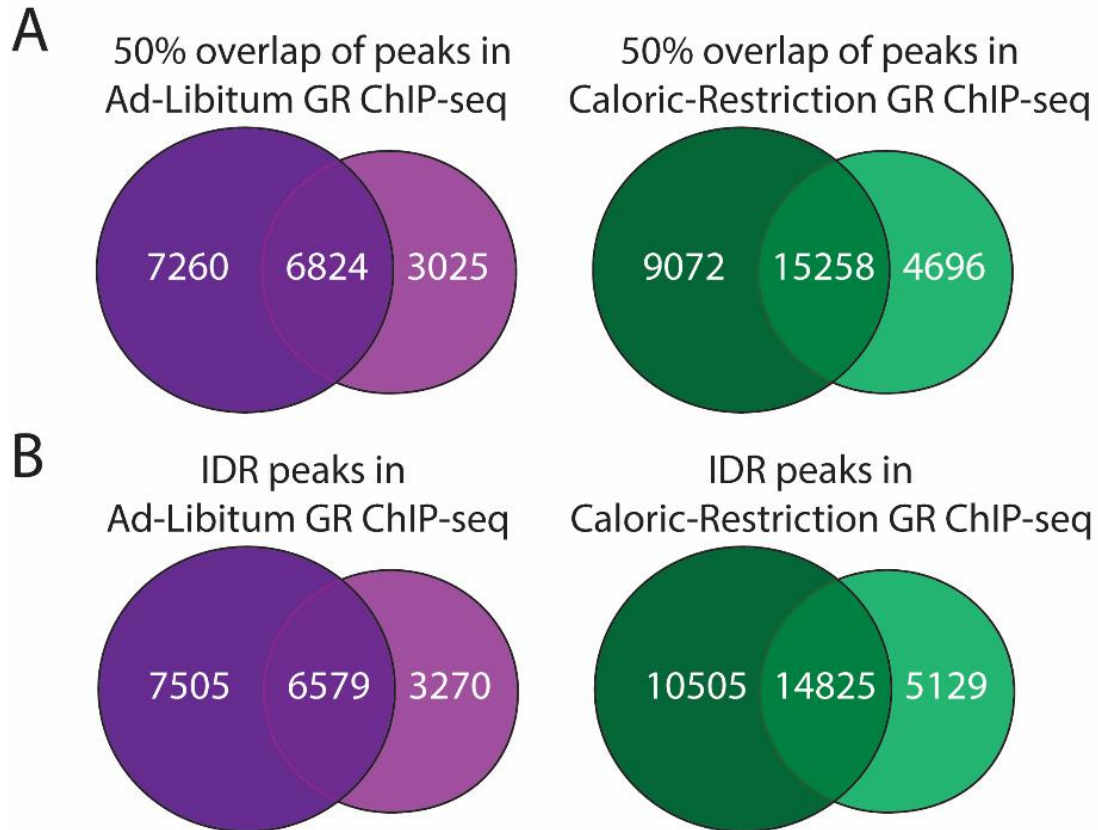
Figure 12: Caloric restriction increases the genome-wide binding profile of hepatic GR.

A: Overlap of the two biological replicates of GR ChIP-seq in both control-fed and restricted mice.
B: IDR analysis displays the reproducible IDR peaks of GR ChIP-seq for both control-fed and restricted mice.

Interestingly, overlap of GR peaks between the *ad-libitum* fed and caloric restricted mice gave a significant percentage of known target gene promoters and enhancers, such as *Per1*, *Pck1*, *G6pc*, *Angptl4*, and *Foxo1*. More specifically, overlap between AL & CR identified 3941 common overlapping GR peaks, leaving 9324 *de novo* GR binding sites specific to caloric restriction conditions (**Figure 13A**). Overlap of the IDR peaks identified 4654 common IDR GR peaks, identifying 9496 unique IDR GR peaks in restriction (**Figure 13B**). Despite the same GR nuclear localization, the excess in glucocorticoids increased GR binding sites in comparison with the *ad-libitum* condition, which reflects the increased GR binding profile.

HOMER motif analysis was further performed on the GR ChIP-seq for both AL and CR condition. Beyond the GRE as the top expected motifs, there were many consensus sites for transcription factors, such as HNF4α, HNF6, FOX, STAT and C/EBP. All these motifs

were previously published in various conditions and they are localized with GR at many hepatic cis-regulatory elements (Greulich et al., 2016; H.-W. Lim et al., 2015; Quagliarini et al., 2019). Comparison of the HOMER motif analysis between the AL and CR GR ChIP-seq identified enrichment for FOX and PPAR/RXR motifs in both cases (**Figure 13C**). FOX motifs have been previously found in GR-bound sites upon fasting-refeeding and high-fat diet in mouse liver (Kalvisa et al., 2018; Quagliarini et al., 2019). In order to understand the differences between the AL and CR GR cistromes, HOMER motif analyses were performed separately in common peaks and unique AL and CR GR IDR peaks. In common IDR peaks, the most enriched motifs were HNF4α, C/EBP, PPAR/RXR, NFIL3, FOX, HNF6 and ATF/CREB motifs (**Figure 13C**). Of note, in the case of the unique AL IDR peaks, STAT5 was identified as a top motif. STAT5 is a transcription factor that participate at the reprogramming of the GR cistrome during high-caloric conditions (Quagliarini et al., 2019). In the remaining unique AL IDR peaks, enriched motifs were than in the common IDR peaks. Surprisingly, unique CR IDR peaks were enriched in HNF4α, PPAR/RXR, NFIL3, FOX, HNF6, and AT/CREB. Both PPAR/RXR and FOX motifs were more enriched in the unique CR GR IDR peaks than in the unique AL GR IDR peaks. Upon caloric restriction, GR has a preference for recognizing sites enriched with PPAR/RXR, FOX, HNF, ATF/CREB motifs than classical GRE motifs (**Figure 13C**).

A: 70% overlap of peaks

B: overlap of IDR peaks (FDR=0.05)

C: HOMER motif analysis in IDR peaks

common peaks

Motif	Factor	P-value
	HNF4a	1E-254
	C/EBP	1E-275
	GRE	1E-222
	PPAR/RXR	1E-174
	NFIL3	1E-155
	FOX	1E-115
	HNF6	1E-91
	ATF/CREB	1E-68

unique peaks in AL

Motif	Factor	P-value
	STAT	1E-58
	GRE	1E-54
	HNF4a	1E-52
	C/EBP	1E-50
	NFIL3	1E-47
	PPAR/RXR	1E-38
	FOX	1E-31
	HNF6	1E-29

unique peaks in CR

Motif	Factor	P-value
	HNF4a	1E-388
	C/EBP	1E-358
	PPAR/RXR	1E-316
	NFIL3	1E-306
	FOX	1E-227
	HNF6	1E-163
	ATF/CREB	1E-129
	GRE	1E-116

Figure 13: Caloric restriction increases the genome-wide binding profile of hepatic GR.

A: GR ChIP peaks overlap between the AL & CR condition without any statistical analysis. **B:** Reproducible GR ChIP peaks overlap between AL & CR. **C:** HOMER analysis presents the enriched transcription factor binding motifs. **D:** Normalized *Foxo1* read counts from published RNA-seq data in GR-LKO mice around the circadian clock (Quagliarini et al., 2019).

Interestingly, FOXO1 factor plays a crucial role for the activation of gluconeogenic and lipid homeostatic genes and it is known to bind many common GR regulated regions, such as distal enhancers, upon fasting (Kalvisa et al., 2018). Additionally, GR binds to the *Foxo1* promoter increasing its expression levels. A 4 hours dexamethasone treatment at the GC trough (ZT0) and peak (ZT12) increased in both cases *Foxo1* expression, while absence of hepatic GR reduces the oscillating *Foxo1* expression (**Figure 14A & 14B**) (Quagliarini et al., 2019).
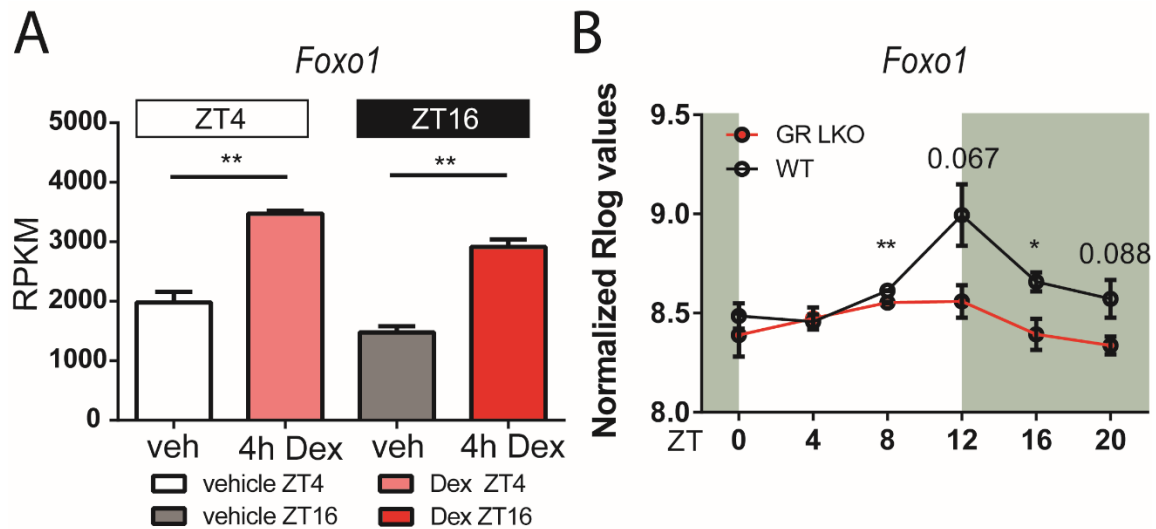
Figure 14: GR controls the Foxo1 expression levels upon dexamethasone treatment and around the clock.

A: *Foxo1* transcript expression in 4h-vehicle (veh) and 4h-dexamethasone (Dex) treated wild type (WT) mice at the ZT0 and ZT12, and sacrificed at ZT4 and ZT16, RPKM (reads per kilobases of transcript per million reads mapped). **B:** Normalized Rlog counts of *Foxo1* transcripts around the circadian clock coming from RNA-seq between low-fat diet-fed WT and GR-LKO mice. ZT: Zeitgeber Time, n =2-3, *p<0.05, **p<0.01 and ns = not significant. Student's t-test (Quagliarini et al., 2019).

4.3.2 Characteristic examples of GR peaks in AL vs CR groups

Since caloric restricted mice secreted 3 times higher corticosterone, this ligand availability is reflected in the GR binding profile. However, classical GR target genes such as *Per1* and *Gck*, were found bound in both cases. Unfortunately, the usage of only two biological replicates in the bioinformatic analysis could not allow *per se* the quantification of the differential peak binding between the two different conditions. Interestingly, hepatic GR binding profile in caloric restriction gave many *de novo* ChIP peaks. These peaks are localized in promoters and enhancers of genes related with the fatty acid metabolism, such as *Fabp1* & *Cpt1α*, the cholesterol transport, such as *Apoa4* & *Apoc3*, and glycolysis/gluconeogenesis, such as *Eno1* (**Figure 15**). In the aforementioned loci, there are many common peaks between *ad-libitum* (purple peaks) and caloric restriction (green peaks). All these examples recapitulate a broader role of hepatic GR binding to many genes related with energy homeostasis, attributing a novel role for this nuclear receptor in caloric restriction.
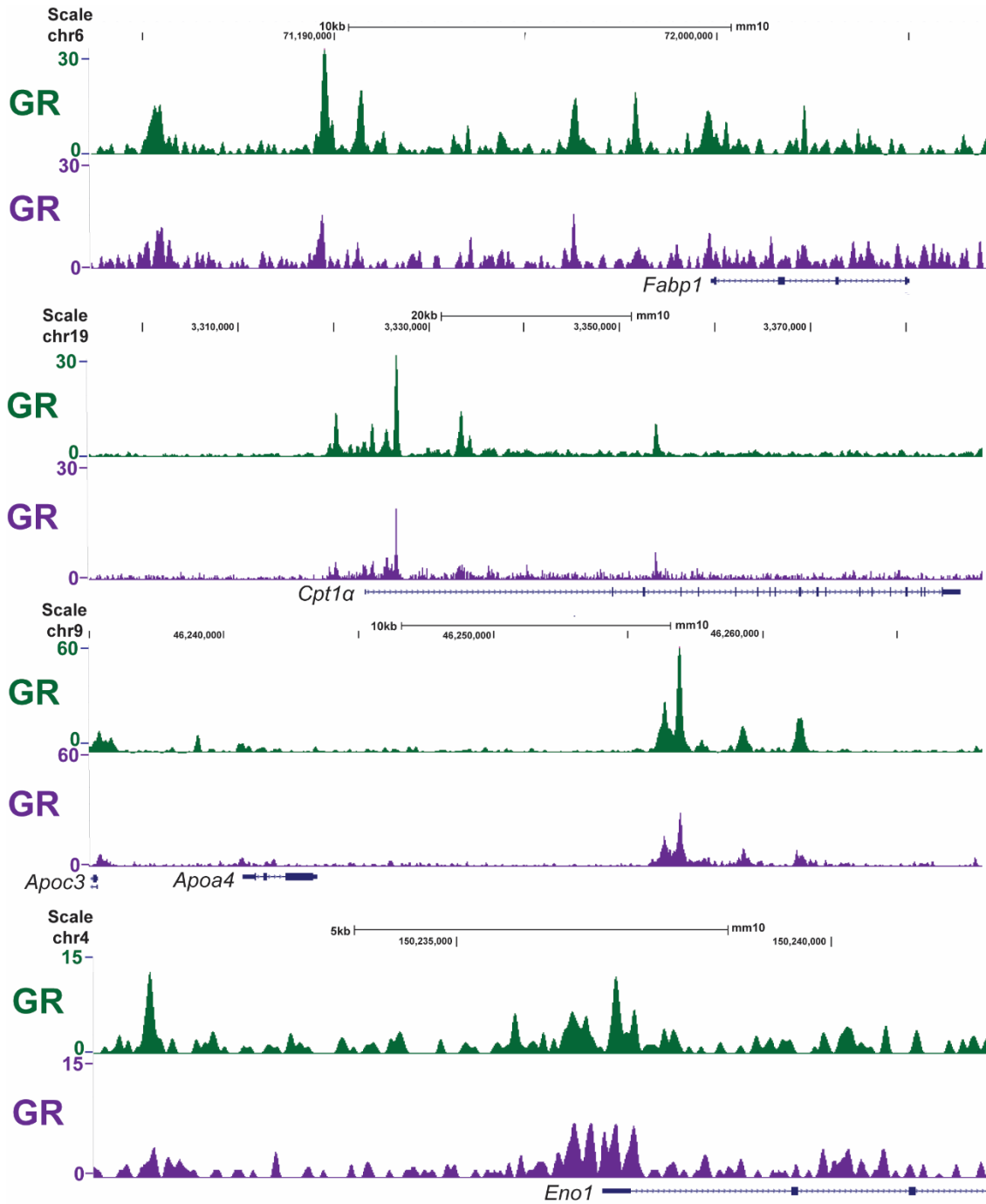
Figure 15: Representative examples of GR ChIP tracks in AL & CR.

Aligned peaks coming from hepatic GR ChIP-seq in both *ad-libitum* fed (purple peaks) and caloric restricted (green peaks) mice, at loci involved in metabolism, such as *Fabp1*, *Cpt1α*, *Apoa4*, *Apoc3*, and *Eno1* at the peak of corticosterone levels (ZT12).

4.3.3   Genome-wide binding profile of hepatic FOXO1 upon Caloric Restriction

To test the hypothesis that FOXO1 factor is a GR co-partner in caloric restriction, ChIP-seq for FOXO1 was performed in the same restricted wild type mouse livers. In the case of FOXO1 factor, only livers from caloric restricted mice at the peak of glucocorticoids were used because we wanted to focus mainly on the caloric restriction, where FOXO1 is enriched. Using a combination of FOXO1 antibodies ChIP-DNA was pulled down, prepared in libraries and sequenced reads were aligned in the mouse mm10 reference genome (**Supplemental Table 1**). Using the same rational, FOXO1 bound regions (peaks) were called by MACS2. Among the two biological replicates, 4324 overlapping peaks were identified while IDR analysis recognized 5102 IDR FOXO1 peaks (**Figure 16A & 16B**). Interestingly, hepatic FOXO1 ChIP peaks were bound to classical gluconeogenic and lipid-homeostatic genes at the peak of hormones in caloric restriction, such as *Pdk4*, *Pck1*, *Gck*, and *Angptl4*. HOMER motif analysis in the FOXO1 bound regions identified peaks with great enrichment in FOX motifs (**Figure 16C**). Moreover, many conserved transcription factor binding motifs, such as HNF4α and HNF6 were observed. Beyond the classical hepatic binding motifs, GRE were also enriched in FOXO1 bound regions, recapitulating the ability of FOXO1 factor to recognize potentially genomic regions with enriched GREs.

A: 70% overlap of peaks

FOXO1 1st Repl.

9504 4324 4410

FOXO1 2nd Repl.

B: IDR peaks

FOXO1 1st Repl.

8726 5102 3632

FOXO1 2nd Repl.
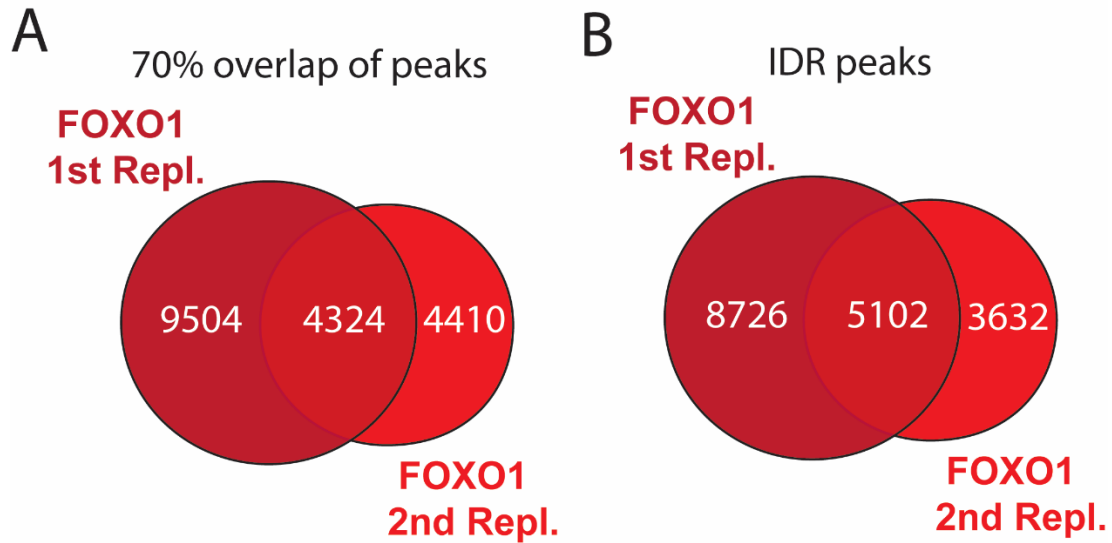
C: HOMER motif analysis in IDR peaks

Motif	Factor	P-value
CTTGTTTACATA	FOX	1E-504
CAGAGGTCAAAGTCCA	HNF4a	1E-275
TAGGGCAAAGGTCA	PPAR/RXR	1E-224
ATTGCGCAAC	C/EBP	1E-205
ATTACGTAATAGTTA	NFIL3	1E-169
GTATTGATCC	HNF6	1E-99
GAGGTCAAAGGTCA	TR4	1E-78
CAGAACATTCTGTTC	GRE	1E-77

Figure 16: Genome-wide binding profile of FOXO1 in caloric restriction reveals gene targets enriched with GRE.

A: Overlap between the two biological replicates (Repl.) from the hepatic FOXO1 ChIP-seq in caloric restriction at the peak of corticosterone levels (ZT12). **B:** IDR analysis displays the reproducible FOXO1 ChIP peaks among the two biological replicates (Repl.). **C:** HOMER motif analysis shows the enriched transcription factor binding sites, which are localized in the FOXO1 ChIP peak coordinates.

4.3.4 GR and FOXO1 binding profile converge on metabolic pathways in caloric restriction

Cistromes for GR and FOXO1 in caloric restriction were compared and revealed a significant overlap of 3071 overlapping IDR peaks (with 70% overlapping genomic coordinates between GR and FOXO1 ChIP-seq) and 1629 IDR peaks (with 70% peak overlap between the IDR caloric restriction unique GR peaks and IDR FOXO1 peaks) (**Figure 17A & 17B**). This confirms that GR and FOXO1 share a large number of binding sites in liver. Representative examples of commonly bound hepatic loci are genes associated with fatty acid metabolism such as *fatty acid binding protein 1* (*Fabp1*), glycogen breakdown, such as phosphorylase enzyme (*Pygl*), circadian clock, such as cryptochrome circadian regulator 1 (*Cry1*) and methionine catabolism such as *s-adenosylmethionine synthase 1a* (*Mat1a*) (**Figure 17C**). Finally, overlap between GR and FOXO1 leads to many commonly bound enhancers and promoters on metabolic genes.
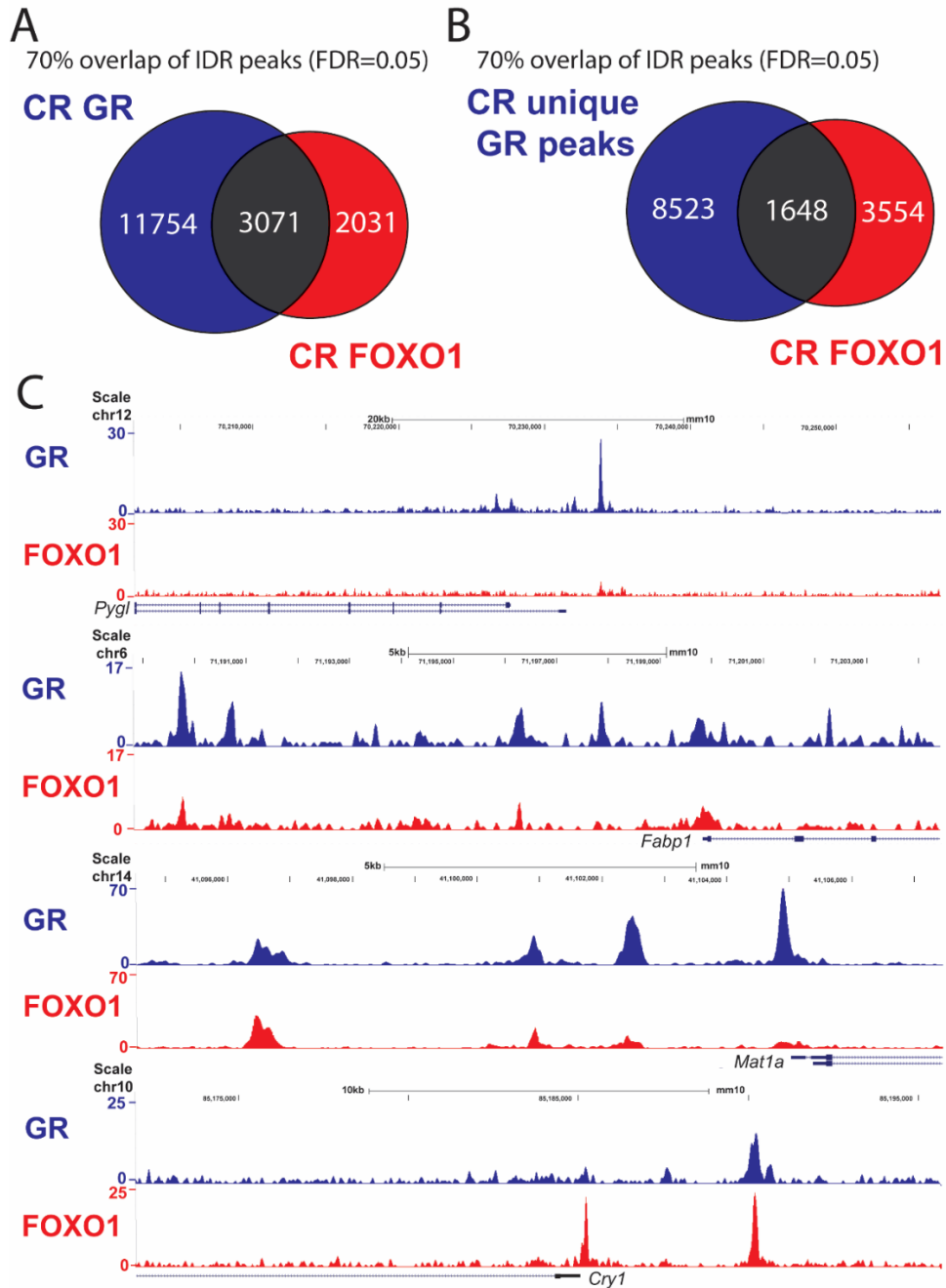
Figure 17: Co-occupancy of GR and FOXO1 at metabolic enhancers and promoters.

A: 70% overlap of CR GR cistrome with the CR FOXO1 cistrome. **B:** 70% overlap of CR unique GR reproducible peaks (after subtracting the AL GR IDR peaks) with the CR FOXO1 cistrome. **C:** Representative ChIP-seq tracks display the common binding of GR and FOXO1 at gene promoters and enhancers related with processes such as fatty acid metabolism, glucose metabolism, glycogen synthesis, methionine metabolism, cholesterol transport and glycolysis in liver. All these ChIP peaks are multiple NGS reads aligned to the mouse mm10 reference genome (**Supplemental Table 1**).

Functional annotation of the commonly bound cis-regulatory elements (peaks) of GR and FOXO1 was performed by ChIP seeker in R in order to cluster them into enriched pathways. For GR and FOXO1, commonly bound regions are located mainly in promoter (22.37%) and intergenic regions (32%) (**Figure 18A**). However, a significant portion of common bound regions are located in intronic regions (**Figure 18A**). Further evaluation of the genomic coordinates of the unique GR and FOXO1 peaks in restriction gave a significant percentage of regions in distal elements (**Figure 18B**). All these unique peaks are distributed far from the transcription start site (TSS) of the genes. More than 70% of these coordinates exceeded 3kb distance downstream and upstream from the transcription start site (**Figure 18B**). The aforementioned peaks were classified into processes related with fatty acid metabolism, cholesterol transport, glucose metabolism (**Figure 18C**). This functional annotation reveals the role of GR and FOXO1 in the regulation of hepatic loci related with the lipid and carbohydrate metabolism. Conclusively, GR and FOXO1 bind cis-regulatory distal elements important for the transition of mice from the lipid homeostasis, which is dominant during their inactive phase to the carbohydrate usage in their active phase.
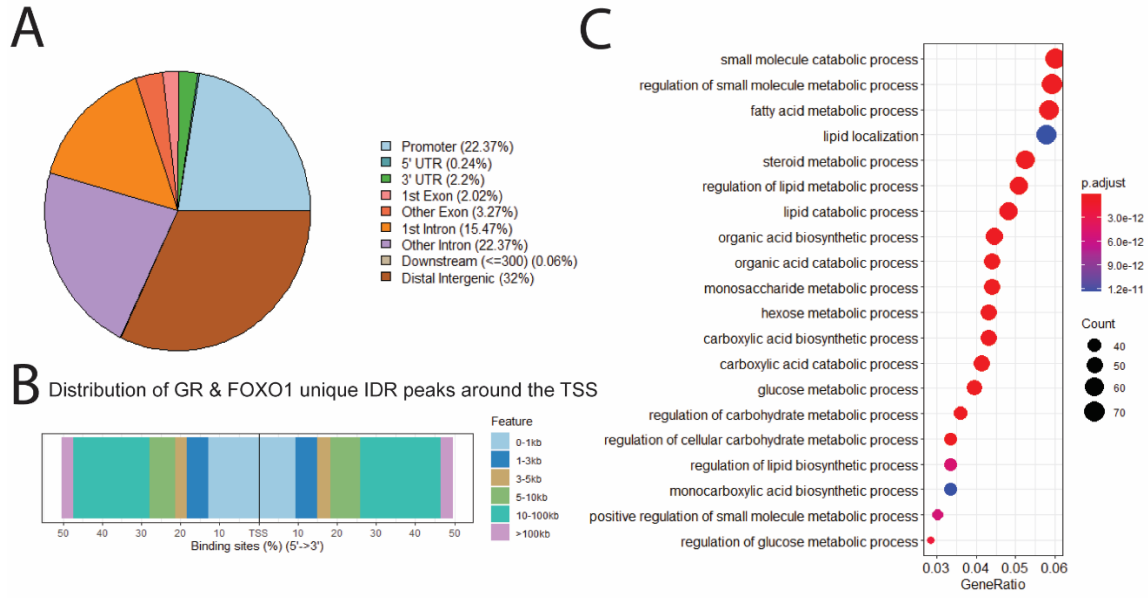
Figure 18: Functional pathway annotation of co-bound loci of GR & FOXO1 in caloric restriction at the peak of glucocorticoids.

A: Annotation of the common GR/FOXO1 bound regions in caloric restriction at the peak of glucocorticoids (ZT12). **B:** Distribution of the commonly bound regions by GR and FOXO1 and their classification by their distance to the transcription start site of the gene targets. **C:** Functional annotation of shared GR-FOXO1 target genes were grouped by GO analysis into pathways. Common ChIP peaks were annotated to the nearest coding gene and clustered into enriched pathways using ChIPseeker annotation tool (Yu et al., 2015).

4.3.5   Transcriptional synergism between GR and FOXO1 in metabolic enhancers in caloric restriction

Analysis of common GR/FOXO1 ChIP regions showed that these factors bind to a great percentage of distal and intronic enhancers. Published data have already shown that GR and FOXO1 are responsible for the activation of promoter regions, such as *Angptl4*, *Pck1* and *Pdk4*. For this reason, in order to elucidate the role between GR and FOXO1 in caloric restriction-related regions, cloned promoters/enhancers, such as *Apoe* and *Apoa4/c3* enhancer region were integrated into constructs upstream of the luciferase promoter. These reporters, were cotransfected together with an overexpressing vector for GR and a constant active FOXO1 mutant (FOXO1ADA) in CV1 cells, which express endogenous GR in low levels (Kitamura et al., 2005). After the transfection of the cells and treatment with dexamethasone, a synthetic glucocorticoid drug, GR/FOXO1ADA transfected cells

treated with dexamethasone gave the maximum luciferase activity in comparison to the vehicle treated cells (**Figure 19**). To conclude with, GR and FOXO1 facilitate transcriptional synergism for these promoter and enhancer regions.
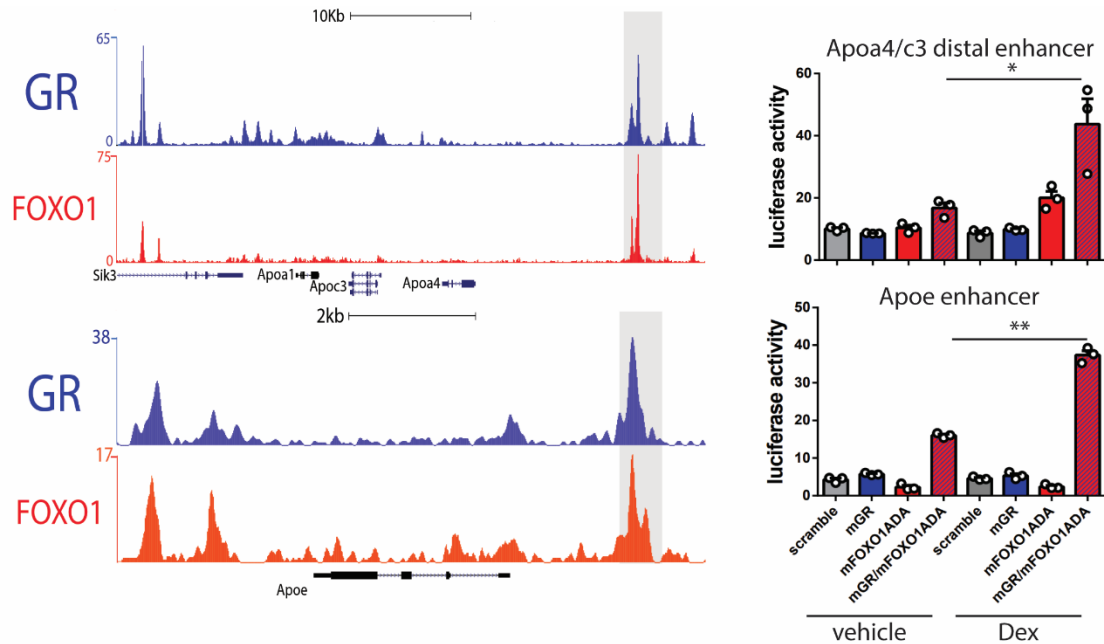
Figure 19: GR and FOXO1 synergism activates enhancer peaks of selected metabolic genes.

A: GR/FOXO1 ChIP tracks from the distal intergenic *Apoa4/c3* enhancer and *Apoe* intergenic enhancer. **B:** Luciferase assay of the cloned genomic gray regions from the respective enhancers in A. The plots represent all the potential combinations of the reporters with co-transfected mGR, constant active mFOXO1ADA, and mix of mGR/mFOXO1ADA in vehicle- and dexamethasone- (Dex) treated CV1 cells. Values represent mean ± SEM, n = 3 replicates. *p<0.05, **p<0.01. Student's t-test.

4.3.6 Genome wide binding profile of hepatic SIN3A overlaps with hepatic GR and FOXO1 upon restriction

GR can either activate or repress gene expression, but its mechanism of action remains unclear. GR can dimerize not only with itself, but also with other co-partners, providing different modes of transcriptional gene regulation. Until now, there are increasing evidence showing GR and FOXO1 synergizing in the transcriptional regulation of energy homeostatic genes, but the role of this nuclear receptor in repression is still a puzzle. Previous study in mice upon high-fat diet showed that hepatic GR was pulled down with the whole SIN3A complex, which has been implicated with FOXO1 repression at the *Gck*

locus (Langlet et al., 2017). Additionally, SIN3A$^{flx;flx}$-Alb-Cre$^+$ (or SIN3A-LKO) showed hepatic steatosis and bile acid deregulation, a similar phenotype described in GR-LKO and FOXO1-LKO mice (Langlet et al., 2017; Matsumoto et al., 2007; Quagliarini et al., 2019). It is thus conceivable that the SIN3A complex can interact with hepatic GR and cause repression in relevant targets.

Hepatic SIN3A complex performs repression in the core-clock machinery BMAL1-CLOCK, when bound to *Per1* promoter (Duong et al., 2011). The maximal binding of this complex is at the peak of corticosterone (ZT12), raising the interest to be examined in association with GR (Duong et al., 2011). The circadian pattern of the hepatic SIN3A complex in the nucleus of caloric restricted WT mice presented a 4 hours shift compared to *ad-libitum* fed mice (peak at ZT12 and ZT16 in the *ad-libitum* and caloric restricted mice, respectively) (**Figure 20A & 20B**). Interestingly, genome-wide binding profile of the hepatic SIN3A catalytic subunit at the peak of glucocorticoids (ZT12) upon low-fat diet in mice showed a massive binding in many gluconeogenic and lipid-homeostatic genes. Intersection between the two biological replicates had 14102 common overlapping ChIP peaks (**Figure 20C**). IDR analysis of the same biological replicates produced 13269 reproducible peaks upon low-fat diet. (**Figure 20C**). However, genome-wide binding profile of hepatic SIN3A in caloric restriction gave a significantly lower number of ChIP peaks (**Figure 20C**). IDR analysis in the same biological replicates produced 8990 reproducible ChIP peaks in restriction (**Figure 20C).**
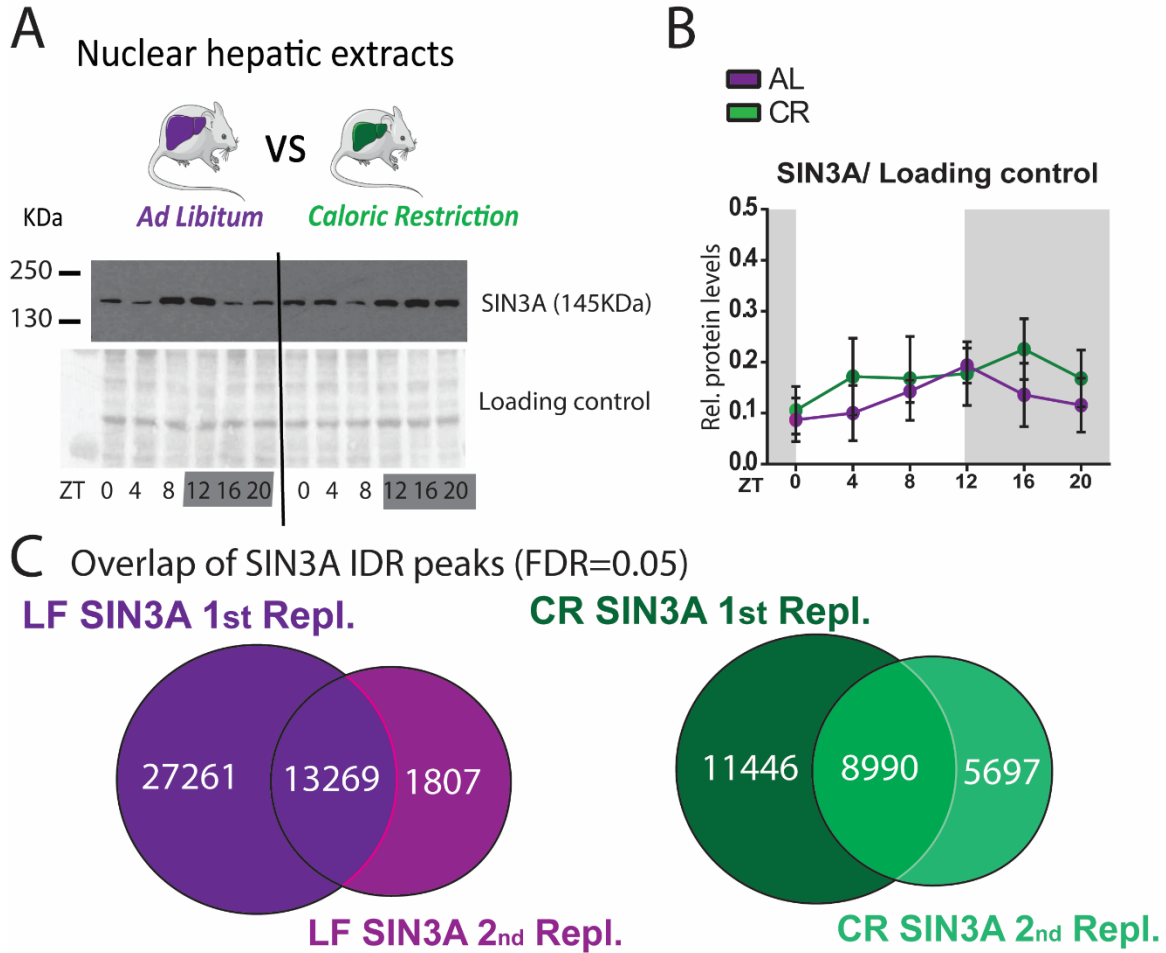
Figure 20: Genome-wide binding profile of SIN3A in caloric restriction reveals a reduced genome-wide binding profile.

A: Western blot in nuclear hepatic extracts from control-fed and restricted mice detecting total SIN3A, and amido black staining was used as a loading control. **B:** Quantification of nuclear hepatic SIN3A levels normalized over the loading control. **C:** Overlap of the two biological replicates of SIN3A ChIP-seq in both control-fed and restricted mice.

Overlap of hepatic SIN3A between low-fat diet and caloric restriction showed roughly 4279 common IDR ChIP peaks between the two conditions (**Figure 21A**). Additionally, performing HOMER motif analysis in the IDR SIN3A peaks in both conditions showed an increased recognition of GC-rich motifs in caloric restriction, such as ELF, ELK, KLF, and SP motifs (**Figure 21B**). In the case of caloric restriction, absence of oxidative stress may lead the SIN3A complex to recognize GC-rich regions in order to protect from potential genome instability. Furthermore, FOX and GRE motifs were less statistical significantly enriched in restriction compared to control-fed mice (**Figure 21D**). Interestingly,

PPAR/RXR motifs were greatly enriched motifs in the unique peaks in low-fat diet. Simultaneously, FOX and GRE motifs were more enriched in this condition showing an increased recognition of common GR/FOXO1 peak regions. In the common IDR peaks, there were many transcription factor motifs related with oxidative stress such as NRF motif, circadian clock, such as BMAL1/CLOCK motif and proliferation, such as ELK/ETS/FLI motifs (**Figure 21B**). In the unique CR SIN3A IDR peaks were mainly GC-rich motifs, beyond the classical hepatocyte specific motifs (**Figure 21D**).

A: HOMER motif analysis in IDR peaks (FDR=0.05)
LF SIN3A / **CR SIN3A**
8990 | 4279 | 4395

B: common peaks

Motif	Factor	P-value
	ELK/FLI/ETS	1E-61
	SP/KLF	1E-43
	NFY	1E-20
	E2F4	1E-12
	RFX	1E-11
	NRF	1E-9
	BMAL1/CLOCK	1E-9
	STAT	1E-7

C: unique peaks in LF

Motif	Factor	P-value
	C/EBP	1E-42
	HNF4a	1E-40
	PPAR/RXR	1E-39
	HNF6	1E-39
	FOX	1E-37
	ELK/FLI/ETS	1E-33
	NFIL3	1E-32
	GRE	1E-26

D: unique peaks in CR

Motif	Factor	P-value
	NFY	1E-24
	SP/KLF	1E-20
	ELK/FLI/ETS	1E-15
	NFIL3	1E-12
	C/EBP	1E-12
	HNF6	1E-8
	FOX	1E-7
	GRE	1E-7

Figure 21: Genome-wide binding profile for hepatic SIN3A overlaps with GR and FOXO1 ChIP peaks at metabolic enhancers and promoters.

A: HOMER analysis in caloric restriction presents the enriched transcription factor binding motifs. **B:** HOMER analysis in common SIN3A IDR peaks presents the enriched transcription factor binding motifs which are recognized in both conditions. **C:** HOMER analysis in low-fat diet unique peaks presents the enriched transcription factor binding motifs only in this condition. **D:** HOMER analysis in caloric restriction unique peaks presents the enriched transcription factor binding motifs only in this condition.

Overlap of SIN3A catalytic subunit with GR and FOXO1 unraveled 201 common IDR ChIP peaks in restriction (**Figure 22A**). For the overlap of the IDR peaks between the three factors were used 70% of their genomic coordinates (**Figure 22A**). Annotation of these common regions gave a great percentage in promoter regions (roughly 65.17%), while a small percentage was close to intronic and intergenic regions (**Figure 22B**). Gene ontology of these genes in the common GR/FOXO1/SIN3A peaks gave enrichment of pathways-related with insulin resistance, circadian rhythms, fatty acid degradation, autophagy, and longevity (**Figure 22C**).

A: 70% overlap of IDR peaks (FDR=0.05)

CR unique GR peaks — 8061, 1447, 3179 — CR FOXO1

201, 462, 375

CR unique SIN3A peaks — 3357

B:
- Promoter (<= 1kb) 65.17%
- Promoter (1-2kb) 6.97%
- Promoter (2-3kb) 2.99%
- 3' UTR 1.49%
- 1st Exon 1.99%
- Other Exon 1.49%
- 1st Intron 4.98%
- Other Intron 5.97%
- Distal Intergenic 8.96%

C:

Term	P-value	Genes
Insulin resistance	5.55E-06	Ppp1cb;Nfkbia;Mlxipl;Creb3l3;Irs1;Insr;Irs2;Ppara
Circadian rhythm	7.43E-06	Per2;Per3;Bhlhe40;Nr1d1;Arntl
Adipocytokine signaling pathway	3.74E-04	Nfkbia;Irs1;Acsl1;Irs2;Ppara
Fatty acid degradation	5.71E-04	Hadhb;Acaa2;Aldh2;Acsl1
Autophagy	0.001435	Sh3glb1;Irs1;Dapk2;Rb1cc1;Irs2;Bcl2l1
Fatty acid elongation	0.001733	Hadhb;Acaa2;Elovl5
Longevity regulating pathway	0.002192	Creb3l3;Irs1;Insr;Rb1cc1;Irs2
Non-alcoholic fatty liver disease	0.002675	Mlxipl;Bcl2l11;Irs1;Insr;Irs2;Ppara
Human T-cell leukemia virus 1 infection	0.00353	Nfkbia;Creb3l3;Canx;E2f3;Tcf3;Mad1l1;Bcl2l1
PPAR signaling pathway	0.0043	Acox2;Acsl1;Ppara;Apoa5

Figure 22: Genome-wide binding profile of hepatic SIN3A overlaps with GR and FOXO1 ChIP peaks at metabolic enhancers and promoters in caloric restriction at the peak of corticosterone levels (ZT12).

A: Intersection of GR/FOXO1/SIN3A IDR ChIP peaks in caloric restriction. **B:** Annotation of the GR/FOXO1/SIN3A common peaks. **C:** KEGG pathway ontology of common GR/FOXO1/SIN3A ChIP peaks in caloric restriction using EnrichR tool. Next to each p-value, were aligned representative genes, which belong to the relevant pathway.

Among the three different factors, the common GR/FOXO1/SIN3A ChIP peaks pointed out that these factors can recognize many interesting insulin- and longevity-related genes, revealing a novel role in caloric restriction. Representative ChIP-tracks from all these factors revealed that GR/FOXO1/SIN3A were bound in genomic enhancers and promoters of genes, such as *Bmal1* (*Arntl*), and *Per2* (**Figure 23**). Even though, the small overlap of hepatic SIN3A catalytic subunit with GR/FOXO1 targets, this complex can bind common peaks with these transcription factors in genes related with longevity, circadian rhythms and insulin resistance.
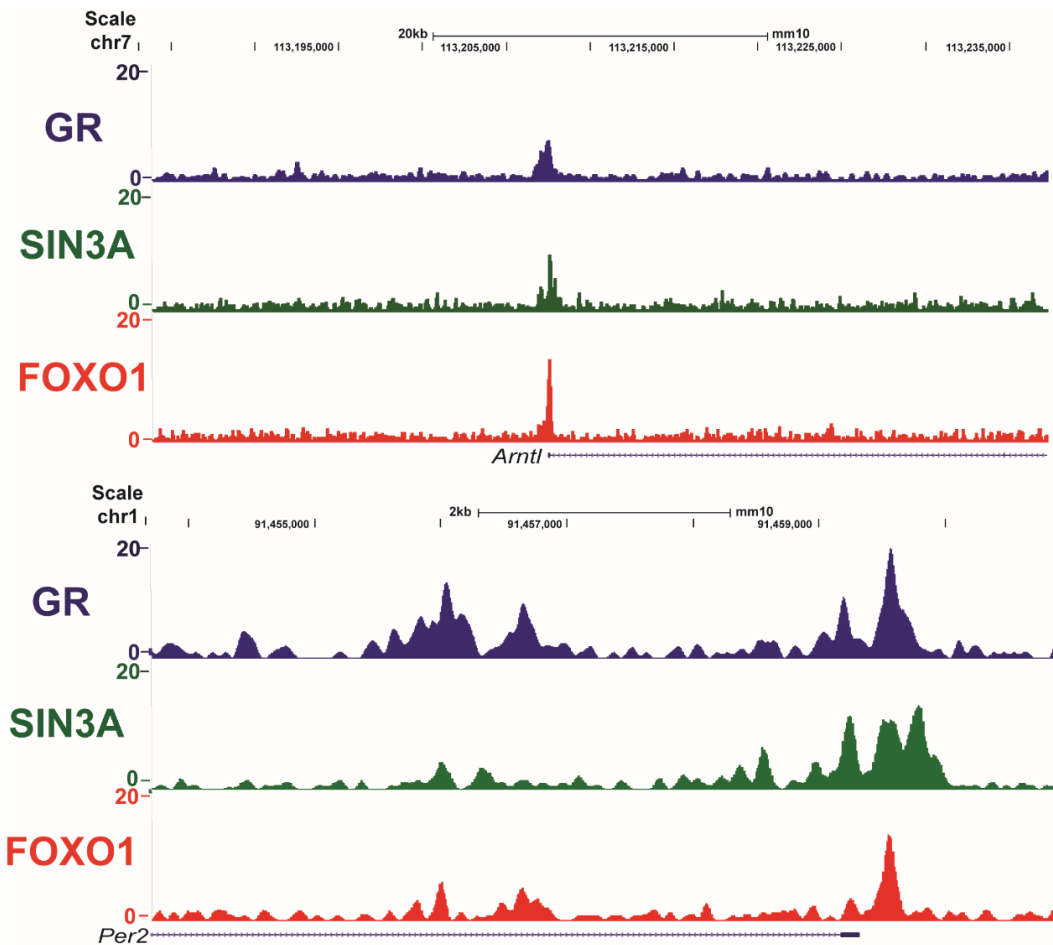
Figure 23: Genome-wide binding profile of hepatic SIN3A overlaps with GR and FOXO1 ChIP peaks at circadian clock-related enhancers and promoters.

ChIP tracks from GR/FOXO1/SIN3A in restriction at two classical circadian clock-related promoters, *Arntl* (known as *Bmal1*) and *Per2* locus, at the peak of corticosterone levels.

4.4 Transcriptomic analysis in caloric restricted WT mice showed the gained GR peaks in genes at the peak of corticosterone

The first aim of this thesis was to identify the connection between caloric restriction and hepatic glucocorticoid receptor. For this reason, WT mice in control (*ad-libitum*) diet and caloric restriction were sacrificed in order to collect their livers at the peak of corticosterone (ZT12) and RNA was extracted for further sequencing. DEseq analysis showed that there were 3195 up-regulated and 3124 down-regulated genes that they were differentially expressed between *ad-libitum* and caloric restriction (**Figure 24A**). A combined analysis of differentially expressed genes exhibiting a binding sequence for GR AL and CR conditions showed 4654 maintained GR ChIP peaks between the two conditions, while 10171 gained GR ChIP peaks in caloric restriction (**Figure 13A**). Filtering the RNA-seq data using the GR cistromes, there were 1479 up-regulated and 1058 down-regulated genes associated with a gained GR ChIP peak in their vicinity (**Figure 24B and 24C**). Interestingly, Kegg pathway annotation analysis by EnrichR pointed cholesterol metabolism, FoxO signaling, AMPK signaling, circadian rhythms and longevity, as top up-regulated processes (**Figure 24B**). In opposite, genes involved in the regulation of peroxisome, bile acid biosynthesis, PPAR signaling and cancer-related pathways were down-regulated (**Figure 24C**). Additionally, glycine, serine and threonine metabolism were also down-regulated. All these processes were already connected with caloric restriction and the induction of pathways related with longevity (Cantó & Auwerx, 2009; Gredilla & Barja, 2005; Ma et al., 2020; Madeo et al., 2019; Roth et al., 2006). Surprisingly, 46.3% of up- and 33.8% of down-regulated genes with a gained GR ChIP peak (**Figure 24D**). In parallel, 26.7% of up- and 18.9% of down-regulated genes were associated with a maintained GR ChIP peak in both conditions (**Figure 24D**). A great percentage of down- and up-regulated genes in caloric restricted WT mice are associated with a gained GR ChIP peak. To conclude with, caloric restriction enhances the hepatic GR binding in many novel genes.

A: ZT12 (Peak of corticosterone levels)

B KEGG pathways

Up-regulated genes (n=1479)	Adj. P-value	Example genes
Cholesterol metabolism	2.21E-06	Scarb1;Abcg8
FoxO signaling pathway	1.43E-04	Cdkn1a;Foxo1
AMPK signaling pathway	1.92E-04	Lepr;Cd36
MAPK signaling pathway	1.92E-04	Flt1;Elk4
Circadian rhythm	4.49E-04	Cry1;Arntl
Insulin resistance	5.74E-04	Pik3ca;Pck1
Fluid shear stress and atherosclerosis	1.24E-03	Ass1;Vegfa
Renal cell carcinoma	1.26E-03	Cdkn1a;Ep300
Longevity regulating pathway	1.68E-03	Irs2;Atf4
Arginine biosynthesis	3.33E-03	Cps1;Arg1

C KEGG pathways

Down-regulated genes (n=1058)	Adj. P-value	Example genes
Peroxisome	2.04E-06	Agxt;Slc27a2
Primary bile acid biosynthesis	2.11E-03	Cyp7b1;Cyp7a1
Thyroid cancer	7.14E-03	Gadd45a;Mapk3
PPAR signaling pathway	7.14E-03	Cpt1a;Acox2
Glyoxylate and dicarboxylate metabolism	7.14E-03	Pcca;Agxt
Glioma	7.14E-03	Rb1;Map2k1
Hepatitis C	1.04E-02	Pik3r1;Rxra
Adherens junction	1.22E-02	Actn1;Egfr
Non-small cell lung cancer	1.24E-02	Cdk4;E2f3
Glycine, serine and threonine metabolism	3.08E-02	Agxt2;Pgam1

Legend (Panel D):
- Up-regulated genes in CR over AL (n=3195)
- Genes with a gained GR peak in CR (n=1479)
- Genes with a maintained GR peak in AL/CR (n=852)
- Down-regulated genes in CR over AL (n=3124)
- Genes with a gained GR peak in CR (n=1058)
- Genes with a maintained GR peak in AL/CR (n=592)

Figure 24: Caloric restriction deregulates genes which are associated with gained and maintained GR ChIP peaks at the peak of corticosterone.

A: Volcano plot showing up-regulated and down-regulated transcripts in caloric restricted compared to control-fed WT mice at the peak of corticosterone levels (at ZT12), FDR <0.05, marked the transcripts with log2foldchange >1, n=3 biological replicates. All transcripts are deregulated with statistical significance less than 0.05. Transcripts for both up- and down-regulated genes are marked as examples. **B:** Functional annotation KEGG pathway analysis by EnrichR in up-regulated genes, which have a gained GR ChIP peak in their vicinity. **C:** Functional annotation KEGG pathway analysis by EnrichR in down-regulated genes, which have a gained GR ChIP peak in their vicinity. **D:** Percentage of genes which are up- and down-regulated in caloric restriction over *ad-libitum* condition and percentage of genes associated with a gained GR peak in caloric restriction and a maintained GR peak in both conditions. AL: *Ad-Libitum*, CR: Caloric Restriction.

5.1 Transcriptomic analysis in caloric restricted GR-LKO mice showed regulation of energy-homeostatic genes at the peak of corticosterone

The second aim of this thesis was to identify those pathways which mediate the caloric restriction response that are altered by the loss GR activity in the liver and to connect the gene expression analysis with GR/FOXO1 DNA binding. For this reason, mice with depletion of hepatic GR (GR-LKO) were restricted following the already described protocol. GR can bind to the target genes based on the ligand availability. Maximum binding of GR is expected at the peak of circulating corticosterone. For FOXO1 is important to be mentioned that maximum binding of this factor is detected upon absence of insulin signaling. So FOXO1 is related to fasting and insulin secretion leads to its cytoplasmic sequestration by the PI3K/AKT phosphorylation. Loss of FOXO1 binding can be detected after food consumption. Based on these considerations, RNA-seq was performed in restricted GR-LKO mice selecting the peak of corticosterone (at ZT12) and 4hr after food intake (at ZT16), in the middle of the post-prandial state. With these two timepoints, it is easier to understand if the restricted GR-LKO mice show an aberrant regulation of energy-homeostatic genes and an altered post-prandial response.

As expected, mice were grouped in both timepoints based on the genotype and nutritional status (**Figure 25A & 25B**). So, they were almost distinct based on the genotype and unfed and fed mice were also separated, when they were included in the same plot in the principal component analysis (**Figure 25C**). Based on the PCA analysis, 2 different mice were excluded, because they were identified as outliers in both timepoints (at ZT12 KO3 & at ZT16 WT1). So, the PCA analysis allowed the distinction from the unfed and fed mice and the GR-LKO and WT mice as well.
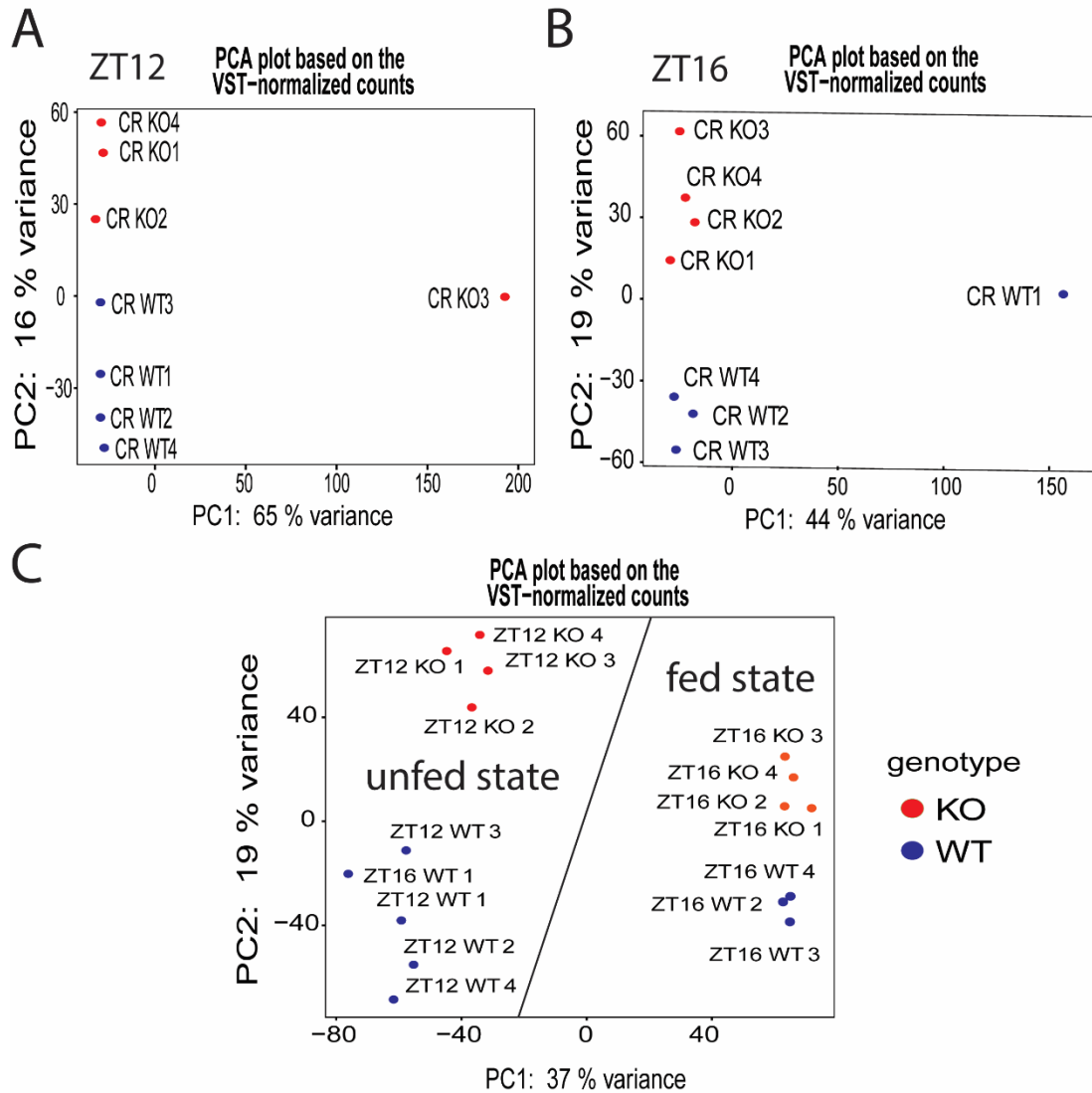
Figure 25: PCA analysis of liver RNA-seq samples based on genotype and feeding status.

A: Principal component analysis (PCA) at the peak of corticosterone levels from RNA-seq data coming from livers of *ad-libitum* fed and restricted WT vs GR-LKO mice. **B:** Principal component analysis from RNA-seq data from liver samples after 4hr of feeding of normal-fed and restricted mice. **C:** Principal component analysis from all the liver samples in both timepoints, at ZT12 and ZT16.

Firstly, DEseq analysis was performed to identify deregulated genes in the caloric restricted GR-LKO compared with the WT mice. In order to study the genes, which were GR- targets in caloric restriction, analysis was performed in the gained GR ChIP peaks, subtracting the common ChIP peaks from the *ad-libitum* condition. Using this analysis, there was sub-selection of genes that they have annotated in their vicinity a gained GR

ChIP peak in caloric restriction. These 10171 gained GR ChIP sites are associated with 4924 genes. The gene overlap between caloric restricted GR-LKO mice versus WT mice showed 515 down-regulated and 541 up-regulated genes (**Figure 26A and 26B**). In total, the gained GR binding sites had overlap with 48.1% (541/1125) of the down-regulated and 57.6% (515/894) of the up-regulated genes (**Figure 26C**). Functional Kegg pathway annotation analysis using EnrichR showed enrichment of processes related to PPAR signaling, peroxisome pathway, fatty acid degradation, butanoate metabolism and catabolism of specific amino acids for up-regulated genes (**Figure 26A**). In the case of down-regulated genes, pathways such as FOXO1 signaling, AMPK signaling and glucagon signaling, circadian rhythms, HIF-1 signaling (related with hypoxia) and arginine biosynthesis were up-regulated (**Figure 26B**). This primary analysis showed that the gained GR ChIP peaks are connected with 48.1% of the down-regulated and 57.6% of the up-regulated genes in GR loss and are associated with processes, such as circadian rhythms, fatty acid catabolism, PPARα and FOXO1 signaling.

A KEGG pathways

Up-regulated genes (n=541)	Adj. P-value	Example genes
PPAR signaling pathway	2.13E-10	Slc27a1;Cpt1a
Peroxisome	5.49E-09	Abcd2;Slc27a2
Fatty acid degradation	5.49E-09	Adh4;Acox1
Butanoate metabolism	2.08E-06	Bdh2;Bdh1
Valine, leucine and isoleucine degradation	2.46E-06	Mcc2;Agxt2
Glyoxylate and dicarboxylate metabolism	4.13E-05	Gcsh;Mcee
Propanoate metabolism	9.98E-05	Acss3;Mcee
Tryptophan metabolism	4.70E-04	Aldh3a2;Gcdh
Biosynthesis of unsaturated fatty acids	2.03E-03	Fads2;Elovl5
Synthesis and degradation of ketone bodies	2.57E-03	Bdh2;Bdh1

B KEGG pathways

Down-regulated genes (n=515)	Adj. P-value	Example genes
Arginine biosynthesis	3.25E-03	Got1;Cps1
HIF-1 signaling pathway	3.25E-03	Eno1;Aldob
Cysteine and methionine metabolism	3.38E-03	Got1;Mat1a
Circadian rhythm	7.89E-03	Clock;Arntl
FoxO signaling pathway	7.89E-03	Crebbp;Cdkn1a
Glucagon signaling pathway	1.97E-02	Ppargc1a;Foxo1
Pathogenic Escherichia coli infection	2.32E-02	Jun;Il1r1
AMPK signaling pathway	3.63E-02	Pck1;Acacb
Transcriptional misregulation in cancer	4.35E-02	Cdkn1a;Foxo1
Glycolysis / Gluconeogenesis	4.41E-02	Eno1;Aldob

Figure 26: Half of the deregulated genes in caloric restricted deleted GR liver are associated with a gained GR ChIP peak at the peak of corticosterone (ZT12).

A-B: Functional annotation KEGG pathway analysis by EnrichR in up-regulated genes (A) and down-regulated genes (B).

At second level, the RNA-seq in caloric restricted GR-LKO mice were overlapped with GR/FOXO1 peak in order to identify direct targets of GR/FOXO1 axis. The ChIP-seq analysis for GR/FOXO1 in caloric restriction provided information about the binding of the factors in 3071 common promoters/enhancers, associated with 1924 genes. Overlap with the RNA-seq helped to narrow down the number of targets. This analysis focused on the common GR/FOXO1 targets, which were deregulated in the caloric restricted GR-LKO mice. Functional pathway annotation of the up-regulated transcripts using EnrichR showed enrichment in KEGG pathways for both ZTs of interest. Interestingly, at the peak

of corticosterone (ZT12) GR-LKO mice showed a great number of up-regulated genes related to fatty acid catabolism, peroxisome and PPAR signaling. It is known that GR represses PPAR signaling, so absence of GR leads to more active PPAR signaling in the liver (Quagliarini et al., 2019) (**Figure 27A and 27B**). In parallel, ABC transporters are up-regulated, while there is a shift in amino acid catabolism in the caloric restricted GR-LKO mice (**Figure 27A and 27B**). These mice also show a preference for elevating valine, leucine, isoleucine, tryptophan, glycine, serine and threonine catabolism in order to sustain their energy needs (**Figure 27A and 27B**). KEGG pathways for the down-regulated transcripts were related to lipid homeostasis, cell cycle progression, circadian rhythms, and differential usage of amino acids (**Figure 27A and 27C**). As lipid homeostatic pathways were FoxO signaling and endocytosis, while significant genes related with glycolysis/gluconeogenesis were dampened as well (**Figure 27A and 27C**). Beyond endocytosis, autophagy was another down-regulated pathway, crucial for the cycling of proteins and lipids. The down-regulation of autophagy implies that caloric restriction may be defective in the liver of the GR-LKO mice. Overlap of the GR/FOXO1 ChIP-seq data and RNA-seq data in this timepoint showed that 24% (275/1167 genes) of the down- and 34% (271/794 genes) of up-regulated transcripts are bound by both factors. Conclusively, the absence of hepatic GR impacts on the energy homeostasis usage and the deregulation of the circadian clock, which are tightly connected with the top KEGG pathways between the down- and the up-regulated genes.

A ZT12 (Peak of corticosterone levels)

B KEGG pathways

Up-regulated genes (n=271)	Adj. P-value	Example Genes
PPAR signaling pathway	2.30E-10	Apoa2;Fabp1
Peroxisome	1.10E-07	Hmgcl;Acox1
Fatty acid degradation	5.26E-06	Aldh3a2;Cpt1a
Synthesis and degradation of ketone bodies	5.26E-06	Hmgcl;Bdh2
Butanoate metabolism	6.91E-05	Bdh2;Bdh1
Valine, leucine and isoleucine degradation	1.20E-04	Acat1;Bcat2
Bile secretion	6.40E-03	Abcc3;Cyp7a1
Biosynthesis of unsaturated fatty acids	1.13E-02	Fads2;Elovl5
Glyoxylate and dicarboxylate metabolism	1.52E-02	Shmt1;Cat
Glutathione metabolism	2.08E-02	Gpx1;Nat8

C KEGG pathways

Down-regulated genes (n=275)	Adj. P-value	Example Genes
FoxO signaling pathway	5.87E-02	Cdkn1b;Foxo1
Glucagon signaling pathway	5.87E-02	Pygl;Acacb
Insulin resistance	5.87E-02	Nfkbia;Stat3
Aldosterone synthesis and secretion	7.40E-02	Camk2b;Scarb1
Ferroptosis	7.40E-02	Map1lc3b;Slc40a1
Autophagy	7.40E-02	Vmp1;Ctsl
Lipid and atherosclerosis	7.40E-02	Nfkbia;Camk2b
Arginine biosynthesis	7.40E-02	Cps1;Arg1
Cholesterol metabolism	7.77E-02	Cyp27a1;Scarb1
Circadian rhythm	1.15E-01	Per1;Cry1

Figure 27: Caloric restricted GR-LKO mice presented altered energy-homeostatic re;ated gene levels at the peak of corticosterone.

A: Volcano plot showing up-regulated and down-regulated transcripts in caloric restricted GR-LKO compared to wild type mice at the peak of corticosterone levels (at ZT12), FDR <0.05, n=3-4 biological replicates. All transcripts are deregulated with statistical significance less than 0.05. Transcripts for both up- and down-regulated genes are marked as examples. **B-C:** Functional annotation KEGG pathway analysis by EnrichR in up-regulated (B) and in down-regulated genes (C).

5.2 Transcriptomic analysis of post-prandial response of restricted GR-LKO mice shows increase in liver glycogen storage and defective lipid clearance

KEGG pathways by EnrichR in caloric restriction after 4 hours of feeding (at ZT16) showed significant up-regulated transcripts related with processes similar to the previous timepoint (ZT12). Among the gained GR ChIP peaks in caloric restriction, 241 and 335 genes were up- and down-regulated, respectively, in caloric restricted GR-LKO mice, at ZT16. Interestingly, there was 59.5% (241/405 genes) and 54.5% (335/615 genes) overlap with the gained GR ChIP peaks for the down- and up-regulated genes respectively. This observation proves that there is at least one gained GR ChIP peak in the half number of the targets, which were deregulated in the absence of hepatic GR in caloric restriction post-prandially. PPAR signaling, fatty acid catabolism, amino acid catabolism, butanoate metabolism, glutathione metabolism, and elongation of fatty acids were top up-regulated

processes (**Figure 28A**). In this case, feeding promotes the fatty acid elongation for the storage of fat in the liver and the glutathione metabolism, which involves enzymes for controlling the redox-state of hepatocytes (**Figure 28A**). Glucocorticoids control the fat catabolism and combined with NFκB signaling modulate the glutathione metabolism changing the redox state of the hepatocytes (Djordjevic et al., 2010; Macfarlane et al., 2008). So, the absence of hepatic glucocorticoid receptor in caloric restriction can reverse these pathways. In the opposite, cholesterol metabolism, cysteine and methionine metabolism, circadian rhythms, fat digestion/absorption, the pluripotency of stem cells and the TGF-β signaling, which modulate the hepatocyte identity, were down-regulated. An increased TGF-β signaling is associated with liver injuries and promotes lipogenesis, leading the hepatocytes to a fibrogenic program (Breitkopf et al., 2006; Yang et al., 2014). The reduction of these pathways indicates that hepatocytes of the GR-LKO mice maintain a specific hepatocyte identity protected from the initiation of a fibrogenic program. Based on the aforementioned, the absence of hepatic GR deregulates processes related with the fat and amino acid catabolism and more than half of the deregulated genes are linked with a gained GR ChIP peak post-prandially.

A KEGG pathways

Up-regulated genes (n=335)	Adj. P-value	Example genes
Peroxisome	1.46E-09	*Abcd2;Abcd3*
PPAR signaling pathway	2.31E-09	*Cd36;Angptl4*
Biosynthesis of unsaturated fatty acids	1.85E-05	*Fads1;Acot4*
Fatty acid degradation	2.98E-05	*Cpt1a;Acox1*
Tryptophan metabolism	2.72E-04	*Gcdh;Maob*
Propanoate metabolism	7.65E-04	*Acss2;Acox1*
Glutathione metabolism	1.53E-03	*Gsta2;Idh2*
Fatty acid elongation	2.29E-03	*Elovl5;Acot4*
Butanoate metabolism	2.44E-03	*Bdh2;Hadh*
Valine, leucine and isoleucine degradation	3.44E-03	*Mcee;Hadh*

B KEGG pathways

Down-regulated genes (n=241)	Adj. P-value	Example genes
Cysteine and methionine metabolism	3.03E-05	*Bhmt;Sds*
Cholesterol metabolism	3.24E-03	*Apoh;Apoa4*
Pluripotency of stem cells	4.46E-03	*Acvr1;Id3*
Glycine, serine and threonine metabolism	6.28E-03	*Cbs;Sdsl*
Fat digestion and absorption	7.76E-02	*Abca1;Scarb1*
Arginine biosynthesis	8.27E-02	*Got1;Arg1*
TGF-beta signaling pathway	1.49E-01	*Id3;Smad7*
Mineral absorption	1.49E-01	*Atp1a1;Atp1b1*
Circadian rhythm	1.49E-01	*Per1;Clock*
Acute myeloid leukemia	1.79E-01	*Pim1;Ppar δ*

Figure 28: More than half number of the deregulated genes in hepatic GR loss in caloric restriction is associated with a gained GR ChIP peak 4 hours after feeding.

A-B: Functional annotation KEGG pathway analysis by EnrichR in up-regulated (A) and in down-regulated genes (B).

Secondarily, filtering the RNA-seq at ZT16 using the common GR/FOXO1 ChIP peaks, there was a focus on the GR/FOXO1 targets after feeding in caloric restriction (post-prandially). In this analysis, GR-LKO mice present up-regulated transcripts in fatty acid catabolism, in PPAR signaling and amino acid catabolism (**Figure 29A and 29B**). These mice cannot switch from energy sources related with fasting which were detected at ZT12. Butanoate (or butyrate) metabolism is another pathway activated at both ZT12 and ZT16

in these mice. Butanoate metabolism is fasting-dependent and can be boosted by prolonged fasting (Shimazu et al., 2013). Butanoate metabolism is connected with all the short-chain fatty acids and short chain alcohols produced by the intestinal fermentation (Donohoe et al., 2011). All these fermented products can be used for the production of ketones bodies, such as β-hydroxybuterate (Donohoe et al., 2011; Shimazu et al., 2013). Moreover, the arachidonic metabolism and steroid hormone synthesis are activated (**Figure 29A and 29B**). In physiological conditions, circulating glucocorticoids activate gluconeogenesis and lipid immobilization for the production of energy and the expression of enzymes which contribute to their own biosynthesis in the liver (Sanderson, 2006; Vegiopoulos & Herzig, 2007). Glucocorticoids are responsible for the expression of steroidogenic enzymes, such as cytochrome P450 enzymes (CYPs), hydroxysteroid dehydrogenases (HSDs), and steroid reductases, which synthesize from cholesterol steroid hormones (Sanderson, 2006; Vegiopoulos & Herzig, 2007). During fasting or caloric restriction, adrenal glands secrete corticosterone favoring the steroid hormone synthesis. For this reason, the absence of hepatic GR in caloric restriction can boost the expression of these enzymes as a compensatory mechanism in order to increase the ligand availability. However, in the case of down-regulated enriched pathways cholesterol transport was one of the top pathways affected by the absence of GR in caloric restriction (**Figure 29C**). Caloric restricted GR-LKO mice showed also down-regulation of transcripts associated with sucrose and starch metabolism, Wnt signaling, FOXO1 signaling, glycolysis/gluconeogenesis, and aldosterone synthesis and secretion (**Figure 29C**). Concerning amino acid metabolism, fed GR-LKO mice upon caloric restriction showed a preference for suppressing catabolizing enzymes related to glycine, serine and threonine (**Figure 29C**). Combined analysis of GR/FOXO1 ChIP-seq and RNA-seq at ZT16 showed 22.3% (137/615 genes) and 44.9% (182/405 genes) overlaps for up- and down-regulated genes, respectively, in caloric restriction. To conclude, fed GR-LKO (ZT16) mice continue to catabolize fatty acids from the breakdown of lipids, present an altered amino acid catabolism usage and produce and degrade more ketones, while they present aberrant cholesterol transport and dampened FoxO signaling.
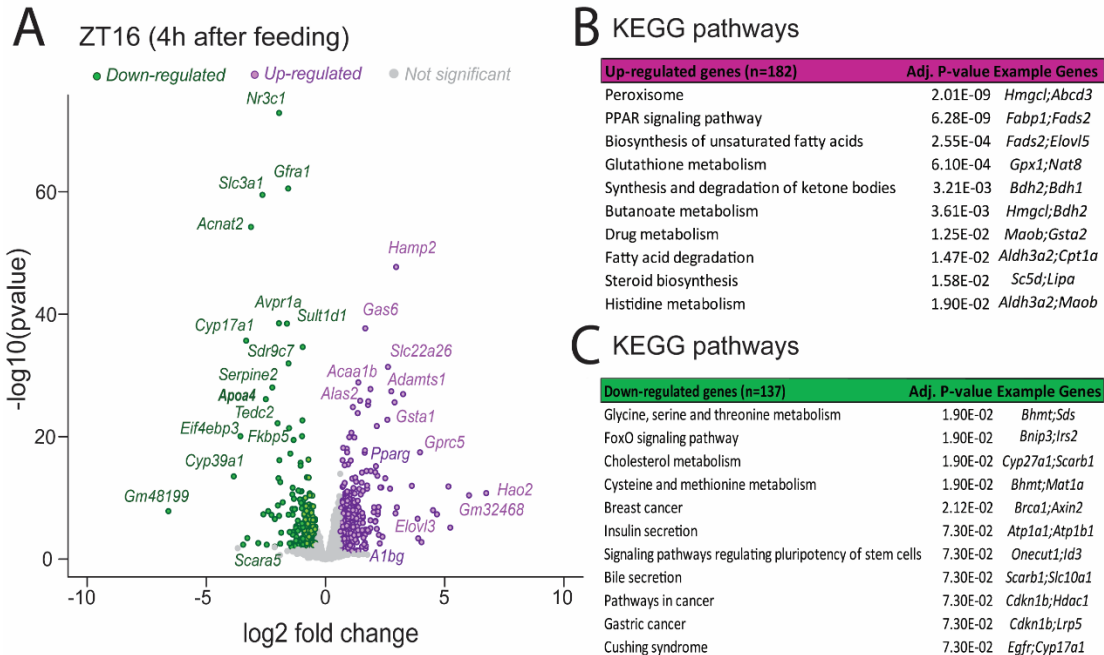
Figure 29: Caloric restricted GR-LKO mice present altered energy-homeostatic gene levels after 4hr of feeding post-prandially.

A: Volcano plot showing up-regulated and down-regulated transcripts in caloric restricted GR-LKO compared to wild type mice 4hr after feeding (at ZT16), FDR <0.05, n=3-4 biological replicates. All transcripts are deregulated with statistical significance less than 0.05. Transcripts for both up- and down-regulated genes are marked as examples. **B-C:** Functional annotation pathway analysis by EnrichR in up-regulated (B) down-regulated genes (C).

5.3   GR-LKO mice presented inactive AKT/FOXO1 signaling in caloric restriction

GR is responsible for the increased expression of the FOXO1 factor and restricted GR-LKO mice showed down-regulation of the FOXO signaling pathway. GR and FOXO1 are necessary for the activation of the gluconeogenesis and other downstream factors, such as cell cycle genes, lipid transporters and metabolism of amino acids (Cournarie et al., 1999; Kalvisa et al., 2018; Kuo et al., 2013; Quagliarini et al., 2019). RNA-seq data in both at ZT12 (peak of hormones) and ZT16 (4h after feeding) showed a clear down-regulation of this pathway (**Figure 27C and 29C**). It is also known that FOXO1 affects the upstream signaling closing the loop of its activation. AKT kinase is upstream of FOXO1 factor and capable of phosphorylating this substrate. Upon feeding/insulin or growth factor stimulation, activation by phosphorylation of AKT kinase at Ser473 leads to subsequent phosphorylation of FOXO1 and its nuclear exclusion (Alessi et al., 1996; Calnan & Brunet,

2008; Kousteni, 2012; Matsuzaki et al., 2003). For this reason, protein levels of the phosphorylated Ser473 and total form of AKT were tested in both timepoints. At ZT12, pAKT levels were not different between restricted GR-LKO and WT mice (**Figure 30A and 30C**). At ZT16, the ratio pAKT over tAKT levels was lower in the caloric restricted GR-LKO mice compared with the WT mice (**Figure 30B and 30D**). In both timepoints, pFOXO1 over the tFOXO1 levels were higher in the restricted GR-LKO over the WT mice. Therefore, absence of hepatic GR leads to dampened AKT signaling and more increased phosphorylation of FOXO1. Conclusively, restricted GR-LKO mice have more inactive FOXO1 levels.
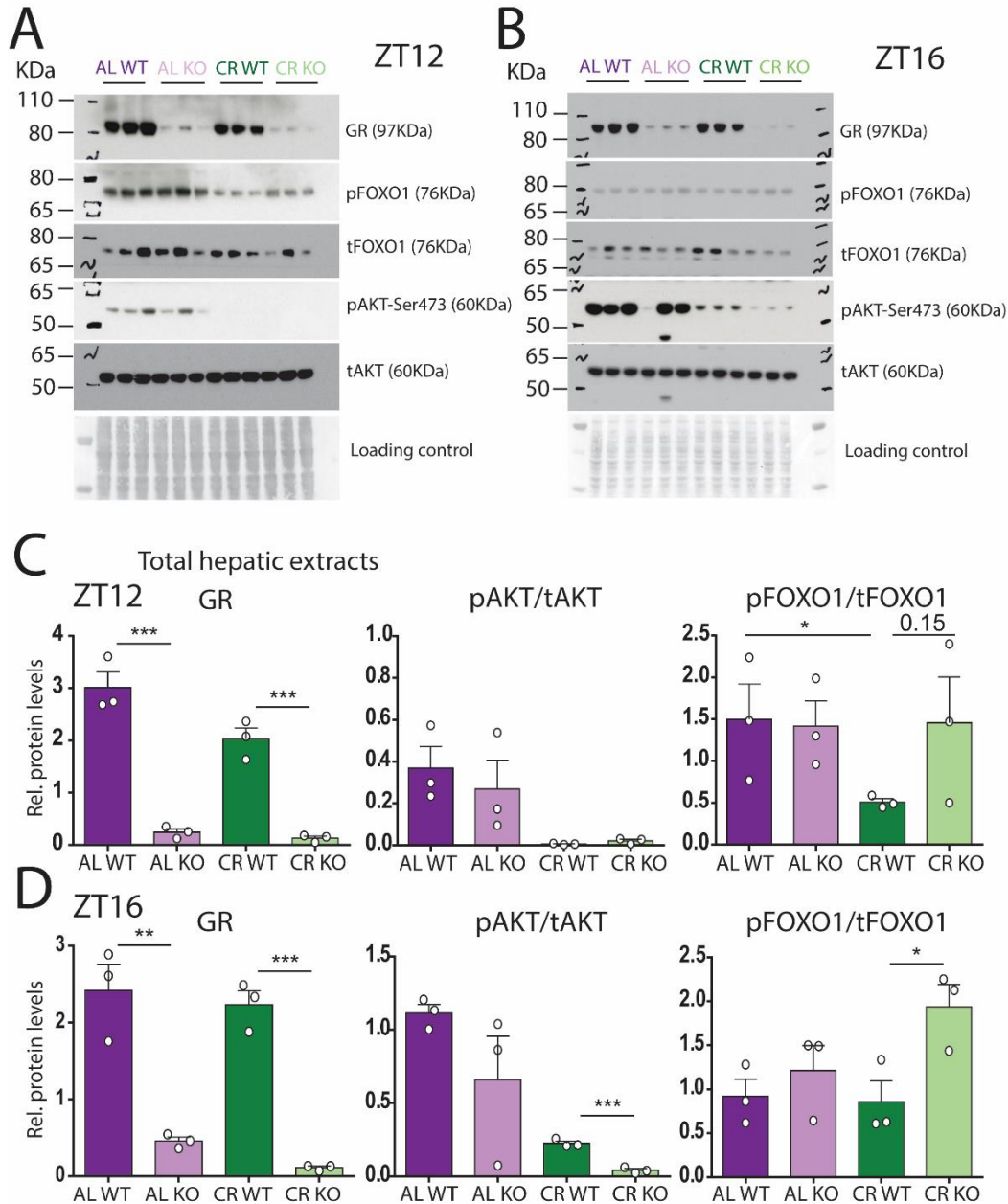
Figure 30: Caloric restricted GR-LKO mice present more inactive AKT/FOXO1 signaling.

A: Western blot in total hepatic extracts from control-fed and restricted GR-LKO and WT mice at the peak of corticosterone levels (ZT12) detecting total GR, pFOXO1, total FOXO1, pAKT (Ser473), total AKT and amido black staining was used as a loading control. **B:** Western blot in total hepatic extracts from control-fed and restricted *GR-LKO* and WT mice 4h after feeding (ZT16) detecting total GR, pFOXO1, total FOXO1, pAKT (Ser473), total AKT and amido black staining was used as a loading control. **C and D:** Quantification of total hepatic GR, pFOXO1/tFOXO1, and pAKT/tAKT levels normalized over the loading control for ZT12 (C) and ZT16 (D). Data are mean ± SEM, n=3 per condition. *p<0.05, **p<0.01, ***p<0.001. Student's t-test.

5.4 Caloric restricted GR-LKO mice present resistance to lose their liver glycogen at the peak of hormones

Glycogen is one of the most potent energy sources in the liver. It acts as an energy reservoir in order to maintain the glucose levels during the period of fasting, hypoglycemia and hypoxia (Rui, 2014b). As an energy source it reassures that all tissues will receive a constant supply of glucose. In opposition to fasting, meals increase the overall glucose levels in the bloodstream. Then liver starts absorbing the free circulating glucose and storing it into glycogen (Kanungo et al., 2018). For glycogen formation, free glucose will be transformed to glucose-6-phosphate by the glucokinase enzyme (*Gck*) (Kanungo et al., 2018). Afterwards, glucose-6-phosphate will be transformed into glucose-1-phosphate by the first reaction of the uronic acid pathway, where UDPG pyrophosphorylase will transform it into UDP-glucose (Kanungo et al., 2018). In the last step of glycogen synthesis, glycogen synthesis and branching enzymes will build up the glycogen. Glycogen synthesis enzyme 2 (*Gys2*) catalyzes the formation of alpha 1,4-glucosidic linkages by transferring glucose from the UDP-glucose to the non-reducing end of glycogen (Kanungo et al., 2018). Glycogen branching enzyme (*Gbe1*) catalyzes the formation of alpha 1,6-glucosidic linkages forming more and more complex structures of glycogen (**Figure 31**). In the case of glucose demand, glycogen breakdown starts with the phosphorylase enzyme (*Pygl*) catalyzing the alpha 1,4-glucosidic enzymes and then the debranching or hydrolyzing enzyme 1 (*Gde1*) removes the alpha 1,6-glucosidic bonds releasing glucose-1-phosphate (Kanungo et al., 2018). Glucose-1-phosphate is converted into glucose-6-phosphate by phosphoglucomutase (*Pgm1/2*). Lastly, glucose-6-phosphate is catalyzed by glucose-6-phosphatase (*G6pc*) releasing free glucose to the bloodstream (Kanungo et al., 2018) (**Figure 31**). Based on the RNA-seq data, caloric restriction seems to induce the expression of the glycogen breakdown enzymes and represses the glycogen synthetic enzymes (**Figure 31**). In absence of hepatic GR in caloric restriction, the expression of these enzymes is reversed, thus enhancing the regulatory role of GR in the glycogen pathway.
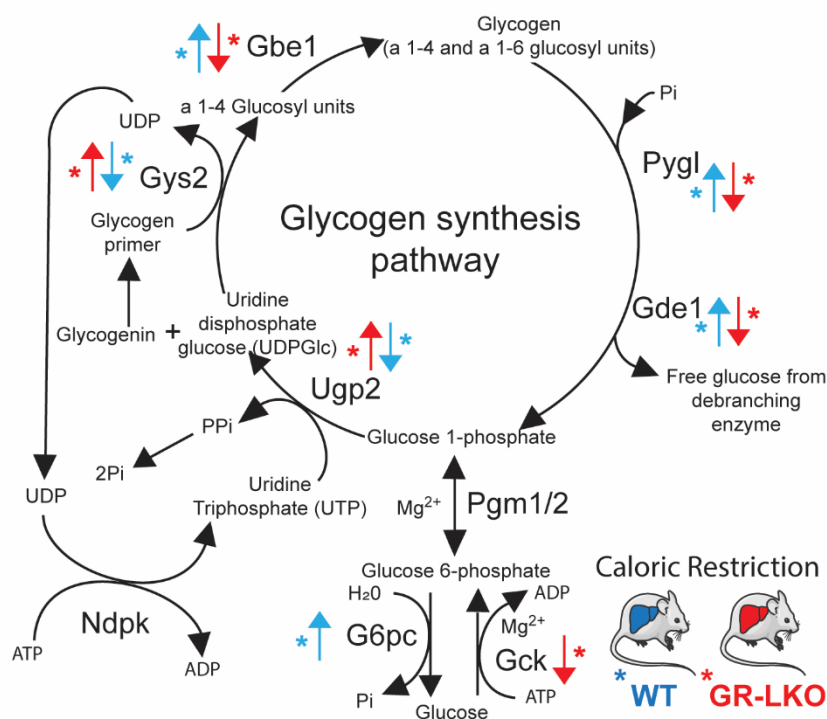
Figure 31: GR is responsible for the hepatic glycogen exhaustion upon caloric restriction.

Schematic representation of the glycogen synthesis/degradation pathway. Down- and up-regulated genes from the RNA-seq between *ad-libitum* and caloric restricted WT mice are marked with blue color, showing their trends. In parallel, down- and up-regulated genes from the RNA-seq between caloric restricted WT and GR-LKO mice are marked with red color, showing their trends in the glycogen pathway.

In GR/FOXO1 ChIP-seq data were many ChIP peaks proximal to genes related with gluconeogenesis and glycogen synthesis/glycogenolysis. In the same time, RNA-seq from the GR-LKO mice showed interesting targets related with these pathways. Until now, it is known that GR is responsible for the activation of gluconeogenesis and one of the classical targets is glucose-6-phosphorylase (*G6pc*). Stress response activate GR binding to this gene and in other gluconeogenic genes, such as *Pck1*, increasing the circulating glucose levels. Moreover, evidences from experiments with MEFs treated with dexamethasone have shown that GR can bind to the glycogen-branching enzyme (*Gbe1*) meaning that GR is necessary for the branching of glycogen during the early stages of life (Escoter-Torres et al., 2020). Based on these evidences, it was interesting to examine the hepatic glycogen levels. Firstly, caloric restricted GR-LKO mice present increased *Gys2* mRNA levels at the peak of corticosterone, at ZT12 (**Figure 32A**). In parallel, expression

levels of *Pygl* were reduced in the caloric restricted GR-LKO mice, at ZT16 (**Figure 32A**). Caloric restricted GR-LKO mice exhibited also a higher glycogen accumulation in the liver at ZT12 (**Figure 32B**). In this case, caloric restricted WT mice have consumed the majority of their glycogen levels at this timepoint (**Figure 32B**). Surprisingly, 4hr after feeding both caloric restricted WT and GR-LKO mice present faster accumulation of glycogen in comparison to the control ab libitum-fed mice (**Figure 32B**). Periodic acid-Schiff (known as PAS) staining of both control-fed and caloric restricted WT and GR-LKO mice showed that GR-LKO have more stained glycogen than the WT mice, at ZT12 (**Figure 32C**). So far, there are many evidence that GR/FOXO1 can bind in novel glycogen-related genes, such as *Gys2* and *Pygl*, altering the glycogen synthesis/breakdown cycle. GR is responsible for the enhanced glycogen breakdown during restriction, underpinning its role in the manipulation of this energy source.
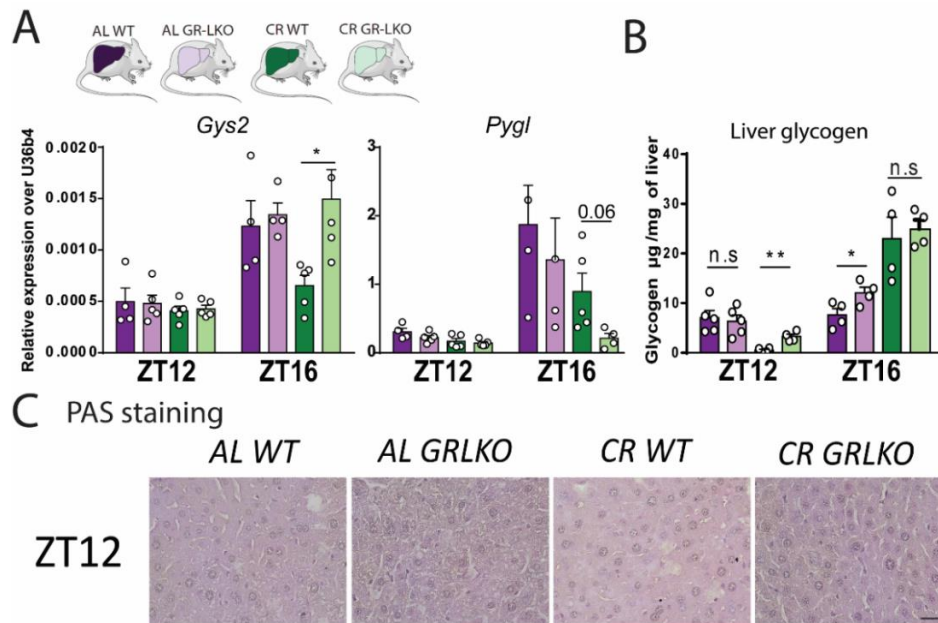
Figure 32: GR is responsible for the hepatic glycogen exhaustion upon caloric restriction.

A: Expression levels of *Gys2* and *Pygl* from qPCR-data from the livers of both *ab-libitum*-fed and caloric restricted WT and GR-LKO mice, at ZT12 and ZT16. All these values were normalized over the housekeeping *U36b4*, gene encoding a ribosomal protein subunit (*Rplp0*), and represent mean ± SEM, n =4-5, *$p<0.05$, **$p<0.01$ and ns = not significant. Student's t-test. **B:** Liver glycogen levels from *ad-libitum* and caloric restricted WT and GR-LKO mice, at ZT12 and ZT16. Values represent mean ± SEM, n =4, *$p<0.05$, **$p<0.01$ and ns = not significant. Student's t-test. **C:** Periodic-acid-Schifff staining (PAS) of liver sections from both al-fed and caloric restricted WT and GR-LKO mice,

at ZT12. For this analysis, were examined n = 3 biological replicates per condition. Scale bar = 100μm. AL: *Ad-Libitum*, CR: Caloric Restriction.

5.5 Caloric restricted GR-LKO mice perform aberrant glycolysis after feeding

Hepatocytes present a great flexibility in switching from one metabolic fuel to another (from glucose to fatty acid and vice versa). This fuel selection is dependent on the hormonal and nutrient availability. In fasted state, circulating glucose levels are low boosting the process of gluconeogenesis and glycogenolysis. In fed state, where the glucose levels are getting high, glycolysis is the dominant process for the production of energy. Glycolytic products and intermediates are used to synthesize amino acids, lipids, and other important molecules, which can be completely oxidized for production of ATP. When hepatocytes are again in fasted state, then they are switching to fatty acid β-oxidation and ketogenesis for energy supply (Ipsen et al., 2018; Rui, 2014b). Glycolysis is a dominant process of producing energy during the prost-prandial state. RNA-seq in caloric restricted WT mice showed increased expression in various glycolytic enzymes, such as *Gpi*, *Pfk1*, *Aldo-a/b*, *Gapdh*, *Pgk1*, and *Eno1*, compared to the *ad-libitum* fed mice. Deletion of hepatic GR shows that all these enzymes are down-regulated in caloric restriction (**Figure 33**). From this overview, it seems that hepatic GR is necessary for the expression of glycolytic enzymes in caloric restriction.
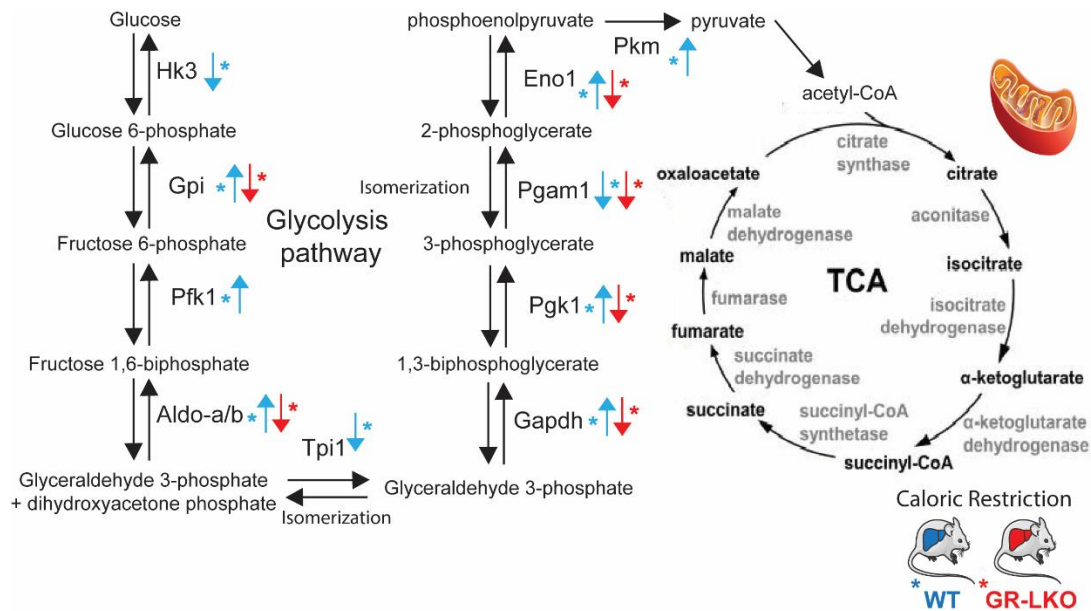
Figure 33: Deletion of hepatic GR reduces the expression levels of glycolytic enzymes in caloric restriction.

Schematic representation of the glycolysis pathway in connection with the TCA cycle in mitochondria. Down- and up-regulated genes from the RNA-seq between *ad-libitum* and caloric restricted WT mice are marked with blue color, showing their trends. In parallel, down- and up-regulated genes from the RNA-seq between caloric restricted WT and GR-LKO mice are marked with red color, showing their trends in the glycolysis pathway. Picture adapted from (Rui, 2014b).

Overlap of GR/FOXO1 ChIP-seq and RNA-seq in the caloric restricted GR-LKO mice showed a great enrichment of gluconeogenesis and glycolysis pathway. Meticulous examination of the targets showed that aldolase-B (*Aldob*) and enolase 1 (*Eno1*) are two characteristic enzymes which show common GR/FOXO1 ChIP peaks. More specifically, they are down-regulated in the caloric restricted GR-LKO mice. The transcripts of these enzymes were lowered both in the pre-prandial (at ZT12) and post-prandial state (at ZT16). Validation of these targets showed that absence of GR in the liver of restricted mice affects the post-prandial expression in these two glycolytic enzymes (**Figure 34A**). Despite the dampened glycolysis, caloric restricted GR-LKO mice present normal glucose levels around the clock (**Figure 34B**).
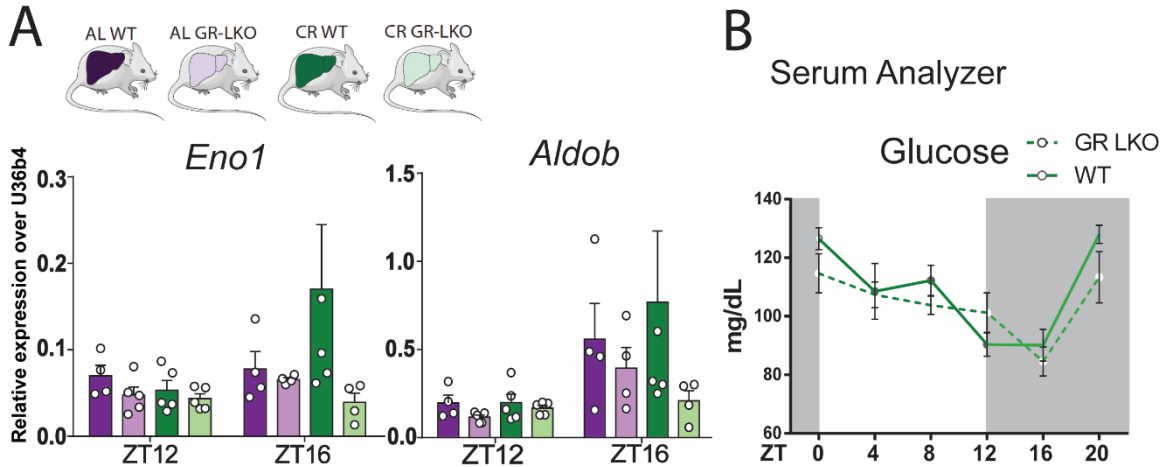
Figure 34: Dampened glycolysis in the deletion of hepatic GR in caloric restriction.

A: Expression levels of *Eno1* and *Aldo-b* from qPCR-data from the livers of both *ab libitum* fed and caloric restricted WT and GR-LKO mice, at ZT12 and ZT16. All these values were normalized over the housekeeping *U36b4*, gene encoding a ribosomal protein subunit (*Rplp0*), and represent mean ± SEM, n =4-5, *$p<0.05$, **$p<0.01$ and ns = not significant. Student's t-test. **B:** Circulating glucose levels from caloric restricted WT and GR-LKO mice, around the clock. Values represent mean ± SEM, n =3-4 for ZT0,4,8,20 and n= 8-10 for ZT12,16, *$p<0.05$, **$p<0.01$ and ns = not significant. Student's t-test.

At the same time, *Pparα* transcript was up-regulated in the caloric restricted GR-LKO mice (**Figure 35A**). PPAR-α signaling is responsible for the suppression of glycolysis during the fasted state and pathway enrichment analysis pointed out the up-regulation of the PPAR-α signaling in both timepoints. It is prominent the direct GR regulation of the glycolytic enzymes by the RNA-seq in the caloric restricted GR-LKO mice. Besides this, validation of the PPAR-α protein levels reveals that absence of hepatic GR in caloric restriction elevates the PPAR-α signaling affecting, as an additional mechanism, the glycolysis turnover (**Figure 35B & 35C**).
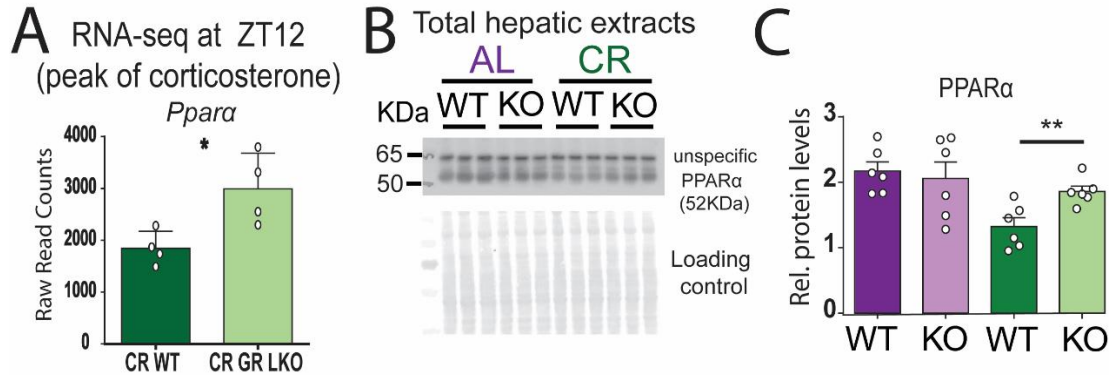
Figure 35: Increased expression and protein levels of PPARα in the caloric restricted GR-LKO mice.

A: *Pparα* expression from liver RNA-seq data of caloric restricted WT and GR-LKO mice, at ZT12. Data represent mean ± SEM, n =4 biological replicates, *p<0.05. Student's t-test. **B:** Western blot in total hepatic extracts from control-fed and restricted mice at ZT12 detecting total PPARα, and amido black staining was used as a loading control. **C:** Quantification of total hepatic PPARα levels normalized over the loading control. Data represent mean ± SEM, n =6 biological replicates, *p<0.05, **p<0.01 and ns = not significant. Student's t-test.

5.6 Caloric restricted GR-LKO mice utilize fatty acid degradation as fuel energy before and after feeding to produce ketones

Lipid homeostasis is tightly connected with gluconeogenesis and energy production. In normal physiological condition, fat depots are immobilized in order to sustain the energy levels of the body. This process of the fat catabolism happens both in human and mouse during their inactive phase in order to maintain their energy levels, while they sleep. In case of fasting or caloric restriction, lipids in white adipose tissue are hydrolyzed leading to the release of fatty acids in the blood circulation (Duszka et al., 2020). These fatty acids will be available to be used as fuels by the muscles or the liver in the lack of nutrients. Circulating fatty acids can be transferred to the hepatic plasma membrane by fatty acid transporters, such as *Cd36* and *Fabp1*, which are mainly regulated by PPARγ and GR (Ipsen et al., 2018; Quagliarini et al., 2019). The inserted fatty acids can follow four different paths inside the hepatocytes. First path is their conversion to triglycerides. As triglycerides can push the hepatocytes to perform *de novo* lipogenesis in association with the SREBP1c/ChREBP axis (Iizuka et al., 2004; Ipsen et al., 2018; Sanders & Griffin, 2016a). This pathway is normally activated by feeding, where high glucose and insulin

contribute to the conversion of glucose and acetate to free fatty and triglycerides (Jensen-Urstad & Semenkovich, 2012; Sanders & Griffin, 2016b). The second path is their transport to mitochondria by the CPT transporters and they can be consumed by the β-oxidation in order to produce energy in the form of ATP and ketones (Ipsen et al., 2018; Reddy & Sambasiva Rao, 2006). The third path is their transport to the peroxisomes. Inside the peroxisomes fatty acid undergo β-oxidation as an alternative path of energy production. In both mitochondria and peroxisomes, β-oxidation of fatty acids produces ATP, ketones and reactive oxygen species (ROS) (G. Wang et al., 2015). In hepatocytes, it is recorded also the ω-oxidation as another energy production source. Last path is their loading in the form of triglycerides with cholesterol into water soluble very-low density lipoprotein particles (known as VLDL) (Ipsen et al., 2018; Reddy & Sambasiva Rao, 2006). Liver is responsible for the production of the VLDL particles, which are the mainly triglyceride and cholesterol carriers (Rustaeus et al., 1999) (**Figure 36**).
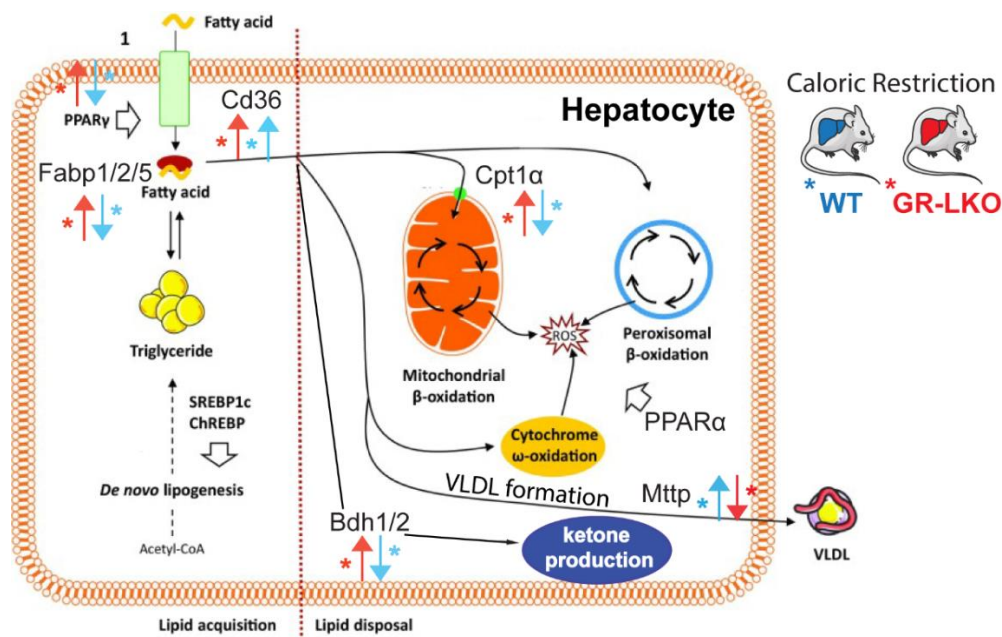
Figure 36: Deletion of hepatic GR elevates the fatty acid oxidation and ketogenesis program in caloric restriction.

Schematic representation of the fatty acid catabolism pathway in connection with the *de novo* lipogenesis and β-oxidation in mitochondria. Down- and up-regulated genes from the RNA-seq between *ad-libitum* and caloric restricted WT mice are marked with blue color, showing their trends. In parallel, down- and up-regulated genes from the RNA-seq between caloric restricted WT and GR-LKO mice are marked with red color, showing their trends in the fatty acid catabolism/oxidation pathway. Picture adapted from (Ipsen et al., 2018).

GR is responsible for the fatty acid metabolism. Indeed, GR binds to the fatty acid transporter *Cd36* repressing this gene. GR-LKO mice have significantly increased PPARγ levels, meaning that GR represses PPARγ expression. Deletion of GR allowed the PPARγ binding to the *Cd36* gene (Quagliarini et al., 2019). The increased fatty acid import can lead to excessive lipid storage (Sanders & Griffin, 2016a). This is reflected in the phenotype of the GR-LKO, which have increased hepatic triglycerides and are prone to develop hepatic steatosis (Quagliarini et al., 2019). In parallel, circulating triglycerides in these mice are lowered. In caloric restriction, both GR/FOXO1 ChIP peaks are in the vicinity of fatty-acid related genes. Moreover, RNA-seq in GR-LKO mice from both ZT12 and ZT16 gave significant enrichment of all the fatty-acid catabolism related pathways. Caloric restricted GR-LKO mice had increased expression levels of both hepatic *Fabp1*, *Cpt1α* and *Bdh-2* genes at ZT12 (**Figure 37A**). Additionally, *Bdh-2* showed flattened expression, which was closely concordant with the dampened circulating ketones levels (**Figure 37B**). Higher activity in the *Bdh2* implied more β-oxidation and increased ketone production. In total, circulating non-esterified fatty acids (NEFAs) and circulating ketones had a dampened rhythm in the caloric restricted GR-LKO mice (**Figure 37B and 37C**). Conclusively, absence of hepatic GR in caloric restriction increases the expression of genes-related with fatty acid transportation and β-oxidation, dampening the rhythm of both fatty acid and ketone cycle.
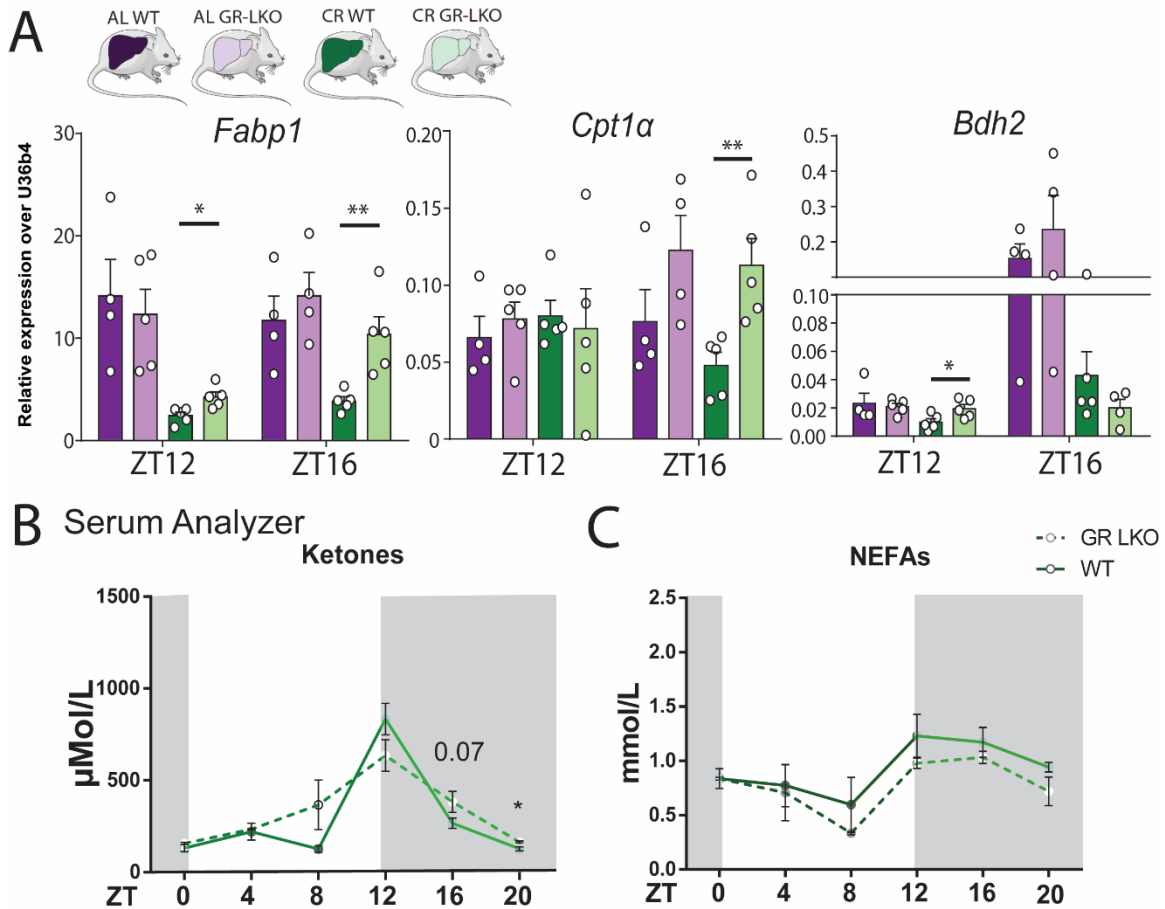
Figure 37: Deletion of GR reduced NEFAs and increased the circulating ketones in caloric restriction.

A: Expression levels of *Fabp1* and *Cpt1α* from liver qPCR-data of both *ad-libitum* fed and restricted WT and GR-LKO mice, at ZT12 and ZT16. All these values were normalized over the housekeeping *U36b4*, gene encoding a ribosomal protein subunit (*Rplp0*), and represent mean ± SEM, n =4-5, *p<0.05, **p<0.01 and ns = not significant. Student's t-test. **B:** Circulating ketone levels from caloric restricted WT and GR-LKO mice, around the clock. Values represent mean ± SEM, n =3 for ZT0,4,8,20 and n= 8-10 for ZT12,16, *p<0.05, **p<0.01 and ns = not significant. Student's t-test. **C:** Circulating NEFAs from both caloric restricted WT and GR-LKO mice, around the clock. For this analysis, were examined n = 3 for ZT0,4,8,20 and n= 8-10 for ZT12,16 *p<0.05, **p<0.01 and ns = not significant. Student's t-test.

5.7 Caloric restricted GR-LKO mice show lowered circulating cholesterol levels after feeding

Circulating cholesterol levels is one of the most important risk factors for developing atherosclerosis (Aguilar-Ballester et al., 2020; Assmann & Gotto, 2004). Aging and diet are two confounding factors, which lead to this condition. Until now, studies have proved the beneficial effects of caloric restriction in preventing atherosclerosis. Long-term caloric restricted human underwent in massive reduction of their LDL, triglycerides and total cholesterol while they have increased their HDL (Fontana et al., 2004). Gradual inflammation plays a critical role for the development of atherosclerosis. Interactions between oxidized cholesterol, macrophages and cellular components in the arterial wall can contribute to this chronic inflammation, forming atheromatic plaques (Fontana et al., 2004). The reduction of calories not only reduces the secretion of cholesterol, LDL and triglycerides, but consequently also protects from the inflammatory-mediated formation of these atheromatic plaques.

Overlap of the GR/FOXO1 co-bound regions with the down-regulated genes in the GR-LKO pointed out as deregulated pathway the cholesterol metabolism before and after feeding (for both timepoints). Indeed, the expression of *Apoa4/c3* and *Scarb1*, two genes encoding apolipoproteins involved in LDL and HDL particles, is down-regulated in the caloric restricted GR-LKO compared with the restricted wild-type mice (**Figure 38A**). Interestingly, while no significant effect could be observed in LDL, caloric restricted GR-LKO mice presented lower circulating total cholesterol and HDL compared with the caloric restricted wild-type mice post-prandially (**Figure 38B, 38C and 38D**). Finally, reduced expression of lipid apolipoprotein transporters is concordant with the dampened post-prandial circulation of total cholesterol and HDL levels in caloric restricted GR-LKO mice.
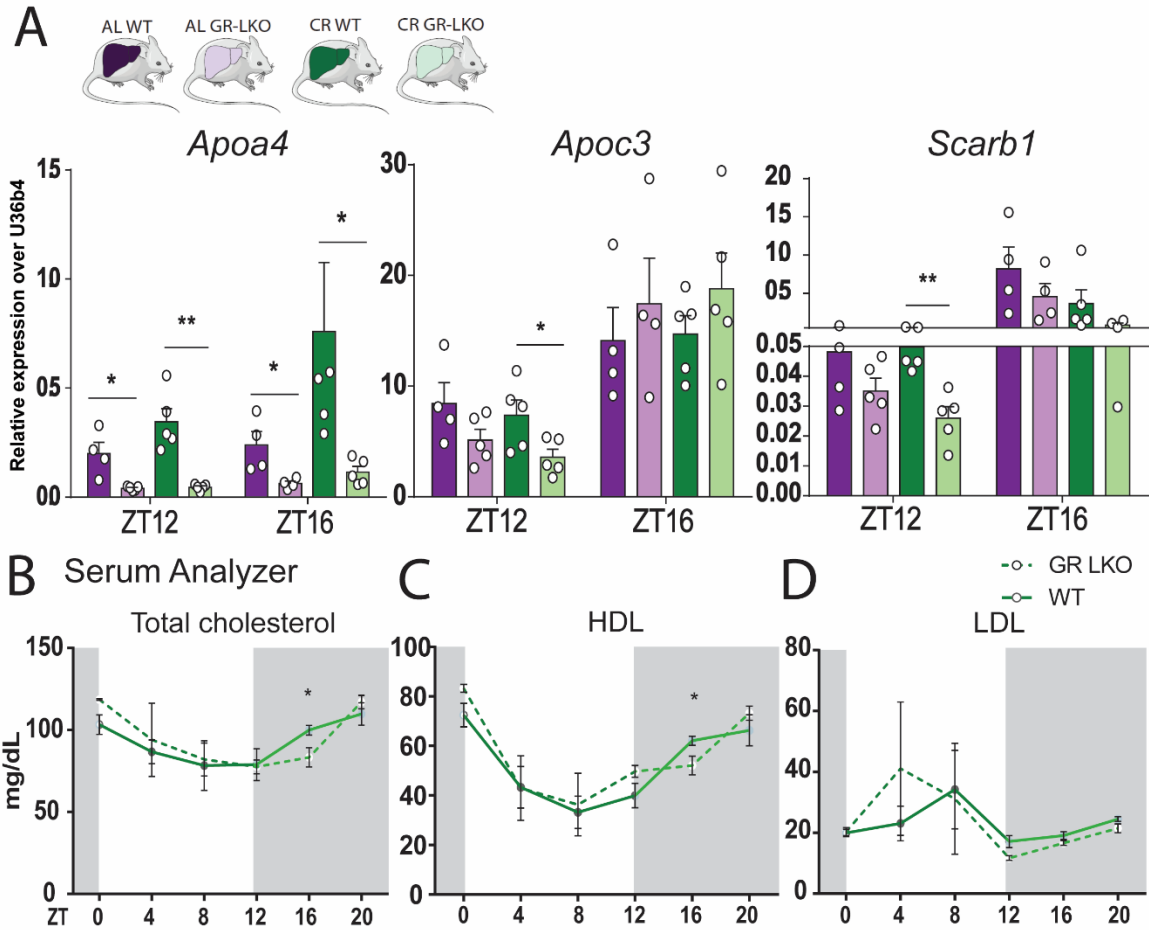
Figure 38: Deletion of GR reduced the post-prandial circulation of HDL and total cholesterol in caloric restriction.

A: Expression levels of *Apoa4*, *Apoc3* and *Scarb1* from qPCR-data from the livers of both *ad-libitum* fed and caloric restricted WT and GR-LKO mice, at ZT12 and ZT16. All these values were normalized over the housekeeping *U36b4*, gene encoding a ribosomal protein subunit (*Rplp0*), and represent mean ± SEM, n =4-5, *p<0.05, **p<0.01 and ns = not significant. Student's t-test. **B-D:** Circulating total cholesterol (B), HDL (C), LDL (D) levels from caloric restricted WT and GR-LKO mice, around the clock. Values represent mean ± SEM, n =3-4 for ZT0,4,8,20 and n= 8-10 for ZT12,16, *p<0.05, **p<0.01 and ns = not significant. Student's t-test.

Surprisingly, enzymes related with cholesterol synthesis in the overlapped ChIP- and RNA-seq data did not show changes between the caloric restricted GR-LKO and wild-type mice. Focusing on these enzymes related with the cholesterol synthesis such as *Sqle*, *Fdps*, and *Hmgcr*, there was no statistical difference between the caloric restricted GR-LKO and wild type mice at the peak of corticosterone levels (**Figure 39**). So, the previously

mentioned results showed that there mainly cholesterol (or lipid) transporters, which are downregulated by the absence of GR in caloric restriction.
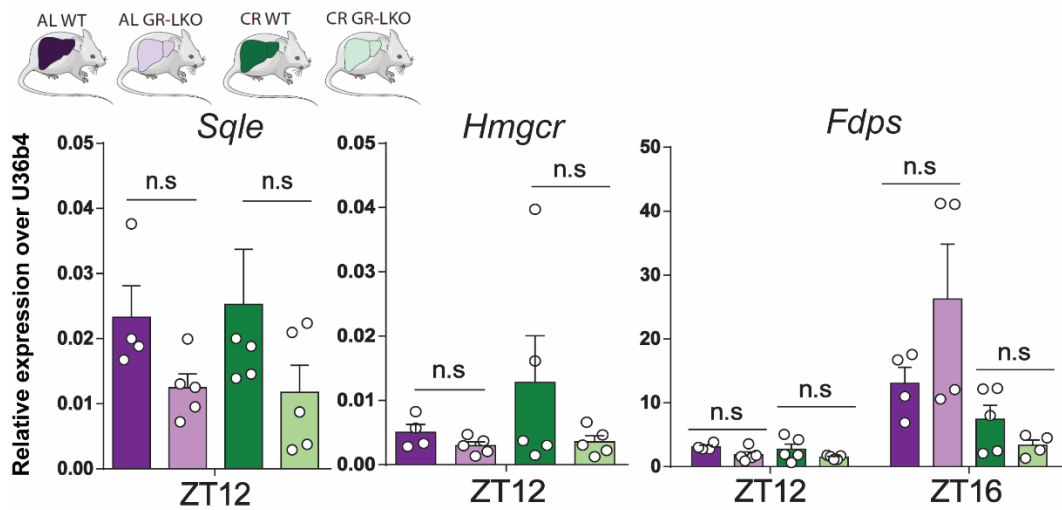
Figure 39: Deletion of GR does not affect the expression levels of cholesterol synthetic enzymes in caloric restriction.

A: Expression levels of liver *Sqle*, *Fdps* and *Hmgcr* from *ad-libitum* fed and caloric restricted WT and GR-LKO mice, at ZT12 and ZT16. All these values were normalized over the housekeeping *U36b4*, gene encoding a ribosomal protein subunit (*Rplp0*), and represent mean ± SEM, n =4-5, *p<0.05, **p<0.01 and ns = not significant. Student's t-test.

5.8 Deletion of GR deregulates the circadian hepatic rhythmicity in caloric restriction

Several hallmarks of aging happen to be consequence of the deterioration of the circadian clock, that is reversible by caloric restriction (García-Gaytán et al., 2020; Makwana et al., 2019b; Sato et al., 2017). The age-dependent decline of the central circadian clock affects all the physiological parameters, altering the rhythmic behavior in mice, such as the locomotor activity and the suprachiasmatic nucleus function (Chang & Guarente, 2014; Sellix et al., 2012). Caloric restriction and other fasting regimens have the ability to extend lifespan, improve healthspan and attenuate the age-dependent phenotype in a clock-dependent manner by rescuing the global protein acetylation and boosting the SIRT1/NAD metabolism (Gill & Panda, 2015; S. A. Patel, Chaudhari, et al., 2016; Zwighaft et al., 2015).

GR/FOXO1 recognize many promoters/enhancers of core circadian factors, such as *Per1*, *Bmal1* (or *Arntl*), *Reverbα*, and *Cry1*. One of the top deregulated pathways in the RNA-

seq data of the caloric restricted GR-LKO mice was the rhythmicity of the clock machinery Previously analysis showed enrichment for circadian clock pathway. *Per1* expression was dampened because is a direct GR target **(Figure 40)**. In the case of *Bmal1* (or *Arntl*), there was a phase delay at ZT12, while its expression was reduced in the GR-LKO compared to the restricted wildtype mice at the peak of corticosterone levels (ZT12). Interestingly, *Reverbα* expression levels were higher during the day in the GR-LKO at ZT4, ZT8 and ZT12, in comparison to the wild type mice. Additionally, *Cry1* expression levels were lower in the caloric restricted GR-LKO mice especially at the peak of corticosterone (ZT12) and during the night (ZT20). Already published data have shown that dexamethasone administration at the trough of hormones (ZT0) upregulates after 4 hours *Per1*, *Bmal1*, and *Cry1* genes (Quagliarini et al., 2019). To sum up, GR is responsible for the enhanced expression of the *Per1*, *Bmal1*, and *Cry1* in caloric restriction at the peak of corticosterone levels (ZT12), and simultaneously increases the *Reverbα* levels during the day at ZT4 to ZT12.
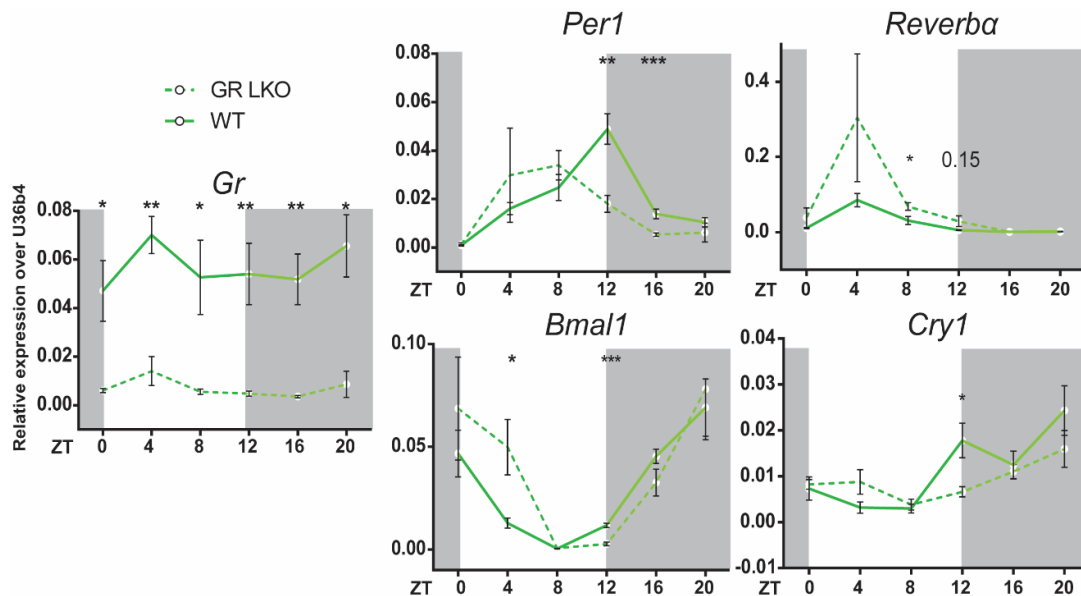
Figure 40: Deletion of GR deregulates the hepatic rhythmicity of the main circadian factors in caloric restriction.

Expression levels of *Gr, Reverbα (or Nr1d1), Bmal1 (or Arntl), Per1* and *Cry1* from liver qPCR-data of both caloric restricted WT and GR-LKO mice around the clock. All these values were normalized over the housekeeping *U36b4*, gene encoding a ribosomal protein subunit (*Rplp0*), data represent mean ± SEM, n =3-4, *$p<0.05$, **$p<0.01$, ***$p<0.001$ and ns = not significant. Student's t-test.

5.9 Caloric restricted GR-LKO mice showed aberrant autophagy at the peak of corticosterone levels

Autophagy is one of the main mechanisms for recycling proteins, metabolites and lipids. The autophagic machinery is activated by caloric restriction through the AMPK signaling, which regulates positively the ULK1 kinase (Aman et al., 2021). The phosphorylated ULK1 stimulates the class III phosphatidylinositol 3-kinase (PI3KC3) complex. This complex is a multiprotein complex, composed of BECN1, ATG14L, VPS15, AMBRA1 and VPS34(Aman et al., 2021). This complex leads to the recruitment of the WIPI proteins, recovering ATG9 positive vesicles and recruiting the ATG5-ATG12-ATG16L1 (E3) conjugating complex. In parallel, LC3 is cleaved by the ATG4 protease in order to form cytosolic LC3-I. LC3-I is recognized by ATG7 (E1), ATG3 (E2) and ATG5-ATG12-ATG16L1 (E3) components, which conjugate it with phosphatidylethanolamine (PE). The processed LC3-I is modified to LC3-II, which via the LIR-containing autophagy motif (such as p62) can recognize the different cargoes and targets their degradation into lysosomes. There acidic hydrolases destroy the cargoes of the mature autophagosomes (Aman et al., 2021) **(Figure 41)**.
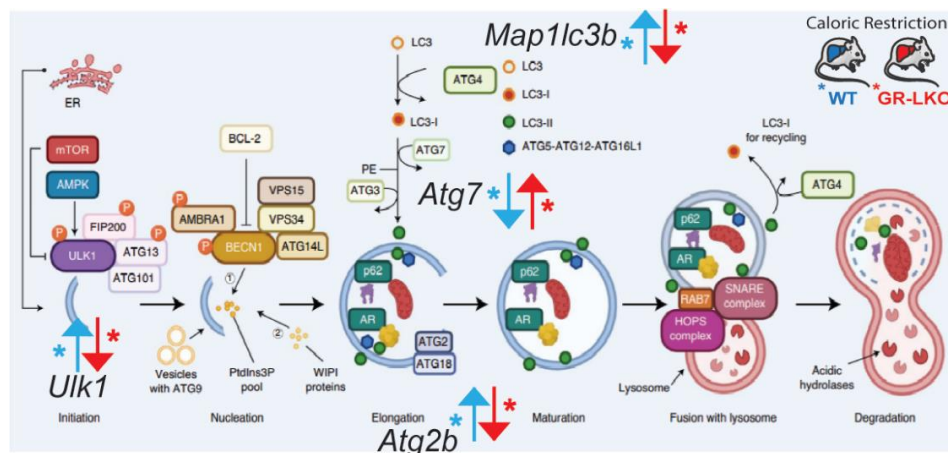
Figure 41: Deletion of hepatic glucocorticoid receptor in caloric restriction downregulates the expression of key genes of the core autophagic machinery.

The core autophagic machinery has multiple stages between the initiation of autophagy until the degradation of the cargoes. AMPK signaling, which is directionally the opposite of mTOR signaling, phosphorylates ULK1 initiating the formation of the autophagosome. Afterwards, various ATG proteins assist for the nucleation, elongation and maturation of the autophagosome until the loading of the cargoes. Fusion of lysosome with the autophagosome leads to the cargo degradation. Down- and up-regulated genes from the RNA-seq between *ad-libitum* and caloric restricted WT mice are

marked with blue color, showing their trends. In parallel, down- and up-regulated genes from the RNA-seq between caloric restricted WT and GR-LKO mice are marked with red color, showing their trends in the autophagy pathway. Picture adapted from Aman et al., 2021.

Upon caloric restriction, WT mice exhibited an up-regulation of many key genes of autophagy genes, such as *Map1lc3b*, *Ulk1*, *Atg7* and *Atg2b* (**Figure 41**). Caloric restricted GR-LKO mice showed down-regulation of these genes both at the peak of corticosterone levels and post-prandially. FOXO1, as initiator of the autophagy-related transcriptional program, is more inactive in caloric restricted GR-LKO mice. Since AKT/FOXO1 signaling is down-regulated, caloric restricted GR-LKO mice probably have aberrant autophagy cycling. Surprisingly, caloric restricted GR-LKO mice had a defect in the transformation from the LC3-I to the LC3-II form and a tendency for reduction in BECN1 and p62 levels **(Figure 42A and 42B)**.
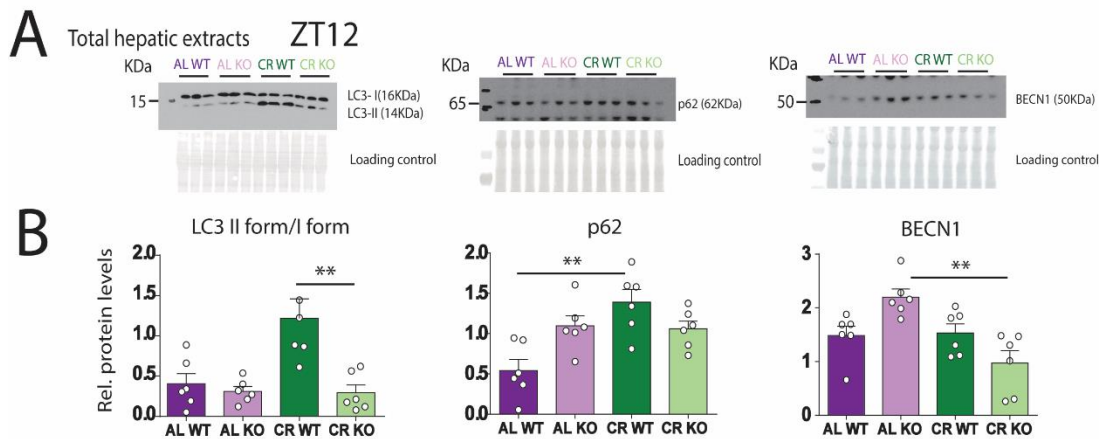
Figure 42: Impaired autophagy in the caloric restricted GR-LKO mice.

A: Western blot in total hepatic extracts from control-fed and caloric restricted WT and GR-LKO mice at ZT12 detecting LC3A/B I/II form, p62, and Beclin1 (BECN1), and amido black staining was used as a loading control. **B:** Quantification of total hepatic LC3A/B I/II form, p62, and Beclin1 (BECN1) levels normalized over the loading control. Data represent mean ± SEM, n=6 biological replicates, *$p<0.05$, **$p<0.01$ and ns = not significant. Student's t-test.

ATG3, ATG16L1, and ATG5 protein expression presented some differences in the conjugation proteins, altering thus potentially the autophagic turnover in the absence of glucocorticoid receptor (**Figure 43A & 43B**). For ATG7 protein there was not observed difference. All these ATG proteins participate in various processes in the autophagosome initiation, elongation and maturation. Concerning the ATG3 protein, caloric restricted GR-LKO mice had higher levels in compared to WT mice. Moreover, ATG5 and ATG16L1

showed different transition from the AL to the CR condition. In conclusion, absence of GR in restriction impairs significant modules of autophagy in multiple stages, primarily in the maturation of autophagosomes and as secondary effects initiation, conjugation of autophagy.
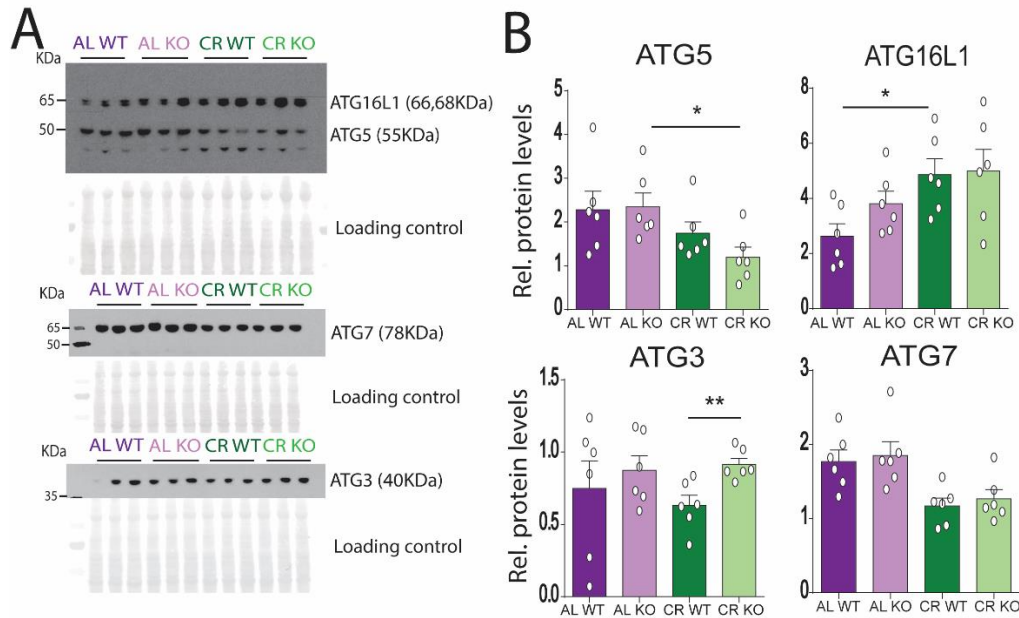
Figure 43: Altered cycling of ATG proteins in the caloric restricted GR-LKO mice.

A-B: Western blot (A) and quantification (B) in total hepatic extracts from control-fed and caloric restricted WT and GR-LKO mice at ZT12 detecting ATG3, ATG5, ATG16L1 and ATG7, and amido black staining was used as a loading control. Data represent mean ± SEM, n=6 biological replicates, *p<0.05, **p<0.01 and ns = not significant. Student's t-test.

5.10 Lipidomic profiling shows accumulation of TGs and reduction of PE in GR-LKO mice in caloric restriction

Lipid species are main regulators for transporting messages through vesicles, such as LDL, HDL and VLDL lipoproteins and through the cytoplasmic membrane. In order to identify the role of hepatic GR in caloric restriction with specific lipid species, lipidome analysis was performed in *ad-libitum* and caloric restricted WT and GR-LKO mice at the peak of corticosterone levels (at ZT12).

Among the 1070 measured lipid species between AL-fed and CR WT and GR-LKO mice, it was followed a specific quality check (GC) analysis as a preprocessing analysis. In the

first step of this QC procedure, lipid species with missing values (NA) equal to or more than 30% in the pool samples were discarded from the dataset. In the second step, the percentage of missing data in the biological samples which clarifies if there is a phenotype related origin of missing values. For example, a lipid which is only observed in one of the biological groups, then it was discarded. Lipids exhibiting a groupwise missingness of 50% in all groups were discarded. Since there were 372 lipids with more than 30% NA in the pool samples and 22 lipids with more than 50% NA per groups, 676 lipid species remained for the analysis. Additionally, lipid species with a coefficient of variation (CV) more than 25% were identified as unreliably measurements. These unreliable lipid species with CVs > 25% were 65 and were excluded from the data set. Among the 611 lipid species, performing a dispersion ratio (D-ratio), technically variable lipid species with D-ratio >= 50% were removed from this analysis, ending up with the final number of 544 lipids (Broadhurst et al., 2018). Due to variation in the lipid species and after performing principal component analysis (PCA), it was necessary the removal of two samples, as outliers. Pre-processing an repeating the same analysis led to 515 lipid species in the principal component analysis, where caloric restricted GR-LKO had a slight swift over the *ad-libitum* fed GR-LKO mice. In the case of the WT genotype, caloric restricted mice showed close grouping between the *ad-libitum* fed and the caloric restricted GR-LKO mice **(Figure 44)**. PCA analysis presented clearly a big dispersion for AL fed GR-LKO mice.
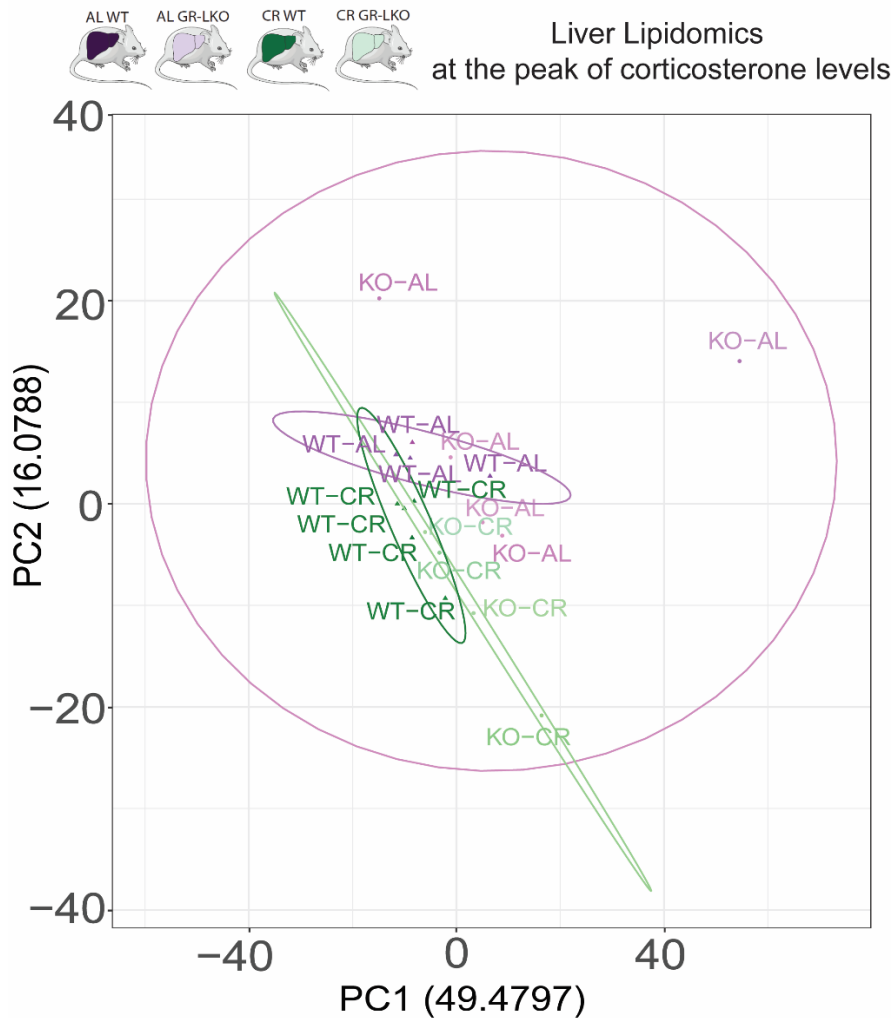
Figure 44: Grouping of liver lipidomic samples based on genotype by performing principal component analysis.

Principal component analysis (PCA) at the peak of corticosterone levels from lipidome data coming from livers of normal-fed and caloric restricted WT vs GR-LKO mice (n=4-5 mice per condition with 515 tested different lipid species).

In order to understand the differences among the different lipid species, clustering of the sum of the concentration of each lipid class was performed. In clustering analysis, GR-LKO mice were grouped mixed between the AL-fed and CR condition, making more difficult their separation. In opposite, WT mice were better separated between these two conditions **(Figure 45A)**. While no big difference could be detected for diacyl-glycerides (DAG), triacyl-glycerides (TAG) showed increased accumulation for both *ad-libitum* fed and caloric restricted GR-LKO mice. Assessing free fatty acids (FFA), they showed

reduced accumulation in the caloric restricted GR-LKO mice, similarly to *ad-libitum* fed GR-LKO mice **(Figure 45B)**.
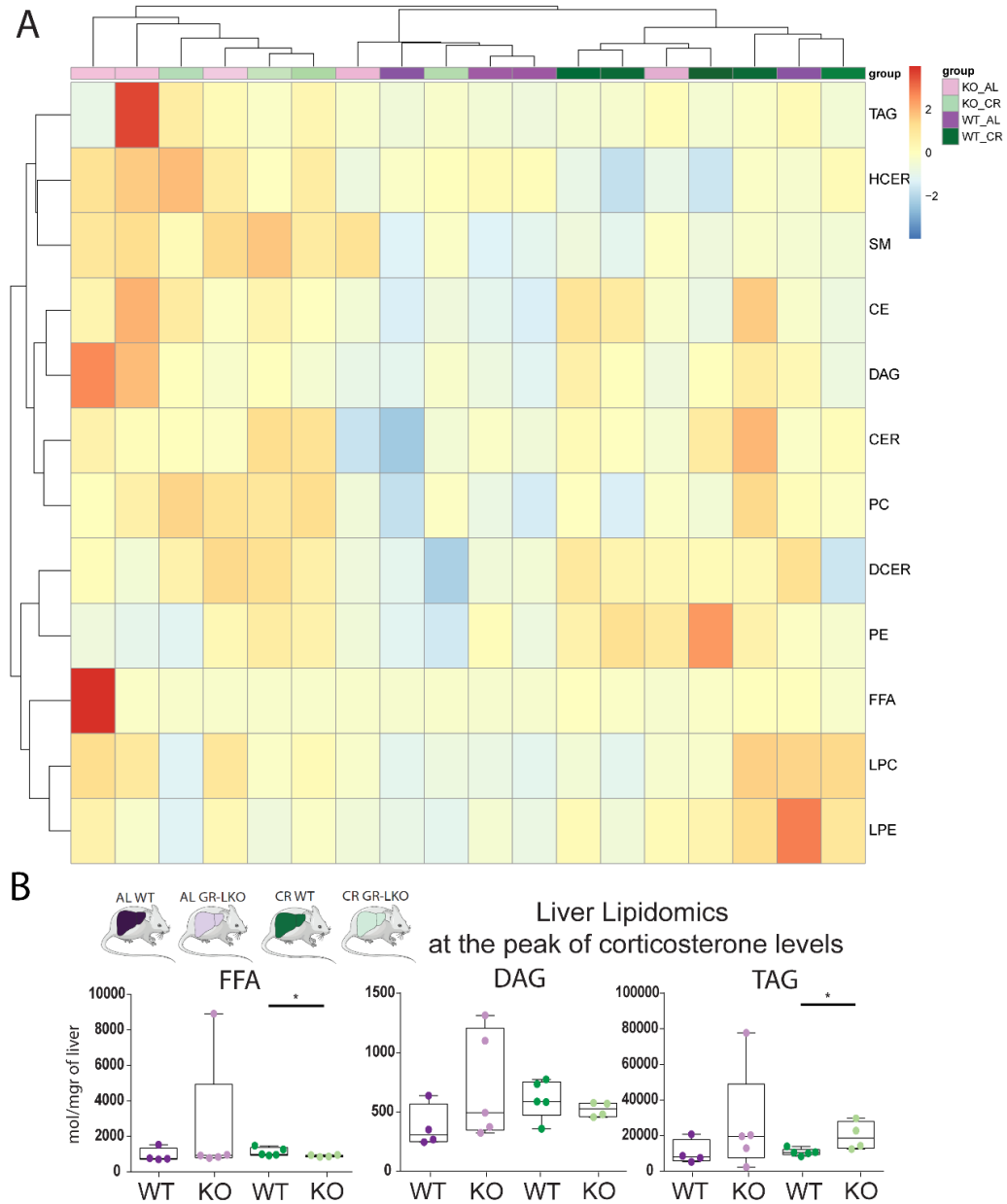
Figure 45: Hierarchical clustering of lipidome of mice shows accumulation of TAG in the restricted GR-LKO mice.

A: Clustering of the 12 main lipid species based on the sum of their lipid concentration. **B:** Box plot with single data points from the sum of concentration of FFA, DAG and TAG from the hepatic lipidome of AL-fed and CR WT and GR-LKO mice (n=4-5 mice per condition with 515 tested different lipid species).

Caloric restricted GR-LKO mice had higher levels of phosphatidylcholine (PC) and lower levels of PE in their livers **(Figure 46)**. These two phospholipid species are abundant, since phosphatidylethanolamine (PE) is contained in 15-25% of the total phospholipids in cell membranes and PC constitutes the 40-50% of total phospholipids in organelles in eykaryotic cells (Calzada et al., 2016; Vance, 2015). Additionally, liver cells produce, through a minor pathway, 30% of their total PC by the trimethylation of PE (Sundler & Akesson, 1975). As a further step of these phospholipids, hepatocytes express the phospolipase A, an enzyme responsible for the hydrolysis of phosphatidylcholines (PC) and phosphatidylethanolamines (PE). This enzymatic reaction of hydrolysis removes one fatty acid group producing lysophosphatidylcholines (LPC) and lysophosphatidylethanolamines (LPE). Caloric restricted GR-LKO mice had the same levels of LPC with the remaining groups, while they contained significantly less LPE **(Figure 46)**. Hepatic PE levels were reduced affecting probably the overall LPE levels. In the case of ceramides, caloric restricted GR-LKO mice have the same levels with the WT mice. Ceramides, as sphingolipids, can induce oxidative stress leading to oxidative damage and activation of apoptosis.
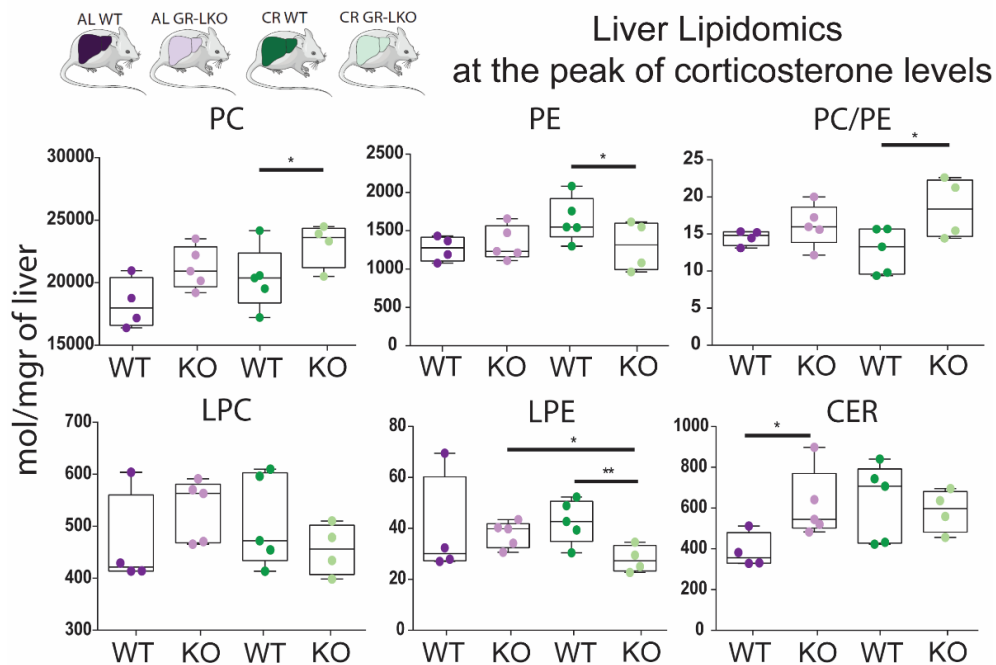
Figure 46: Hepatic lipidome of caloric restricted GR-LKO mice shows reduced PE and increased PC levels.

Box plot with single data points from the sum of concentration of PC, PE, PC/PE, LPC, LPE and CER from the hepatic lipidome of AL-fed and CR WT and GR-LKO mice (n=4-5 mice per condition with 544 tested different lipid species).

Ceramides act as significant precursors of sphingolipids and play an important role in membrane homeostasis and in cellular signaling (Kogot-Levin & Saada, 2014). In the ceramide production pathways, there are four different possible pathways, responsible for their production: (i) the *de novo* synthesis pathway, (ii) the sphingomyelinase pathway, (iii) the salvage pathway and (iv) the catabolism of the exogenous ceramides (Apostolopoulou et al., 2018; Kogot-Levin & Saada, 2014). Dihydroceramides (DCER) can produce, through the *de novo* synthesis pathway, hepatic ceramides. In this pathway, RNA-seq in caloric restricted GR-LKO mice showed up-regulation of *Sptlc2*, which is a subunit of the palmitoyltransferase SPT (Dawkins et al., 2001, 2002). In the same time, complex sphingolipids can be degraded in lysosomes into hexosylceramides (HCER) and these can be re-cycled through the salvage pathway for the ceramide production **(Figure 47A)** (Apostolopoulou et al., 2018). RNA-seq data showed that absence of hepatic GR down-regulates *Asah2*, which encodes ceramidase for the degradation of sphingolipids (Kono et al., 2006). The reduced *Asah2* levels can explain by part the higher HCER levels of caloric restricted GR-LKO mice over the WT mice **(Figure 47B)**. During the transformation of dihydroceramides to ceramides, DES enzyme is responsible for this desaturase process (Casasampere et al., 2016). At the same time, DCER levels were the same among the different groups because there was no difference in *Des* gene between caloric restricted WT and GR-LKO mice **(Figure 47B)**. Another interesting pathway was the catabolism of exogenous ceramides. *S1pr1* and *Plpp3* were up-regulated in the caloric restricted GR-LKO mice compared to WT mice. *S1pr1* is a novel receptor of sphingosine 1-phosphate, while *Plpp3* encodes an integral membrane enzyme responsible for the dephosphorylation of phosphate esters in glycerol- and sphingophospholipids (Tang et al., 2015; L. Zhang et al., 2012). It seems that caloric restricted WT mice express higher levels of *Sgms1/2* and *Smpd1*, enhancing the sphingomyelin synthesis and breakdown, respectively. However, it seems that absence of hepatic GR in caloric restriction reduces the expression of *Smpd2*, which is responsible for the transformation of sphingomyelin to ceramides (**Figure 47A**). The down-regulation of *Smpd2* in combination with the increased *S1pr1* signaling can explain the accumulation of sphingomyelin in the *ad-libitum* and caloric restricted GR-LKO mice. Conclusively, absence of hepatic GR increased the synthesis of hepatic SM in both *ad-libitum* and caloric restriction, while HCER was only increased in caloric restriction.
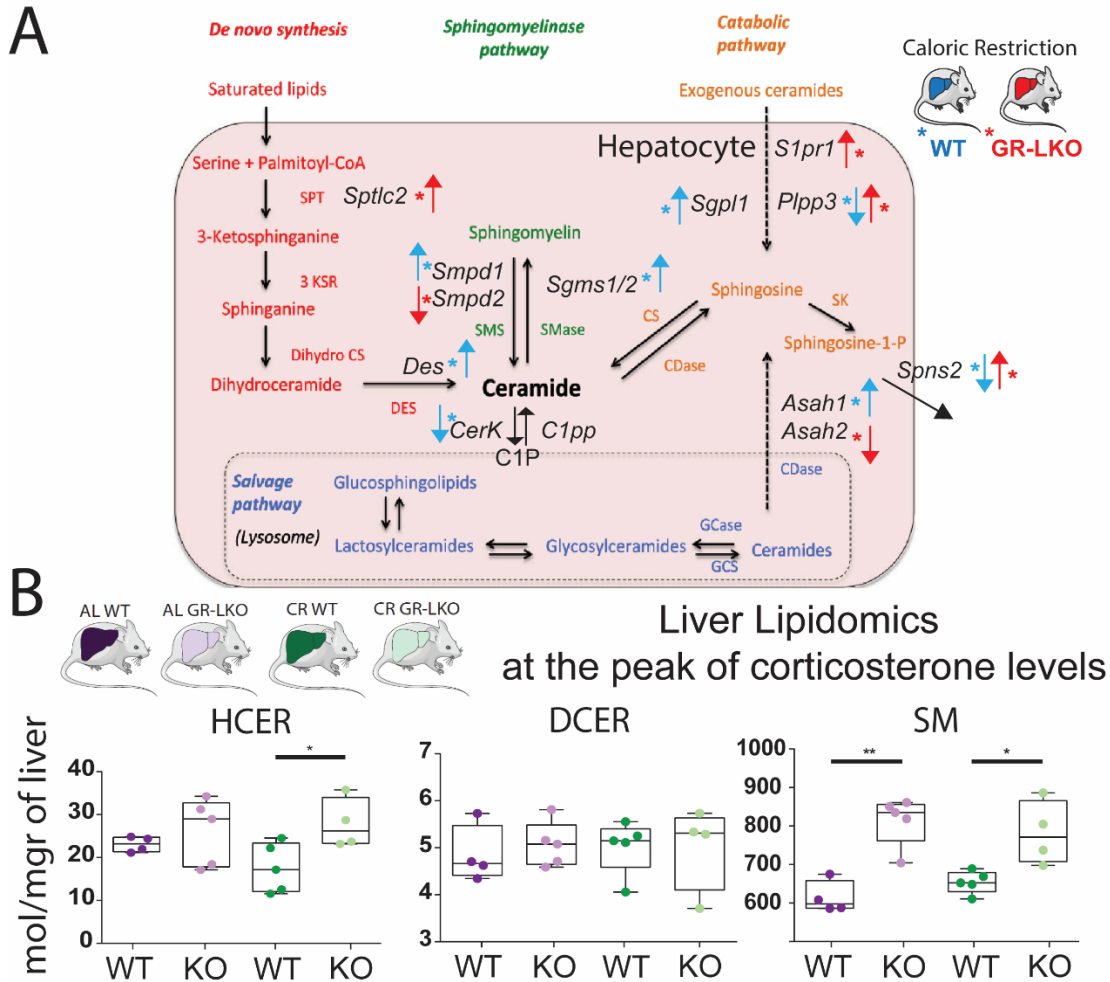
Figure 47: Hepatic lipidome of caloric restricted GR-LKO mice shows increased HCER and SM levels.

A: The different pathways of ceramide production. Picture adapted from Apostolopoulou et al., 2018. **B:** Box plot with single data points from the sum of concentration of HCER, DCER and SM from the hepatic lipidome of *ad-libitum* fed and caloric restricted WT and GR-LKO mice (n=4-5 mice per condition with 515 tested different lipid species). Down- and up-regulated genes from the RNA-seq between *ad-libitum* and caloric restricted WT mice are marked with blue color, showing their trends. In parallel, down- and up-regulated genes from the RNA-seq between caloric restricted WT and GR-LKO mice are marked with red color, showing their trends in the ceramide synthesis pathway.

5.11 GR deletion in liver affects the total activity and the energy expenditure post-prandially in caloric restriction

Until now, GR down-regulates fatty acid catabolism and activates glycogen breakdown and glycolysis for the production of energy. Given the fact that liver is the main organ for the energy production, we assessed their energy status. Since AKT/FOXO1 signaling was dampened and many energy-related genes were repressed, caloric restricted GR-LKO mice were measured in metabolic cages. Indirect calorimetry, locomotor activity and energy expenditure were measured during 4 consecutive days of the 5th week of caloric restricted GR-LKO mice at 23 ºC and 12hr light-12hr dark daily cycle. Data shown are the average of these 4 days of measurements of all animals for each group.

Initially, the body composition of *ad-libitum* and caloric restricted GR-LKO mice was measured by NMR for assessing their body composition at the 5th week of the caloric restriction regimen. No significant difference among the different groups was observed for both fat and lean mass (**Figure 48A and 48B**).
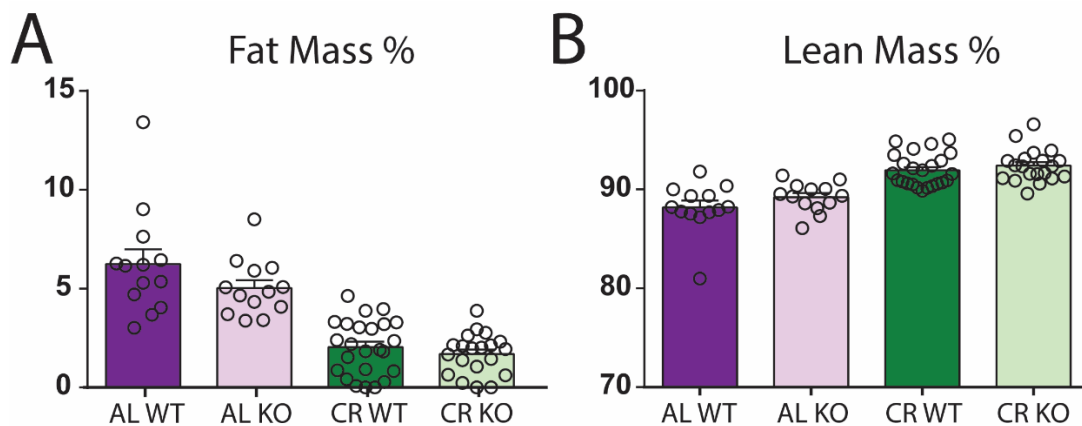
Figure 48: Deletion of hepatic GR does not affect the body composition during caloric restriction.

A-B: Percentage of fat mass (A) and lean mass (B) from *ad-libitum* fed and caloric restricted WT and GR-LKO mice measured by NMR. n= 10-15 biological replicates per condition, WT: Wild Type; KO: GR liver specific knock-out; AL: *Ad-Libitum*; CR: Caloric Restriction.

Interestingly, caloric restricted GR-LKO mice showed a reduced locomotor activity in multiple moments during the day and the night (**Figure 49A**). During the day, caloric restricted GR-LKO mice present less locomotor activity between ZT4 and ZT11, while

during the night mainly between ZT12 and ZT16 (**Figure 49A**). In the case of using all the values between only the day and only the night, there is a slight tendency on average for less activity of the caloric restricted GR-LKO compared to the wild type mice during the day (**Figure 49B**). Given the fact that caloric restricted GR-LKO mice present the same body composition with the WT mice and lower locomotor activity, they are probably not able to utilize the same energy sources. Considering both day and night, all data points showed that GR-LKO mice move significantly less compared with the wild type mice, probably due to their increased glycogen accumulation and facilitate glycolysis in the liver (**Figure 49B**).
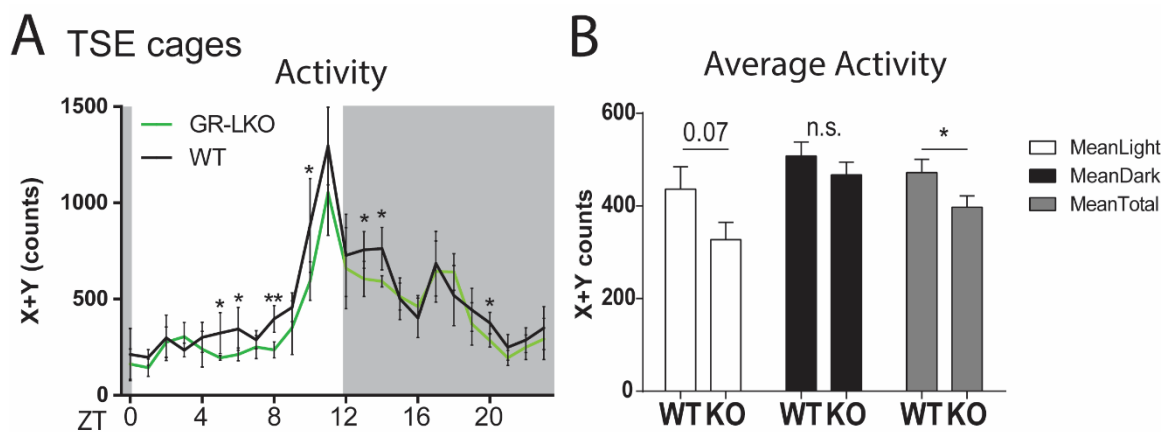
Figure 49: Caloric restricted GR-LKO mice showed significant less activity both during the day and the night.

A: Hourly locomotor activity on the XY axis measured in beam breaks per hour. **B:** Average locomotor activity pooling the average values for each hour during the day, the night and the whole day-night cycle. XY counts represent mean ± SEM, n =7-8 mice, *p<0.05, **p<0.01, and ns = not significant. Student's t-test.

Another important parameter of evaluating the use of energy source in the caloric restricted GR-LKO mice was their respiratory exchange ratio (RER), which is equivalent to the ratio between CO_2 production and O_2 consumption. A RER around 0.7 indicates fat is the predominant fuel source, while a value of 1 corresponds to the utilization of both fat and carbohydrates (Matarese, 1997; Spriet, 2014). Undoubtedly, caloric restricted WT and GR-LKO mice showed a similar respiratory curve with significant differences at specific timepoints between ZT0 and ZT10 (**Figure 50**). During the night caloric restricted GR-LKO mice showed a reduced respiration rate between ZT15 and ZT17, a time window, where all their food consumption was fully done (**Figure 50A**). Unfortunately, data points both

from the day and night were similar between the caloric restricted GR-LKO and wild type mice (**Figure 50B**). So, absence of hepatic GR does not attribute significantly to a defective transition from fat to carbohydrate and fat usage, albeit the resistance of mice to lose glycogen, observing significant fluctuations of respiration at specific timepoints.
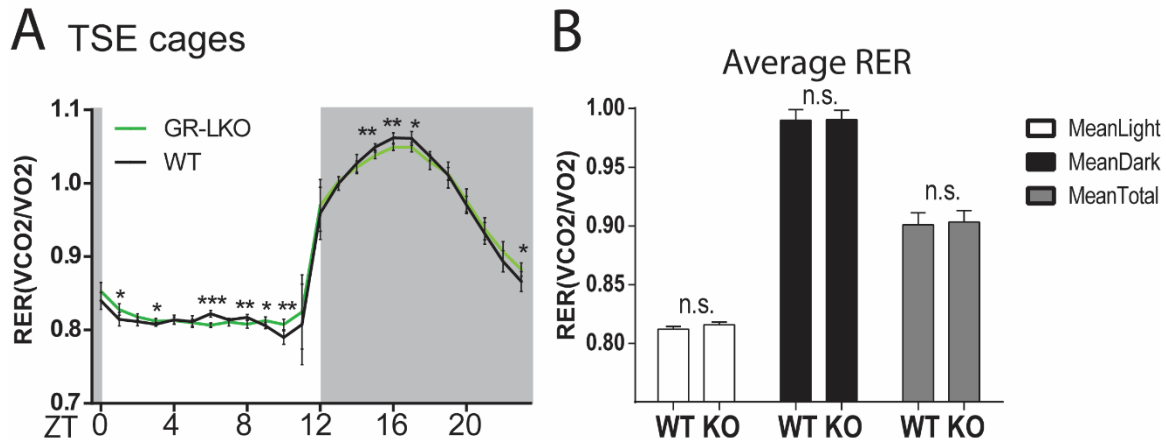
Figure 50: Caloric restricted GR-LKO mice show no difference in respiratory exchange ratio.

A: Hourly respiratory exchange ratio calculated as the ratio between VCO_2 and VO_2. **B:** Average respiratory exchange ratio only during the day, the night and the whole day cycle. RER counts represent mean ± SEM, n =7-8 mice, *$p<0.05$, **$p<0.01$, and ns = not significant. Student's t-test.

In addition, energy expenditure was measured in kcal per hour, showing same levels of consumed kcals during the day in both caloric restricted WT and GR-LKO, while during the night an increased post-prandial peak was detected in GR-LKO mice (**Figure 51A**). This post-prandial peak is concordant with the lower peak of respiratory exchange ratio and the lower locomotor activity, around ZT16. This could be due to the activation of PPAR-α signaling, based on the RNA-seq data at this timepoint (**Figure 29**). Interestingly, the liver mass over the total body mass in the caloric restricted GR-LKO mice was higher than in wild type, probably by the accumulation of glycogen and other carbohydrates (**Figure 51B**). Based on the aforementioned data, caloric restricted GR-LKO mice have less locomotor activity and heavier livers, which were caused by the resistance of these mice to burn carbohydrates in the liver. Despite this defect in the liver, GR-LKO mice are able to switch efficiently from the lipid usage to the carbohydrate utilization program without having massive systemic metabolic changes.
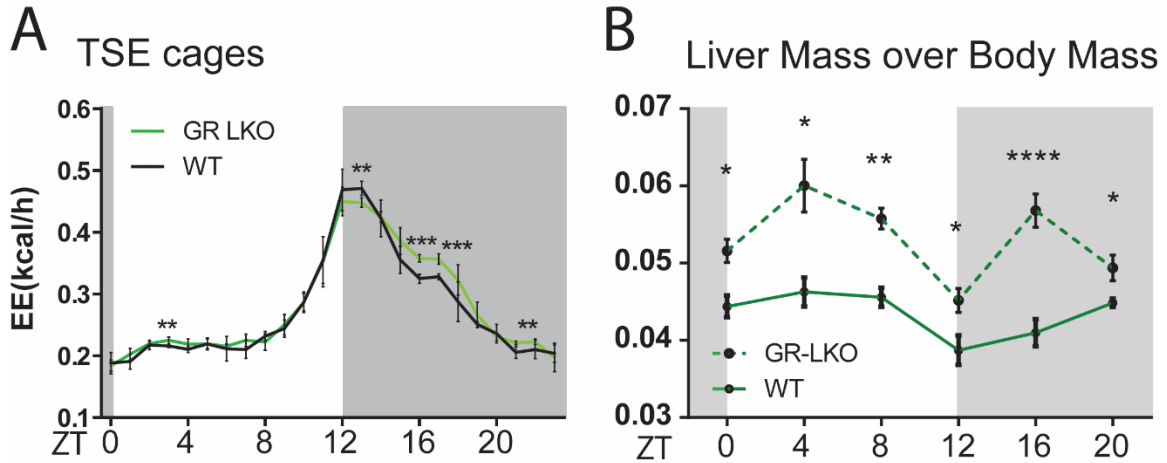
Figure 51: Caloric restricted GR-LKO mice show a post-prandial increase in the energy expenditure and increased liver mass.

A: Hourly energy expenditure measured in kcal per hour. **B:** Liver mass over the body mass in caloric restricted GR-LKO and WT mice around the clock. Values represent mean ± SEM, n =3-8 mice per timepoint, *p<0.05, **p<0.01, ***p<0.001, ****p<0.0001 and ns = not significant. Student's t-test. ZT: Zeitgeber.

6 Discussion

We performed a comprehensive study that linked next-generation sequencing data and mouse phenotyping. We thus used wild type and genetically-modified mice for the caloric restriction regimen in order to study the effects of hepatic GR in this nutritional status.

The main conclusion of this work is that caloric restriction enhances the GR activity, which is necessary for the reprogramming by caloric restriction. Hepatic GR in association with FOXO1 are necessary for the transcriptional program of autophagy, insulin sensitivity, cholesterol metabolism, glycogen breakdown and sharper transition from fatty acid metabolism to carbohydrate usage. The absence of GR/FOXO1 axis activates in response to oxidative stress the PPAR alpha signaling, as a counterbalance mechanism.

This discovery has important implications for finding novel caloric restriction mimetics that potentially can be included in the whole armamentarium of these substances (Madeo et al., 2019). The goal of understanding the role of hepatic GR in association with FOXO1 can deepen our knowledge for modulating this axis in the right timing.

6.1 Hepatic reprogramming by GR and FOXO1 are necessary for the effects of caloric restriction

Caloric restriction is a specific feeding-fasting regimen with a reduced food intake, which has many beneficial effects not only in mice but also in worms, flies, monkeys and humans (Madeo et al., 2019; Trepanowski et al., 2011). All these models have shown an anti-aging phenotype and protection from many metabolic abnormalities. At the basis of caloric restriction, the absence of calories dampens insulin signaling, which modulates downstream transcription factors, such as the FOXO transcription factors (Golson & Kaestner, 2016; Zhu, 2016). At the same time, this caloric consumption lessens the circulating glucose levels, forcing the adrenal glands to secrete glucocorticoids. This combined enhanced glucocorticoid and dampened insulin secretion can be called caloric stress (**Figure 10**) (Leakey et al., 1994). Caloric stress can increase sharply the nuclear residency of both GR and FOXO1, reprogramming the energy status of the hepatocytes (**Figure 11**). This FOXO1 function of reprogramming the hepatocytes has been observed also in other cell types, such as neurons or myocytes (Doan et al., 2016; Gopal et al.,

2017). Different diet regimens, such as time-restricted feeding and caloric restriction, affect FOXO1 signaling and localization (D. H. Kim et al., 2015; Regmi & Heilbronn, 2020). This enhanced FOXO1 activity can protect from disease, such as Alzheimer and diabetes, which are associated with insulin resistance, oxidative stress and recycling of proteins. Based on previous studies, GR binds to the *Foxo1* promoter and increases its expression (**Figure 14**). This function of GR, elevating the FOXO1 levels, increases the synergism for the expression of gluconeogenic genes upon feeding-fasting cycle and prolonged starvation (Kalvisa et al., 2018; Matsumoto et al., 2007; Quagliarini et al., 2019; Waddell et al., 2008). For this reason, studying the co-occupancy of these factors in genome-wide level can reveal their role in caloric restriction.

Genomic studies of both hepatic GR and FOXO1 in fasting have revealed an enrichment of FOX and GRE motifs respectively (Kalvisa et al., 2018; Shin et al., 2012). This increased recognition of the motifs implies that they cooperate for the expression of liver fatty acid-related and gluconeogenic genes, such as *Angptl4*, *Gck*, and *Pck1*. Until now, validation in the promoters of these genes have shown strong synergism between GR and FOXO1 in both hepatocytes and myocytes (Kalvisa et al., 2018; Waddell et al., 2008). The same transcriptional synergism was proved in other promoters and enhancers, where we had strong binding from GR and FOXO1 (**Figure 19**). Interestingly, during fasting both hepatic GR and FOXO1 resided in distal genomic elements (enhancers) facilitating transcriptional activation. In the case of *in vitro* hepatocyte studies, only *Gck* promoter has been extensively studied, showing the importance of this synergism for the gluconeogenesis (Langlet et al., 2017). The multiple GR binding with FOXO1 revealed that they are responsible for the expression of this gene (Præstholm et al., 2021b). However, the way GR and FOXO1 perform transcriptional activation versus repression still remains elusive. Until now, *Gck*, is the only locus showing that SIN3A, a FOXO1 co-repressor complex, can perform repression through the recruitment of HDACs (Zullo et al., 2019). Our ChIP-seq data for the hepatic SIN3A showed a smaller genome-wide binding profile in restriction (**Figure 20 and 21**). Common GR/FOXO1/SIN3A target loci (promoters or enhancers) in caloric restriction, were involved in insulin- and molecular clock-related processes (**Figure 22**). So far, this complex was connected with genome instability in yeast studies, while in our hepatic ChIP-seq data were addtional pathways in the overlap with GR and FOXO1, such as autophagy, insulin resistance, and fatty acid elongation (**Figure 22**). Additionally, the SIN3A complex can be affected by multiple factors, such as HDAC inhibitors (Shimazu et al., 2013). The increased circulating hydroxybutyrate levels in fasting or caloric

restriction can pause the HDAC activity, blocking the repression action of SIN3A complex (Shimazu et al., 2013). The reduced SIN3A-HDAC activity can explain the proportional transcriptional activation of the GR/FOXO1 synergism at the peak of corticosterone levels. Our ChIP-seq data revealed that caloric restriction reduced the genome-wide SIN3A binding profile (**Figure 21**). The retained SIN3A occupancy in this condition indicates that this complex constantly binds to promoter regions of insulin- and clock-related genes. For the aforementioned reasons, it will be interesting to measure the circulating and hepatic hydroxybutyrate levels in the restricted and synchronized ad-libitum-fed mice, in order to understand the inhibitory role of this metabolite. Evaluation of SIN3A and HDAC1 binding at the peak of hormones in the restricted mice, through ChIP-qPCR, can give further insight in relevant loci. On the other side, the common GR/FOXO1 binding sites are equally distributed in promoter, intergenic and intronic enhancers (**Figure 18**). The common GR/FOXO1 genome-wide binding profile can explain the phenotypical outcome of the mice when one of the two factors is missing. GR-LKO and FOXO1-LKO mice are prone to develop hepatic steatosis through accumulation of triglycerides and other lipid species, recapitulating the role of GR/FOXO1 in the liver (Quagliarini et al., 2019; K. Zhang et al., 2012). It is necessary though to validate the increased recruitment of GR/FOXO1 in the caloric-restricted promoters/enhancers caused by caloric stress.

At the transcriptional level, studies in GR-LKO mice upon HFD and fasting have shown deregulation of pathways related with carbohydrate-, fatty acid-, and bile acid-related targets (Kalvisa et al., 2018; Quagliarini et al., 2019). Performing transcriptomic analysis in restricted GR-LKO mice at the peak of hormones and post-prandially, we observed an inability of mice to switch from fatty acid oxidation to carbohydrate metabolism at the peak of hormones (**Figure 27**). Absence of hepatic GR attenuates the FOXO transcriptional program, shutting down the glucose production. Gluconeogenesis, glycogen breakdown and glycolysis were significantly reduced, providing less energy in these mice (**Figure 27, 29, 32, 34, 37 and 38**). It is known that FOXO1 factor blocks the expression of SREBP-1c, repressing fatty acid oxidation and glycolysis (Matsumoto, 2006; W. Zhang et al., 2006). Therefore, the blocked FoxO signaling drives the liver to continue using fatty acid oxidation and peroxidation for energy production. At the same time, the absence of GR/FOXO1 signaling attenuates the autophagy program leading to aggregated harmful products, which were not recycled in the liver. Furthermore, GR-LKO mice present a phenotype of insulin resistance, since AKT/FOXO1 signaling is not responsive in the same level as in the caloric restricted WT mice (Chen et al., 2010; Hay, 2011; Ni et al., 2007).

Insulin resistance can be explained by the fact that FOXO1 binds and regulates genes upstream in the same pathway. The increased inactive FOXO1 signaling leads to negative feedback loop for the activation of AKT by the insulin in the GR-LKO mice. It is important to be mentioned that dexamethasone, an artificial glucocorticoid, can induce the *Foxo1* expression by GR, recruiting the protein to the common GR sites. The overactivation of the FOXO1 action can give many unpleasant side-effects. For this reason, it is necessary to induce the GR/FOXO1 axis in the right timing and under specific condition. In the case of caloric restriction, high NAD^+ availability increases the NAD-dependent deacetylase SIRT1, which potentially, removes acetyl group not only from FOXO1 but also from histone marks (Boily et al., 2008; Chang & Guarente, 2014). The modulation of FOXO1 by the AMPK signaling and NAD production pathway can probably explain that they are potentially specific post-translational modifications in FOXO1, which can modulate its function. A further analysis of specific post-translational modification of FOXO1 can give new insights for the transcriptional mechanism between GR and FOXO1 in caloric restriction. Addition to in vivo evidence, in vitro primary hepatocyte cultures can give a cleaner outcome in the regulation of these targets. Ablation of each factor and treatment with dexamethasone and insulin can help defining better the transcriptional program between GR/FOXO1 and SIN3A complex. Conclusively the GR/FOXO1 synergism plays a central role in the hepatic adaptation to the caloric restriction for the efficient transition from lipids to carbohydrates.

6.2 Carbohydrates and lipids as energy fuels in the liver during caloric restriction

Previous studies have shown that caloric restriction activates essential mechanisms for the energy production from all the possible energy sources. Published works have shown that starvation, caloric restriction and intermittent fasting can mobilize fat in order to release fatty acids and supply the organs with energy through the fatty acid oxidation (the first alternative energy source). In condition of a prolonged lack of nutrients, liver utilizes fatty acids to produce ketones and supply with energy the remaining organs. Liver lacks of the enzyme thiophorase (β-ketoacyl-CoA transferase), which metabolizes the ketone bodies. Consequently, only the peripheral organs, such as brain and muscles, can metabolize ketone bodies in order to sustain their energy levels. Proteins can also be degraded into amino acids and used for ATP production. In opposite, in liver, glycogen, glucose, fatty acids and amino acids can be degraded in order to be utilized for energy.

More specifically, glycogen can be transformed into glucose and enter the glycolysis pathway to produce, through the TCA cycle, ATP molecules in mitochondria (Rui, 2014). The same fate applies for the amino acids, which will enter in the glycolysis pathway and through again the TCA cycle will produce ATP molecules. In the case of fasting, fatty acids can produce energy through the β oxidation in mitochondria and generate ketones for supplementing with energy the extrahepatic organs (Rui, 2014). In our study, we observed that caloric restricted GR-LKO mice were consuming the same energy levels, while they were moving less. They had fluctuations of energy expenditure during the day in specific timepoints and during the night post-prandially compared to the caloric restricted WT mice. Caloric restricted GR-LKO mice have a differential post-prandial response in respiratory exchange ratio (RER) and energy expenditure, showing a defect for this transition. Our RNA-seq data in the GR-LKO mice have shown increased PPARα signaling and dampened FOXO1 signaling, both at the peak of hormones and post-prandially. This prolonged PPARα signaling transcriptionally in the liver can attribute to these slight metabolic changes that we observed in the GR-LKO mice. Additionally, circulating levels of HDL, which are high in caloric restriction and concordant to the total cholesterol levels seem that they have a phase shift in secretion **(Figure 32)**. This transition in energy utilization is the key of caloric stress, in which liver starts instead of lipids, using carbohydrates before the initiation point of the active phase. Hepatic transcriptional program in caloric restriction is tightly coordinated in order to prepare the liver to express all the necessary enzymes for the process and storage of carbohydrates in order to sustain the energy levels. Hepatic GR deletion does not disrupt systematically the fuel switching, but alters the post-prandial energy utilization right after feeding.

6.3 Carbohydrate and lipid metabolism are cross-connected with the molecular clock and autophagy under caloric restriction

Molecular clock and autophagy are two processes strongly associated with the functionality of hepatocytes. Through aging, both molecular clock and autophagy processes are dampened lowering the whole cell functionality and disrupting the hepatic autonomous and non-autonomous functions (cross-organ communication). There are evidences that core circadian clock factors are degraded in lysosomes with the process of autophagy affecting the glucose production (Toledo et al., 2018). In case of CRY1

protein, there is a distinct LIR motif, which gives the ability of recognition from the LC3 mature autophagosomes and direct degradation from the lysosomes (Toledo et al., 2018). CRY1 suppresses the hepatic gluconeogenesis by rhythmic repression of GR and decreasing nuclear FOXO1 (Jang et al., 2016; Lamia et al., 2011; E. E. Zhang et al., 2010). For this reason, autophagy degrades CRY1 permitting GR and FOXO1 to activate gluconeogenesis. Considering all these events at the peak of glucocorticoids, it is possible that maximal autophagy flux leads to CRY1 degradation contributing to glucose production (Toledo et al., 2018).

At the peak of corticosterone levels (at ZT12), caloric restricted WT mice showed fully maturation of LC3 protein, which was blocked in the absence of GR (**Figure 42**). This lower LC3 transition from the I to II form can be justified by the common binding of GR/FOXO1 in *Map1lc3b* locus. The lower activation of this locus can change its expression levels and the LC3 turnover for the final maturation of autophagosomes, altering the whole process of autophagy. In parallel, hepatic PE levels in restricted GR-LKO mice were lower than in WT, which underlies the importance of hepatic GR/FOXO1 axis in the final autophagosome maturation. Examining key autophagic protein, which participate in various stages of autophagy, caloric restricted GR-LKO mice showed an altered turnover in the conjugation system between LC3 and PE, which can be caused mainly by their levels. It is remarkable that high PE levels in both mammals and flies positively regulate longevity (Calzada et al., 2016). As secondary effects, absence of hepatic GR blunts the p62 protein levels, which has a LIR motif, and reduces Beclin1 protein levels, which is necessary for the initiation of the phagopore formation (**Figure 42**). To conclude, absence of hepatic GR/FOXO1 axis disrupts the LC3 levels and the PE coupling to the mature autophagosomes, blocking the process of autophagy in the final stage and giving an aged liver phenotype (**Figure 52**).

Time-restricted feeding (TRF) protects clock mutant mice from obesity and serum hyperlipidemia. More specifically, Chaix et al showed that TRF can protect BMAL1-LKO, REV-ERBα/β-LDKO (double LKO) and CRY1/CRY2-KO (double KO) from metabolic abnormalities, when they controlled their fasting-feeding cycle. This imposed feeding behavior by TRF increased their energy expenditure and respiratory exchange ratio during their active phase. The higher RER during the feeding period of these mice indicates that TRF led to a relatively higher usage of carbohydrates and higher lipid usage during their fasting period. Additionally, the higher oxygen consumption increased transiently their

overall oxidative metabolism (Chaix et al., 2014, 2019; Hatori et al., 2012). Consequently, TRF drives a rhythm in substrate utilization without having a functional clock. Mechanistically, TRF increased the expression of genes related with cellular maintenance pathways, such as macromolecule quality control and repair pathways in DNA, RNA, and protein level. From the activation of these pathways, clock mutant mice were protected by liver fat accumulation. In the case of the *ad-libitum* GR-LKO mice, synchronization is exactly the same rational regimen with TRF. Surprisingly, synchronization of GR-LKO mice did not correct liver fat accumulation, showing the central role of GR/FOXO1 axis (**Figure 51B**). Even with caloric restriction, GR-LKO mice had increased oxidative metabolism (**Figure 34 and 51**). The higher post-prandial energy expenditure peak implies that caloric restricted GR-LKO mice consumed more energy in order to store carbohydrates in the form of lipids than using them for moving. This is the reason, that even upon caloric restriction, the reduced expression of the molecular clock factors in the absence of GR drives to liver fat accumulation. In opposition to the TR-fed clock mutant mice, the expression of PPARα and PPARγ in caloric restricted GR-LKO mice were up-regulated. These evidences prove that GR in both HFD and CR suppresses the PPARα and PPARγ levels (Quagliarini et al., 2019). The activation of the PPARα and PPARγ signaling can reveal another alternative hub of activation in the crosstalk between GR and other nuclear receptors. Lastly, clock-deficient mice in TRF were protected by insulin resistance, which remains to be validated in the caloric restricted GR-LKO mice (Chaix et al., 2019). Aberrant hepatic GR/FOXO1 axis causes reduced pAKT levels in these mice, leading to insulin resistance phenotype. Interestingly, liver lipidomics in these mice showed increased accumulation of sphingolipid species, such as hexosylceramides and sphingomyelin, which are correlated with oxidative stress and insulin resistance in non-alcoholic-fatty liver disease (NAFLD) (Apostolopoulou et al., 2018). To sum up, absence of hepatic GR impairs autophagy, the molecular clock machinery, insulin sensitivity and the transition from fatty acid to carbohydrate utilization program (**Figure 52**).
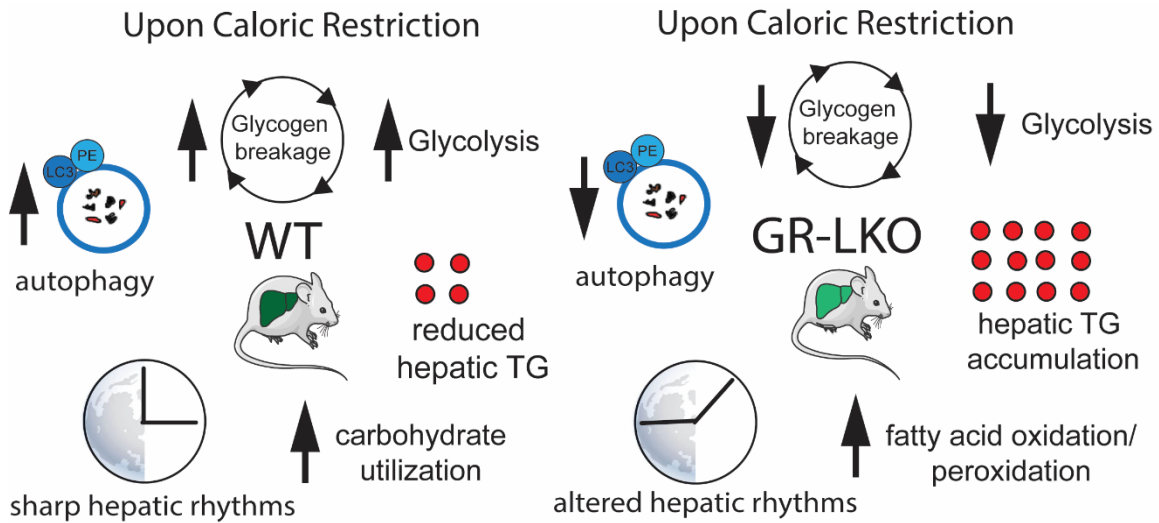
Figure 52: Phenotypical outcome of caloric restricted WT and GR-LKO mice.

In caloric restriction, WT mice present increased utilization of carbohydrates for production of energy. As energy supplying pathways, glycogen breakage and glycolysis are increased, in parallel with reduced TG levels, sharper hepatic rhythms and increased autophagy. In deletion of hepatic GR, mice have lower autophagy, and reduced glycogen breakage and glycolysis. In the same time, mice accumulate TGs and they have altered hepatic rhythms, which are reflected as imbalances in energy expenditure and activity, and continuous fatty acid oxidation/peroxidation at the peak of hormones and post-prandially.

6.4 Defects in energy production reveals peroxisomal signaling as another compensatory mechanism related with caloric restriction and aging

Genomic and transcriptomic studies pointed to enhanced PPARα signaling in the absence of hepatic GR in CR. Furthermore, the phenotype of the caloric restricted GR-LKO mice was related with cholesterol trafficking, ketogenesis, β-oxidation and lipid (TAG) accumulation, processes governed by the PPAR family (Duszka et al., 2020; Zardi et al., 2013). Examining the PPARα and PPARγ levels, the former was elevated in both mRNA and protein level in the caloric restricted GR-LKO mice (**Figure 35**). In the case of PPARγ, it is less abundant in the liver. The fact that hepatic free fatty acids were less in the GR-LKO mice could explain their use by the PPARα (**Figure 37 and 44**). Also, CR increases the NAD-dependent SIRT3, which deacetylates and activates mainly PPARα and modulates the AMPK-mTORC1 signaling for maintaining mitochondrial function and autophagy in macrophages and hepatocytes (J. Kim & Guan, 2019; T. S. Kim et al., 2019).

113

For this reason, it would be interesting to test the levels of SIRT3 and study the AMPK-mTORC1 signaling in the caloric restricted GR-LKO mice. Validating this pathway will enhance the theory that absence of GR permits PPARα to facilitate its function in order to compensate the energy losses and deters from lipotoxicity (Duszka et al., 2020). Careful examination of the PPARα signaling can give new insights for the reprogramming of the hepatocytes in absence of GR in CR.

Recent genomic studies in fasting revealed that FOXO1 and PPARα have a differential pattern between triglyceride homeostatic and glucose process related loci (Kitamoto et al., 2021). Distribution of annotated FOXO1 ChIP peaks in both fasting and feeding gave a statistically significant enrichment of triglyceride genes in introns, while for glucose metabolism genes in intergenic and distal gene regions (Kitamoto et al., 2021). In case of CR, common GR/FOXO1 annotated peaks were distributed relatively equally between the intronic, intergenic and promoter regions (**Figure 18**). It would be interesting since we detected enrichment of PPAR/RXR motif in the HOMER motif analysis in our datasets to distinguish the pattern of FOXO1 annotated peaks between the glucose and triglycerides genes in caloric restriction. This analysis will give a better view for the modulation of the common GR/FOXO1 targets. Moreover, PPARα ChIP-seq in caloric restriction will complete the genes that are regulated by the crosstalk between GR/FOXO1/PPARα. However, we would expect that absence of GR and FOXO1 leads to overactivation and increased PPARα binding, which remains to be validated in the caloric restricted GR-LKO and FOXO1-LKO mice. During insulin resistance, Kitamoto et al., propose that FOXO1 has a spreading binding pattern in resilient enhancers in the lipid and lipoprotein genes. *In vitro* studies in dexamethasone and insulin-treated primary FOXO1KO hepatocytes did not gave any difference which by part can be explained by PPARα binding (data not shown). These evidences enhance the idea that PPARα can recognize same sites with FOXO1 and regulate the same targets in the absence of hepatic GR in CR. For this reason, it would be encouraging to test the PPARα activity in these studies. This proposed model can recapitulate our hypothesis that absence of GR rewires the hepatic reprogramming from FOXO1 to PPARα signaling in caloric restriction (**Figure 53**).
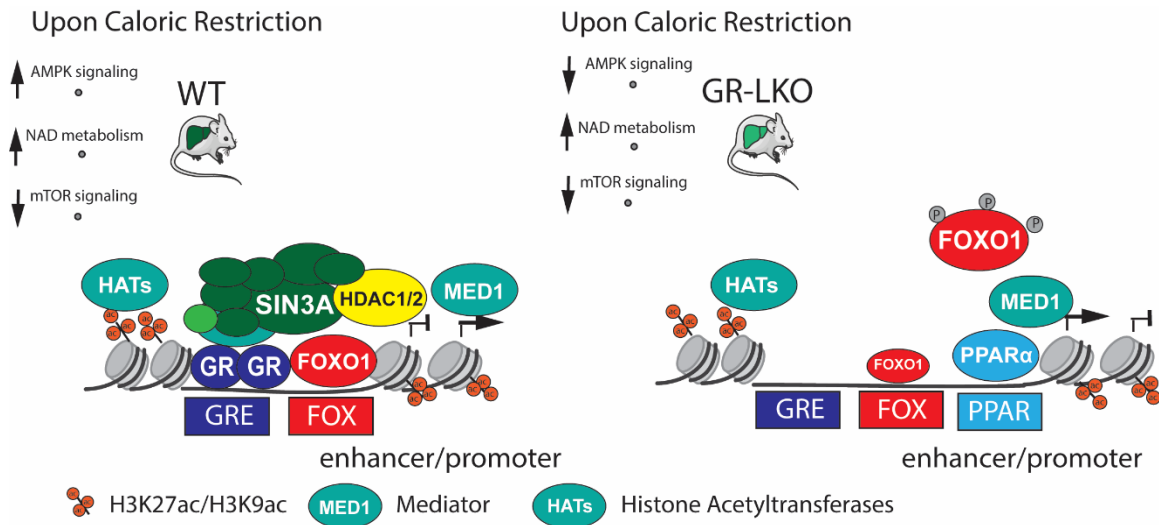
Figure 53: Graphical model of GR/FOXO1/PPARα in caloric restriction.

In caloric restriction, peak of glucocorticoids and low insulin levels lead to GR/FOXO1 recruitment in enhancers/promoters of metabolic genes (such as *Per1*, *Map1lc3b*, and *Gck*). In the same time, increased AMPK signaling and NAD metabolism probably reshape the chromatin acetylation pattern permitting positive regulation of transcription (by MED1, HATs) in the respective loci. In clock and insulin-related genes, there is recruitment of SIN3A/HDAC complex, which may close the loop of transcription, repressing these GR/FOXO1 targets. In the absence of hepatic GR, mice switch from FOXO1 to PPARα transcriptional program, affecting the cholesterol secretion, the switch from fatty acid to carbohydrate metabolism, autophagy, glycogen breakdown and lipid homeostasis.

6.5 The yin and the yan of glucocorticoids reveals a translational aspect

Chronic exposure to glucocorticoids has been connected with many unpleasant side-effects, which are opposite to the role of caloric restriction. In the context of caloric restriction, rodents were having high corticosterone levels in combination with low insulin (**Figure 10**). This signaling affects GR and all the insulin-mediated copartners of this nuclear receptor. Until now, we have observed that GR has a differential role based on the neighboring copartner. For example, high fat diet increases the damage to the liver activating the STAT5 signaling and boosting their association (Quagliarini et al., 2019). In high-fat diet GR-LKO mice, the reduced GR/STAT5 cross-talk leads to a worsened hepatic steatosis, which is contradictory to the hepatic GR deletion in the db/db mice (Lemke et al., 2008). In db/db mice, the transient hepatic GR deletion improved the hepatic steatosis

because it de-represses the *Hes1* and compensates this phenotypical outcome by normalizing triglyceride levels. Moreover, the silencing of GR with the virus in the adult liver can potentially give a differential outcome in comparison to the constitutive Alb-Cre+ mice, where hepatic deletion occurs early in development. Based on the aforementioned, timing and metabolic background of hepatic GR deletion can alter this phenotypical outcome.

In the case of other cell types, such as macrophages, there is also recruitment of complexes, such as the COMPASS, SWI/SNF and COREST complex (Greulich et al., 2021). In the case of caloric restriction, the role of FOXO1 and PPARα is important for the regulation of processes related with the energy hepatic status. However, it remains puzzling if the timing of the secreted glucocorticoids can impact differently on the activation of the respective factors. For this reason, it would be interesting to synchronize the feeding behavior in rodents and administer exogenously corticosterone in order to mimic the hypercorticosterolemia of caloric restriction. Assessing the recruitment of GR, FOXO1, PPARα and SIN3A/HDAC complex, by chromatin immunoprecipitation coupled with quantitative PCR, can elucidate the mechanism of activation versus repression in CR. Further validation of positive transcription marks can be proved via ChIP-qPCR of histone marks, such as H3K27ac and H3K9ac in the respective loci. Comparing this experimental set up with the caloric restriction regimen, we will understand if there is a difference in the recruitment of these factors. Moreover, it would be valuable to see how the insulin sensitivity of caloric restriction and activation of protective pathways, such as AMPK signaling and NAD metabolism, can facilitate epigenetic regulation of these transcription factors and manipulate these chromatin marks. Studying the post-translational modifications of GR and FOXO1 in caloric restriction versus this acute hypercorticosterolemia can drive an altered transcriptional programming. In further comparison between acute hypercorticosterolemia and caloric restriction regimen, it would be wise to perform chromatin immunoprecipitation coupled with sequencing in order to assess the genome-wide binding profile of GR versus the GR cistrome in CR. In case that the GR cistrome will be the same and the recruitment of FOXO1 and PPARα comparable with CR, then it would be really encouraging to administer glucocorticoids at the beginning of the active phase in humans and following a reduction of calories. Of course, caloric restriction is not a favorable method for the western society. As an alternative perspective, exercise or cortisol in combination with specific caloric restriction mimetics can be administered to humans in order to protect from the side-effects of glucocorticoids.

Understanding the role of glucocorticoids can improve our view for these anti-inflammatory drugs and treat patients with metabolic abnormalities trying to align all the GR-mediated processes. Despite that chronic exposure to these drugs leads to many side-effects, the precise manipulation of the hepatic metabolism by glucocorticoids can reduce the side-effects without misaligning the aging clock.

7 References

Acosta-Rodríguez, V. A., de Groot, M. H. M., Rijo-Ferreira, F., Green, C. B., & Takahashi, J. S. (2017). Mice under Caloric Restriction Self-Impose a Temporal Restriction of Food Intake as Revealed by an Automated Feeder System. *Cell Metabolism*, *26*(1), 267-277.e2. https://doi.org/10.1016/j.cmet.2017.06.007

Aguilar-Ballester, M., Herrero-Cervera, A., Vinué, Á., Martínez-Hervás, S., & González-Navarro, H. (2020). Impact of Cholesterol Metabolism in Immune Cell Function and Atherosclerosis. *Nutrients*, *12*(7), 2021. https://doi.org/10.3390/nu12072021

Alers, S., Löffler, A. S., Wesselborg, S., & Stork, B. (2012). Role of AMPK-mTOR-Ulk1/2 in the Regulation of Autophagy: Cross Talk, Shortcuts, and Feedbacks. *Molecular and Cellular Biology*, *32*(1), 2–11. https://doi.org/10.1128/MCB.06159-11

Alessi, D. R., Andjelkovic, M., Caudwell, B., Cron, P., Morrice, N., Cohen, P., & Hemmings, B. A. (1996). Mechanism of activation of protein kinase B by insulin and IGF-1. *The EMBO Journal*, *15*(23), 6541–6551.

Almlöf, T., Wright, A. P. H., & Gustafsson, J.-Å. (1995). Role of Acidic and Phosphorylated Residues in Gene Activation by the Glucocorticoid Receptor. *Journal of Biological Chemistry*, *270*(29), 17535–17540. https://doi.org/10.1074/jbc.270.29.17535

Aman, Y., Schmauck-Medina, T., Hansen, M., Morimoto, R. I., Simon, A. K., Bjedov, I., Palikaras, K., Simonsen, A., Johansen, T., Tavernarakis, N., Rubinsztein, D. C., Partridge, L., Kroemer, G., Labbadia, J., & Fang, E. F. (2021). Autophagy in healthy aging and disease. *Nature Aging*, *1*(8), 634–650. https://doi.org/10.1038/s43587-021-00098-4

Aparicio, O., Geisberg, J. v, & Struhl, K. (2004). Chromatin immunoprecipitation for determining the association of proteins with specific genomic sequences in vivo. *Current Protocols in Cell Biology*, *Chapter 17*, Unit 17.7. https://doi.org/10.1002/0471143030.cb1707s23

Apostolopoulou, M., Gordillo, R., Koliaki, C., Gancheva, S., Jelenik, T., de Filippo, E., Herder, C., Markgraf, D., Jankowiak, F., Esposito, I., Schlensak, M., Scherer, P. E., & Roden, M. (2018). Specific Hepatic Sphingolipids Relate to Insulin Resistance, Oxidative Stress, and Inflammation in Nonalcoholic Steatohepatitis. *Diabetes Care*, *41*(6), 1235–1243. https://doi.org/10.2337/dc17-1318

Assmann, G., & Gotto, A. M. (2004). HDL Cholesterol and Protective Factors in Atherosclerosis. *Circulation*, *109*(23_suppl_1). https://doi.org/10.1161/01.CIR.0000131512.50667.46

Atger, F., Mauvoisin, D., Weger, B., Gobet, C., & Gachon, F. (2017). Regulation of Mammalian Physiology by Interconnected Circadian and Feeding Rhythms. *Frontiers in Endocrinology*, *8*. https://doi.org/10.3389/fendo.2017.00042

Ayer, D. E., Lawrence, Q. A., & Eisenman, R. N. (1995). Mad-Max transcriptional repression is mediated by ternary complex formation with mammalian homologs of yeast repressor Sin3. *Cell*, *80*(5), 767–776. https://doi.org/10.1016/0092-8674(95)90355-0

Barnett, D. W., Garrison, E. K., Quinlan, A. R., Stromberg, M. P., & Marth, G. T. (2011). BamTools: a C++ API and toolkit for analyzing and managing BAM files. *Bioinformatics*, *27*(12), 1691–1692. https://doi.org/10.1093/bioinformatics/btr174

Biggs III, W. H., & Cavenee Karen C., W. K. (2001). Identification and characterization of members of the FKHR (FOX O) subclass of winged-helix transcription factors in the mouse. *Mammalian Genome*, *12*(6), 416–425. https://doi.org/10.1007/s003350020002

Boily, G., Seifert, E. L., Bevilacqua, L., He, X. H., Sabourin, G., Estey, C., Moffat, C., Crawford, S., Saliba, S., Jardine, K., Xuan, J., Evans, M., Harper, M.-E., & McBurney, M. W. (2008). SirT1 Regulates Energy Metabolism and Response to Caloric Restriction in Mice. *PLoS ONE*, *3*(3), e1759. https://doi.org/10.1371/journal.pone.0001759

Bolger, A. M., Lohse, M., & Usadel, B. (2014). Trimmomatic: a flexible trimmer for Illumina sequence data. *Bioinformatics*, *30*(15), 2114–2120. https://doi.org/10.1093/bioinformatics/btu170

Bonkowski, M. S., Rocha, J. S., Masternak, M. M., al Regaiey, K. A., & Bartke, A. (2006). Targeted disruption of growth hormone receptor interferes with the beneficial actions of calorie restriction. *Proceedings of the National Academy of Sciences*, *103*(20), 7901–7905. https://doi.org/10.1073/pnas.0600161103

Bookout, A. L., Jeong, Y., Downes, M., Yu, R. T., Evans, R. M., & Mangelsdorf, D. J. (2006). Anatomical Profiling of Nuclear Receptor Expression Reveals a Hierarchical Transcriptional Network. *Cell*, *126*(4), 789–799. https://doi.org/10.1016/j.cell.2006.06.049

Bordone, L., & Guarente, L. (2005). Calorie restriction, SIRT1 and metabolism: understanding longevity. *Nature Reviews. Molecular Cell Biology*, *6*(4), 298–305. https://doi.org/10.1038/nrm1616

Breitkopf, K., Godoy, P., Ciuclan, L., Singer, M., & Dooley, S. (2006). TGF-β/Smad Signaling in the Injured Liver. *Zeitschrift Für Gastroenterologie*, *44*(01), 57–66. https://doi.org/10.1055/s-2005-858989

Broadhurst, D., Goodacre, R., Reinke, S. N., Kuligowski, J., Wilson, I. D., Lewis, M. R., & Dunn, W. B. (2018). Guidelines and considerations for the use of system suitability and quality control samples in mass spectrometry assays applied in untargeted clinical metabolomic studies. *Metabolomics*, *14*(6), 72. https://doi.org/10.1007/s11306-018-1367-3

Brunet, A., Bonni, A., Zigmond, M. J., Lin, M. Z., Juo, P., Hu, L. S., Anderson, M. J., Arden, K. C., Blenis, J., & Greenberg, M. E. (1999). Akt Promotes Cell Survival by Phosphorylating and Inhibiting a Forkhead Transcription Factor. *Cell*, *96*(6), 857–868. https://doi.org/10.1016/S0092-8674(00)80595-4

Brunet, A., Sweeney, L. B., Sturgill, J. F., Chua, K. F., Greer, P. L., Lin, Y., Tran, H., Ross, S. E., Mostoslavsky, R., Cohen, H. Y., Hu, L. S., Cheng, H.-L., Jedrychowski, M. P., Gygi, S. P., Sinclair, D. A., Alt, F. W., & Greenberg, M. E. (2004). Stress-Dependent

Regulation of FOXO Transcription Factors by the SIRT1 Deacetylase. *Science*, *303*(5666), 2011–2015. https://doi.org/10.1126/science.1094637

Calnan, D. R., & Brunet, A. (2008). The FoxO code. *Oncogene*, *27*(16), 2276–2288. https://doi.org/10.1038/onc.2008.21

Calzada, E., Onguka, O., & Claypool, S. M. (2016). *Phosphatidylethanolamine Metabolism in Health and Disease* (pp. 29–88). https://doi.org/10.1016/bs.ircmb.2015.10.001

Cantó, C., & Auwerx, J. (2009). Caloric restriction, SIRT1 and longevity. *Trends in Endocrinology & Metabolism*, *20*(7), 325–331. https://doi.org/10.1016/j.tem.2009.03.008

Cantó, C., Gerhart-Hines, Z., Feige, J. N., Lagouge, M., Noriega, L., Milne, J. C., Elliott, P. J., Puigserver, P., & Auwerx, J. (2009). AMPK regulates energy expenditure by modulating NAD+ metabolism and SIRT1 activity. *Nature*, *458*(7241), 1056–1060. https://doi.org/10.1038/nature07813

Cantó, C., Jiang, L. Q., Deshmukh, A. S., Mataki, C., Coste, A., Lagouge, M., Zierath, J. R., & Auwerx, J. (2010). Interdependence of AMPK and SIRT1 for Metabolic Adaptation to Fasting and Exercise in Skeletal Muscle. *Cell Metabolism*, *11*(3), 213–219. https://doi.org/10.1016/j.cmet.2010.02.006

Caratti, G., Iqbal, M., Hunter, L., Kim, D., Wang, P., Vonslow, R. M., Begley, N., Tetley, A. J., Woodburn, J. L., Pariollaud, M., Maidstone, R., Donaldson, I. J., Zhang, Z., Ince, L. M., Kitchen, G., Baxter, M., Poolman, T. M., Daniels, D. A., Stirling, D. R., … Ray, D. W. (2018). REVERBa couples the circadian clock to hepatic glucocorticoid action. *Journal of Clinical Investigation*, *128*(10), 4454–4471. https://doi.org/10.1172/JCI96138

Casasampere, M., Ordoñez, Y. F., Pou, A., & Casas, J. (2016). Inhibitors of dihydroceramide desaturase 1: Therapeutic agents and pharmacological tools to decipher the role of dihydroceramides in cell biology. *Chemistry and Physics of Lipids*, *197*, 33–44. https://doi.org/10.1016/j.chemphyslip.2015.07.025

Chaix, A., Lin, T., Le, H. D., Chang, M. W., & Panda, S. (2019). Time-Restricted Feeding Prevents Obesity and Metabolic Syndrome in Mice Lacking a Circadian Clock. *Cell Metabolism*, *29*(2), 303-319.e4. https://doi.org/10.1016/j.cmet.2018.08.004

Chaix, A., Zarrinpar, A., Miu, P., & Panda, S. (2014). Time-Restricted Feeding Is a Preventative and Therapeutic Intervention against Diverse Nutritional Challenges. *Cell Metabolism*, *20*(6), 991–1005. https://doi.org/10.1016/j.cmet.2014.11.001

Challet, E. (2015). Keeping circadian time with hormones. *Diabetes, Obesity and Metabolism*, *17*, 76–83. https://doi.org/10.1111/dom.12516

Chang, H.-C., & Guarente, L. (2014). SIRT1 and other sirtuins in metabolism. *Trends in Endocrinology & Metabolism*, *25*(3), 138–145. https://doi.org/10.1016/j.tem.2013.12.001

Chen, C.-C., Jeon, S.-M., Bhaskar, P. T., Nogueira, V., Sundararajan, D., Tonic, I., Park, Y., & Hay, N. (2010). FoxOs Inhibit mTORC1 and Activate Akt by Inducing the

Expression of Sestrin3 and Rictor. *Developmental Cell*, *18*(4), 592–604. https://doi.org/10.1016/j.devcel.2010.03.008

Civitarese, A. E., Carling, S., Heilbronn, L. K., Hulver, M. H., Ukropcova, B., Deutsch, W. A., Smith, S. R., & Ravussin, E. (2007). Calorie Restriction Increases Muscle Mitochondrial Biogenesis in Healthy Humans. *PLoS Medicine*, *4*(3), e76. https://doi.org/10.1371/journal.pmed.0040076

Clark, K. L., Halay, E. D., Lai, E., & Burley, S. K. (1993). Co-crystal structure of the HNF-3/fork head DNA-recognition motif resembles histone H5. *Nature*, *364*(6436), 412–420. https://doi.org/10.1038/364412a0

Clotman, F., Lannoy, V. J., Reber, M., Cereghini, S., Cassiman, D., Jacquemin, P., Roskams, T., Rousseau, G. G., & Lemaigre, F. P. (2002). The onecut transcription factor HNF6 is required for normal development of the biliary tract. *Development*, *129*(8), 1819–1828. https://doi.org/10.1242/dev.129.8.1819

Cohen, H. Y., Miller, C., Bitterman, K. J., Wall, N. R., Hekking, B., Kessler, B., Howitz, K. T., Gorospe, M., de Cabo, R., & Sinclair, D. A. (2004). Calorie Restriction Promotes Mammalian Cell Survival by Inducing the SIRT1 Deacetylase. *Science*, *305*(5682), 390–392. https://doi.org/10.1126/science.1099196

Cole, T. J., Blendy, J. A., Monaghan, A. P., Krieglstein, K., Schmid, W., Aguzzi, A., Fantuzzi, G., Hummler, E., Unsicker, K., & Schütz, G. (1995). Targeted disruption of the glucocorticoid receptor gene blocks adrenergic chromaffin cell development and severely retards lung maturation. *Genes & Development*, *9*(13), 1608–1621. https://doi.org/10.1101/gad.9.13.1608

Collins, N., Han, S.-J., Enamorado, M., Link, V. M., Huang, B., Moseman, E. A., Kishton, R. J., Shannon, J. P., Dixit, D., Schwab, S. R., Hickman, H. D., Restifo, N. P., McGavern, D. B., Schwartzberg, P. L., & Belkaid, Y. (2019). The Bone Marrow Protects and Optimizes Immunological Memory during Dietary Restriction. *Cell*, *178*(5), 1088-1101.e15. https://doi.org/10.1016/j.cell.2019.07.049

Colman, R. J., Beasley, T. M., Kemnitz, J. W., Johnson, S. C., Weindruch, R., & Anderson, R. M. (2014). Caloric restriction reduces age-related and all-cause mortality in rhesus monkeys. *Nature Communications*, *5*(1), 3557. https://doi.org/10.1038/ncomms4557

Contreras, G. A., Bell, C. S., del Bianco, G. P., Perez, N., Kleinosky, M. T., Murphy, J. R., & Heresi, G. P. (2013). Prevalence and risk factors associated with resistance-associated mutations to etravirine in a cohort of perinatally HIV-infected children. *Journal of Antimicrobial Chemotherapy*. https://doi.org/10.1093/jac/dkt198

Cournarie, F., Azzout-Marniche, D., Foretz, M., Guichard, C., Ferre, P., & Foufelle, F. (1999). The inhibitory effect of glucose on phosphoenolpyruvate carboxykinase gene expression in cultured hepatocytes is transcriptional and requires glucose metabolism. *FEBS Letters*, *460*(3), 527–532. https://doi.org/10.1016/S0014-5793(99)01407-6

Dahlman-Wright, K., Wright, A., Gustafsson, J. A., & Carlstedt-Duke, J. (1991). Interaction of the glucocorticoid receptor DNA-binding domain with DNA as a dimer is mediated

by a short segment of five amino acids. *Journal of Biological Chemistry*, *266*(5), 3107–3112. https://doi.org/10.1016/S0021-9258(18)49960-7

Dawkins, J. L., Brahmbhatt, S., Auer-Grumbach, M., Wagner, K., Hartung, H.-P., Verhoeven, K., Timmerman, V., de Jonghe, P., Kennerson, M., LeGuern, E., & Nicholson, G. A. (2002). Exclusion of serine palmitoyltransferase long chain base subunit 2 (SPTLC2) as a common cause for hereditary sensory neuropathy. *Neuromuscular Disorders*, *12*(7–8), 656–658. https://doi.org/10.1016/S0960-8966(02)00015-9

Dawkins, J. L., Hulme, D. J., Brahmbhatt, S. B., Auer-Grumbach, M., & Nicholson, G. A. (2001). Mutations in SPTLC1, encoding serine palmitoyltransferase, long chain base subunit-1, cause hereditary sensory neuropathy type I. *Nature Genetics*, *27*(3), 309–312. https://doi.org/10.1038/85879

Dhahbi, J. M., Mote, P. L., Wingo, J., Rowley, B. C., Cao, S. X., Walford, R. L., & Spindler, S. R. (2001). Caloric restriction alters the feeding response of key metabolic enzyme genes. *Mechanisms of Ageing and Development*, *122*(10), 1033–1048. https://doi.org/10.1016/S0047-6374(01)00230-5

Dhahbi, J. M., Mote, P. L., Wingo, J., Tillman, J. B., Walford, R. L., & Spindler, S. R. (1999). Calories and aging alter gene expression for gluconeogenic, glycolytic, and nitrogen-metabolizing enzymes. *American Journal of Physiology-Endocrinology and Metabolism*, *277*(2), E352–E360. https://doi.org/10.1152/ajpendo.1999.277.2.E352

Djordjevic, J., Djordjevic, A., Adzic, M., Niciforovic, A., & Radojcic, M. (2010). Chronic stress differentially affects antioxidant enzymes and modifies the acute stress response in liver of Wistar rats. *Physiological Research*, 729–736. https://doi.org/10.33549/physiolres.931862

Doan, K. v., Kinyua, A. W., Yang, D. J., Ko, C. M., Moh, S. H., Shong, K. E., Kim, H., Park, S.-K., Kim, D.-H., Kim, I., Paik, J.-H., DePinho, R. A., Yoon, S. G., Kim, I. Y., Seong, J. K., Choi, Y.-H., & Kim, K. W. (2016). FoxO1 in dopaminergic neurons regulates energy homeostasis and targets tyrosine hydroxylase. *Nature Communications*, *7*(1), 12733. https://doi.org/10.1038/ncomms12733

Dobin, A., Davis, C. A., Schlesinger, F., Drenkow, J., Zaleski, C., Jha, S., Batut, P., Chaisson, M., & Gingeras, T. R. (2013). STAR: ultrafast universal RNA-seq aligner. *Bioinformatics*, *29*(1), 15–21. https://doi.org/10.1093/bioinformatics/bts635

Donohoe, D. R., Garge, N., Zhang, X., Sun, W., O'Connell, T. M., Bunger, M. K., & Bultman, S. J. (2011). The Microbiome and Butyrate Regulate Energy Metabolism and Autophagy in the Mammalian Colon. *Cell Metabolism*, *13*(5), 517–526. https://doi.org/10.1016/j.cmet.2011.02.018

Duncan, S. A. (2000). Transcriptional regulation of liver development. *Developmental Dynamics : An Official Publication of the American Association of Anatomists*, *219*(2), 131–142. https://doi.org/10.1002/1097-0177(2000)9999:9999<::aid-dvdy1051>3.3.co;2-e

Dunn, S. E., Kari, F. W., French, J., Leininger, J. R., Travlos, G., Wilson, R., & Barrett, J. C. (1997). Dietary restriction reduces insulin-like growth factor I levels, which modulates apoptosis, cell proliferation, and tumor progression in p53-deficient mice. *Cancer Research*, *57*(21), 4667–4672.

Duong, H. A., Robles, M. S., Knutti, D., & Weitz, C. J. (2011). A Molecular Mechanism for Circadian Clock Negative Feedback. *Science*, *332*(6036), 1436–1439. https://doi.org/10.1126/science.1196766

Duszka, K., Gregor, A., Guillou, H., König, J., & Wahli, W. (2020). Peroxisome Proliferator-Activated Receptors and Caloric Restriction—Common Pathways Affecting Metabolism, Health, and Longevity. *Cells*, *9*(7), 1708. https://doi.org/10.3390/cells9071708

Escoter-Torres, L., Caratti, G., Mechtidou, A., Tuckermann, J., Uhlenhaut, N. H., & Vettorazzi, S. (2019). Fighting the Fire: Mechanisms of Inflammatory Gene Regulation by the Glucocorticoid Receptor. *Frontiers in Immunology*, *10.* https://doi.org/10.3389/fimmu.2019.01859

Escoter-Torres, L., Greulich, F., Quagliarini, F., Wierer, M., & Uhlenhaut, N. H. (2020). Anti-inflammatory functions of the glucocorticoid receptor require DNA binding. *Nucleic Acids Research*, *48*(15), 8393–8407. https://doi.org/10.1093/nar/gkaa565

Evans, R. M. (1988). The Steroid and Thyroid Hormone Receptor Superfamily. *Science*, *240*(4854), 889–895. https://doi.org/10.1126/science.3283939

Evans, R. M., & Mangelsdorf, D. J. (2014). Nuclear Receptors, RXR, and the Big Bang. *Cell*, *157*(1), 255–266. https://doi.org/10.1016/j.cell.2014.03.012

Feige, J. N., Lagouge, M., Canto, C., Strehle, A., Houten, S. M., Milne, J. C., Lambert, P. D., Mataki, C., Elliott, P. J., & Auwerx, J. (2008). Specific SIRT1 Activation Mimics Low Energy Levels and Protects against Diet-Induced Metabolic Disorders by Enhancing Fat Oxidation. *Cell Metabolism*, *8*(5), 347–358. https://doi.org/10.1016/j.cmet.2008.08.017

Flurkey, K., Papaconstantinou, J., Miller, R. A., & Harrison, D. E. (2001). Lifespan extension and delayed immune and collagen aging in mutant mice with defects in growth hormone production. *Proceedings of the National Academy of Sciences*, *98*(12), 6736–6741. https://doi.org/10.1073/pnas.111158898

Fontana, L. (2007). Aging, Adiposity, and Calorie Restriction. *JAMA*, *297*(9), 986. https://doi.org/10.1001/jama.297.9.986

Fontana, L., Meyer, T. E., Klein, S., & Holloszy, J. O. (2004). Long-term calorie restriction is highly effective in reducing the risk for atherosclerosis in humans. *Proceedings of the National Academy of Sciences*, *101*(17), 6659–6663. https://doi.org/10.1073/pnas.0308291101

Fontana, L., Weiss, E. P., Villareal, D. T., Klein, S., & Holloszy, J. O. (2008). Long-term effects of calorie or protein restriction on serum IGF-1 and IGFBP-3 concentration in humans. *Aging Cell*, *7*(5), 681–687. https://doi.org/10.1111/j.1474-9726.2008.00417.x

Fulco, M., Cen, Y., Zhao, P., Hoffman, E. P., McBurney, M. W., Sauve, A. A., & Sartorelli, V. (2008). Glucose Restriction Inhibits Skeletal Myoblast Differentiation by Activating SIRT1 through AMPK-Mediated Regulation of Nampt. *Developmental Cell*, *14*(5), 661–673. https://doi.org/10.1016/j.devcel.2008.02.004

García-Gaytán, A. C., Miranda-Anaya, M., Turrubiate, I., López-De Portugal, L., Bocanegra-Botello, G. N., López-Islas, A., Díaz-Muñoz, M., & Méndez, I. (2020). Synchronization of the circadian clock by time-restricted feeding with progressive increasing calorie intake. Resemblances and differences regarding a sustained hypocaloric restriction. *Scientific Reports*, *10*(1), 10036. https://doi.org/10.1038/s41598-020-66538-0

Gerhart-Hines, Z., Rodgers, J. T., Bare, O., Lerin, C., Kim, S.-H., Mostoslavsky, R., Alt, F. W., Wu, Z., & Puigserver, P. (2007). Metabolic control of muscle mitochondrial function and fatty acid oxidation through SIRT1/PGC-1α. *The EMBO Journal*, *26*(7), 1913–1923. https://doi.org/10.1038/sj.emboj.7601633

Gill, S., & Panda, S. (2015). A Smartphone App Reveals Erratic Diurnal Eating Patterns in Humans that Can Be Modulated for Health Benefits. *Cell Metabolism*, *22*(5), 789–798. https://doi.org/10.1016/j.cmet.2015.09.005

Glass, C. K., & Saijo, K. (2010). Nuclear receptor transrepression pathways that regulate inflammation in macrophages and T cells. *Nature Reviews Immunology*, *10*(5), 365–376. https://doi.org/10.1038/nri2748

Golson, M. L., & Kaestner, K. H. (2016). Fox transcription factors: from development to disease. *Development*, *143*(24), 4558–4570. https://doi.org/10.1242/dev.112672

Gopal, K., Saleme, B., al Batran, R., Aburasayn, H., Eshreif, A., Ho, K. L., Ma, W. K., Almutairi, M., Eaton, F., Gandhi, M., Park, E. A., Sutendra, G., & Ussher, J. R. (2017). FoxO1 regulates myocardial glucose oxidation rates via transcriptional control of pyruvate dehydrogenase kinase 4 expression. *American Journal of Physiology-Heart and Circulatory Physiology*, *313*(3), H479–H490. https://doi.org/10.1152/ajpheart.00191.2017

Gredilla, R., & Barja, G. (2005). Minireview: The Role of Oxidative Stress in Relation to Caloric Restriction and Longevity. *Endocrinology*, *146*(9), 3713–3717. https://doi.org/10.1210/en.2005-0378

Green, C. B., Takahashi, J. S., & Bass, J. (2008). The Meter of Metabolism. *Cell*, *134*(5), 728–742. https://doi.org/10.1016/j.cell.2008.08.022

Green, S., Walter, P., Kumar, V., Krust, A., Bornert, J.-M., Argos, P., & Chambon, P. (1986). Human oestrogen receptor cDNA: sequence, expression and homology to v-erb-A. *Nature*, *320*(6058), 134–139. https://doi.org/10.1038/320134a0

Greene, G. L., Gilna, P., Waterfield, M., Baker, A., Hort, Y., & Shine, J. (1986). Sequence and Expression of Human Estrogen Receptor Complementary DNA. *Science*, *231*(4742), 1150–1154. https://doi.org/10.1126/science.3753802

Greulich, F., Hemmer, M. C., Rollins, D. A., Rogatsky, I., & Uhlenhaut, N. H. (2016). There goes the neighborhood: Assembly of transcriptional complexes during the regulation

of metabolism and inflammation by the glucocorticoid receptor. *Steroids*, *114*, 7–15. https://doi.org/10.1016/j.steroids.2016.05.003

Greulich, F., Wierer, M., Mechtidou, A., Gonzalez-Garcia, O., & Uhlenhaut, N. H. (2021). The glucocorticoid receptor recruits the COMPASS complex to regulate inflammatory transcription at macrophage enhancers. *Cell Reports*, *34*(6), 108742. https://doi.org/10.1016/j.celrep.2021.108742

Grøntved, L., John, S., Baek, S., Liu, Y., Buckley, J. R., Vinson, C., Aguilera, G., & Hager, G. L. (2013). C/EBP maintains chromatin accessibility in liver and facilitates glucocorticoid receptor recruitment to steroid response elements. *The EMBO Journal*, *32*(11), 1568–1583. https://doi.org/10.1038/emboj.2013.106

Guo, S., Rena, G., Cichy, S., He, X., Cohen, P., & Unterman, T. (1999). Phosphorylation of Serine 256 by Protein Kinase B Disrupts Transactivation by FKHR and Mediates Effects of Insulin on Insulin-like Growth Factor-binding Protein-1 Promoter Activity through a Conserved Insulin Response Sequence. *Journal of Biological Chemistry*, *274*(24), 17184–17192. https://doi.org/10.1074/jbc.274.24.17184

Gustafsson, J.-A. (2016). Historical overview of nuclear receptors. *The Journal of Steroid Biochemistry and Molecular Biology*, *157*, 3–6. https://doi.org/10.1016/j.jsbmb.2015.03.004

Gwinn, D. M., Shackelford, D. B., Egan, D. F., Mihaylova, M. M., Mery, A., Vasquez, D. S., Turk, B. E., & Shaw, R. J. (2008). AMPK Phosphorylation of Raptor Mediates a Metabolic Checkpoint. *Molecular Cell*, *30*(2), 214–226. https://doi.org/10.1016/j.molcel.2008.03.003

Haeusler, R. A., Kaestner, K. H., & Accili, D. (2010). FoxOs Function Synergistically to Promote Glucose Production. *Journal of Biological Chemistry*, *285*(46), 35245–35248. https://doi.org/10.1074/jbc.C110.175851

Hagopian, K., Ramsey, J. J., & Weindruch, R. (2004). Krebs cycle enzymes from livers of old mice are differentially regulated by caloric restriction. *Experimental Gerontology*, *39*(8), 1145–1154. https://doi.org/10.1016/j.exger.2004.04.009

Hagopian, K., Soo Hoo, R., López-Domínguez, J. A., & Ramsey, J. J. (2013). Calorie restriction influences key metabolic enzyme activities and markers of oxidative damage in distinct mouse liver mitochondrial sub-populations. *Life Sciences*, *93*(24), 941–948. https://doi.org/10.1016/j.lfs.2013.10.006

Halleck, M. S., Pownall, S., Harder, K. W., Duncan, A. M., Jirik, F. R., & Schlegel, R. A. (1995a). A widely distributed putative mammalian transcriptional regulator containing multiple paired amphipathic helices, with similarity to yeast SIN3. *Genomics*, *26*(2), 403–406. https://doi.org/10.1016/0888-7543(95)80229-f

Halleck, M. S., Pownall, S., Harder, K. W., Duncan, A. M., Jirik, F. R., & Schlegel, R. A. (1995b). A widely distributed putative mammalian transcriptional regulator containing multiple paired amphipathic helices, with similarity to yeast SIN3. *Genomics*, *26*(2), 403–406. https://doi.org/10.1016/0888-7543(95)80229-f

Hallows, W. C., Yu, W., & Denu, J. M. (2012). Regulation of Glycolytic Enzyme Phosphoglycerate Mutase-1 by Sirt1 Protein-mediated Deacetylation. *Journal of Biological Chemistry*, *287*(6), 3850–3858. https://doi.org/10.1074/jbc.M111.317404

Hancock, M. L., Meyer, R. C., Mistry, M., Khetani, R. S., Wagschal, A., Shin, T., Ho Sui, S. J., Näär, A. M., & Flanagan, J. G. (2019). Insulin Receptor Associates with Promoters Genome-wide and Regulates Gene Expression. *Cell*, *177*(3), 722-736.e22. https://doi.org/10.1016/j.cell.2019.02.030

Hardie, D. G., & Alessi, D. R. (2013). LKB1 and AMPK and the cancer-metabolism link - ten years after. *BMC Biology*, *11*(1), 36. https://doi.org/10.1186/1741-7007-11-36

Hassig, C. A., Fleischer, T. C., Billin, A. N., Schreiber, S. L., & Ayer, D. E. (1997). Histone Deacetylase Activity Is Required for Full Transcriptional Repression by mSin3A. *Cell*, *89*(3), 341–347. https://doi.org/10.1016/S0092-8674(00)80214-7

Hatori, M., Vollmers, C., Zarrinpar, A., DiTacchio, L., Bushong, E. A., Gill, S., Leblanc, M., Chaix, A., Joens, M., Fitzpatrick, J. A. J., Ellisman, M. H., & Panda, S. (2012). Time-Restricted Feeding without Reducing Caloric Intake Prevents Metabolic Diseases in Mice Fed a High-Fat Diet. *Cell Metabolism*, *15*(6), 848–860. https://doi.org/10.1016/j.cmet.2012.04.019

Hay, N. (2011). Interplay between FOXO, TOR, and Akt. *Biochimica et Biophysica Acta (BBA) - Molecular Cell Research*, *1813*(11), 1965–1970. https://doi.org/10.1016/j.bbamcr.2011.03.013

Heinz, S., Benner, C., Spann, N., Bertolino, E., Lin, Y. C., Laslo, P., Cheng, J. X., Murre, C., Singh, H., & Glass, C. K. (2010). Simple Combinations of Lineage-Determining Transcription Factors Prime cis-Regulatory Elements Required for Macrophage and B Cell Identities. *Molecular Cell*, *38*(4), 576–589. https://doi.org/10.1016/j.molcel.2010.05.004

Hemmer, M. C., Wierer, M., Schachtrup, K., Downes, M., Hübner, N., Evans, R. M., & Uhlenhaut, N. H. (2019). E47 modulates hepatic glucocorticoid action. *Nature Communications*, *10*(1), 306. https://doi.org/10.1038/s41467-018-08196-5

Herman, J. P., McKlveen, J. M., Ghosal, S., Kopp, B., Wulsin, A., Makinson, R., Scheimann, J., & Myers, B. (2016). Regulation of the Hypothalamic-Pituitary-Adrenocortical Stress Response. In *Comprehensive Physiology* (pp. 603–621). Wiley. https://doi.org/10.1002/cphy.c150015

Holczer, M., Hajdú, B., Lőrincz, T., Szarka, A., Bánhegyi, G., & Kapuy, O. (2019). A Double Negative Feedback Loop between mTORC1 and AMPK Kinases Guarantees Precise Autophagy Induction upon Cellular Stress. *International Journal of Molecular Sciences*, *20*(22), 5543. https://doi.org/10.3390/ijms20225543

Hollenberg, S. M., Weinberger, C., Ong, E. S., Cerelli, G., Oro, A., Lebo, R., Brad Thompson, E., Rosenfeld, M. G., & Evans, R. M. (1985). Primary structure and expression of a functional human glucocorticoid receptor cDNA. *Nature*, *318*(6047), 635–641. https://doi.org/10.1038/318635a0

Horton, J. D., Goldstein, J. L., & Brown, M. S. (2002). SREBPs: activators of the complete program of cholesterol and fatty acid synthesis in the liver. *Journal of Clinical Investigation*, *109*(9), 1125–1131. https://doi.org/10.1172/JCI15593

Hou, X., Xu, S., Maitland-Toolan, K. A., Sato, K., Jiang, B., Ido, Y., Lan, F., Walsh, K., Wierzbicki, M., Verbeuren, T. J., Cohen, R. A., & Zang, M. (2008). SIRT1 Regulates Hepatocyte Lipid Metabolism through Activating AMP-activated Protein Kinase. *Journal of Biological Chemistry*, *283*(29), 20015–20026. https://doi.org/10.1074/jbc.M802187200

Hughes, M. E., DiTacchio, L., Hayes, K. R., Vollmers, C., Pulivarthy, S., Baggs, J. E., Panda, S., & Hogenesch, J. B. (2009). Harmonics of Circadian Gene Transcription in Mammals. *PLoS Genetics*, *5*(4), e1000442. https://doi.org/10.1371/journal.pgen.1000442

Hunter A.L, Poolman T., Kim D., Gonzalez F.J., Bechtold D.A., Loudon A.S.I., Iqbal M., & a Ray D.W. (2021). HNF4A is required to specify glucocorticoid action in the liver. *bioRχiv*. **doi:** https://doi.org/10.1101/2021.04.10.438998

Iizuka, K., Bruick, R. K., Liang, G., Horton, J. D., & Uyeda, K. (2004). From The Cover: Deficiency of carbohydrate response element-binding protein (ChREBP) reduces lipogenesis as well as glycolysis. *Proceedings of the National Academy of Sciences*, *101*(19), 7281–7286. https://doi.org/10.1073/pnas.0401516101

Ikeno, Y., Bronson, R. T., Hubbard, G. B., Lee, S., & Bartke, A. (2003). Delayed Occurrence of Fatal Neoplastic Diseases in Ames Dwarf Mice: Correlation to Extended Longevity. *The Journals of Gerontology Series A: Biological Sciences and Medical Sciences*, *58*(4), B291–B296. https://doi.org/10.1093/gerona/58.4.B291

Inoki, K., Zhu, T., & Guan, K.-L. (2003). TSC2 Mediates Cellular Energy Response to Control Cell Growth and Survival. *Cell*, *115*(5), 577–590. https://doi.org/10.1016/S0092-8674(03)00929-2

Ipsen, D. H., Lykkesfeldt, J., & Tveden-Nyborg, P. (2018). Molecular mechanisms of hepatic lipid accumulation in non-alcoholic fatty liver disease. *Cellular and Molecular Life Sciences*, *75*(18), 3313–3327. https://doi.org/10.1007/s00018-018-2860-6

Itoh, M., Adachi, M., Yasui, H., Takekawa, M., Tanaka, H., & Imai, K. (2002). Nuclear Export of Glucocorticoid Receptor is Enhanced by c-Jun N-Terminal Kinase-Mediated Phosphorylation. *Molecular Endocrinology*, *16*(10), 2382–2392. https://doi.org/10.1210/me.2002-0144

Iwafuchi-Doi, M., Donahue, G., Kakumanu, A., Watts, J. A., Mahony, S., Pugh, B. F., Lee, D., Kaestner, K. H., & Zaret, K. S. (2016). The Pioneer Transcription Factor FoxA Maintains an Accessible Nucleosome Configuration at Enhancers for Tissue-Specific Gene Activation. *Molecular Cell*, *62*(1), 79–91. https://doi.org/10.1016/j.molcel.2016.03.001

Jackson, J. G., Kreisberg, J. I., Koterba, A. P., Yee, D., & Brattain, M. G. (2000). Phosphorylation and nuclear exclusion of the forkhead transcription factor FKHR

after epidermal growth factor treatment in human breast cancer cells. *Oncogene*, *19*(40), 4574–4581. https://doi.org/10.1038/sj.onc.1203825

Jang, H., Lee, G. Y., Selby, C. P., Lee, G., Jeon, Y. G., Lee, J. H., Cheng, K. K. Y., Titchenell, P., Birnbaum, M. J., Xu, A., Sancar, A., & Kim, J. B. (2016). SREBP1c-CRY1 signalling represses hepatic glucose production by promoting FOXO1 degradation during refeeding. *Nature Communications*, *7*(1), 12180. https://doi.org/10.1038/ncomms12180

Jenniskens, M., Weckx, R., Dufour, T., vander Perre, S., Pauwels, L., Derde, S., Téblick, A., Güiza, F., van den Berghe, G., & Langouche, L. (2018). The Hepatic Glucocorticoid Receptor Is Crucial for Cortisol Homeostasis and Sepsis Survival in Humans and Male Mice. *Endocrinology*, *159*(7), 2790–2802. https://doi.org/10.1210/en.2018-00344

Jensen-Urstad, A. P. L., & Semenkovich, C. F. (2012). Fatty acid synthase and liver triglyceride metabolism: Housekeeper or messenger? *Biochimica et Biophysica Acta (BBA) - Molecular and Cell Biology of Lipids*, *1821*(5), 747–753. https://doi.org/10.1016/j.bbalip.2011.09.017

Jones, J. I., & Clemmons, D. R. (1995). Insulin-Like Growth Factors and Their Binding Proteins: Biological Actions*. *Endocrine Reviews*, *16*(1), 3–34. https://doi.org/10.1210/edrv-16-1-3

Jouffe, C., Cretenet, G., Symul, L., Martin, E., Atger, F., Naef, F., & Gachon, F. (2013). The Circadian Clock Coordinates Ribosome Biogenesis. *PLoS Biology*, *11*(1), e1001455. https://doi.org/10.1371/journal.pbio.1001455

Kalvisa, A., Siersbæk, M. S., Præstholm, S. M., Christensen, L. J. L., Nielsen, R., Stohr, O., Vettorazzi, S., Tuckermann, J., White, M., Mandrup, S., & Grøntved, L. (2018). Insulin signaling and reduced glucocorticoid receptor activity attenuate postprandial gene expression in liver. *PLOS Biology*, *16*(12), e2006249. https://doi.org/10.1371/journal.pbio.2006249

Kanungo, S., Wells, K., Tribett, T., & El-Gharbawy, A. (2018). Glycogen metabolism and glycogen storage disorders. *Annals of Translational Medicine*, *6*(24), 474–474. https://doi.org/10.21037/atm.2018.10.59

Kaufmann, E., & Knöchel, W. (1996). Five years on the wings of fork head. *Mechanisms of Development*, *57*(1), 3–20. https://doi.org/10.1016/0925-4773(96)00539-4

Kim, D. H., Park, M. H., Lee, E. K., Choi, Y. J., Chung, K. W., Moon, K. M., Kim, M. J., An, H. J., Park, J. W., Kim, N. D., Yu, B. P., & Chung, H. Y. (2015). The roles of FoxOs in modulation of aging by calorie restriction. *Biogerontology*, *16*(1), 1–14. https://doi.org/10.1007/s10522-014-9519-y

Kim, J., & Guan, K.-L. (2019). mTOR as a central hub of nutrient signalling and cell growth. *Nature Cell Biology*, *21*(1), 63–71. https://doi.org/10.1038/s41556-018-0205-1

Kim, T. S., Jin, Y. B., Kim, Y. S., Kim, S., Kim, J. K., Lee, H.-M., Suh, H.-W., Choe, J. H., Kim, Y. J., Koo, B.-S., Kim, H.-N., Jung, M., Lee, S.-H., Kim, D.-K., Chung, C., Son, J.-W., Min, J.-J., Kim, J.-M., Deng, C.-X., … Jo, E.-K. (2019). SIRT3 promotes

antimycobacterial defenses by coordinating mitochondrial and autophagic functions. *Autophagy*, *15*(8), 1356–1375. https://doi.org/10.1080/15548627.2019.1582743

Kishi, T., Hirooka, Y., Nagayama, T., Isegawa, K., Katsuki, M., Takesue, K., & Sunagawa, K. (2015). Calorie Restriction Improves Cognitive Decline via Up-Regulation of Brain-Derived Neurotrophic Factor. *International Heart Journal*, *56*(1), 110–115. https://doi.org/10.1536/ihj.14-168

Kitamoto, T., Kuo, T., Okabe, A., Kaneda, A., & Accili, D. (2021). An integrative transcriptional logic model of hepatic insulin resistance. *Proceedings of the National Academy of Sciences*, *118*(45), e2102222118. https://doi.org/10.1073/pnas.2102222118

Kitamura, Y. I., Kitamura, T., Kruse, J.-P., Raum, J. C., Stein, R., Gu, W., & Accili, D. (2005). FoxO1 protects against pancreatic β cell failure through NeuroD and MafA induction. *Cell Metabolism*, *2*(3), 153–163. https://doi.org/10.1016/j.cmet.2005.08.004

Kogot-Levin, A., & Saada, A. (2014). Ceramide and the mitochondrial respiratory chain. *Biochimie*, *100*, 88–94. https://doi.org/10.1016/j.biochi.2013.07.027

Kono, M., Dreier, J. L., Ellis, J. M., Allende, M. L., Kalkofen, D. N., Sanders, K. M., Bielawski, J., Bielawska, A., Hannun, Y. A., & Proia, R. L. (2006). Neutral Ceramidase Encoded by the Asah2 Gene Is Essential for the Intestinal Degradation of Sphingolipids. *Journal of Biological Chemistry*, *281*(11), 7324–7331. https://doi.org/10.1074/jbc.M508382200

Korenfeld, N., Finkel, M., Buchshtab, N., Bar-Shimon, M., Charni-Natan, M., & Goldstein, I. (2021). Fasting Hormones Synergistically Induce Amino Acid Catabolism Genes to Promote Gluconeogenesis. *Cellular and Molecular Gastroenterology and Hepatology*, *12*(3), 1021–1036. https://doi.org/10.1016/j.jcmgh.2021.04.017

Kousteni, S. (2012). FoxO1, the transcriptional chief of staff of energy metabolism. *Bone*, *50*(2), 437–443. https://doi.org/10.1016/j.bone.2011.06.034

Krstic, M. D., Rogatsky, I., Yamamoto, K. R., & Garabedian, M. J. (1997). Mitogen-activated and cyclin-dependent protein kinases selectively and differentially modulate transcriptional enhancement by the glucocorticoid receptor. *Molecular and Cellular Biology*, *17*(7), 3947–3954. https://doi.org/10.1128/MCB.17.7.3947

Kuleshov, M. v., Jones, M. R., Rouillard, A. D., Fernandez, N. F., Duan, Q., Wang, Z., Koplev, S., Jenkins, S. L., Jagodnik, K. M., Lachmann, A., McDermott, M. G., Monteiro, C. D., Gundersen, G. W., & Ma'ayan, A. (2016). Enrichr: a comprehensive gene set enrichment analysis web server 2016 update. *Nucleic Acids Research*, *44*(W1), W90–W97. https://doi.org/10.1093/nar/gkw377

Kumar, R., & Thompson, E. B. (2005). Gene regulation by the glucocorticoid receptor: Structure:function relationship. *The Journal of Steroid Biochemistry and Molecular Biology*, *94*(5), 383–394. https://doi.org/10.1016/j.jsbmb.2004.12.046

Kume, S., Uzu, T., Horiike, K., Chin-Kanasaki, M., Isshiki, K., Araki, S., Sugimoto, T., Haneda, M., Kashiwagi, A., & Koya, D. (2010). Calorie restriction enhances cell

adaptation to hypoxia through Sirt1-dependent mitochondrial autophagy in mouse aged kidney. *Journal of Clinical Investigation*, *120*(4), 1043–1055. https://doi.org/10.1172/JCI41376

Kuo, T., Chen, T.-C., Yan, S., Foo, F., Ching, C., McQueen, A., & Wang, J.-C. (2014). Repression of glucocorticoid-stimulated angiopoietin-like 4 gene transcription by insulin. *Journal of Lipid Research*, *55*(5), 919–928. https://doi.org/10.1194/jlr.M047860

Kuo, T., Harris, C. A., & Wang, J.-C. (2013). Metabolic functions of glucocorticoid receptor in skeletal muscle. *Molecular and Cellular Endocrinology*, *380*(1–2), 79–88. https://doi.org/10.1016/j.mce.2013.03.003

Laherty, C. D., Yang, W.-M., Sun, J.-M., Davie, J. R., Seto, E., & Eisenman, R. N. (1997). Histone Deacetylases Associated with the mSin3 Corepressor Mediate Mad Transcriptional Repression. *Cell*, *89*(3), 349–356. https://doi.org/10.1016/S0092-8674(00)80215-9

Lamia, K. A., Papp, S. J., Yu, R. T., Barish, G. D., Uhlenhaut, N. H., Jonker, J. W., Downes, M., & Evans, R. M. (2011). Cryptochromes mediate rhythmic repression of the glucocorticoid receptor. *Nature*, *480*(7378), 552–556. https://doi.org/10.1038/nature10700

Lan, F., Cacicedo, J. M., Ruderman, N., & Ido, Y. (2008). SIRT1 Modulation of the Acetylation Status, Cytosolic Localization, and Activity of LKB1. *Journal of Biological Chemistry*, *283*(41), 27628–27635. https://doi.org/10.1074/jbc.M805711200

Landt, S. G., Marinov, G. K., Kundaje, A., Kheradpour, P., Pauli, F., Batzoglou, S., Bernstein, B. E., Bickel, P., Brown, J. B., Cayting, P., Chen, Y., DeSalvo, G., Epstein, C., Fisher-Aylor, K. I., Euskirchen, G., Gerstein, M., Gertz, J., Hartemink, A. J., Hoffman, M. M., … Snyder, M. (2012). ChIP-seq guidelines and practices of the ENCODE and modENCODE consortia. *Genome Research*, *22*(9), 1813–1831. https://doi.org/10.1101/gr.136184.111

Langlais, D., Couture, C., Balsalobre, A., & Drouin, J. (2012). The Stat3/GR Interaction Code: Predictive Value of Direct/Indirect DNA Recruitment for Transcription Outcome. *Molecular Cell*, *47*(1), 38–49. https://doi.org/10.1016/j.molcel.2012.04.021

Langlet, F., Haeusler, R. A., Lindén, D., Ericson, E., Norris, T., Johansson, A., Cook, J. R., Aizawa, K., Wang, L., Buettner, C., & Accili, D. (2017). Selective Inhibition of FOXO1 Activator/Repressor Balance Modulates Hepatic Glucose Handling. *Cell*, *171*(4), 824-835.e18. https://doi.org/10.1016/j.cell.2017.09.045

Leakey, J. E. A., Chen, S., Manjgaladze, M., Turturro, A., Duffy, P. H., Pipkin, J. L., & Hart, R. W. (1994). Role of Glucocorticoids and "Caloric Stress" in Modulating the Effects of Caloric Restriction in Rodents. *Annals of the New York Academy of Sciences*, *719*(1 The Aging Clo), 171–194. https://doi.org/10.1111/j.1749-6632.1994.tb56828.x

Leavens, K. F., & Birnbaum, M. J. (2011). Insulin signaling to hepatic lipid metabolism in health and disease. *Critical Reviews in Biochemistry and Molecular Biology*, *46*(3), 200–215. https://doi.org/10.3109/10409238.2011.562481

Lee, C., Safdie, F. M., Raffaghello, L., Wei, M., Madia, F., Parrella, E., Hwang, D., Cohen, P., Bianchi, G., & Longo, V. D. (2010). Reduced Levels of IGF-I Mediate Differential Protection of Normal and Cancer Cells in Response to Fasting and Improve Chemotherapeutic Index. *Cancer Research*, *70*(4), 1564–1572. https://doi.org/10.1158/0008-5472.CAN-09-3228

Lee, I. H., & Finkel, T. (2009). Regulation of Autophagy by the p300 Acetyltransferase. *Journal of Biological Chemistry*, *284*(10), 6322–6328. https://doi.org/10.1074/jbc.M807135200

Lemke, U., Krones-Herzig, A., Diaz, M. B., Narvekar, P., Ziegler, A., Vegiopoulos, A., Cato, A. C. B., Bohl, S., Klingmüller, U., Screaton, R. A., Müller-Decker, K., Kersten, S., & Herzig, S. (2008). The Glucocorticoid Receptor Controls Hepatic Dyslipidemia through Hes1. *Cell Metabolism*, *8*(3), 212–223. https://doi.org/10.1016/j.cmet.2008.08.001

Levine, B., & Klionsky, D. J. (2004). Development by Self-Digestion. *Developmental Cell*, *6*(4), 463–477. https://doi.org/10.1016/S1534-5807(04)00099-1

Li, H., & Durbin, R. (2010). Fast and accurate long-read alignment with Burrows–Wheeler transform. *Bioinformatics*, *26*(5), 589–595. https://doi.org/10.1093/bioinformatics/btp698

Li, H., Ruan, J., & Durbin, R. (2008). Mapping short DNA sequencing reads and calling variants using mapping quality scores. *Genome Research*, *18*(11), 1851–1858. https://doi.org/10.1101/gr.078212.108

Li, K., Qiu, C., Sun, P., Liu, D., Wu, T., Wang, K., Zhou, Y., Chang, X., Yin, Y., Chen, F., Zhu, Y., & Han, X. (2019). Ets1-Mediated Acetylation of FoxO1 Is Critical for Gluconeogenesis Regulation during Feed-Fast Cycles. *Cell Reports*, *26*(11), 2998-3010.e5. https://doi.org/10.1016/j.celrep.2019.02.035

Li, Q., Brown, J. B., Huang, H., & Bickel, P. J. (2011). Measuring reproducibility of high-throughput experiments. *The Annals of Applied Statistics*, *5*(3). https://doi.org/10.1214/11-AOAS466

Li, Z., Schug, J., Tuteja, G., White, P., & Kaestner, K. H. (2011). The nucleosome map of the mammalian liver. *Nature Structural & Molecular Biology*, *18*(6), 742–746. https://doi.org/10.1038/nsmb.2060

Liao, Y., Smyth, G. K., & Shi, W. (2014). featureCounts: an efficient general purpose program for assigning sequence reads to genomic features. *Bioinformatics*, *30*(7), 923–930. https://doi.org/10.1093/bioinformatics/btt656

Lightman, S. L. (2008). The Neuroendocrinology of Stress: A Never Ending Story. *Journal of Neuroendocrinology*, *20*(6), 880–884. https://doi.org/10.1111/j.1365-2826.2008.01711.x

Lim, H.-W., Uhlenhaut, N. H., Rauch, A., Weiner, J., Hübner, S., Hübner, N., Won, K.-J., Lazar, M. A., Tuckermann, J., & Steger, D. J. (2015). Genomic redistribution of GR monomers and dimers mediates transcriptional response to exogenous

glucocorticoid in vivo. *Genome Research*, *25*(6), 836–844. https://doi.org/10.1101/gr.188581.114

Lim, J.-H., Lee, Y.-M., Chun, Y.-S., Chen, J., Kim, J.-E., & Park, J.-W. (2010). Sirtuin 1 Modulates Cellular Responses to Hypoxia by Deacetylating Hypoxia-Inducible Factor 1α. *Molecular Cell*, *38*(6), 864–878. https://doi.org/10.1016/j.molcel.2010.05.023

Lin, K., Dorman, J. B., Rodan, A., & Kenyon, C. (1997). *daf-16*: An HNF-3/forkhead Family Member That Can Function to Double the Life-Span of *Caenorhabditis elegans*. *Science*, *278*(5341), 1319–1322. https://doi.org/10.1126/science.278.5341.1319

Liu, Y., Dentin, R., Chen, D., Hedrick, S., Ravnskjaer, K., Schenk, S., Milne, J., Meyers, D. J., Cole, P., III, J. Y., Olefsky, J., Guarente, L., & Montminy, M. (2008). A fasting inducible switch modulates gluconeogenesis via activator/coactivator exchange. *Nature*, *456*(7219), 269–273. https://doi.org/10.1038/nature07349

Liu, Y., Yan, C., Wang, Y., Nakagawa, Y., Nerio, N., Anghel, A., Lutfy, K., & Friedman, T. C. (2006). Liver X Receptor Agonist T0901317 Inhibition of Glucocorticoid Receptor Expression in Hepatocytes May Contribute to the Amelioration of Diabetic Syndrome in *db/db* Mice. *Endocrinology*, *147*(11), 5061–5068. https://doi.org/10.1210/en.2006-0243

Lombard, D. B., Alt, F. W., Cheng, H.-L., Bunkenborg, J., Streeper, R. S., Mostoslavsky, R., Kim, J., Yancopoulos, G., Valenzuela, D., Murphy, A., Yang, Y., Chen, Y., Hirschey, M. D., Bronson, R. T., Haigis, M., Guarente, L. P., Farese, R. v., Weissman, S., Verdin, E., & Schwer, B. (2007). Mammalian Sir2 Homolog SIRT3 Regulates Global Mitochondrial Lysine Acetylation. *Molecular and Cellular Biology*, *27*(24), 8807–8814. https://doi.org/10.1128/MCB.01636-07

Love, M. I., Huber, W., & Anders, S. (2014). Moderated estimation of fold change and dispersion for RNA-seq data with DESeq2. *Genome Biology*, *15*(12), 550. https://doi.org/10.1186/s13059-014-0550-8

Lu, N. Z., & Cidlowski, J. A. (2006). Glucocorticoid receptor isoforms generate transcription specificity. *Trends in Cell Biology*, *16*(6), 301–307. https://doi.org/10.1016/j.tcb.2006.04.005

Lu, Y., Zhang, Z., Xiong, X., Wang, X., Li, J., Shi, G., Yang, J., Zhang, X., Zhang, H., Hong, J., Xia, X., Ning, G., & Li, X. (2012). Glucocorticoids Promote Hepatic Cholestasis in Mice by Inhibiting the Transcriptional Activity of the Farnesoid X Receptor. *Gastroenterology*, *143*(6), 1630-1640.e8. https://doi.org/10.1053/j.gastro.2012.08.029

Luo, L., Jiang, S., Huang, D., Lu, N., & Luo, Z. (2015). MLK3 Phophorylates AMPK Independently of LKB1. *PLOS ONE*, *10*(4), e0123927. https://doi.org/10.1371/journal.pone.0123927

Ma, S., Sun, S., Geng, L., Song, M., Wang, W., Ye, Y., Ji, Q., Zou, Z., Wang, S., He, X., Li, W., Esteban, C. R., Long, X., Guo, G., Chan, P., Zhou, Q., Belmonte, J. C. I., Zhang, W., Qu, J., & Liu, G.-H. (2020). Caloric Restriction Reprograms the Single-

Cell Transcriptional Landscape of Rattus Norvegicus Aging. *Cell*, *180*(5), 984–1001.e22. https://doi.org/10.1016/j.cell.2020.02.008

Macfarlane, D. P., Forbes, S., & Walker, B. R. (2008). Glucocorticoids and fatty acid metabolism in humans: fuelling fat redistribution in the metabolic syndrome. *Journal of Endocrinology*, *197*(2), 189–204. https://doi.org/10.1677/JOE-08-0054

Madeo, F., Carmona-Gutierrez, D., Hofer, S. J., & Kroemer, G. (2019). Caloric Restriction Mimetics against Age-Associated Disease: Targets, Mechanisms, and Therapeutic Potential. *Cell Metabolism*, *29*(3), 592–610. https://doi.org/10.1016/j.cmet.2019.01.018

Makwana, K., Gosai, N., Poe, A., & Kondratov, R. v. (2019). Calorie restriction reprograms diurnal rhythms in protein translation to regulate metabolism. *The FASEB Journal*, *33*(3), 4473–4489. https://doi.org/10.1096/fj.201802167R

Mangelsdorf, D. J., Thummel, C., Beato, M., Herrlich, P., Schütz, G., Umesono, K., Blumberg, B., Kastner, P., Mark, M., Chambon, P., & Evans, R. M. (1995). The nuclear receptor superfamily: The second decade. *Cell*, *83*(6), 835–839. https://doi.org/10.1016/0092-8674(95)90199-X

Margagliotti, S., Clotman, F., Pierreux, C. E., Beaudry, J.-B., Jacquemin, P., Rousseau, G. G., & Lemaigre, F. P. (2007). The Onecut transcription factors HNF-6/OC-1 and OC-2 regulate early liver expansion by controlling hepatoblast migration. *Developmental Biology*, *311*(2), 579–589. https://doi.org/10.1016/j.ydbio.2007.09.013

Masri, S., & Sassone-Corsi, P. (2018). The emerging link between cancer, metabolism, and circadian rhythms. *Nature Medicine*, *24*(12), 1795–1803. https://doi.org/10.1038/s41591-018-0271-8

Matarese, L. E. (1997). Indirect Calorimetry. *Journal of the American Dietetic Association*, *97*(10), S154–S160. https://doi.org/10.1016/S0002-8223(97)00754-2

Matsumoto, M. (2006). Dual role of transcription factor FoxO1 in controlling hepatic insulin sensitivity and lipid metabolism. *Journal of Clinical Investigation*. https://doi.org/10.1172/JCI27047

Matsumoto, M., Pocai, A., Rossetti, L., DePinho, R. A., & Accili, D. (2007). Impaired Regulation of Hepatic Glucose Production in Mice Lacking the Forkhead Transcription Factor Foxo1 in Liver. *Cell Metabolism*, *6*(3), 208–216. https://doi.org/10.1016/j.cmet.2007.08.006

Matsuzaki, H., Daitoku, H., Hatta, M., Tanaka, K., & Fukamizu, A. (2003). Insulin-induced phosphorylation of FKHR (Foxo1) targets to proteasomal degradation. *Proceedings of the National Academy of Sciences*, *100*(20), 11285–11290. https://doi.org/10.1073/pnas.1934283100

Mattison, J. A., Colman, R. J., Beasley, T. M., Allison, D. B., Kemnitz, J. W., Roth, G. S., Ingram, D. K., Weindruch, R., de Cabo, R., & Anderson, R. M. (2017). Caloric restriction improves health and survival of rhesus monkeys. *Nature Communications*, *8*(1), 14063. https://doi.org/10.1038/ncomms14063

Medema, R. H., Kops, G. J. P. L., Bos, J. L., & Burgering, B. M. T. (2000). AFX-like Forkhead transcription factors mediate cell-cycle regulation by Ras and PKB through p27kip1. *Nature, 404*(6779), 782–787. https://doi.org/10.1038/35008115

Meley, D., Bauvy, C., Houben-Weerts, J. H. P. M., Dubbelhuis, P. F., Helmond, M. T. J., Codogno, P., & Meijer, A. J. (2006). AMP-activated Protein Kinase and the Regulation of Autophagic Proteolysis. *Journal of Biological Chemistry*, *281*(46), 34870–34879. https://doi.org/10.1074/jbc.M605488200

Mitchell, S. E., Tang, Z., Kerbois, C., Delville, C., Konstantopedos, P., Bruel, A., Derous, D., Green, C., Aspden, R. M., Goodyear, S. R., Chen, L., Han, J. J. D., Wang, Y., Promislow, D. E. L., Lusseau, D., Douglas, A., & Speakman, J. R. (2015). The effects of graded levels of calorie restriction: I. impact of short term calorie and protein restriction on body composition in the C57BL/6 mouse. *Oncotarget*, *6*(18), 15902–15930. https://doi.org/10.18632/oncotarget.4142

Morselli, E., Mariño, G., Bennetzen, M. v., Eisenberg, T., Megalou, E., Schroeder, S., Cabrera, S., Bénit, P., Rustin, P., Criollo, A., Kepp, O., Galluzzi, L., Shen, S., Malik, S. A., Maiuri, M. C., Horio, Y., López-Otín, C., Andersen, J. S., Tavernarakis, N., … Kroemer, G. (2011). Spermidine and resveratrol induce autophagy by distinct pathways converging on the acetylproteome. *Journal of Cell Biology*, *192*(4), 615–629. https://doi.org/10.1083/jcb.201008167

Most, J., Gilmore, L. A., Smith, S. R., Han, H., Ravussin, E., & Redman, L. M. (2018). Significant improvement in cardiometabolic health in healthy nonobese individuals during caloric restriction-induced weight loss and weight loss maintenance. *American Journal of Physiology-Endocrinology and Metabolism*, *314*(4), E396–E405. https://doi.org/10.1152/ajpendo.00261.2017

Most, J., & Redman, L. M. (2020). Impact of calorie restriction on energy metabolism in humans. *Experimental Gerontology*, *133*, 110875. https://doi.org/10.1016/j.exger.2020.110875

Motta, M. C., Divecha, N., Lemieux, M., Kamel, C., Chen, D., Gu, W., Bultsma, Y., McBurney, M., & Guarente, L. (2004). Mammalian SIRT1 Represses Forkhead Transcription Factors. *Cell*, *116*(4), 551–563. https://doi.org/10.1016/S0092-8674(04)00126-6

Nagy, L., Kao, H. Y., Chakravarti, D., Lin, R. J., Hassig, C. A., Ayer, D. E., Schreiber, S. L., & Evans, R. M. (1997). Nuclear receptor repression mediated by a complex containing SMRT, mSin3A, and histone deacetylase. *Cell*, *89*(3), 373–380. https://doi.org/10.1016/s0092-8674(00)80218-4

Nakagawa, T., Lomb, D. J., Haigis, M. C., & Guarente, L. (2009). SIRT5 Deacetylates Carbamoyl Phosphate Synthetase 1 and Regulates the Urea Cycle. *Cell*, *137*(3), 560–570. https://doi.org/10.1016/j.cell.2009.02.026

Nan, X., Ng, H.-H., Johnson, C. A., Laherty, C. D., Turner, B. M., Eisenman, R. N., & Bird, A. (1998). Transcriptional repression by the methyl-CpG-binding protein MeCP2 involves a histone deacetylase complex. *Nature*, *393*(6683), 386–389. https://doi.org/10.1038/30764

Ni, Y. G., Wang, N., Cao, D. J., Sachan, N., Morris, D. J., Gerard, R. D., Kuro-o, M., Rothermel, B. A., & Hill, J. A. (2007). FoxO transcription factors activate Akt and attenuate insulin signaling in heart by inhibiting protein phosphatases. *Proceedings of the National Academy of Sciences*, *104*(51), 20517–20522. https://doi.org/10.1073/pnas.0610290104

Oakhill, J. S., Steel, R., Chen, Z.-P., Scott, J. W., Ling, N., Tam, S., & Kemp, B. E. (2011). AMPK Is a Direct Adenylate Charge-Regulated Protein Kinase. *Science*, *332*(6036), 1433–1435. https://doi.org/10.1126/science.1200094

Oakley, R. H., & Cidlowski, J. A. (2011). Cellular Processing of the Glucocorticoid Receptor Gene and Protein: New Mechanisms for Generating Tissue-specific Actions of Glucocorticoids. *Journal of Biological Chemistry*, *286*(5), 3177–3184. https://doi.org/10.1074/jbc.R110.179325

Oakley, R. H., & Cidlowski, J. A. (2013). The biology of the glucocorticoid receptor: New signaling mechanisms in health and disease. *Journal of Allergy and Clinical Immunology*, *132*(5), 1033–1044. https://doi.org/10.1016/j.jaci.2013.09.007

Obsil, T., & Obsilova, V. (2011). Structural basis for DNA recognition by FOXO proteins. *Biochimica et Biophysica Acta (BBA) - Molecular Cell Research*, *1813*(11), 1946–1953. https://doi.org/10.1016/j.bbamcr.2010.11.025

Ogg, S., Paradis, S., Gottlieb, S., Patterson, G. I., Lee, L., Tissenbaum, H. A., & Ruvkun, G. (1997). The Fork head transcription factor DAF-16 transduces insulin-like metabolic and longevity signals in C. elegans. *Nature*, *389*(6654), 994–999. https://doi.org/10.1038/40194

Oosterman, J. E., Kalsbeek, A., la Fleur, S. E., & Belsham, D. D. (2015). Impact of nutrients on circadian rhythmicity. *American Journal of Physiology-Regulatory, Integrative and Comparative Physiology*, *308*(5), R337–R350. https://doi.org/10.1152/ajpregu.00322.2014

Opherk, C., Tronche, F., Kellendonk, C., Kohlmüller, D., Schulze, A., Schmid, W., & Schütz, G. (2004). Inactivation of the Glucocorticoid Receptor in Hepatocytes Leads to Fasting Hypoglycemia and Ameliorates Hyperglycemia in Streptozotocin-Induced Diabetes Mellitus. *Molecular Endocrinology*, *18*(6), 1346–1353. https://doi.org/10.1210/me.2003-0283

Paik, J.-H., Kollipara, R., Chu, G., Ji, H., Xiao, Y., Ding, Z., Miao, L., Tothova, Z., Horner, J. W., Carrasco, D. R., Jiang, S., Gilliland, D. G., Chin, L., Wong, W. H., Castrillon, D. H., & DePinho, R. A. (2007). FoxOs Are Lineage-Restricted Redundant Tumor Suppressors and Regulate Endothelial Cell Homeostasis. *Cell*, *128*(2), 309–323. https://doi.org/10.1016/j.cell.2006.12.029

Panda, S. (2016). Circadian physiology of metabolism. *Science*, *354*(6315), 1008–1015. https://doi.org/10.1126/science.aah4967

Partch, C. L., Green, C. B., & Takahashi, J. S. (2014). Molecular architecture of the mammalian circadian clock. *Trends in Cell Biology*, *24*(2), 90–99. https://doi.org/10.1016/j.tcb.2013.07.002

Parviz, F., Matullo, C., Garrison, W. D., Savatski, L., Adamson, J. W., Ning, G., Kaestner, K. H., Rossi, J. M., Zaret, K. S., & Duncan, S. A. (2003). Hepatocyte nuclear factor 4α controls the development of a hepatic epithelium and liver morphogenesis. *Nature Genetics*, *34*(3), 292–296. https://doi.org/10.1038/ng1175

Patel, N., & Finch, C. (2002). The glucocorticoid paradox of caloric restriction in slowing brain aging. *Neurobiology of Aging*, *23*(5), 707–717. https://doi.org/10.1016/S0197-4580(02)00017-9

Patel, R., McIntosh, L., McLaughlin, J., Brooke, S., Nimon, V., & Sapolsky, R. (2002). Disruptive effects of glucocorticoids on glutathione peroxidase biochemistry in hippocampal cultures. *Journal of Neurochemistry*, *82*(1), 118–125. https://doi.org/10.1046/j.1471-4159.2002.00948.x

Patel, S. A., Chaudhari, A., Gupta, R., Velingkaar, N., & Kondratov, R. v. (2016). Circadian clocks govern calorie restriction-mediated life span extension through BMAL1- and IGF-1-dependent mechanisms. *FASEB Journal: Official Publication of the Federation of American Societies for Experimental Biology*, *30*(4), 1634–1642. https://doi.org/10.1096/fj.15-282475

Patel, S. A., Velingkaar, N., Makwana, K., Chaudhari, A., & Kondratov, R. (2016). Calorie restriction regulates circadian clock gene expression through BMAL1 dependent and independent mechanisms. *Scientific Reports*, *6*(1), 25970. https://doi.org/10.1038/srep25970

Porstmann, T., Santos, C. R., Griffiths, B., Cully, M., Wu, M., Leevers, S., Griffiths, J. R., Chung, Y.-L., & Schulze, A. (2008). SREBP Activity Is Regulated by mTORC1 and Contributes to Akt-Dependent Cell Growth. *Cell Metabolism*, *8*(3), 224–236. https://doi.org/10.1016/j.cmet.2008.07.007

Potter, G. D. M., Skene, D. J., Arendt, J., Cade, J. E., Grant, P. J., & Hardie, L. J. (2016). Circadian Rhythm and Sleep Disruption: Causes, Metabolic Consequences, and Countermeasures. *Endocrine Reviews*, *37*(6), 584–608. https://doi.org/10.1210/er.2016-1083

Præstholm, S. M., Correia, C. M., Goitea, V. E., Siersbæk, M. S., Jørgensen, M., Havelund, J. F., Pedersen, T. Å., Færgeman, N. J., & Grøntved, L. (2021). Impaired glucocorticoid receptor expression in liver disrupts feeding-induced gene expression, glucose uptake, and glycogen storage. *Cell Reports*, *37*(5), 109938. https://doi.org/10.1016/j.celrep.2021.109938

Præstholm, S. M., Correia, C. M., & Grøntved, L. (2020). Multifaceted Control of GR Signaling and Its Impact on Hepatic Transcriptional Networks and Metabolism. *Frontiers in Endocrinology*, *11*. https://doi.org/10.3389/fendo.2020.572981

Pratt, W. B., & Toft, D. O. (1997). Steroid Receptor Interactions with Heat Shock Protein and Immunophilin Chaperones*. *Endocrine Reviews*, *18*(3), 306–360. https://doi.org/10.1210/edrv.18.3.0303

Purushotham, A., Schug, T. T., Xu, Q., Surapureddi, S., Guo, X., & Li, X. (2009). Hepatocyte-Specific Deletion of SIRT1 Alters Fatty Acid Metabolism and Results in

Hepatic Steatosis and Inflammation. *Cell Metabolism*, *9*(4), 327–338. https://doi.org/10.1016/j.cmet.2009.02.006

Quagliarini, F., Mir, A. A., Balazs, K., Wierer, M., Dyar, K. A., Jouffe, C., Makris, K., Hawe, J., Heinig, M., Filipp, F. V., Barish, G. D., & Uhlenhaut, N. H. (2019). Cistromic Reprogramming of the Diurnal Glucocorticoid Hormone Response by High-Fat Diet. *Molecular Cell*, *76*(4), 531-545.e5. https://doi.org/10.1016/j.molcel.2019.10.007

Quinlan, A. R., & Hall, I. M. (2010). BEDTools: a flexible suite of utilities for comparing genomic features. *Bioinformatics*, *26*(6), 841–842. https://doi.org/10.1093/bioinformatics/btq033

Ratman, D., Mylka, V., Bougarne, N., Pawlak, M., Caron, S., Hennuyer, N., Paumelle, R., De Cauwer, L., Thommis, J., Rider, M. H., Libert, C., Lievens, S., Tavernier, J., Staels, B., & De Bosscher, K. (2016). Chromatin recruitment of activated AMPK drives fasting response genes co-controlled by GR and PPARα. *Nucleic Acids Research*, *44*(22), 10539–10553. https://doi.org/10.1093/nar/gkw742

Ravussin, E., Redman, L. M., Rochon, J., Das, S. K., Fontana, L., Kraus, W. E., Romashkan, S., Williamson, D. A., Meydani, S. N., Villareal, D. T., Smith, S. R., Stein, R. I., Scott, T. M., Stewart, T. M., Saltzman, E., Klein, S., Bhapkar, M., Martin, C. K., Gilhooly, C. H., … Roberts, S. B. (2015). A 2-Year Randomized Controlled Trial of Human Caloric Restriction: Feasibility and Effects on Predictors of Health Span and Longevity. *The Journals of Gerontology Series A: Biological Sciences and Medical Sciences*, *70*(9), 1097–1104. https://doi.org/10.1093/gerona/glv057

Reddy, J. K., & Sambasiva Rao, M. (2006). Lipid Metabolism and Liver Inflammation. II. Fatty liver disease and fatty acid oxidation. *American Journal of Physiology-Gastrointestinal and Liver Physiology*, *290*(5), G852–G858. https://doi.org/10.1152/ajpgi.00521.2005

Regmi, P., & Heilbronn, L. K. (2020). Time-Restricted Eating: Benefits, Mechanisms, and Challenges in Translation. *IScience*, *23*(6), 101161. https://doi.org/10.1016/j.isci.2020.101161

Reppert, S. M., & Weaver, D. R. (2001). Molecular Analysis of Mammalian Circadian Rhythms. *Annual Review of Physiology*, *63*(1), 647–676. https://doi.org/10.1146/annurev.physiol.63.1.647

Rodgers, J. T., Lerin, C., Haas, W., Gygi, S. P., Spiegelman, B. M., & Puigserver, P. (2005). Nutrient control of glucose homeostasis through a complex of PGC-1α and SIRT1. *Nature*, *434*(7029), 113–118. https://doi.org/10.1038/nature03354

Rogatsky, I., Waase, C. L. M., & Garabedian, M. J. (1998). Phosphorylation and Inhibition of Rat Glucocorticoid Receptor Transcriptional Activation by Glycogen Synthase Kinase-3 (GSK-3). *Journal of Biological Chemistry*, *273*(23), 14315–14321. https://doi.org/10.1074/jbc.273.23.14315

Rosales, R., Romero, M. R., Vaquero, J., Monte, M. J., Requena, P., Martinez-Augustin, O., Sanchez de Medina, F., & Marin, J. J. G. (2013). FXR-dependent and -independent interaction of glucocorticoids with the regulatory pathways involved in

the control of bile acid handling by the liver. *Biochemical Pharmacology*, *85*(6), 829–838. https://doi.org/10.1016/j.bcp.2013.01.001

Rose, A. J., Díaz, M. B., Reimann, A., Klement, J., Walcher, T., Krones-Herzig, A., Strobel, O., Werner, J., Peters, A., Kleyman, A., Tuckermann, J. P., Vegiopoulos, A., & Herzig, S. (2011). Molecular Control of Systemic Bile Acid Homeostasis by the Liver Glucocorticoid Receptor. *Cell Metabolism*, *14*(1), 123–130. https://doi.org/10.1016/j.cmet.2011.04.010

Roth, G. S., Ingram, D. K., & Lane, M. A. (2006). Caloric Restriction in Primates and Relevance to Humans. *Annals of the New York Academy of Sciences*, *928*(1), 305–315. https://doi.org/10.1111/j.1749-6632.2001.tb05660.x

Ruderman, N. B., Carling, D., Prentki, M., & Cacicedo, J. M. (2013). AMPK, insulin resistance, and the metabolic syndrome. *Journal of Clinical Investigation*, *123*(7), 2764–2772. https://doi.org/10.1172/JCI67227

Rui, L. (2014). Energy Metabolism in the Liver. In *Comprehensive Physiology* (pp. 177–197). Wiley. https://doi.org/10.1002/cphy.c130024

Rustaeus, S., Lindberg, K., Stillemark, P., Claesson, C., Asp, L., Larsson, T., Borén, J., & Olofsson, S.-O. (1999). Assembly of Very Low Density Lipoprotein: A Two-Step Process of Apolipoprotein B Core Lipidation. *The Journal of Nutrition*, *129*(2), 463S-466S. https://doi.org/10.1093/jn/129.2.463S

Sabatino, F., Masoro, E. J., McMahan, C. A., & Kuhn, R. W. (1991). Assessment of the Role of the Glucocorticoid System in Aging Processes and in the Action of Food Restriction. *Journal of Gerontology*, *46*(5), B171–B179. https://doi.org/10.1093/geronj/46.5.B171

Sacitharan, P. K., Gharios, G. B., & Edwards, J. R. (2019). Spermidine restores dysregulated autophagy and polyamine synthesis in aged and osteoarthritic chondrocytes via EP300: response to correspondence by Borzì et al. *Experimental & Molecular Medicine*, *51*(3), 1–2. https://doi.org/10.1038/s12276-019-0225-3

Sanders, F. W. B., & Griffin, J. L. (2016a). *De novo* lipogenesis in the liver in health and disease: more than just a shunting yard for glucose. *Biological Reviews*, *91*(2), 452–468. https://doi.org/10.1111/brv.12178

Sanders, F. W. B., & Griffin, J. L. (2016b). *De novo* lipogenesis in the liver in health and disease: more than just a shunting yard for glucose. *Biological Reviews*, *91*(2), 452–468. https://doi.org/10.1111/brv.12178

Sanderson, J. T. (2006). The Steroid Hormone Biosynthesis Pathway as a Target for Endocrine-Disrupting Chemicals. *Toxicological Sciences*, *94*(1), 3–21. https://doi.org/10.1093/toxsci/kfl051

Sato, S., Solanas, G., Peixoto, F. O., Bee, L., Symeonidi, A., Schmidt, M. S., Brenner, C., Masri, S., Benitah, S. A., & Sassone-Corsi, P. (2017). Circadian Reprogramming in the Liver Identifies Metabolic Pathways of Aging. *Cell*, *170*(4), 664-677.e11. https://doi.org/10.1016/j.cell.2017.07.042

Schneider, A., Dhahbi, J. M., Atamna, H., Clark, J. P., Colman, R. J., & Anderson, R. M. (2017). Caloric restriction impacts plasma microRNAs in rhesus monkeys. *Aging Cell*, *16*(5), 1200–1203. https://doi.org/10.1111/acel.12636

Sellix, M. T., Evans, J. A., Leise, T. L., Castanon-Cervantes, O., Hill, D. D., DeLisser, P., Block, G. D., Menaker, M., & Davidson, A. J. (2012). Aging Differentially Affects the Re-entrainment Response of Central and Peripheral Circadian Oscillators. *Journal of Neuroscience*, *32*(46), 16193–16202. https://doi.org/10.1523/JNEUROSCI.3559-12.2012

Shaw, R. J., Kosmatka, M., Bardeesy, N., Hurley, R. L., Witters, L. A., DePinho, R. A., & Cantley, L. C. (2004). The tumor suppressor LKB1 kinase directly activates AMP-activated kinase and regulates apoptosis in response to energy stress. *Proceedings of the National Academy of Sciences*, *101*(10), 3329–3335. https://doi.org/10.1073/pnas.0308061100

Shimazu, T., Hirschey, M. D., Newman, J., He, W., Shirakawa, K., le Moan, N., Grueter, C. A., Lim, H., Saunders, L. R., Stevens, R. D., Newgard, C. B., Farese, R. v., de Cabo, R., Ulrich, S., Akassoglou, K., & Verdin, E. (2013). Suppression of Oxidative Stress by β-Hydroxybutyrate, an Endogenous Histone Deacetylase Inhibitor. *Science*, *339*(6116), 211–214. https://doi.org/10.1126/science.1227166

Shin, D.-J., Joshi, P., Hong, S.-H., Mosure, K., Shin, D.-G., & Osborne, T. F. (2012). Genome-wide analysis of FoxO1 binding in hepatic chromatin: Potential involvement of FoxO1 in linking retinoid signaling to hepatic gluconeogenesis. *Nucleic Acids Research*, *40*(22), 11499–11509. https://doi.org/10.1093/nar/gks932

Silverstein, R. A., & Ekwall, K. (2005). Sin3: a flexible regulator of global gene expression and genome stability. *Current Genetics*, *47*(1), 1–17. https://doi.org/10.1007/s00294-004-0541-5

Someya, S., Yu, W., Hallows, W. C., Xu, J., Vann, J. M., Leeuwenburgh, C., Tanokura, M., Denu, J. M., & Prolla, T. A. (2010). Sirt3 Mediates Reduction of Oxidative Damage and Prevention of Age-Related Hearing Loss under Caloric Restriction. *Cell*, *143*(5), 802–812. https://doi.org/10.1016/j.cell.2010.10.002

Son, G. H., Chung, S., & Kim, K. (2011). The adrenal peripheral clock: Glucocorticoid and the circadian timing system. *Frontiers in Neuroendocrinology*, *32*(4), 451–465. https://doi.org/10.1016/j.yfrne.2011.07.003

Sonntag, W. E., Lynch, C. D., Cefalu, W. T., Ingram, R. L., Bennett, S. A., Thornton, P. L., & Khan, A. S. (1999). Pleiotropic Effects of Growth Hormone and Insulin-like Growth Factor (IGF)-1 on Biological Aging: Inferences From Moderate Caloric-Restricted Animals. *The Journals of Gerontology Series A: Biological Sciences and Medical Sciences*, *54*(12), B521–B538. https://doi.org/10.1093/gerona/54.12.B521

Spencer, R. L., Chun, L. E., Hartsock, M. J., & Woodruff, E. R. (2018). Glucocorticoid hormones are both a major circadian signal and major stress signal: How this shared signal contributes to a dynamic relationship between the circadian and stress systems. *Frontiers in Neuroendocrinology*, *49*, 52–71. https://doi.org/10.1016/j.yfrne.2017.12.005

Spriet, L. L. (2014). New Insights into the Interaction of Carbohydrate and Fat Metabolism During Exercise. *Sports Medicine*, *44*(S1), 87–96. https://doi.org/10.1007/s40279-014-0154-1

Starick, S. R., Ibn-Salem, J., Jurk, M., Hernandez, C., Love, M. I., Chung, H.-R., Vingron, M., Thomas-Chollier, M., & Meijsing, S. H. (2015). ChIP-exo signal associated with DNA-binding motifs provides insight into the genomic binding of the glucocorticoid receptor and cooperating transcription factors. *Genome Research*, *25*(6), 825–835. https://doi.org/10.1101/gr.185157.114

Sternberg, P. W., Stern, M. J., Clark, I., & Herskowitz, I. (1987). Activation of the yeast HO gene by release from multiple negative controls. *Cell*, *48*(4), 567–577. https://doi.org/10.1016/0092-8674(87)90235-2

Sundler, R., & Akesson, B. (1975). Biosynthesis of phosphatidylethanolamines and phosphatidylcholines from ethanolamine and choline in rat liver. *Biochemical Journal*, *146*(2), 309–315. https://doi.org/10.1042/bj1460309

Tang, X., Benesch, M. G. K., & Brindley, D. N. (2015). Lipid phosphate phosphatases and their roles in mammalian physiology and pathology. *Journal of Lipid Research*, *56*(11), 2048–2060. https://doi.org/10.1194/jlr.R058362

Taniguchi, C. M., Emanuelli, B., & Kahn, C. R. (2006). Critical nodes in signalling pathways: insights into insulin action. *Nature Reviews Molecular Cell Biology*, *7*(2), 85–96. https://doi.org/10.1038/nrm1837

Titchenell, P. M., Quinn, W. J., Lu, M., Chu, Q., Lu, W., Li, C., Chen, H., Monks, B. R., Chen, J., Rabinowitz, J. D., & Birnbaum, M. J. (2016). Direct Hepatocyte Insulin Signaling Is Required for Lipogenesis but Is Dispensable for the Suppression of Glucose Production. *Cell Metabolism*, *23*(6), 1154–1166. https://doi.org/10.1016/j.cmet.2016.04.022

Toledo, M., Batista-Gonzalez, A., Merheb, E., Aoun, M. L., Tarabra, E., Feng, D., Sarparanta, J., Merlo, P., Botrè, F., Schwartz, G. J., Pessin, J. E., & Singh, R. (2018). Autophagy Regulates the Liver Clock and Glucose Metabolism by Degrading CRY1. *Cell Metabolism*, *28*(2), 268-281.e4. https://doi.org/10.1016/j.cmet.2018.05.023

Trapp, J. (2006). The Role of NAD+ Dependent Histone Deacetylases (sirtuins) in Ageing. *Current Drug Targets*, *7*(11), 1553–1560. https://doi.org/10.2174/138945011060701553

Trepanowski, J. F., Canale, R. E., Marshall, K. E., Kabir, M. M., & Bloomer, R. J. (2011). Impact of caloric and dietary restriction regimens on markers of health and longevity in humans and animals: a summary of available findings. *Nutrition Journal*, *10*(1), 107. https://doi.org/10.1186/1475-2891-10-107

Tronche, F., Kellendonk, C., Kretz, O., Gass, P., Anlag, K., Orban, P. C., Bock, R., Klein, R., & Schütz, G. (1999). Disruption of the glucocorticoid receptor gene in the nervous system results in reduced anxiety. *Nature Genetics*, *23*(1), 99–103. https://doi.org/10.1038/12703

Vance, J. E. (2015). Phospholipid Synthesis and Transport in Mammalian Cells. *Traffic*, *16*(1), 1–18. https://doi.org/10.1111/tra.12230

Vegiopoulos, A., & Herzig, S. (2007). Glucocorticoids, metabolism and metabolic diseases. *Molecular and Cellular Endocrinology*, *275*(1–2), 43–61. https://doi.org/10.1016/j.mce.2007.05.015

Waddell, D. S., Baehr, L. M., van den Brandt, J., Johnsen, S. A., Reichardt, H. M., Furlow, J. D., & Bodine, S. C. (2008). The glucocorticoid receptor and FOXO1 synergistically activate the skeletal muscle atrophy-associated MuRF1 gene. *American Journal of Physiology-Endocrinology and Metabolism*, *295*(4), E785–E797. https://doi.org/10.1152/ajpendo.00646.2007

Wang, G., Bonkovsky, H. L., de Lemos, A., & Burczynski, F. J. (2015). Recent insights into the biological functions of liver fatty acid binding protein 1. *Journal of Lipid Research*, *56*(12), 2238–2247. https://doi.org/10.1194/jlr.R056705

Wang, H., & Stillman, D. J. (1993). Transcriptional repression in Saccharomyces cerevisiae by a SIN3-LexA fusion protein. *Molecular and Cellular Biology*, *13*(3), 1805–1814. https://doi.org/10.1128/mcb.13.3.1805-1814.1993

Webb, A. E., Kundaje, A., & Brunet, A. (2016). Characterization of the direct targets of <scp>FOXO</scp> transcription factors throughout evolution. *Aging Cell*, *15*(4), 673–685. https://doi.org/10.1111/acel.12479

Weigel, D., Jürgens, G., Küttner, F., Seifert, E., & Jäckle, H. (1989). The homeotic gene fork head encodes a nuclear protein and is expressed in the terminal regions of the Drosophila embryo. *Cell*, *57*(4), 645–658. https://doi.org/10.1016/0092-8674(89)90133-5

Weir, J. B. de v. (1949). New methods for calculating metabolic rate with special reference to protein metabolism. *The Journal of Physiology*, *109*(1–2), 1–9. https://doi.org/10.1113/jphysiol.1949.sp004363

Wondisford, A. R., Xiong, L., Chang, E., Meng, S., Meyers, D. J., Li, M., Cole, P. A., & He, L. (2014). Control of Foxo1 Gene Expression by Co-activator P300. *Journal of Biological Chemistry*, *289*(7), 4326–4333. https://doi.org/10.1074/jbc.M113.540500

Wong, C.-W., & Privalsky, M. L. (1998). Transcriptional Silencing Is Defined by Isoform- and Heterodimer-Specific Interactions between Nuclear Hormone Receptors and Corepressors. *Molecular and Cellular Biology*, *18*(10), 5724–5733. https://doi.org/10.1128/MCB.18.10.5724

Woods, A., Johnstone, S. R., Dickerson, K., Leiper, F. C., Fryer, L. G. D., Neumann, D., Schlattner, U., Wallimann, T., Carlson, M., & Carling, D. (2003). LKB1 Is the Upstream Kinase in the AMP-Activated Protein Kinase Cascade. *Current Biology*, *13*(22), 2004–2008. https://doi.org/10.1016/j.cub.2003.10.031

Wu, Y., Pan, Q., Yan, H., Zhang, K., Guo, X., Xu, Z., Yang, W., Qi, Y., Guo, C. A., Hornsby, C., Zhang, L., Zhou, A., Li, L., Chen, Y., Zhang, W., Sun, Y., Zheng, H., Wondisford, F., He, L., & Guo, S. (2018). Novel Mechanism of Foxo1 Phosphorylation in Glucagon

Signaling in Control of Glucose Homeostasis. *Diabetes*, *67*(11), 2167–2182. https://doi.org/10.2337/db18-0674

Xiao, B., Sanders, M. J., Underwood, E., Heath, R., Mayer, F. v., Carmena, D., Jing, C., Walker, P. A., Eccleston, J. F., Haire, L. F., Saiu, P., Howell, S. A., Aasland, R., Martin, S. R., Carling, D., & Gamblin, S. J. (2011). Structure of mammalian AMPK and its regulation by ADP. *Nature*, *472*(7342), 230–233. https://doi.org/10.1038/nature09932

Yang, L., Roh, Y. S., Song, J., Zhang, B., Liu, C., Loomba, R., & Seki, E. (2014). Transforming growth factor beta signaling in hepatocytes participates in steatohepatitis through regulation of cell death and lipid metabolism in mice. *Hepatology*, *59*(2), 483–495. https://doi.org/10.1002/hep.26698

Yao, C., Carraro, G., Konda, B., Guan, X., Mizuno, T., Chiba, N., Kostelny, M., Kurkciyan, A., David, G., McQualter, J. L., & Stripp, B. R. (2017). Sin3a regulates epithelial progenitor cell fate during lung development. *Development*. https://doi.org/10.1242/dev.149708

Yi, C., Ma, M., Ran, L., Zheng, J., Tong, J., Zhu, J., Ma, C., Sun, Y., Zhang, S., Feng, W., Zhu, L., Le, Y., Gong, X., Yan, X., Hong, B., Jiang, F.-J., Xie, Z., Miao, D., Deng, H., & Yu, L. (2012). Function and Molecular Mechanism of Acetylation in Autophagy Regulation. *Science*, *336*(6080), 474–477. https://doi.org/10.1126/science.1216990

Young, E., Abelson, J., & Lightman, S. (2004). Cortisol pulsatility and its role in stress regulation and health. *Frontiers in Neuroendocrinology*, *25*(2), 69–76. https://doi.org/10.1016/j.yfrne.2004.07.001

Yu, G., Wang, L.-G., & He, Q.-Y. (2015). ChIPseeker: an R/Bioconductor package for ChIP peak annotation, comparison and visualization. *Bioinformatics*, *31*(14), 2382–2383. https://doi.org/10.1093/bioinformatics/btv145

Zardi, E., Navarini, L., Sambataro, G., Piccinni, P., Sambataro, F., Spina, C., & Dobrina, A. (2013). Hepatic PPARs: Their Role in Liver Physiology, Fibrosis and Treatment. *Current Medicinal Chemistry*, *20*(27), 3370–3396. https://doi.org/10.2174/09298673113209990136

Zhang, E. E., Liu, Y., Dentin, R., Pongsawakul, P. Y., Liu, A. C., Hirota, T., Nusinow, D. A., Sun, X., Landais, S., Kodama, Y., Brenner, D. A., Montminy, M., & Kay, S. A. (2010). Cryptochrome mediates circadian regulation of cAMP signaling and hepatic gluconeogenesis. *Nature Medicine*, *16*(10), 1152–1156. https://doi.org/10.1038/nm.2214

Zhang, K., Li, L., Qi, Y., Zhu, X., Gan, B., DePinho, R. A., Averitt, T., & Guo, S. (2012). Hepatic Suppression of Foxo1 and Foxo3 Causes Hypoglycemia and Hyperlipidemia in Mice. *Endocrinology*, *153*(2), 631–646. https://doi.org/10.1210/en.2011-1527

Zhang, L., Orban, M., Lorenz, M., Barocke, V., Braun, D., Urtz, N., Schulz, C., von Brühl, M.-L., Tirniceriu, A., Gaertner, F., Proia, R. L., Graf, T., Bolz, S.-S., Montanez, E., Prinz, M., Müller, A., von Baumgarten, L., Billich, A., Sixt, M., … Massberg, S. (2012). A novel role of sphingosine 1-phosphate receptor S1pr1 in mouse thrombopoiesis.

Journal of Experimental Medicine, *209*(12), 2165–2181. https://doi.org/10.1084/jem.20121090

Zhang, W., Patil, S., Chauhan, B., Guo, S., Powell, D. R., Le, J., Klotsas, A., Matika, R., Xiao, X., Franks, R., Heidenreich, K. A., Sajan, M. P., Farese, R. v., Stolz, D. B., Tso, P., Koo, S.-H., Montminy, M., & Unterman, T. G. (2006). FoxO1 Regulates Multiple Metabolic Pathways in the Liver. *Journal of Biological Chemistry*, *281*(15), 10105–10117. https://doi.org/10.1074/jbc.M600272200

Zhang, Y., Iratni, R., Erdjument-Bromage, H., Tempst, P., & Reinberg, D. (1997). Histone Deacetylases and SAP18, a Novel Polypeptide, Are Components of a Human Sin3 Complex. *Cell*, *89*(3), 357–364. https://doi.org/10.1016/S0092-8674(00)80216-0

Zhang, Y., Liu, T., Meyer, C. A., Eeckhoute, J., Johnson, D. S., Bernstein, B. E., Nussbaum, C., Myers, R. M., Brown, M., Li, W., & Liu, X. S. (2008). Model-based Analysis of ChIP-Seq (MACS). *Genome Biology*, *9*(9), R137. https://doi.org/10.1186/gb-2008-9-9-r137

Zheng, W.-H., Kar, S., & Quirion, R. (2002). FKHRL1 and its homologs are new targets of nerve growth factor Trk receptor signaling. *Journal of Neurochemistry*, *80*(6), 1049–1061. https://doi.org/10.1046/j.0022-3042.2002.00783.x

Zhu, H. (2016). Forkhead box transcription factors in embryonic heart development and congenital heart disease. *Life Sciences*, *144*, 194–201. https://doi.org/10.1016/j.lfs.2015.12.001

Zullo, J. M., Drake, D., Aron, L., O'Hern, P., Dhamne, S. C., Davidsohn, N., Mao, C.-A., Klein, W. H., Rotenberg, A., Bennett, D. A., Church, G. M., Colaiácovo, M. P., & Yankner, B. A. (2019). Regulation of lifespan by neural excitation and REST. *Nature*, *574*(7778), 359–364. https://doi.org/10.1038/s41586-019-1647-8

Zwighaft, Z., Aviram, R., Shalev, M., Rousso-Noori, L., Kraut-Cohen, J., Golik, M., Brandis, A., Reinke, H., Aharoni, A., Kahana, C., & Asher, G. (2015). Circadian Clock Control by Polyamine Levels through a Mechanism that Declines with Age. *Cell Metabolism*, *22*(5), 874–885. https://doi.org/10.1016/j.cmet.2015.09.011

8 Supplementary data

Supplementary figure 1: Validation of GR-, FOXO1-, and SIN3A-ChIP-seq in both AL and CR in liver.

Validation of ChIP-seq at the peak of corticosterone levels (at ZT12) in the liver using ChIP-qPCR for GR (at both AL and CR), FOXO1 (in CR), and SIN3A (in CR). For GR ChIP-seq, as negative control was in ChIP-qPCR *Foxl2* locus and as positive loci: *Per1* (*Peak#1*), *Per1* (*Peak#2*), and *Fkbp5* locus. Prominently, from the GR ChIP-seq between AL and CR, we can observe increased GR recruitment in caloric restriction over *ad-libitum*. For FOXO1 ChIP-seq in caloric restriction, as negative loci in the ChIP-qPCR were used *Foxl2* and *Trim63* locus and as positive loci: *Abcg8* and *Pdk4* locus. For SIN3A ChIP-seq in caloric restriction, as negative loci in the ChIP-qPCR were used *Foxl2* and *Trim63* locus and as positive loci: *Abcg8* and *Per1* (*Peak#2*) locus. Data represent mean ± SEM, n =3 biological replicates, *p<0.05, **p<0.01 and ns = not significant. Student's t-test.

ChIP-seq at the peak of corticosterone levels (at ZT12)
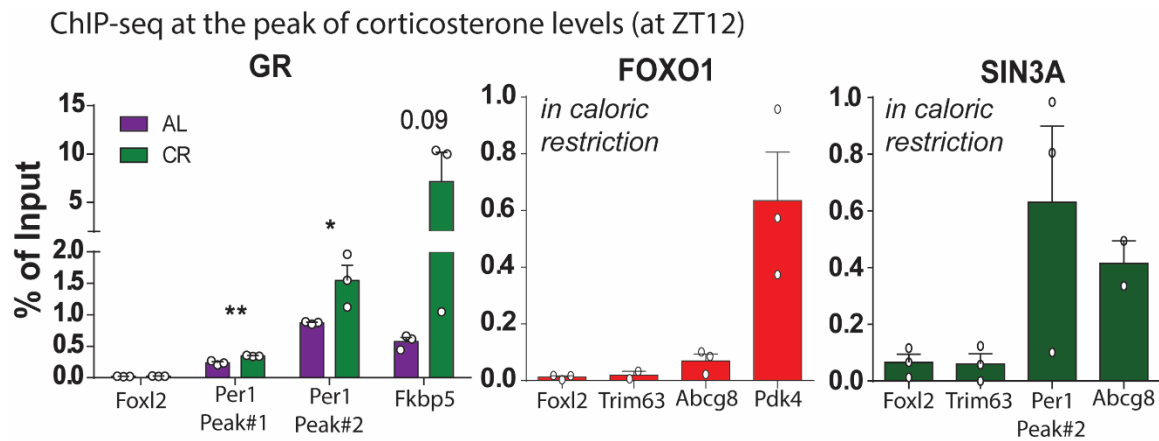
Supplementary Table 1: Quality check of ChIP-seq samples.

Sample Name	Total Read Fastq	Total Reads BAM	Reads after removing duplicates	Reads after removing multimappers	Nº of duplicates	Nº of multimappers	FriP score	Nº of peaks FDR < 0.05 (unfiltered.narrowPeak)	Nº of IDR peaks
AL_GR_R1	29358420	58717837	25609476	18788360	33108361	6821116	0.079	2330	6579
AL_GR_R2	30893147	61787475	44792421	36295377	16995054	8497044	0.088	12978	6579
AL_GR_R3	109507800	219018677	96504590	74392012	122514087	22112578	0.046	7125	6579
CR_GR_R1	42741581	41714980	27987082	22690852	13727898	5296230	0.119	23271	14828
CR_GR_R2	65749121	131499950	45498411	33150660	86001539	12347751	0.099	17245	14828
CR_FOXO1_R1	51474836	50375451	36047940	28906266	14327511	7141674	0.050	7581	5102
CR_FOXO1_R2	135958842	271924108	64052432	9346439	207871676	54705993	0.124	13748	5102
LF_SIN3A_R1	75270622	73228428	35063590	19494035	38164838	15569555	0.193	22295	13269
LF_SIN3A_R2	78384812	79936150	40496489	35527232	39439661	4969257	0.219	39567	13269
CR_SIN3A_R1	43559729	42618595	12373512	8329822	30245083	4043690	0.133	14197	8990
CR_SIN3A_R2	37655270	75311554	58589847	49058498	16721707	9531349	0.065	13846	8990

Supplementary list 1: Selected GR ChIP-seq peaks.

Gene	Chromosome	Start	End	Annotation	Gene strand
Apoc3	chr9	46235333	46235731	Promoter (<=1kb)	-
Arntl	chr7	113260578	113260976	Intron	+
Atg7	chr6	114657075	114657473	Promoter (<=1kb)	+
Atg7	chr6	114787713	114788111	Intron	+
Atg7	chr6	114781782	114782180	Intron	+
Cpt1α	chr19	3320086	3320484	Promoter (1-2kb)	+
Cry1	chr10	85190102	85190500	Distal Intergenic	-
Fabp1	chr6	71173008	71173406	Distal Intergenic	+
Fabp1	chr6	71189604	71190002	Distal Intergenic	+
Fabp1	chr6	71173008	71173406	Distal Intergenic	+
Fabp1	chr6	71185171	71185569	Distal Intergenic	+
Fabp1	chr6	71196051	71196449	Distal Intergenic	+
Gde1	chr7	118703191	118703589	Promoter (1-2kb)	-
Pygl	chr12	70233637	70234035	Promoter (2-3kb)	-
Nr1d1	chr11	98773849	98774247	Promoter (1-2kb)	-
Per1	chr11	69096873	69097271	Promoter (1-2kb)	+
Ulk1	chr5	110808001	110808399	Promoter (1-2kb)	-

Supplementary list 2: Selected common GR/FOXO1 ChIP-seq peaks.

Gene	Chromosome	Start*	End*	Annotation	Gene strand
Cry1	chr10	85190101	85190500	Distal Intergenic	-
Fabp1	chr6	71173007	71173406	Distal Intergenic	+
Fabp1	chr6	71185170	71185569	Distal Intergenic	+
Map1lc3b	chr8	121585308	121585707	Intron	+
Mat1a	chr14	41096371	41096770	Distal Intergenic	+
Mat1a	chr14	41100662	41101061	Distal Intergenic	+
Per1	chr11	69094836	69095235	Promoter	+
Per1	chr11	69096872	69097271	Intron	+
Per2	chr1	91436408	91436807	Intron	-
Pparα	chr15	85732200	85732599	Distal Intergenic	+
Pparα	chr15	85787300	85787699	Intron	+
Pygl	chr12	70233636	70234035	Exon	-
Aldob	chr4	49559949	49560348	Distal Intergenic	-

*Overlap of the common GR/FOXO1 ChIP peaks with 400bp coverage.

Supplementary list 3: Differentially expressed genes between AL vs CR in liver.

Results from RNA-seq in liver of caloric restricted WT versus *ad-libitum* WT mice at the peak of corticosterone levels (at ZT12) indicating the fold change (FC) in gene expression as log2 (log2FC). The top 50 up- and down-regulated genes (FC>1.5; p-value <0.05) are listed.

Gene name	baseMean	log2FC	Padj CR over AL
Fmo3	19246.36	10.65	9.74E-85
Cyp2b9	6145.01	10.16	3.12E-83
Cyp2b13	67.98	8.61	2.06E-10
Cyp2b10	56.07	6.84	9.43E-13
4931429L15Rik	375.35	6.11	9.54E-15
Cux2	551.51	5.99	3.99E-88
Slc22a26	339.19	5.96	2.75E-12
Cyp2c69	529.26	5.86	3.21E-10
Fam107a	276.92	5.86	2.74E-71
Slc22a27	208.69	5.84	6.46E-16
Nipal1	1214.47	5.72	1.19E-17
Ddit4	2682.32	5.67	0.00E+00
Cdkn1a	1254.34	5.62	9.68E-146
Pdk4	2399.21	5.55	1.61E-11
Pdgfrl	348.79	5.45	7.62E-20
Sult1e1	138.55	5.18	1.21E-34
Ppp1r3g	1682.08	5.15	3.18E-16
Igfbp1	19342.81	5.11	1.95E-21
Cyp4a14	53253.14	4.71	1.29E-27
Arntl	342.93	4.19	2.43E-77
Gadd45b	121.46	4.19	1.17E-14
Cyp2a4	462.01	4.06	2.06E-09
Nr4a1	281.04	3.91	6.91E-04
Gm11843	188.71	3.86	7.27E-24
Dusp8	89.70	3.80	3.29E-11
Il22ra1	450.05	3.80	1.07E-54
Cyp2c40	546.68	3.65	1.01E-08
Bud13	1596.45	3.59	2.60E-57
Acnat2	829.38	3.54	4.69E-68
Myom1	152.54	3.51	3.53E-18
Dhrs9	61.52	3.49	1.79E-17
Cyp39a1	3983.88	3.46	1.51E-136
Cyp2c39	283.16	3.44	3.53E-22
Fam222a	343.51	3.40	3.45E-26
Mroh6	172.17	3.40	2.66E-40
Sftpa1	439.34	3.32	3.46E-10

4921513D11Rik	153.95	3.26	8.01E-23
Fmo2	6052.15	3.22	6.40E-51
Plin4	1605.61	3.13	1.71E-53
Lepr	5106.75	3.06	1.41E-160
Atoh8	855.90	3.02	9.74E-76
Tat	153691.44	2.97	1.27E-63
Hamp2	2558.52	2.96	1.64E-08
Slc16a5	1289.83	2.88	7.29E-11
Mpzl1	191.68	2.86	3.99E-16
1810053B23Rik	86.69	2.85	1.04E-20
AA986860	652.14	2.85	3.45E-22
Adrb2	68.56	2.75	6.42E-15
Gm43305	1406.04	2.74	2.34E-04
Cyp17a1	2922.19	2.72	2.33E-04
Cib3	169.03	-3.81	8.48E-23
Klhdc7a	649.29	-3.86	1.19E-13
Gbp10	92.91	-3.89	2.44E-20
Bhlhe41	89.53	-3.94	3.78E-24
Mup-ps13	151.00	-3.97	3.61E-06
Fam83f	60.73	-4.05	1.46E-10
3110082I17Rik	223.68	-4.08	1.27E-09
Fam65b	135.87	-4.20	3.08E-39
Gm13775	172.43	-4.24	4.83E-07
Nudt7	16647.27	-4.41	1.05E-164
C330002G04Rik	55.17	-4.46	1.68E-19
Mup2	181.89	-4.47	1.83E-04
Slco1a1	10297.62	-4.48	6.80E-07
RP24-82M4,2	135.48	-4.52	3.15E-23
Prok1	131.47	-4.56	4.60E-30
Gm38070	49.33	-4.65	1.34E-13
Mup21	7641.42	-4.65	2.69E-19
Mup10	13405.27	-4.94	6.05E-08
Slc22a28	255.20	-5.11	7.84E-54
Mup-ps16	157.97	-5.14	8.63E-10
Nat8f5	262.44	-5.28	2.40E-12
Obox4-ps3	49.13	-5.32	8.20E-17
Nrep	2323.44	-5.41	2.20E-17
Serpina9	61.07	-5.44	6.33E-17
Ces4a	77.38	-5.46	3.16E-23
Mup16	345.85	-5.52	3.52E-52
Gbp11	838.28	-5.57	3.18E-17
C4a	3697.31	-5.72	3.80E-211
Xirp1	67.33	-6.28	1.38E-18

Mup20	95849.28	-6.35	3.48E-153
Cyp21a1	92.46	-6.48	5.43E-23
RP23-306P12,3	49.37	-6.57	3.50E-12
Selenbp2	7872.78	-6.76	1.29E-174
Mup-ps19	107.12	-6.96	3.03E-22
Ugt2b38	593.20	-6.99	2.05E-79
Cyp4a12b	2829.26	-7.15	2.46E-34
Hsd3b5	4556.34	-7.16	3.18E-11
Moxd1	139.25	-7.32	7.12E-07
Mup12	357.75	-7.42	8.01E-14
Serpina1e	55641.38	-7.62	8.14E-26
Mup1	270.53	-7.81	3.98E-17
Cyp4a12a	5094.03	-7.87	5.26E-19
Serpina4-ps1	9253.07	-8.27	0.00E+00
Mup17	2928.99	-8.37	2.26E-28
Mup15	2214.42	-8.40	5.56E-33
Mup11	3712.44	-8.56	1.54E-27
Mup18	129.98	-8.57	8.00E-15
Mup19	164.57	-8.91	7.99E-16
Mup14	4423.42	-8.97	1.34E-27
Mup7	17057.73	-9.28	2.95E-37

Supplementary list 4: Differentially expressed genes between CR WT vs CR GR-LKO mice in liver, at the peak of corticosterone levels (at ZT12).

Results from RNA-seq in liver of caloric restricted GR-LKO versus WT mice at the peak of corticosterone levels (at ZT12) indicating the fold change (FC) in gene expression as log2 (log2FC). The top 50 up- and down-regulated genes (FC>1.5; p-value <0.05) are listed.

Gene name	baseMean	log2FC	Padj. val. in CR GR-LKO
Gm32468	359.05	7.90	7.21E-08
Rps3a3	204.39	7.39	5.73E-05
Cd1d2	79.91	7.31	3.14E-04
Cyp2b13	1115.66	7.23	1.05E-05
Mup-ps16	174.45	6.82	9.33E-32
Hao2	95.32	6.74	9.81E-07
Gm13775	240.33	5.70	1.96E-13
Nrep	664.66	5.64	4.09E-20
Gprc5b	101.89	5.59	5.26E-06

Gbp11	244.47	5.50	2.91E-05
Gm45724	52.70	4.81	1.61E-04
Hamp2	1237.50	4.65	5.39E-08
Slc22a26	1112.81	4.23	2.35E-05
Clstn3	328.98	4.03	1.98E-32
Tcf24	48.92	3.88	3.43E-12
Cyp2a22	1069.03	3.74	1.18E-04
Klhdc7a	361.03	3.70	4.20E-44
Osbpl3	262.88	3.68	5.62E-39
Vnn1	540.74	3.61	4.06E-41
Gm49012	27.33	3.59	9.14E-06
Car3	23271.48	3.56	8.30E-44
Cyp4a12a	1279.55	3.53	3.54E-02
Dlec1	115.83	3.43	1.32E-11
Lgals1	344.35	3.40	7.84E-22
Bhlhb9	62.49	3.35	2.97E-11
Gm2788	102.78	3.31	1.37E-02
Gask1a	53.50	3.22	1.49E-07
A530020G20Rik	68.67	3.20	3.77E-14
Mmd2	200.44	3.20	1.30E-27
Gpx6	112.85	3.07	1.72E-27
Gm15998	80.55	3.05	6.14E-14
Serpina7	564.38	3.02	3.24E-07
Fads3	560.20	3.01	1.41E-53
G0s2	1083.41	3.00	2.50E-06
Serpinb1a	57.68	2.94	1.28E-07
Ntrk2	155.14	2.91	4.18E-03
Fam83f	16.70	2.85	2.52E-04
Fitm1	257.83	2.84	1.03E-17
Paqr9	3445.23	2.84	2.24E-61
Tpm2	78.58	2.82	8.77E-14
Gm15564	110.79	2.78	2.13E-02
Clec2h	262.55	2.72	3.14E-02
Cyp2d36-ps	45.25	2.69	2.82E-06
Gadd45a	48.60	2.69	1.82E-08
Gm32063	82.48	2.66	5.12E-14
A630031M04Rik	71.07	2.57	4.52E-10
Gm11266	44.82	2.57	1.89E-08
Tlr5	145.07	2.55	8.21E-29
Gm37691	25.76	2.55	4.75E-05
Pparg	290.82	2.54	1.72E-19
Gm16573	187.31	-1.95	1.70E-22
Slco3a1	57.07	-1.97	1.32E-07

Serpine2	128.20	-2.02	7.28E-12
Gldc	2838.90	-2.03	5.69E-13
Mpzl1	56.39	-2.03	1.54E-08
Abcd4	345.03	-2.07	1.29E-24
Shld2	632.71	-2.12	4.54E-17
Fbxo31	1108.69	-2.15	3.54E-49
Fmo5	29531.09	-2.17	3.79E-22
St3gal5	3747.52	-2.22	3.57E-22
Mt1	437.06	-2.24	1.05E-17
Tsku	1825.11	-2.24	1.86E-03
Arrdc2	93.31	-2.25	2.05E-15
Extl1	101.67	-2.26	1.12E-06
Fam222a	65.13	-2.27	6.60E-11
Marco	71.14	-2.36	3.74E-02
Tcim	207.70	-2.39	1.91E-24
Mfsd2a	2922.85	-2.47	1.49E-19
Gstm3	2329.64	-2.47	3.09E-04
Pfkfb3	239.58	-2.63	2.01E-23
Cpm	76.69	-2.69	4.70E-16
Gadd45g	294.05	-2.70	3.24E-02
Plin5	1243.61	-2.73	5.29E-26
Gm15889	115.00	-2.78	1.11E-16
Atp2b2	10.14	-2.80	2.51E-02
Gm27252	117.46	-2.83	3.38E-13
Srrm4	61.91	-2.88	4.49E-16
Fkbp5	3009.37	-2.93	9.25E-33
Arntl	91.52	-3.01	1.32E-12
Apoa4	1118.75	-3.04	4.65E-36
Rrm2	118.01	-3.10	2.10E-19
Slc3a1	332.52	-3.16	2.75E-31
Rasgef1b	556.39	-3.26	1.68E-30
Il1r1	1034.21	-3.28	2.09E-52
Rpl3-ps1	107.32	-3.32	1.15E-02
Tmc7	188.54	-3.38	3.54E-49
Cyp17a1	199.14	-3.51	3.23E-06
Igfbp1	2015.50	-3.58	1.69E-31
Ddit4	500.79	-3.75	2.89E-29
Il22ra1	149.60	-3.80	8.00E-27
Zbtb16	789.51	-3.86	1.01E-41
Lpin1	9487.71	-4.06	1.82E-112
Acnat2	331.67	-4.17	4.31E-56
1810053B23Rik	94.52	-4.22	1.19E-28
AA986860	161.63	-4.37	4.51E-37

Gene name			
Eif4ebp3	155.89	-5.07	4.30E-49
Scara5	67.17	-5.21	5.83E-04
Cyp39a1	930.23	-5.32	5.20E-11
Cdkn1a	194.51	-5.35	1.65E-36
Gm48199	222.79	-6.47	9.08E-08
Fam107a	130.07	-7.32	1.63E-12

Supplementary list 5: Differentially expressed genes between CR WT vs CR-LKO mice in liver, 4h after feeding (at ZT16).

Results from RNA-seq in liver of caloric restricted GR-LKO versus WT mice 4 h after feeding (at ZT16) indicating the fold change (FC) in gene expression as log2 (log2FC). The top 50 up- and down-regulated genes (FC>1.5; p-value <0.05) are listed.

Gene name	baseMean	log2FC	Padj CR GR-LKO
Gm32468	105.21	6.74	1.75E-11
Hao2	200.92	6.02	3.70E-11
Gm8730	187.16	5.24	6.90E-06
Gprc5b	183.42	5.16	1.34E-12
Mup-ps16	95.60	4.68	4.96E-08
Gm13775	141.21	4.51	1.03E-08
Mup11	10.02	4.03	1.78E-03
Gsta1	545.73	3.96	3.68E-18
Cyp4a12a	853.18	3.89	4.11E-04
Elovl3	129.48	3.86	2.63E-07
Cyp2b13	3464.96	3.62	1.15E-12
Tcf24	80.06	3.26	1.09E-27
Gm3776	202.59	2.99	3.35E-09
Hamp2	1974.44	2.96	1.94E-48
Sult2a7	179.67	2.93	3.25E-08
Adamts15	140.11	2.90	2.38E-26
Cyp2b10	569.88	2.76	4.05E-28
Car3	55691.68	2.71	3.04E-12
Slc22a26	1767.53	2.61	3.95E-32
Fitm1	221.47	2.59	1.69E-23
Serpina7	2273.06	2.51	5.98E-14
H2-Q1	93.30	2.39	2.25E-04
Gm15998	62.95	2.35	2.03E-12
Osbpl3	52.50	2.31	1.94E-12
Cyp4a12b	102.45	2.28	2.80E-03

Lgals1	317.50	2.24	1.10E-04
Bhlhb9	45.74	2.23	3.29E-09
Vnn1	554.08	2.20	1.64E-08
Clstn3	777.29	2.19	5.10E-08
Ttc39a	77.45	2.18	2.54E-14
Tpm2	143.84	2.15	1.81E-22
Chrna4	453.58	2.15	1.17E-05
Cidec	112.11	2.14	1.97E-08
Rad51b	139.49	2.11	7.10E-16
Orm2	1894.46	2.10	6.21E-07
Arhgef9	126.53	2.09	6.62E-15
Gpx6	87.31	2.08	7.50E-07
Cyp2a4	2592.47	2.04	3.67E-09
BC023105	112.00	2.02	2.16E-08
Pparg	225.92	1.89	4.22E-15
Acaa1b	17829.43	1.89	1.68E-28
Saa1	269.25	1.88	9.55E-06
Dlec1	74.39	1.88	4.77E-07
Ntrk2	49.06	1.81	3.52E-05
Alas2	781.61	1.79	1.75E-26
Slc22a27	569.45	1.79	6.37E-26
Gm4841	89.42	1.78	1.92E-05
Raet1d	318.02	1.74	9.85E-13
Gbp11	130.98	1.74	3.06E-12
Slc10a2	308.90	1.72	4.07E-15
Wfdc21	2426.82	-1.23	9.67E-04
Gm45470	71.24	-1.23	4.71E-06
Brca1	42.14	-1.24	7.86E-06
Peg3	166.53	-1.25	2.23E-05
Mfsd2a	1193.20	-1.27	6.08E-09
Chic1	201.54	-1.31	7.07E-09
Cyp2c70	4141.49	-1.33	1.43E-10
Tango2	307.03	-1.34	3.55E-20
Cd9	144.03	-1.37	2.29E-12
Cdkn1a	243.43	-1.37	5.58E-08
Epop	48.31	-1.38	3.67E-05
Lrg1	1743.09	-1.38	9.79E-05
Sall2	107.75	-1.39	2.70E-11
Ppard	330.76	-1.39	6.41E-09
Hcn3	237.87	-1.45	2.53E-03
Srgap3	209.16	-1.48	5.64E-18
Igsf23	13.38	-1.50	2.63E-03
Srrm4	37.61	-1.51	3.95E-05

Fkbp5	737.55	-1.53	4.07E-22
Sdr9c7	1055.93	-1.55	1.06E-32
Slc1a5	86.59	-1.56	5.33E-08
Gfra1	1940.34	-1.56	3.21E-61
Sult1d1	2149.55	-1.62	3.37E-39
Enho	50.62	-1.79	5.41E-10
Gm43305	512.56	-1.85	4.62E-05
Slc34a2	293.49	-1.90	3.18E-03
Cpm	60.68	-1.90	2.71E-13
Ccnf	155.62	-1.93	7.42E-17
AA986860	28.85	-1.94	8.73E-08
Nr3c1	808.74	-1.95	1.44E-73
Avpr1a	366.17	-1.95	2.94E-39
Urad	355.04	-1.97	6.28E-14
Gm27252	34.35	-1.99	1.77E-09
Tedc2	627.04	-2.01	6.13E-23
Rrm2	67.34	-2.12	2.98E-07
Serpine2	154.35	-2.23	8.92E-29
Zbtb16	89.16	-2.26	6.03E-08
Gm15889	27.22	-2.40	1.48E-08
Gm8893	1375.73	-2.47	4.54E-03
Apoa4	869.24	-2.50	7.39E-27
Serpina3k	36250.71	-2.60	4.67E-08
Slc3a1	367.26	-2.64	3.39E-60
Fam107a	7.75	-2.82	2.39E-03
Acnat2	702.21	-3.13	5.72E-55
1810053B23Rik	41.08	-3.28	3.45E-04
Cyp17a1	376.38	-3.33	2.12E-36
Scara5	3.78	-3.46	4.27E-03
Eif4ebp3	58.95	-3.57	8.10E-21
Cyp39a1	827.37	-3.85	2.93E-14
Gm48199	12.38	-6.58	1.42E-08

Supplementary list 6: Lipid species concentration between ad-libitum and caloric restricted WT vs GR-LKO mice in liver, at the peak of corticosterone levels (at ZT12).

All the raw values of the 13 different measured lipid class concentrations from livers of all conditions at the peak of corticosterone. For the normalization of the data, reference plasma was used in order to quantify the measured samples. Also, the blank samples were used in order to have the baseline levels of the buffers in the Lipidyzer.

Name	CE	CER	DAG	DCER	FFA	HCER	LCER	LPC	LPE	PC	PE	SM	TAG
Blank_01	1.17	0.06	1.77	0.56	82.20	.	.	.	.	1.22	0.39	3.26	2.06
Blank_02	0.58	0.05	1.59	0.57	93.63	.	.	.	.	.	.	3.29	1.05
Blank_03	0.53	0.06	2.01	0.51	98.98	.	.	.	.	.	.	3.10	0.76
RefPlasma_01	2794.42	4.43	44.87	0.74	1129.08	2.50	2.80	386.45	3.62	1892.81	98.49	412.01	956.14
Pool_01	131.04	15.17	147.56	1.23	336.69	6.46	.	104.07	7.97	4769.56	1473.09	498.37	2223.95
WT-CR-R1	148.86	15.38	151.71	1.52	356.97	4.67	0.13	92.66	7.84	4624.05	1374.45	460.81	753.05
KO-AL-R1	97.00	10.86	65.92	0.92	201.64	4.64	.	97.11	6.27	4323.43	1909.63	440.08	906.07
WT-AL-R1	66.12	13.50	49.93	1.30	185.75	6.15	.	85.48	5.66	3816.13	1693.30	415.47	379.77
KO-CR-R1	266.95	14.18	104.25	1.04	222.13	5.59	0.14	119.85	8.09	5151.48	1379.45	496.28	4887.35
WT-AL-R2	66.38	9.33	54.85	1.35	169.67	5.46	.	85.83	5.49	3762.89	1676.48	369.41	534.83
KO-CR-R2	111.94	17.78	91.63	1.30	212.58	7.23	.	104.41	6.91	5269.55	2546.30	481.23	1614.27
WT-CR-R2	86.80	15.14	72.87	1.17	223.49	6.00	.	122.14	10.02	4515.41	2088.08	468.29	593.14
KO-AL-R2	109.03	14.59	99.86	1.38	213.85	7.06	0.22	116.98	8.06	5236.62	1529.55	517.22	1429.80
WT-AL-R3	79.98	11.01	240.93	0.62	668.54	4.39	0.10	98.72	16.29	3471.52	1344.14	360.26	9486.21
WT-CR-R3	84.77	16.95	117.81	1.46	257.86	3.73	.	96.86	8.69	4528.79	1878.96	467.44	721.92
RefPlasma_02	2807.89	4.50	50.04	0.75	1239.69	2.94	2.96	400.84	3.75	1863.88	121.88	428.67	979.64
Pool_02	113.69	13.10	152.11	0.96	465.79	5.28	.	111.05	8.02	4325.99	1750.50	422.01	1580.79
KO-AL-R3	129.04	16.22	278.97	2.06	3152.94	7.64	.	121.18	8.79	4666.17	1232.80	494.75	161.81
WT-AL-R4	102.77	14.47	130.80	1.15	435.63	5.21	.	124.61	14.40	4691.91	1258.74	483.07	1531.04
KO-CR-R3	139.18	14.97	114.23	1.06	208.46	8.65	.	81.16	4.41	5330.08	1842.13	408.88	2090.55
KO-AL-R4	104.48	13.97	76.22	1.31	193.54	4.47	.	95.61	8.05	4594.61	2231.49	468.05	1385.44
WT-AL-R5	76.70	14.57	71.35	1.24	176.97	6.34	.	88.07	6.57	4186.19	1163.05	469.69	613.13
KO-CR-R4	127.23	18.14	116.65	1.37	244.61	5.91	.	97.41	5.89	5310.06	2297.09	481.09	1019.74
WT-CR-R4	168.58	19.54	156.82	1.24	411.01	6.10	.	125.07	10.57	5382.06	2474.60	511.78	1007.99
WT-CR-R5	141.64	14.80	119.09	1.55	279.71	3.31	.	84.52	6.09	4008.53	1633.95	402.20	766.78
KO-CR-R5	91.29	13.61	96.18	0.93	219.36	6.08	.	88.80	4.93	4554.48	1705.23	389.92	879.77
KO-AL-R5	179.80	15.26	220.30	0.89	235.06	8.08	0.27	116.07	6.92	5113.04	1061.35	456.07	5323.43
RefPlasma_03	3330.78	5.69	59.67	0.91	1330.53	3.26	3.28	477.65	4.66	2222.45	117.66	480.07	1151.81
Pool_03	123.16	14.45	137.47	1.22	343.35	5.83	.	95.49	7.23	4785.40	2188.86	445.11	1955.85
LCBlank_00	570.27	.	.	.	1228.13	.	.	.	.	.	.	.	1831.57

9 Publications

1. Quagliarini, F., Mir, A. A., Balazs, K., Wierer, M., Dyar, K. A., Jouffe, C., **Makris, K**., Hawe, J., Heinig, M., Filipp, F. V., Barish, G. D., & Uhlenhaut, N. H. (2019). Cistromic Reprogramming of the Diurnal Glucocorticoid Hormone Response by High-Fat Diet. *Molecular Cell*, *76*(4), 531-545.e5. https://doi.org/10.1016/j.molcel.2019.10.007

10 Conference attendance and poster presentations

1. **K. Makris**, F. Quagliarini, M. Wierer, C. Hemmer, N.H. UhlenhautI. Transcriptional complexes mediating hepatic GR action. Spetses FEBS course 2019, Spetses, Greece.

2. **K. Makris**, F. Quagliarini, K. Balasz and N.H. Uhlenhaut. The role of glucocorticoids in the adaptive response to Caloric Restriction in mouse liver. Chromatin and Metabolism Spetses Summer school 2018, Spetses. Greece.

11 Curriculum Vitae

Konstantinos Makris

Date of birth: 18/05/1993

Place of birth: Cholargos, Athens

Nationality: Greek

Education

15/02/2018-14/02/2022   **PhD in Molecular Biology**

AG Prof. Dr.rer. nat. N.H. Uhlenhaut, Institute for Diabetes and Endocrinology

Helmholtz Zentrum München & Ludwig Maximilians University, Munich

Title of PhD thesis

"The role of glucocorticoid in hepatic adaptive response to caloric restriction"

10/2015-10/2017   **Master of Science (MSc) in Molecular Biology-Biomedicine, 120 Credits**

Interdepartmental program between Faculty of Biology, School of Medicine and IMBB-FORTH, **University of Crete**, **Greece**

Average grade: *9.11/10 (with High Honors)*

Master Thesis, Title: "Pharmacokinetic regulation of ERF, as a therapeutic approach for the ERF-related craniosynostosis in mouse"

09/2011-09/2015   **Bachelor of Science (BSc) in Molecular Biology and Biotechnology, 240 Credits**

Faculty of Biology, School of Sciences and Engineering, **University of Crete, Greece**

Average grade: *8.17/10* (***with Honors***)

Bachelor Thesis, Title: "Pharmacokinetic study of inhibitors of nuclear export, as a therapy for ERF-related craniosynostosis in mouse"

09/2008-06/2011   2nd General Lyceum of Livadeia, Greece, Average grade: **18.9/20**